

**Chemistry of Transition Metal Complexes with O- and/or N-
Donor Ligands: Synthesis, Characterization and Study of
Reactivity**

*Dissertation submitted to the
National Institute of Technology Rourkela
in partial fulfillment of the requirements
of the degree of
Doctor of Philosophy*

*in
Chemistry*

by

Satabdi Roy

(Roll No. 512CY105)

Under the supervision of

Prof. Rupam Dinda



January, 2017

**Department of Chemistry
National Institute of Technology, Rourkela
Rourkela-769008, Odisha, India**



Department of Chemistry
National Institute of Technology Rourkela

Certificate of Examination

Roll Number: 512CY105

Name: Satabdi Roy

Title of Dissertation: "Chemistry of Transition Metal Complexes with O- and/or N- Donor Ligands: Synthesis, Characterization and Study of Reactivity"

We the below signed, after checking the dissertation mentioned above and the official record book (s) of the student, hereby state our approval of the dissertation submitted in partial fulfillment of the requirements of the degree of Doctor of Philosophy in Chemistry at National Institute of Technology Rourkela. We are satisfied with the volume, quality, correctness, and originality of the work.

Rupam Dinda
Supervisor

Debasish Sarkar
Member (DSC)

Saurav Chatterjee
Member (DSC) & HOD

V. Sivakumar
Member (DSC)

Examiner

Garudadhvaj Hota
Chairman (DSC)



Department of Chemistry
National Institute of Technology Rourkela

Prof. Rupam Dinda
Associate Professor

Supervisor's Certificate

This is to certify that the work presented in this dissertation entitled “*Chemistry of Transition Metal Complexes with O- and/or N- Donor Ligands: Synthesis, Characterization and Study of Reactivity*” by **Satabdi Roy, Roll No. 512CY105** of the Department of Chemistry, National Institute of Technology, Rourkela, India, for the degree of **Doctor of Philosophy** is a record of bona fide research work carried out by her under my guidance and supervision. I am satisfied that the thesis has reached the standard fulfilling the requirements of the regulations relating to the nature of the degree. To the best of my knowledge, the matter embodied in the thesis has not been submitted to any other University/Institute for the award of any degree or diploma.

Supervisor

Place: Rourkela

Date:

Dr. Rupam Dinda,
Department of Chemistry
National Institute of Technology,
Rourkela-769008, Odisha,
India

Declaration of Originality

I, Satabdi Roy, Roll Number 512CY105 hereby declare that this dissertation entitled *“Chemistry of Transition Metal Complexes with O- and/or N- Donor Ligands: Synthesis, Characterization and Study of Reactivity”* represents my original work carried out as a doctoral student of NIT Rourkela and, to the best of my knowledge, it contains no material previously published or written by another person, nor any material presented for the award of any other degree or diploma of NIT Rourkela or any other institution. Any contribution made to this research by others, with whom I have worked at NIT Rourkela or elsewhere, is explicitly acknowledged in the dissertation. Works of other authors cited in this dissertation have been duly acknowledged under the section "References". I have also submitted my original research records to the scrutiny committee for evaluation of my dissertation.

I am fully aware that in case of any non-compliance detected in future, the Senate of NIT Rourkela may withdraw the degree awarded to me on the basis of the present dissertation.

Date:

NIT Rourkela

Satabdi Roy

Acknowledgements

This thesis is the account of four and a half years of work in the field of coordination chemistry in relation to their biological and magnetic application at Department of Chemistry, National Institute of Technology, Rourkela, India, which would not have been possible without the help of many.

I would like to express my gratitude to my supervisor Dr. Rupam Dinda, Associate Professor, Department of Chemistry, National Institute of Technology, Rourkela for his guidance, constant encouragement and constructive criticisms. I would sincerely acknowledge him for patiently scrutinizing my thesis and making this project a success.

I am thankful to the Director, National Institute of Technology, Rourkela for providing me the use of all infrastructural facilities. I would also like to thank Dr. S. Chatterjee, HOD, Department of Chemistry, for providing me the various laboratory and instrumental facilities during my Ph.D. work.

I sincerely thank my DSC members, Dr. D. Sarkar, Department of Ceramic Engineering, Dr. S. Chatterjee and Dr. V. Siva Kumar for their valuable comments and evaluation of my progress reports and seminars during the Ph. D. program. I am sincerely thankful to all the faculty members and staff of our Department for their constant help. Helps received from Dr. Debayan Sarkar deserves special mention. I am thankful to the members of our research group Sagarika Pasayat, Saswati, Sudarshana Majumder, Atanu Banerjee, Monalisa Mohanty and Subhashree P. Dash for their active cooperation during my research work.

I would like to express my gratitude to Mokshada Varma, Manasi R. Hardikar, K. Senthilguru, Ayon Chakraborty, Raquel M. S. N. Sampaio, Martin Recheilt, Michael Böhme, and Axel Buchholz for their kind cooperation.

I am thankful to Prof. Indranil Banerjee, Department of Biotechnology, NIT Rourkela, Dr. Bimba N. Joshi, Agharkar Research Institute, Prof. Ashis Biswas, IIT Bhubaneswar and Prof. Adolfo Horn Jr., Universidade Federal de Santa Catarina Brazil for the pharmacological studies. I also acknowledge Prof. Dr. Winfried Plass, Institut für Anorganische und Analytische Chemie, Germany for magnetochemical and theoretical

studies. I am thankful to Prof. S. K. Chattopadhyay, Department of Chemistry, IEST, Shibpur, for his generous help in electrochemical studies.

I am grateful to, Prof. Dr. Hans Reuter, Institute of Chemistry of New Materials, University of Osnabrueck, Prof. Ekkehard Sinn, Department of Chemistry, Western Michigan University, Kalamazoo, Dr. Werner Kaminsky, Department of Chemistry, University of Washington and Prof. Cassandra Eagle, Department of Chemistry, East Tennessee State University for their kind cooperation in determining the X-ray structures of synthesized complexes.

I would like to acknowledge NIT Rourkela for providing research fellowship during my Ph. D tenure. Financial assistance received from the Council of Scientific and Industrial Research, New Delhi [Grant No. 01(2735)/13/EMR-II] and DBT, Govt. of India [Grant No. 6241 P112/RGCB/PMD/DBT/RPDA/2015] is gratefully acknowledged.

Last but not the least; it would not have been possible to complete this project without the love and support of my parents whose unflinching faith in my abilities helped me to overcome many obstacles and march ahead in spite of failures. I would like to dedicate this project to my family.

Date:

Satabdi Roy

ABSTRACT

Chemistry of Transition Metal Complexes with O- and/or N- Donor Ligands: Synthesis, Characterization and Study of Reactivity

Satabdi Roy

Department of Chemistry, National Institute of Technology, Rourkela-769008, Odisha,
India

Chapter 1: In this chapter the scope of the present investigation is delineated briefly along with the aim of the work.

Chapter 2: The synthesis of ethoxido bridged divanadium(IV/IV) complexes $[(VOL^{1-3})_2(\mu-OEt)][Et_3NH]$ (**1-3**) of three azo dyes, 2-(2'-carboxy-5'-X-phenylazo)-4-methylphenol (where X = H (H_2L^1); X = NO_2 (H_2L^2)) and 2-(2'-carboxy-5'-Br-phenylazo)-2-naphthol (H_2L^3), differing in the substituents of the phenyl ring, in order to discern their influence, if any, on their redox potentials, biological activities and magnetochemistry, has been discussed. All the synthesized ligands and the vanadium(IV) complexes were successfully characterized by various physico-chemical techniques, viz. elemental analysis, IR, UV-vis and NMR spectroscopy, ESI-MS and cyclic voltammetry. Molecular structures of $[(VOL^{1,3})_2(\mu-OEt)][Et_3NH]$ (**1** and **3**) have been determined by X-ray crystallography. Antiferromagnetic coupling interaction was observed between the vanadium d^1-d^1 centers of the complexes and this phenomenon was also established theoretically. The complexes were further screened for their *in vitro* cytotoxicity against HeLa and HT-29 cancer cell lines.

Chapter 3: Three new monooxidovanadium(IV) $[V^{IV}OL^{1-3}]$ (**1-3**) and two alkoxido bridged vanadium(IV) trimeric $[V^{IV}_3O_3(\mu-OMe)_3(\mu_3-OMe)L^{4,5}]$ (**4** and **5**), complexes have been reported, which were obtained upon reaction of 2-((2-X)-diazol)-4-methylphenol (where X = benzo[1,3]dioxol-5-yl (HL^1), phenyl (HL^2) and 4-methoxyphenyl (HL^3)), 1-(2-(thiazol-2-yl)diazenyl)naphthalene-2-ol (HL^4) and 2-(2-(thiazol-2-yl)diazenyl)-4-methylphenol (HL^5)) with $VOSO_4 \cdot 5H_2O$. The synthesized complexes were successfully characterized by elemental analysis, IR, UV-vis spectroscopy, ESI-MS and their redox properties studied by cyclic voltammetry. Molecular structure of **4** has been determined by single crystal X-ray diffraction study. The complexes were probed for their *in vitro* insulin-mimetic activity against insulin responsive L6 myoblast cells. The complexes (**1-5**) have also been screened for their cytotoxicity in human breast adenocarcinoma cell line, MCF-7. The insulin-mimetic activity of complexes **1-5** was also probed on rat L6 myoblast cells. To further confirm whether these compounds act via insulin signaling pathway, the immunoblot analysis for IRS-1 was also carried out.

Chapter 4: The reaction of 2-(aryloxy)phenols (HL) with $[Ru(PPh_3)_3Cl_2]$ in an ethanolic medium under basic conditions afforded two organometallic Ru(II) complexes, $[RuL(PPh_3)_2(CO)]$ (**1**) and $[RuL(PPh_3)_2(CH_3CN)]$ (**2**). A similar reaction of HL with $[Ir(PPh_3)_3Cl]$ resulted in the formation of the organometallic Ir(III) complex, $[IrL(PPh_3)_2(H)]$ (**3**). The 2-(aryloxy)phenolate ligand is coordinated to the metal center in each complex (**1-3**) as a tridentate C, N, O-donor via metal assisted C-H activation of the ligand. The plausible solvent assisted mechanistic pathway for the unprecedented CO coordination to the Ru(II) center in the case of **1** has been explained. The synthesized complexes have been characterized by various spectroscopic techniques (viz., IR, UV-vis

and NMR spectroscopy), ESI-MS and their electrochemical behavior studied by cyclic voltammetry. Molecular structures of **1–3** have been determined by X-ray crystallography.

Chapter 5: Seven hexacoordinated *cis*-dioxidomolybdenum(VI) complexes, [MoO₂L^{1–7}] (**1–7**) derived from various substituted tetradentate diamino bis(phenolato) “salan” ligands, *N,N'*-dimethyl-*N,N'*-bis-(2-hydroxy-3-X-5-Y-6-Z-benzyl)-1,2-diaminoethane (H₂L¹, X = Br, Y = Me, Z = H; H₂L², X = Me, Y = Cl, Z = H; H₂L³, X = ⁱPr, Y = Cl, Z = Me) and *N,N'*-bis-(2-hydroxy-3-X-5-Y-6-Z-benzyl)-1,2-diaminopropane (H₂L⁴, X = Y = ^tBu, Z = H; H₂L⁵, X = Y = Me, Z = H; H₂L⁶, X = ⁱPr, Y = Cl, Z = Me; H₂L⁷, X = Y = Br, Z = H) containing O–N donor atoms, have been isolated and structurally characterized. The formation of *cis*-dioxidomolybdenum(VI) complexes was confirmed by elemental analysis, IR, UV-vis and NMR spectroscopy, ESI-MS and cyclic voltammetry measurements. X-ray crystallography showed the O₂N₂ donor set to define an octahedral geometry in each case. [MoO₂L^{1–7}] (**1–7**) showed moderate DNA binding propensity with binding constants ranging from 10⁴–10⁵ M⁻¹. The experimental results showed that the complexes **1–7** effectively interact with CT-DNA by both minor and major groove binding mode, while complex **2** additionally interacts by partial intercalative mode of binding. The dioxidomolybdenum(VI) complexes (**1–3**) showed moderate photo-induced cleavage of pUC19 supercoiled plasmid DNA. All the complexes (**1–7**) were tested for their *in vitro* antiproliferative activity against HT-29 and HeLa cancer cell lines. Some of the complexes proved to be as active as the clinical referred drugs, and the greater potency of **6** and **7** may be dependent on the substituents in the salan ligand environment coordinated to the metal.

Chapter 6: The synthesis and characterization (elemental analysis, UV-vis spectroscopy, ESI-MS and cyclic voltammetry) of Cu(II) complexes ([CuL^{1,2}] (**1** and **2**) and [CuL^{3,4}]₂ (**3** and **4**)) using salan ligands, *N,N'*-dimethyl-*N,N'*-bis-(2-hydroxy-3-X-5-Y-6-Z-benzyl)-1,2-diaminoethane (H₂L¹, X = ⁱPr, Y = Cl, Z = Me; H₂L², X = OCH₃, Y = allyl, Z = H) and *N,N'*-bis-(2-hydroxy-3-X-5-Y-6-Z-benzyl)-1,2-diaminopropane (H₂L³, X = ⁱPr, Y = Cl, Z = Me; H₂L⁴, X = Y = CH₃, Z = H), have been discussed. Molecular structures of **1** and **3** have been determined by X-ray crystallography. An unprecedented ligand transformation occurs in the case of **3** and **4**, leading to the formation of phenolato bridged Cu(II) dimeric complexes, [CuL^{3,4}]₂. The organic transformation in the ligand has been mechanistically elucidated to be Cu(II) catalysed. This unusual chemistry of **3** and **4** has been compared with Ni^{II}, Fe^{III} and Mo^{VI} complexes (**5–7**) with similar ligand environment. The anomaly in ligand structure was however not observed in the case of other transition metal complexes (**5–7**). The superoxide dismutase (SOD) activity of the Cu(II) complexes (**1–3**) has also been investigated; the activity follows the order **3** > **1** > **2**. Due to the deliquescent nature of **4**, its SOD activity could not be evaluated.

Chapter 7: In this chapter a brief resume of the work embodied in the thesis and concluding remarks are stated. The scope for future research work has also been discussed.

Keywords: Azo; Salan; Variable valence transition metals (V(IV), Ru(II), Ir(III), Mo(VI), Cu(II)); X-ray crystal structure; Biological activity (DNA interaction, Cytotoxicity, Insulin-mimetic, Superoxide Dismutase Mimics); Magnetochemistry; Theoretical Study

Contents

| | Page No. | |
|-----------------------------------|---|-----------|
| Certificate of Examination | ii | |
| Supervisor's Certificate | iii | |
| Declaration of Originality | iv | |
| Acknowledgements | v | |
| Abstract | vii | |
| Preface | 1 | |
| Chapter 1 | Scope of the Present Investigation | 4 |
| | Abstract | 5 |
| 1.1. | Reviews on transition metal complexes of azo ligands | 5 |
| 1.1.1. | Vanadium complexes of azo ligands | 5 |
| 1.1.2. | Ruthenium and Iridium complexes of azo ligands | 9 |
| 1.2. | Reviews on transition metal complexes of salan ligands | 15 |
| 1.2.1. | Molybdenum complexes of salan ligands | 15 |
| 1.2.2. | Copper complexes of salan ligands | 18 |
| 1.3. | Aim of the present work | 23 |
| 1.4. | The main objectives of the present study | 26 |
| 1.5. | References | 28 |
| Chapter 2 | Magnetic exchange coupling interaction of μ-ethoxido bridged azo functionalized oxidovanadium(IV) dimeric anions: Synthesis, X-ray structure, characterization and cytotoxicity | 33 |
| | Abstract | 34 |
| 2.1. | Introduction | 35 |
| 2.2. | Experimental section | 38 |
| 2.2.1. | General methods and materials | 38 |
| 2.2.2. | Synthesis of ligands (H_2L^{1-3}) | 38 |
| 2.2.3. | Synthesis of complexes, $[(VOL^{1,3})_2(\mu-OEt)][Et_3NH]$ (1-3) | 39 |
| 2.2.4. | X-ray Crystallography | 40 |
| 2.2.5. | Magnetic Susceptibility Study | 43 |

| | | |
|------------------|---|-----------|
| 2.2.6. | Computational Studies | 43 |
| 2.2.7. | Cytotoxicity | 44 |
| 2.3. | Results and discussion | 45 |
| 2.3.1. | Synthesis | 45 |
| 2.3.2. | Spectral characteristics | 46 |
| 2.3.2.1. | IR spectroscopy | 46 |
| 2.3.2.2. | UV-vis spectroscopy | 47 |
| 2.3.3. | ESI-MS | 48 |
| 2.3.4. | Electrochemical properties | 51 |
| 2.3.5. | Description of X-ray crystallographic structure of [(VOL ^{1,3}) ₂ (μ-OEt)][Et ₃ NH] (1 and 3) | 53 |
| 2.3.6. | Magnetic Susceptibility Study | 61 |
| 2.3.7. | Computational Studies | 62 |
| 2.3.8. | Cytotoxicity Study | 69 |
| 2.4. | Conclusion | 73 |
| 2.5. | References | 74 |
| Chapter 3 | <i>Synthesis, structure and characterization of mono- and trinuclear oxidovanadium(IV) azo complexes: Study of antiproliferative and insulin-mimetic activity</i> | 82 |
| | Abstract | 83 |
| 3.1. | Introduction | 84 |
| 3.2. | Experimental section | 87 |
| 3.2.1. | General methods and materials | 87 |
| 3.2.2. | Synthesis of ligands (HL ¹⁻⁵) | 87 |
| 3.2.3. | Synthesis of complexes, [VOL ¹⁻³ ₂] (1-3) and [V ^{IV} ₃ O ₃ (μ-OMe) ₃ (μ ₃ -OMe)L ^{4,5} ₂] (4 and 5) | 88 |
| 3.2.4. | X-ray crystallography | 90 |
| 3.2.5. | Cytotoxicity Studies | 92 |
| 3.2.5.1. | MTT assay | 92 |
| 3.2.5.2. | Nuclear Morphology study using DAPI Staining | 92 |
| 3.2.6. | <i>In vitro</i> insulin-mimetic activity | 93 |

| | | |
|------------------|---|------------|
| 3.2.7. | Immunoblot analysis | 93 |
| 3.2.7.1. | Analysis of accumulation of IRS-1 in L6 myotubes in presence of vanadium complexes | 93 |
| 3.2.7.2. | Immunoblot analysis for IRS-1 | 93 |
| 3.3. | Results and discussion | 95 |
| 3.3.1. | Synthesis | 95 |
| 3.3.2. | Spectral characteristics | 97 |
| 3.3.2.1. | IR spectroscopy | 97 |
| 3.3.2.2. | UV-vis spectroscopy | 98 |
| 3.3.3. | ESI-MS | 99 |
| 3.3.4. | Electrochemical properties | 103 |
| 3.3.5. | Description of X-ray structure of $[V^{IV}_3O_3(\mu\text{-OMe})_3(\mu_3\text{-OMe})L^4_2]$ | 107 |
| | (4) | |
| 3.3.6. | Cytotoxicity Studies | 110 |
| 3.3.6.1. | MTT assay | 110 |
| 3.3.6.2. | Nuclear Morphology study using DAPI Staining | 113 |
| 3.3.7. | <i>In vitro</i> insulin-mimetic activity | 116 |
| 3.3.8. | Immunoblot analysis | 118 |
| 3.4. | Conclusion | 120 |
| 3.5. | References | 121 |
| Chapter 4 | <i>Synthesis, characterization and study of reactivity of Ru and Ir complexes of 2-arylazophenols: Solvent assisted CO insertion and formation of metal (Ru, Ir)–carbon bond</i> | 129 |
| | Abstract | 130 |
| 4.1. | Introduction | 131 |
| 4.2. | Experimental section | 133 |
| 4.2.1. | General methods and materials | 133 |
| 4.2.2. | Synthesis of complexes | 133 |
| 4.2.3. | X–ray crystallography | 134 |
| 4.3. | Results and disscussion | 137 |
| 4.3.1. | Synthesis of complexes (1–3) | 137 |

| | | |
|------------------|--|------------|
| 4.3.2. | Spectral characteristics | 139 |
| 4.3.2.1. | IR spectroscopy | 139 |
| 4.3.2.2. | UV-vis spectroscopy | 141 |
| 4.3.2.3. | NMR spectroscopy | 143 |
| 4.3.3. | ESI-MS | 146 |
| 4.3.4. | Electrochemical properties | 149 |
| 4.3.5. | Description of X-ray structure of [RuL(PPh ₃) ₂ (CO)] (1), [RuL(PPh ₃) ₂ (CH ₃ CN)] (2) and [IrL(PPh ₃) ₂ (H)] (3) | 151 |
| 4.4. | Conclusion | 156 |
| 4.5. | References | 157 |
| Chapter 5 | <i>Synthesis, structure, DNA interaction and cytotoxicity of a series of dioxidomolybdenum(VI) complexes featuring salan ligands</i> | 160 |
| | Abstract | 161 |
| 5.1. | Introduction | 162 |
| 5.2. | Experimental section | 165 |
| 5.2.1. | General methods and materials | 165 |
| 5.2.2. | Synthesis of ligands (H ₂ L ¹⁻⁷) | 166 |
| 5.2.3. | Synthesis of complexes [MoO ₂ L ¹⁻⁷] (1-7) | 168 |
| 5.2.4. | X-ray crystallography | 170 |
| 5.2.5. | DNA binding experiments | 173 |
| 5.2.6. | DNA cleavage experiments | 174 |
| 5.2.7. | Cytotoxic Activity | 175 |
| 5.3. | Results and discussion | 177 |
| 5.3.1. | Synthesis | 177 |
| 5.3.2. | Spectral characteristics | 178 |
| 5.3.3. | ESI-MS | 181 |
| 5.3.4. | Electrochemical properties | 185 |
| 5.3.5. | Description of X-ray structures of [MoO ₂ L ¹⁻⁶] (1-6) | 186 |
| 5.3.6. | DNA binding studies | 191 |
| 5.3.7. | DNA cleavage studies | 206 |

| | | |
|------------------|---|------------|
| 5.3.8. | Cytotoxicity | 212 |
| 5.4. | Conclusion | 216 |
| 5.5. | References | 217 |
| <i>Chapter 6</i> | <i>Synthesis, characterization and superoxide dismutase activity of</i> | 224 |
| | <i>Cu(II) salan complexes: Unprecedented Cu(II) catalyzed acetal</i> | |
| | <i>formation</i> | |
| | Abstract | 225 |
| 6.1. | Introduction | 226 |
| 6.2. | Experimental section | 228 |
| 6.2.1. | General methods and materials | 228 |
| 6.2.2. | Synthesis of ligands (H ₂ L ¹⁻⁴) | 228 |
| 6.2.3. | Synthesis of Cu(II) complexes (1-4) | 229 |
| 6.2.4. | Synthesis of [Ni ^{II} L ³] (5), [Fe ^{III} L ³ (Cl)] (6) and [Mo ^{VI} O ₂ L ³] (7) complexes. | 229 |
| 6.2.5. | X-ray Crystallography | 230 |
| 6.2.6 | Superoxide Dismutase activity | 234 |
| 6.3. | Results and discussion | 235 |
| 6.3.1. | Synthesis | 235 |
| 6.3.2. | Spectral characteristics | 239 |
| 6.3.3 | ESI-MS | 242 |
| 6.3.4. | Electrochemical Properties | 246 |
| 6.3.5. | Description of X-ray structure of [CuL ¹] (1) and [CuL ³] ₂ (3) | 247 |
| 6.3.6. | Superoxide Dismutase activity | 251 |
| 6.4. | Conclusion | 254 |
| 6.5. | References | 255 |
| <i>Chapter 7</i> | <i>Conclusion and Scope for Further Research</i> | 259 |
| 7.1. | <i>A Brief Resume of the Work Embodied in this Dissertation and</i> <i>Concluding Remarks</i> | 260 |
| 7.2. | <i>Scope for Further Research</i> | 263 |
| | <i>Dissemination</i> | 264 |
| | <i>Curriculum Vitae</i> | 267 |

Preface

The present dissertation describes the design, synthesis, characterization and the exploration of chemical and electrochemical properties and the study of bio- and magnetochemistry of a series of variable valence transition metal (V, Ru and Ir) complexes of bi- and tridentate ON, ONN and ONO donating arylazo ligands and Mo(VI) and Cu(II) complexes derived from tetradentate ONNO donating salan ligands. Structures of some of the important transition metal (V, Ru, Ir, Mo and Cu) complexes are determined by single crystal X-ray analysis. Structure-reactivity relations are discussed and implications of structure determination on the design of new complexes using the structurally characterized compounds as precursors are elaborated. All the complexes described in this dissertation are characterized by various physico-chemical techniques such as elemental analysis, IR, UV-vis and NMR spectroscopy and ESI-MS. Electrochemical characterization of the complexes were studied by cyclic voltammetry. Biological activities particularly, DNA interaction, antiproliferative, insulin-mimetic and superoxide dismutase activity of the complexes and the magnetic exchange coupling interactions between the metal centers in bridged vanadium(IV) complexes were also studied. The subject matter of this dissertation is divided into seven chapters containing an the chemistry of V(IV), Ru(II) and Ir(III) ligated to azo ligands, and the Mo(VI) and Cu(II) salan complexes, followed by the concluding remarks and future scope of research. *Chapter 1* is a literature survey and general introduction to the entire work described in the present dissertation and spells out the objectives of the thesis. The objectives of the works are placed at the end of the general introduction. The entire subject matter of this dissertation is organized in the consecutive chapters.

Chapter 2 deals with the synthesis of ethoxido bridged divanadium(IV/IV) complexes $[(VOL^{1-3})_2(\mu-OEt)][Et_3NH]$ (**1-3**) of three azo dyes, 2-(2'-carboxy-5'-X-phenylazo)-4-methylphenol (H_2L^1 , X = H; H_2L^2 , X = NO₂) and 2-(2'-carboxy-5'-Br-phenylazo)-2-naphthol (H_2L^3), differing in the substituents of the phenyl ring, in order to discern their influence, if any, on the redox potentials, bio- and magnetochemistry of the complexes has been discussed. All the synthesized ligands and the vanadium(IV) complexes are successfully characterized by various physicochemical techniques, viz. elemental analysis, IR, UV-vis and NMR spectroscopy, ESI-MS and cyclic voltammetry. Molecular

structures of $[(VOL^{1,3})_2(\mu-OEt)][Et_3NH]$ (**1** and **3**) have been determined by X-ray crystallography. Antiferromagnetic exchange interaction was observed between the vanadium d^1-d^1 centers of the complexes and this phenomenon was also established by density functional theory (DFT) study. The complexes were also screened for their *in vitro* cytotoxicity against HeLa and HT-29 cancer cell lines and the results indicated that the synthesized azo functionalized vanadium(IV) complexes were cytotoxic in nature, with **1** being the most potent against HeLa cancer cell line.

Chapter 3 describes the synthesis of three new monooxidovanadium(IV), $[V^{IV}OL^{1-3}]$ (**1-3**), and two new alkoxido bridged trioxidovanadium(IV), $[V^{IV}_3O_3(\mu-OMe)_3(\mu_3-OMe)L^{4,5}]$ (**4** and **5**), complexes obtained upon reaction of 2-((2-X)-diazol)-4-methylphenol (where X = benzo[1,3]dioxol-5-yl (HL^1), phenyl (HL^2) and 4-methoxyphenyl (HL^3)), 1-(2-(thiazol-2-yl)diazenyl)naphthalene-2-ol (HL^4) and 2-(2-(thiazol-2-yl)diazenyl)-4-methylphenol (HL^5) with $VOSO_4 \cdot 5H_2O$. The synthesized complexes were successfully characterized by elemental analysis, IR and UV-vis spectroscopy, ESI-MS and their redox properties analysed by cyclic voltammetry. Molecular structure of complex **4** has also been characterized by X-ray crystallography. The complexes (**1-5**) were screened for their cytotoxicity in MCF-7 cancer cell line. The insulin-mimetic activity of **1-5** was probed on rat L6 myoblast cells. Insulin signaling mechanism of the complexes **2** and **4** was studied by immunoblot analysis for IRS-1.

Chapter 4 describes the reaction of 2-(aryloxy)phenols (HL) with $[Ru(PPh_3)_3Cl_2]$ in ethanolic medium under basic conditions to afford two organometallic Ru(II) complexes, $[Ru(PPh_3)_2L(CO)]$ (**1**) and $[Ru(PPh_3)_2L(CH_3CN)]$ (**2**). A similar reaction of HL with $[Ir(PPh_3)_3Cl]$ results in formation of the organometallic Ir(III) complex, $[IrL(PPh_3)_2(H)]$ (**3**). The 2-(aryloxy)phenolate ligand is coordinated to the metal center in each complex (**1-3**) as a tridentate C, N, O-donor via C-H activation of the ligand. The sixth coordination site in the equatorial plane of **1-3** is occupied by CO, CH_3CN and H^- , respectively. The plausible solvent assisted mechanistic pathway for the unprecedented CO coordination to the Ru(II) center in the case of **1** has been explained. The synthesized complexes have been characterized by various spectroscopic techniques (viz., IR, UV-vis and NMR spectroscopy), ESI-MS and their electrochemical behavior studied by cyclic voltammetry. Molecular structures of **1-3** have been determined by X-ray crystallography.

In **Chapter 5** the synthesis and structural characterization of seven hexacoordinated *cis* dioxidomolybdenum(VI) complexes $[\text{MoO}_2\text{L}^{1-7}]$ (**1–7**) derived from various substituted tetradentate diamino bis(phenolato) “salan” ligands containing O–N donor atoms, have been discussed. The formation of *cis*-dioxidomolybdenum(VI) complexes was confirmed by elemental analysis, IR, UV-vis and NMR spectroscopy, ESI-MS and cyclic voltammetry measurements. Molecular structures of **1–6** were solved by X-ray crystallography. The complexes (**1–7**) were tested for their DNA binding and cleavage activity. In addition, the *in vitro* antiproliferative activity of **1–7** was studied against HT-29 and HeLa cancer cells.

In **Chapter 6** the synthesis and characterization (elemental analysis, UV-vis spectroscopy and ESI-MS) of Cu(II) complexes ($[\text{CuL}^{1,2}]$ (**1** and **2**) and $[\text{CuL}^{3,4'}]_2$ (**3** and **4**)) using tetradentate diamino bis(phenolato) “salan” ligands, have been discussed. The redox property of the complexes has been ascertained by cyclic voltammetry. Molecular structures of the complexes (**1** and **3**) have been determined by X-ray crystallography. While **1** and **2** have the expected square planar geometry, with the ligand coordinating to the metal center in the usual tetradentate fashion, an unprecedented ligand transformation occurs in the case of **3** and **4**, leading to the formation of phenolato bridged Cu(II) dimeric complexes, $[\text{CuL}^{3,4'}]_2$, having an elongated octahedron structure. The organic transformation in the ligands (H_2L^3 and H_2L^4) has been mechanistically elucidated to be Cu(II) catalysed. In order to fortify the ligand transformation to be Cu(II) assisted, the corresponding Ni^{II} , Fe^{III} and Mo^{VI} complexes (**5–7**) with the same ligand environment, were synthesized and characterized. The anomaly in the ligand backbone was however not observed in the case of other transition metal complexes (**5–7**). In addition, the superoxide dismutase (SOD) activity of the Cu(II) complexes (**1–3**) has also been investigated; the activity follows the order **3** > **1** > **2**. Due to the deliquescent nature of $[\text{CuL}^{4'}]_2$ (**4**), its SOD activity could not be evaluated.

Chapter 7 is a brief resume of the work embodied in this research work, followed by the scope for future research work.

Chapter 1

Scope of the Present Investigation

Chapter 1

Scope of the present investigation

Abstract: In this chapter the scope of the present investigation is delineated briefly along with the aim of the work. The chapter is divided into two sections. Section 1.1 deals with the reviews on transition metal complexes of aromatic azo ligands, while a review on transition metal complexes of salan ligands is discussed in Section 1.2.

1.1. REVIEWS ON TRANSITION METAL COMPLEXES OF AZO LIGANDS

The coordination behavior of transition metals with azo ($-N=N-$) ligands is of interest for their π -acidity, interesting coordination modes and molecular structures, dyes and pigmenting behavior, redox, photo-physical, catalytic and biological properties.¹⁻⁹ These properties are attributed to the low lying π^* orbitals of the azo functionality. Transition metal chelates incorporating arylazooximes,⁵ arylazophenols,⁶ arylazoimines,⁷ alkylthioazobenzenes⁸ and sulfenylazobenzenes,⁹ are some of the notable examples. Azo-compounds containing an imidazole moiety have been reported to have the potential to photoregulate biofunctions, such as gene-expression and enzymatic action.^{3b}

1.1.1. Vanadium complexes of azo ligands

The coordination chemistry of vanadium attracts increasing interest due to the use of vanadium complexes as models for the biological functions,¹⁰⁻¹³ such as haloperoxidation,¹⁴ phosphorylation,¹⁵ insulin mimicking,¹⁶⁻²⁰ nitrogen fixation,²¹ tumor growth inhibition and prophylaxis against carcinogenesis.²²

A. Chakravorty et al. reported the chemistry of first structurally characterized O and N ligated VO^{+3} in variable valence $V^{IV}O(ONO)(NN)$ (Figure 1.1a) and $V^VO(ONO)(ON)$ (Figure 1.1b) families of azophenolato ligands and elucidated that such complexes incorporating the V^VO^{3+} moiety are of special interest in the context of bromoperoxidase bioinorganic chemistry.²³ Similar V^VO^{3+} moiety containing mixed ligand vanadium(V) complex with tridentate 2-hydroxy-2'-carboxy-5-methylazobenzene and bidentate quinolin-8-ol was synthesized by the same group and the low temperature EPR parameters of its electrogenerated anionic complex were found to be close to those of reduced bromoperoxidase (low pH).²⁴ In addition they also investigated the chemistry of mono and binuclear oxido V^V , V^VV^V , and V^VV^{IV} azophenolates (Scheme 1.1).²⁵

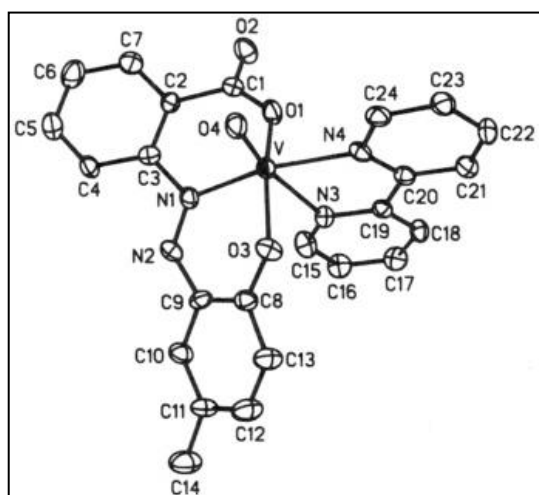


Figure 1.1a

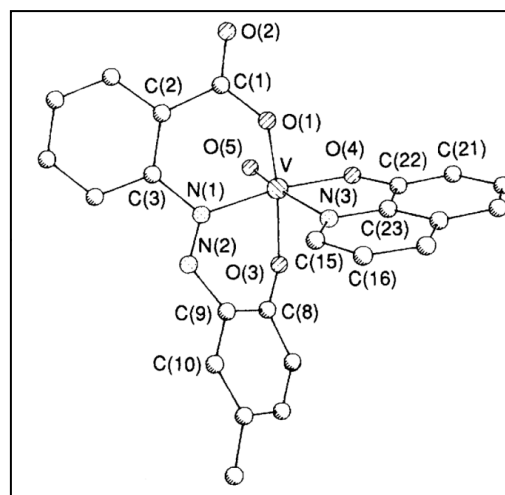
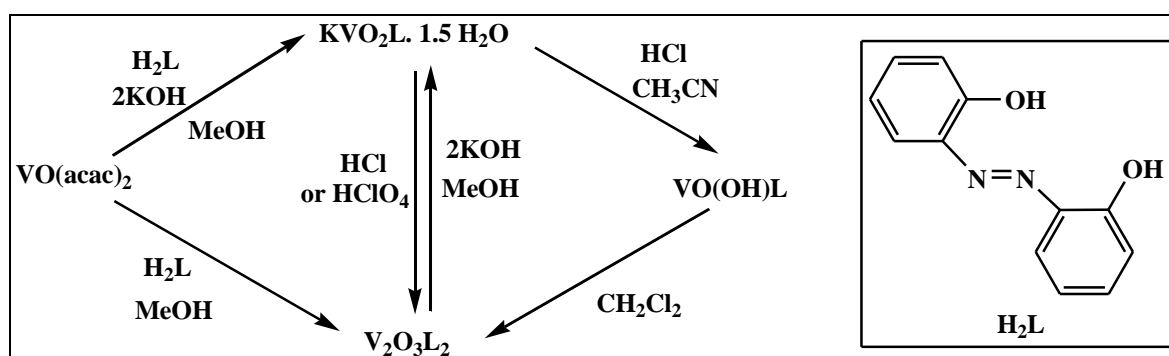


Figure 1.1b



Scheme 1.1

The formation of “bare” V(IV) complexes formed by tridentate (ONO) azo ligands was unambiguously proved in aqueous solution around the physiological pH and in the solid state by E. Garibba et al.²⁶ DFT calculations were used to predict the structure (Figure 1.2a) and ⁵¹V hyperfine coupling tensor A of the non-oxido species (Figure 1.2b). It was observed that the flexibility of the ligands resulted in an unsymmetric facial coordination with a geometry intermediate between the octahedron and the trigonal prism.

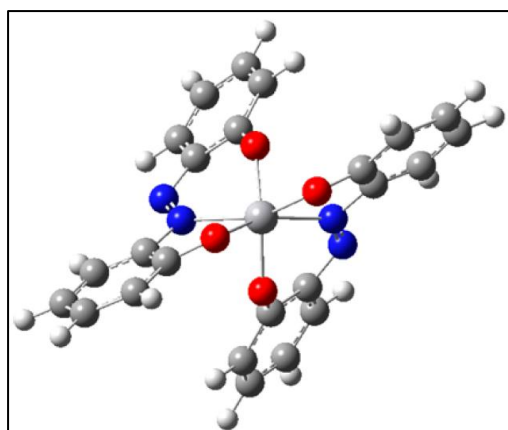


Figure 1.2a

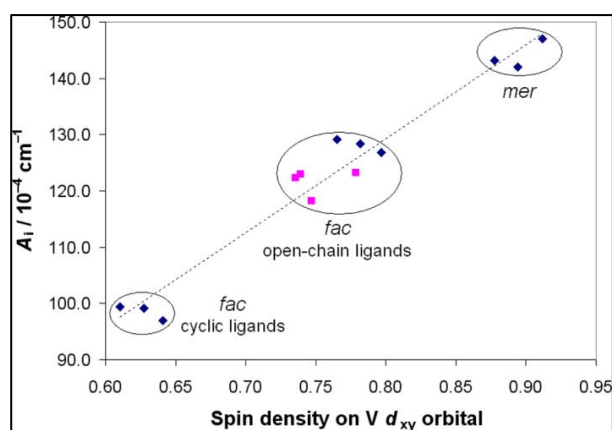


Figure 1.2b

T. Ghosh et al.²⁷ reported the synthesis of mixed-ligand vanadyl(IV) and vanadyl(V) complexes derived from tridentate ONO donor azophenolalcoholate [viz., 2-hydroxy-2'-hydroxymethyl-5-methylazobenzene] and bidentate NO [viz., 8-hydroxyquinoline (Hhq)] or NN [viz., 2,2'-bipyridine (bipy) and 1,10-phenanthroline (phen)] and reported their spectroscopic (Figure 1.3a and 1.3b) and electrochemical behavior. Further characterization revealed that they exist in two isomeric solid forms viz., monomers and polymers, whereas vanadyl(V) complexes exist only in the monomeric form. The azo complex synthesized was one of the first reported examples of hepta-coordinated alkoxido-bonded mixed-ligand oxovanadium(IV) complexes.

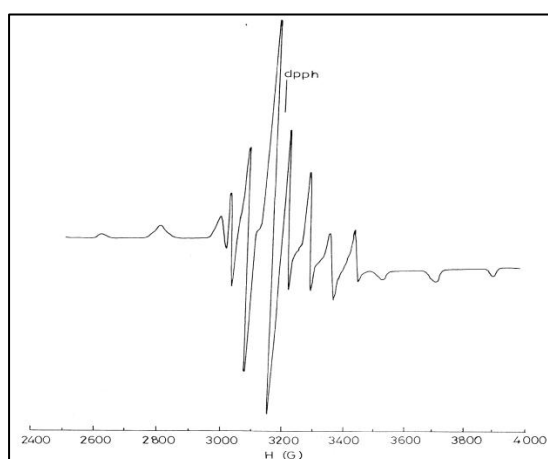


Figure 1.3a

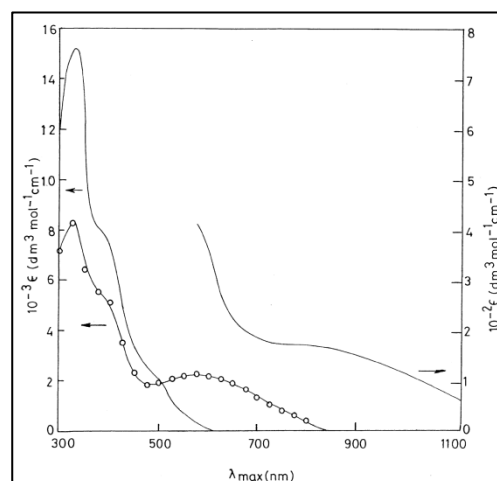
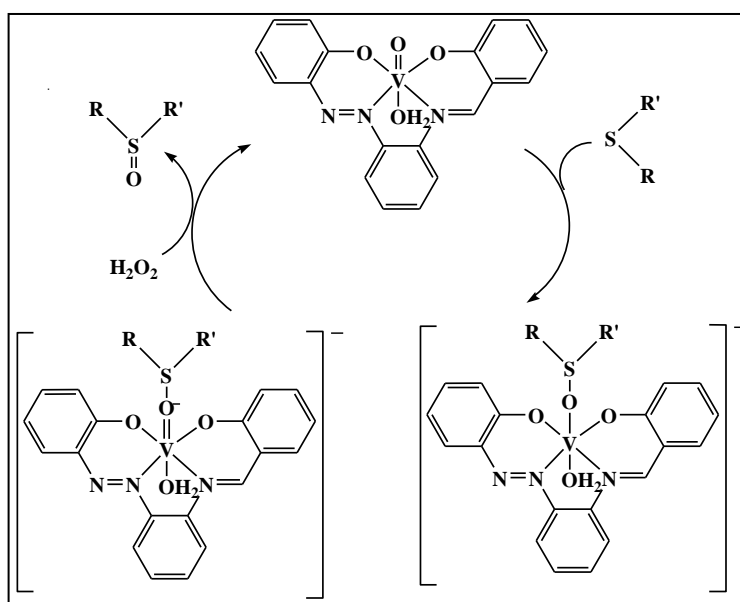


Figure 1.3b

A series of V(IV) azosalophen complexes were synthesized by varying the ligand backbone and these were examined by S. Chattopadhyay et al.²⁸ for their catalytic activity towards H₂O₂ induced oxidation of organic thioethers to sulfoxide and sulphones (Scheme 1.2). Further studies on the cytotoxicity of these azosalophen complexes of V(IV) on human lung cancer cells (A549) showed apoptotic pattern of cell death due to increase in hypoploid DNA increase in the cells (Figure 1.4a and 1.4b).



Scheme 1.2

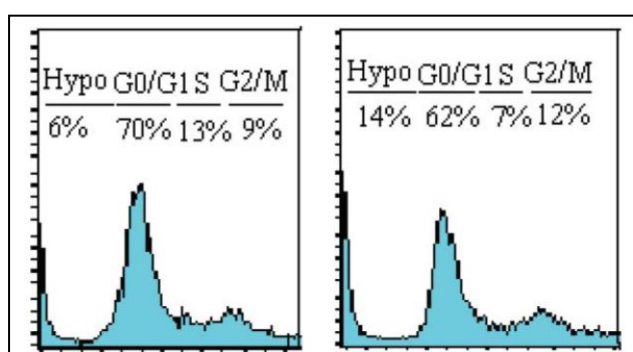


Figure 1.4a

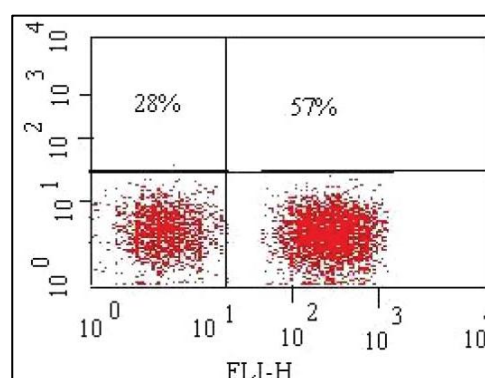
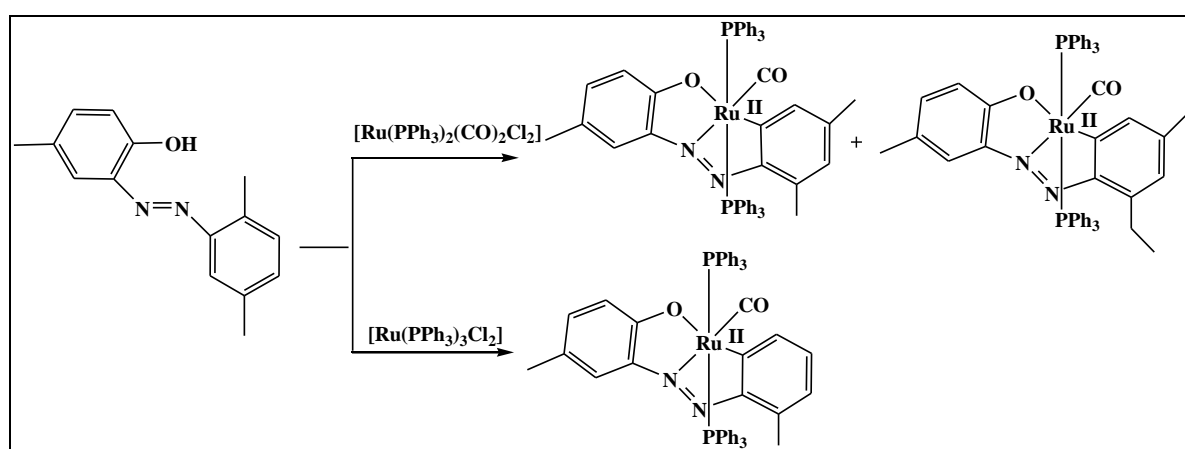


Figure 1.4b

1.1.2. Ruthenium and Iridium complexes of azo ligands

S. Bhattacharya et al. had observed an unprecedented chemical transformation of 2-(2',6'-dimethylphenylazo)-4-methylphenol upon its reaction with differing Ru metal precursors.^{29,30} It was observed that when $[\text{Ru}(\text{PPh}_3)_3\text{Cl}_2]$ was employed as the starting material, one of the methyl group from the phenyl ring of the arylazo fragment migrated to the metal center via oxidation to CO, whereas upon its reaction with $[\text{Ru}(\text{PPh}_3)_2(\text{CO})_2\text{Cl}_2]$, the methyl group at the 2' position underwent migration to the 4' or 6' position (Scheme 1.3).



Scheme 1.3

Chakravorty et al. isolated and structurally characterized the first azo anion radical complexes of ruthenium by the reaction of different substituted 2-arylazopyridine ligands with $\text{Ru}(\text{H})(\text{Cl})(\text{CO})(\text{PPh}_3)_3$ (Figure 1.5a). Upon changing the metal precursor to $\text{RuCl}_3 \cdot 3\text{H}_2\text{O}$ and $\text{RuCl}_2(\text{bpy})_2$, the resulting products were however observed to be of a different nature. The reaction of the corresponding 2-arylaazoimidazoles with RuCl_3 yielded two isomers from the same reaction mixture with *cis-trans-cis* and *trans-cis-cis* configuration. With the change in configuration the redox and spectral properties (Figure 1.5b) of the isomeric complexes also varied. It was also observed that a shift of Ru(III)/Ru(II) couple to more positive potential and blue shift of MLCT bands occurred on going from azoimidazole to azopyridine-ruthenium(II) complexes.³¹

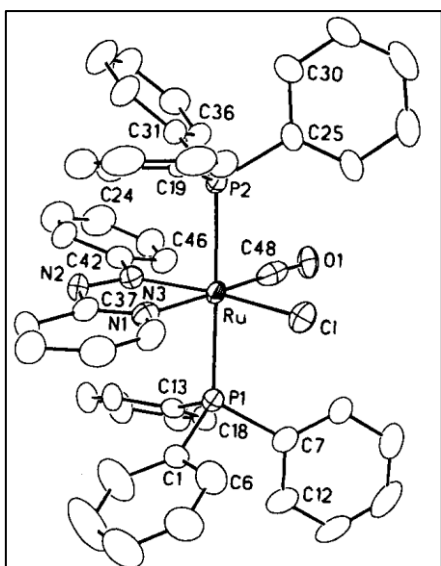


Figure 1.5a

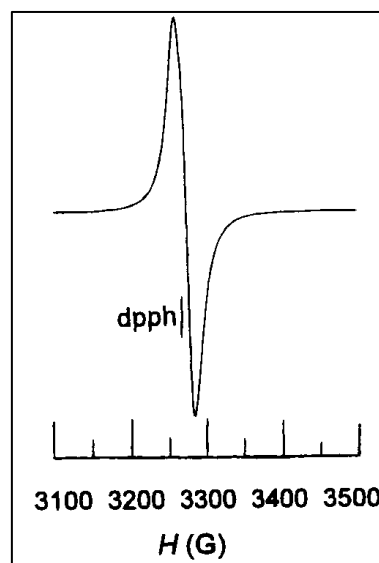
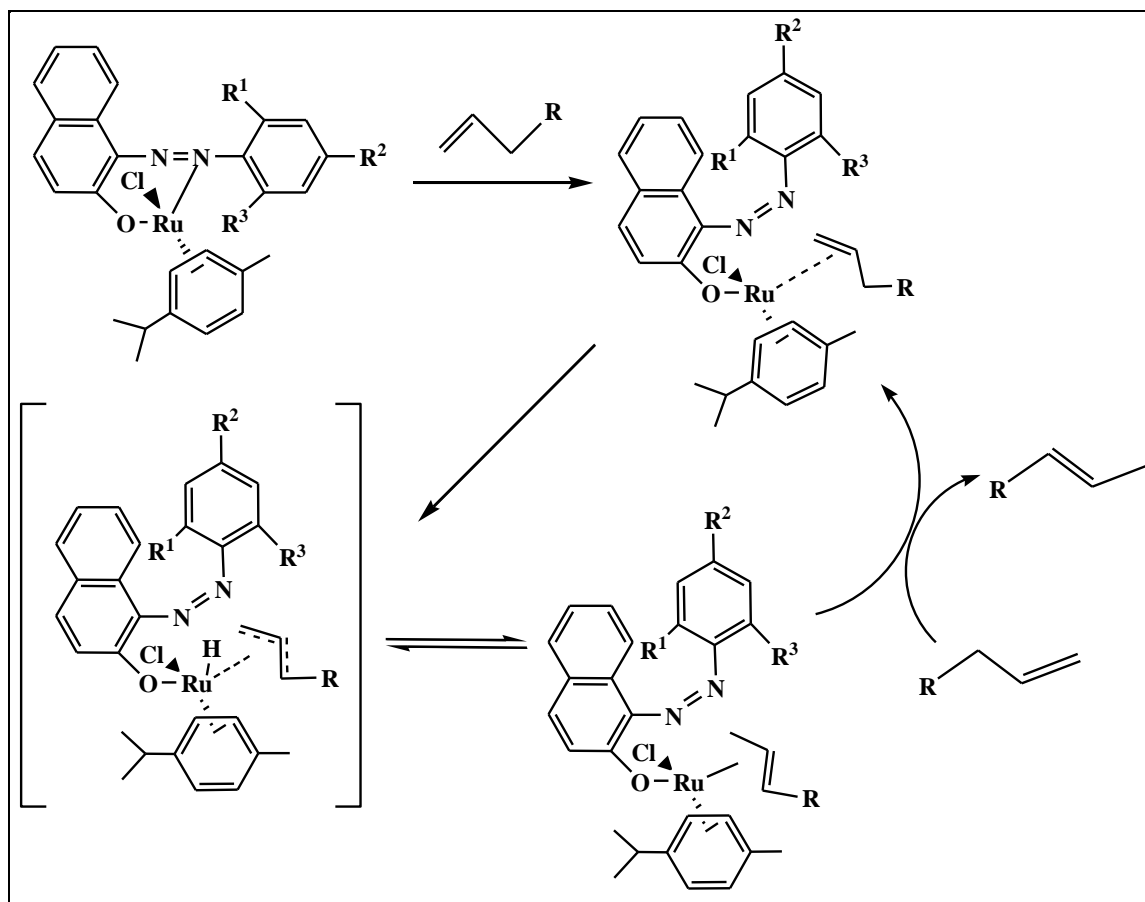


Figure 1.5b

Ding et al. synthesized a series of Ru-azo complexes $[(\eta^6\text{-}p\text{-cymene})\text{RuCl}(\text{L})]$ (L = azonaphthol/azophenyl group) and studied their catalytic activity in olefin isomerization (using allylbenzene and 1-octene as model substrates) (Scheme 1.4).³² These Ru complexes were highly specific for isomerization, without any dimerization or oligomerization and revealed that their catalytic activity for 1-octene strongly depends on the steric and electronic effects of the Ru environment. A noteworthy advantage of these catalysts is their inertness towards air and moisture, thus preventing a meticulous pretreatment.



Scheme 1.4

Juan Xie et al.³³ synthesized a series of photoswitchable arene ruthenium complexes containing *o*-sulfonamide azobenzene ligands (Figure 1.6) and found that they exhibit uncommon coordination pattern with an exocyclic N=N bond. These complexes undergo E→Z photoisomerization upon irradiation, followed by thermal Z→E isomerization (upon resting in the dark) (Figure 1.6), the rate being dependent on the solvent, nature of the arene group, sulfonamide moiety, and azobenzene substitution, as revealed by structure–property studies.

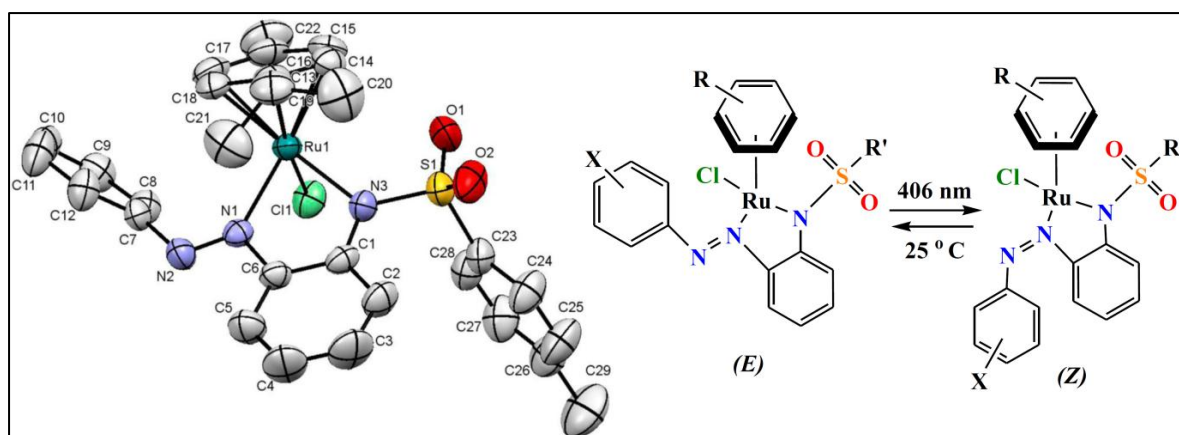


Figure 1.6

C. Das et al. achieved regioselective *para* amination at three coordinated 2-(phenylazo)pyridine ligands in $[\text{Ru}(\text{pap})_3]^{2+}$ (Figure 1.7 and Scheme 1.5). They established the role of the mediator complex with respect to site selectivity of the amination reaction. Thus they established that for a labile complex, an *ortho*-fusion process is favored. This seems reasonable since prior coordination of an amine residue at the vacant site of the metal ion would bring it in close proximity to the *ortho*-CH of the pendent phenyl ring. In the absence of any such vacant site at the metal center, as it occurs in the case of a substitutionally inert mediator complex, ArNH_2 cannot approach the *ortho*-carbon and hence fusion occurs only at the *para*-carbon. The generality of the fusion reaction was established by the use of different ArNH_2 species. The aminated ligand HL_2 , thus formed, has both donor and acceptor chromophores and shows interesting optical as well as redox properties.³⁴

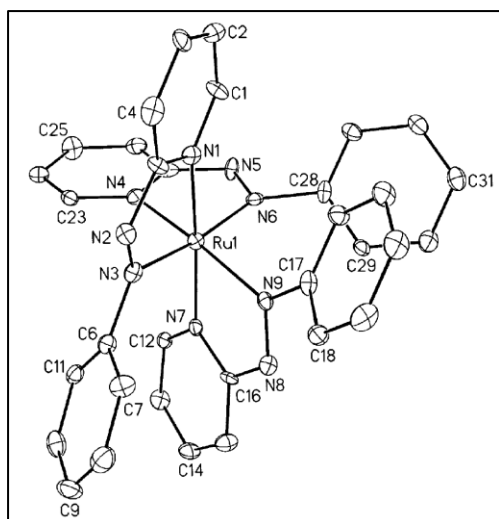
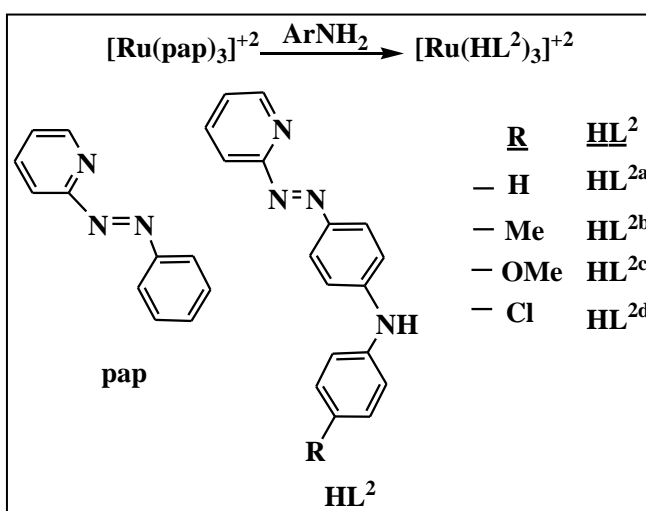


Figure 1.7



Scheme 1.5

An interesting chemistry of Ir-azo complexes was observed by R. Acharyya et al., who had isolated and structurally characterized three different Ir(III) complexes in a single reaction using 2-aryldiazophenols, viz., $[\text{Ir}(\text{PPh}_3)_2(\text{NO-R})(\text{H})\text{Cl}]$ ($\text{R} = \text{OCH}_3, \text{CH}_3, \text{H}, \text{Cl}$ and NO_2) (Figure 1.8a), $[\text{Ir}(\text{PPh}_3)_2(\text{NO-R})(\text{H})_2]$ and $[\text{Ir}(\text{PPh}_3)_2(\text{CNO-R})(\text{H})]$ in ethanol medium, but the same ligand and metal precursor in toluene medium gave two C–H activated products, $[\text{Ir}(\text{PPh}_3)_2(\text{CNO-R})(\text{H})]$ and $[\text{Ir}(\text{PPh}_3)_2(\text{CNO-R})\text{Cl}]$ (Figure 1.8b).³⁵

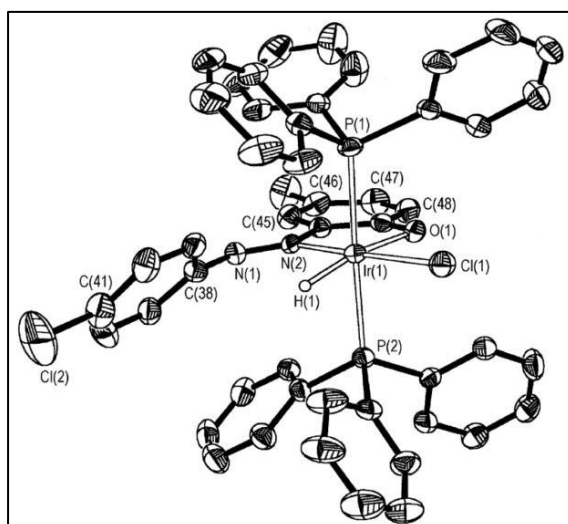


Figure 1.8a

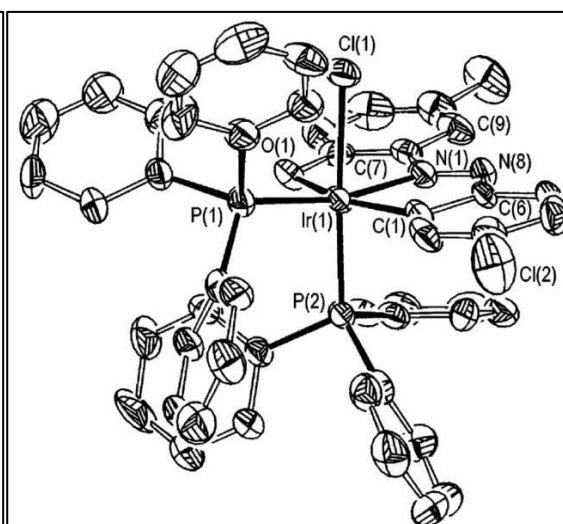


Figure 1.8b

This work describes the synthesis and structural characterization of iridium(I)–carbonyl complexes of coumarinazoimidazoles, $[\text{Ir}(\text{CZ-X})(\text{CO})(\text{PPh}_3)_2]$ derived from Vaska’s complex (Figure 1.9a). The structural characterization shows a distorted square pyramidal geometry. The complexes exhibit emissions at room temperature and are redox active. DFT calculations revealed that the effect of the phenyl group is more prominent than that of the methyl group in the imidazole moiety to tune the energy of the HOMO to a significant extent and substantially reduce the energy gap between the HOMO and the LUMO (Figure 1.9b).³⁶

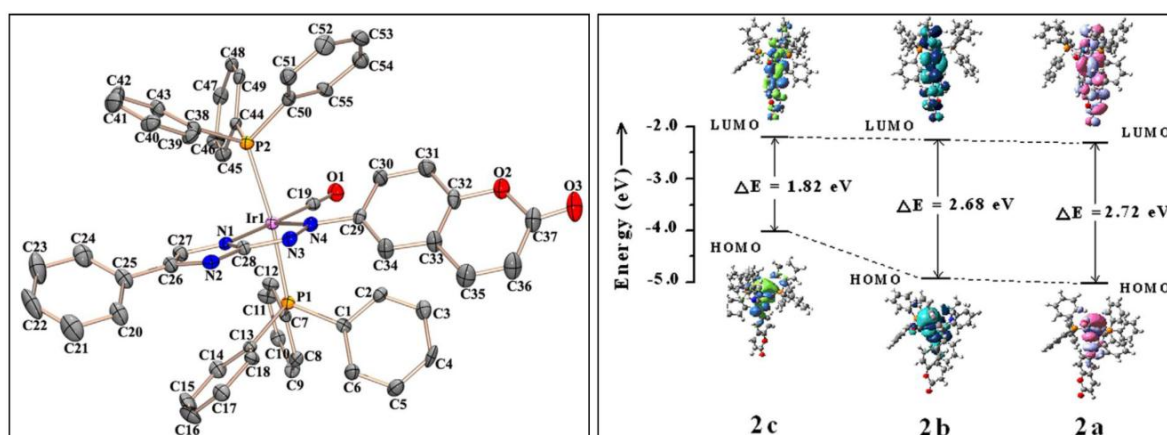


Figure 1.9a

Figure 1.9b

M. Panda et al. studied the isolation and characterization of bis-chelated Ir(III) and mixed ligand Ir(V) complexes of 2-arylazopyridines, obtained from the reaction of hydrated iridium(III) chloride (Figure 1.10a). Interestingly, the same ligand coordinates both as an anionic C, N-donor as well as a neutral N, N donor in the trivalent iridium complex. They further investigated the aromatic ring para-amination reaction of the coordinated ligand of the iridium complexes, which they proposed to have occurred via chloride substitution and reduction of the intermediate complex (Figure 1.10b).³⁷

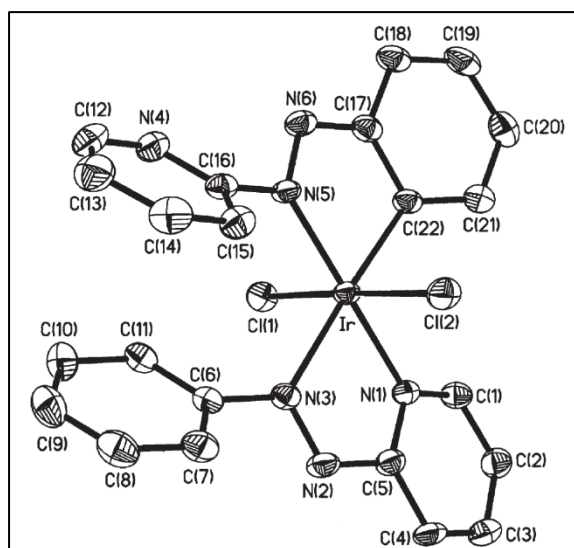


Figure 1.10a

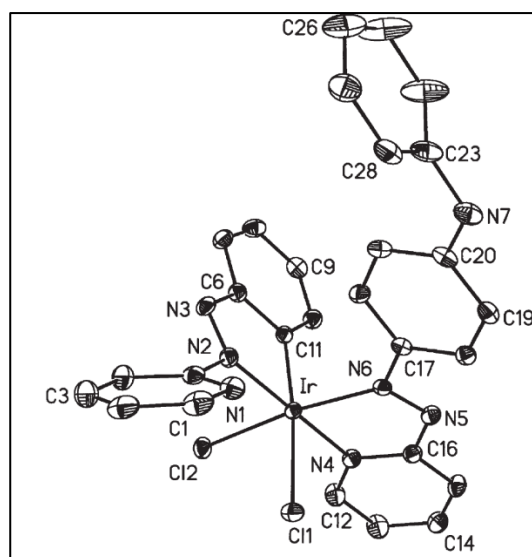


Figure 1.10b

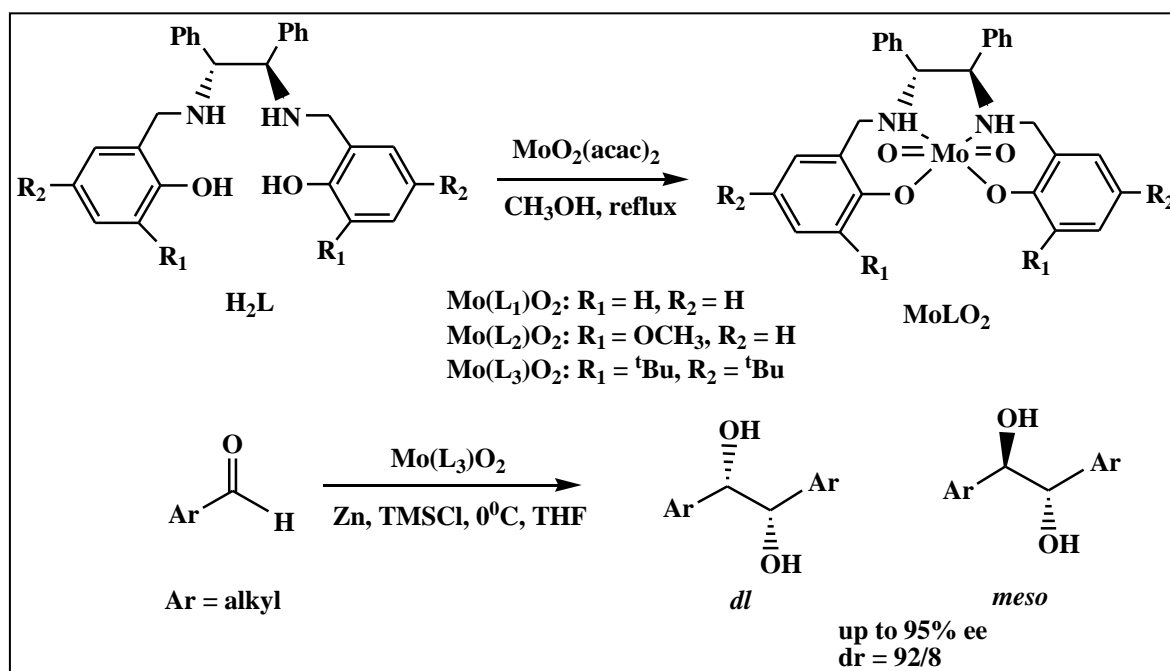
1.2 REVIEWS ON TRANSITION METAL COMPLEXES OF SALAN (TETRAHYDROGENATED ANALOGUE OF SCHIFF BASE) LIGANDS

Use of the salen ligand (Schiff bases(SB)) framework in transition-metal chemistry is well-documented, especially in the area of asymmetric catalysis,³⁸ however, less common is the related salan (hydrogenated analogue of SB) complexes, which often display different structural conformation, due to greater flexibility as a consequence of C=N bond hydrogenation and increased N-basicity, which leads to different reactivity and selectivity.³⁹ In contrast to the salen complexes, where the imine moiety is prone to decomposition in the presence of water, the higher resistance to hydrolytic decomposition of reduced SB compounds deserve special mention.⁴⁰

1.2.1. Molybdenum complexes of salan ligands

Dioxidomolybdenum(VI) complexes have a long standing and successful history in mimicking active sites of molybdenum containing enzymes, especially of the sulfite oxidase family.⁴¹⁻⁴⁶ It has been known that the presence of sulfur atoms coordinated to molybdenum is favorable for complexes of molybdenum to have oxotransfer activity, and many model compounds that mimic such oxotransferases have been studied.⁴⁷⁻⁵⁰

H. Yang et al reported the synthesis and characterization of a series of chiral salan-Mo(VI) dioxido complexes (Scheme 1.6),⁵¹ which were the first optically active Mo(VI) dioxido complexes used in asymmetric reactions, particularly as precatalysts for the synthesis of chiral diols by enantioselective pinacol coupling of aryl aldehydes (Scheme 1.6).



Scheme 1.6

C. J. Whiteoak et al. reported a series of molybdenum(VI) *cis*-dioxido complexes containing tetradentate salan ligands with different *para*-substitutions on the phenoxy group (Figure 1.11a) and studied their catalytic role in the oxygen atom transfer reaction between dimethylsulfoxide and triphenylphosphine.⁵² It was observed that during oxo transfer catalysis, the complexes were resistant to formation of catalytically inactive oxido-bridged dimeric Mo(V) complexes. Structure-activity correlations established by electrochemical behavior and Hammett correlations of the Mo(VI)-salan complexes showed a linear correlation between the $E_{1/2}$ values and the Hammett σ_p parameter (Figure 1.11b).

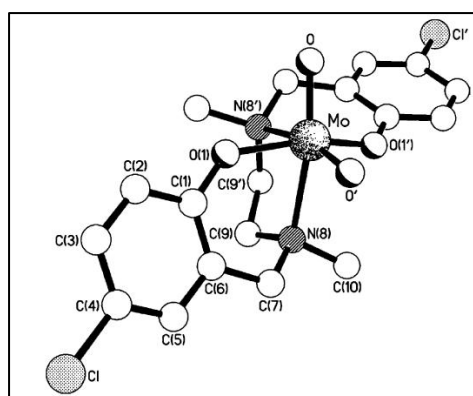


Figure 1.11a

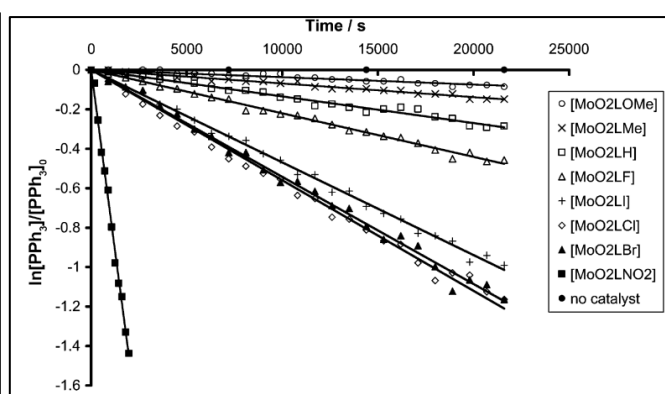
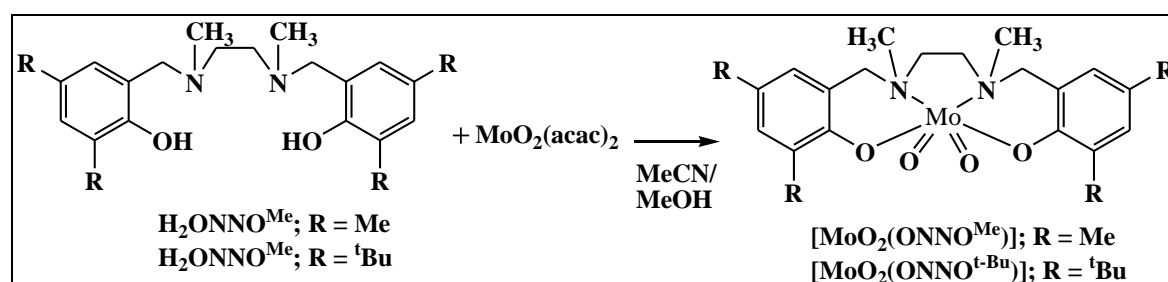


Figure 1.11b

Lehtonen et al. synthesised monomeric Mo-salan complexes, $[\text{MoO}_2(\text{ONNO}^{\text{Me}})]$ and $[\text{MoO}_2(\text{ONNO}^{\text{tBu}})]$, derived from $\text{MoO}_2(\text{acac})_2$ and the tetradentate ligands, $\text{N,N}'$ -bis(2-hydroxy-3,5-dimethylbenzyl)- $\text{N,N}'$ -dimethylethane-1,2-diamine ($\text{H}_2\text{ONNO}^{\text{Me}}$) and $\text{N,N}'$ -bis(2-hydroxy-3,5-di-tert-butylbenzyl)- $\text{N,N}'$ -dimethylethane-1,2-diamine ($\text{H}_2\text{ONNO}^{\text{tBu}}$) respectively (Scheme 1.7) and studied their activity towards oxotransfer reactions between DMSO and benzoin or triphenylphosphine.⁵³ They further studied the catalytic activity of the synthesized complexes in ring opening metathesis polymerization of norbornene, using a Et_2AlCl .



Scheme 1.7

N. C. Mösch-Zanetti et al. synthesized dioxidomolybdenum(VI) complexes with a *cis-α* configuration containing ligands with bipyrrrolidine backbone, as efficient catalysts for olefin epoxidation (Figure 1.12).⁵⁴ These bis-phenolate ligands were considerably more

stable and soluble than analogous compounds with a diazepane backbone with *cis*- β configuration.

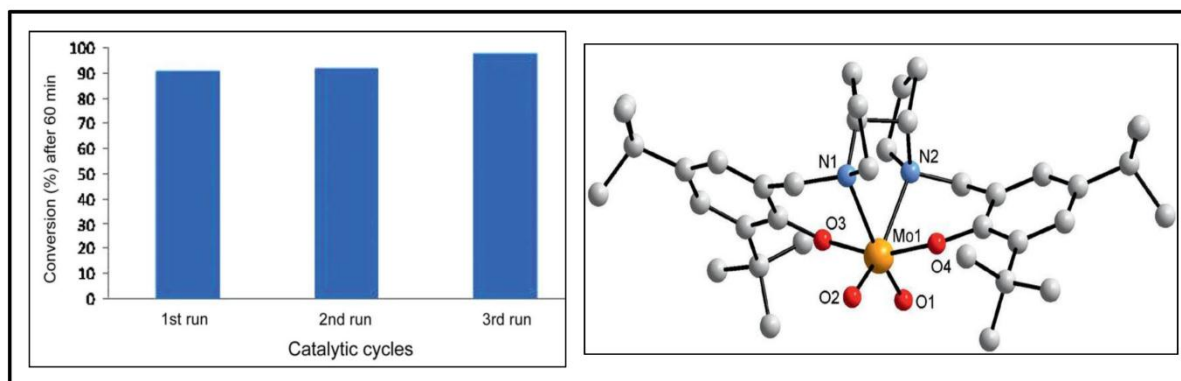
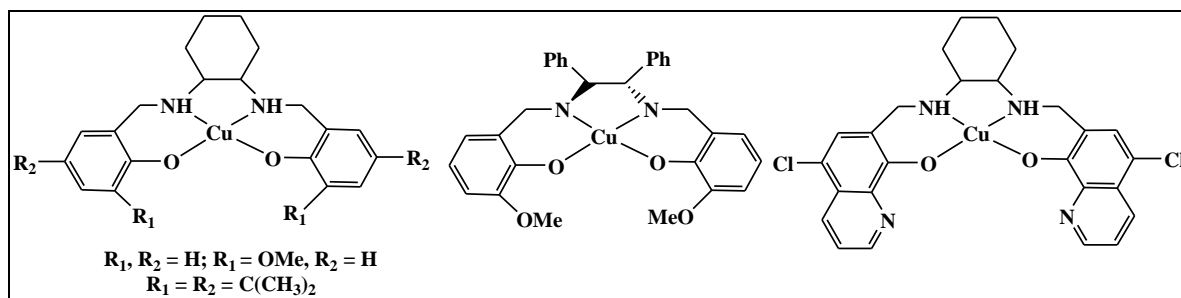


Figure 1.12

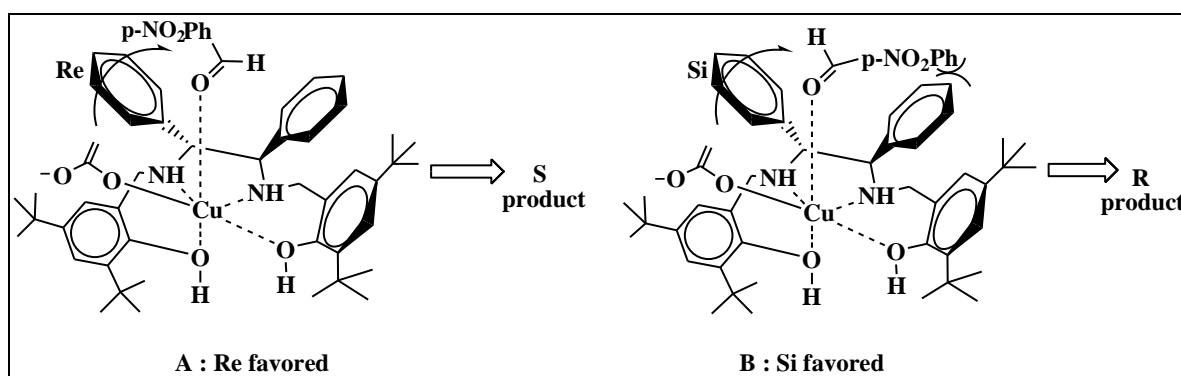
1.2.2. Copper complexes of salen ligands: Copper, an essential element for most aerobic organisms is employed as a structural and catalytic cofactor, and is thus involved in many biological pathways.⁵⁵ Copper forms diverse coordination complexes in oxidation states Cu(II) and Cu(I), and rare copper(III) compounds, with ligands of different hapticity, from monodentate to hexadentate, and characterized by different donor atoms (O, N, S, P, and C) which gave rise to different geometrical arrangements.⁵⁶ Synthesis of Cu-salen complexes have started as early as 1993,⁵⁷ and developments in this field are still in progress.^{58–63}

P. Adão et al.⁵⁸ evaluated the catalytic efficiency of optically active Cu(II)-salen compounds (Scheme 1.8) in sulfoxidation, alkene oxidation, and oxidative naphthol coupling. Their synthesized Cu(II) complexes undergo degradation by oxidative dehydrogenation of the ligand when in the presence of H₂O₂, as observed during the ESI-MS experiments and also during EPR, CD and electronic absorption studies. They had also isolated and characterized the main oxidative dehydrogenation product the “half-salen” variant.



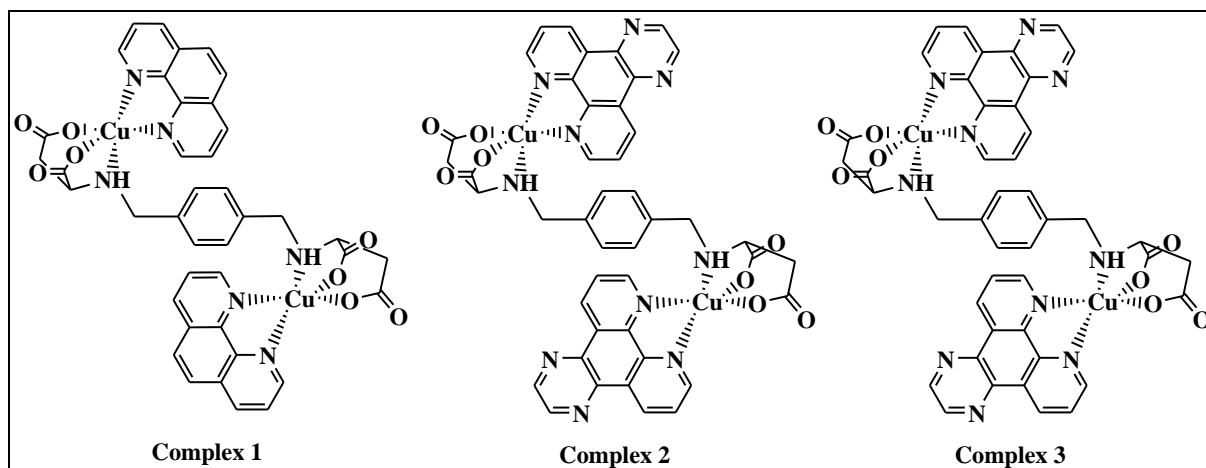
Scheme 1.8

CuI-[H₄]salen-catalyzed asymmetric Henry reaction have been reported to deliver excellent enantioselectivities for aromatic, heteroaromatic, enal, and aliphatic aldehydes (Scheme 1.9). Predominantly, the Cu catalysts have been successfully applied to the synthesis of (S)-norphenylephrine, starting from commercially available m-hydroxybenzaldehyde. Moreover the catalytic pathway is air tolerant and can be easily manipulated with readily available reagents.⁵⁹



Scheme 1.9

L. Jia et al.⁶⁰ studied the antitumor activity of three ternary dinuclear copper (II) complexes with a reduced Schiff base ligand and diimine coligands (Scheme 1.10), *in vitro* and *in vivo*. The DNA binding of these complexes occurs primarily through intercalative interactions and were found to reduce cell viability and induce apoptosis in human tumor cell lines HeLa, PC3, and HepG2 in a dose-dependent manner (Figure 1.13). In addition, the complexes inhibited human tumor cell growth *in vivo* using a nude mouse xenograft model.



Scheme 1.10

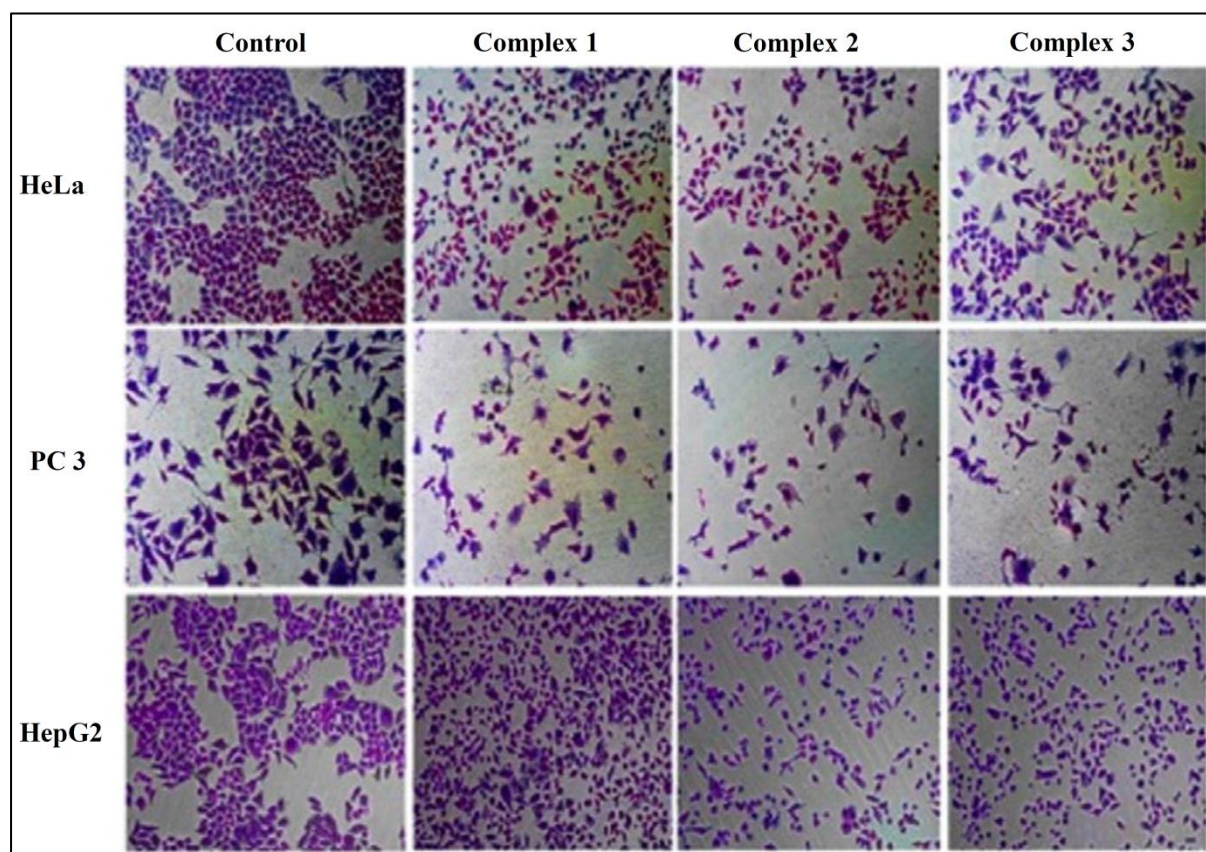


Figure 1.13

H. Hosseini et al.⁶¹ synthesized two new dimeric Cu(II) complexes bridged by phenoxide-O atom using $\text{Cu}(\text{NO}_3)_2 \cdot 3\text{H}_2\text{O}$ and salan ligands, *N,N'*-bis(*o*-hydroxybenzyl)-1,2-diaminocyclohexane ($\text{H}_2[\text{H}_4]\text{L}^1$); *N,N'*-bis(*o*-hydroxybromobenzyl)-1,2-diaminocyclohexane $\text{H}_2[\text{H}_4]\text{L}^2$, and characterized them by spectroscopic techniques and determined their molecular structures by X-ray diffraction analyses (Figure 1.14a). Interestingly while $\text{H}_2[\text{H}_4]\text{L}^1$ coordinates to copper centers as a monoanionic ligand in a tetradentate mode, $[\text{Cu}(\text{H}[\text{H}_4]\text{L}^1)]_2 \cdot 2\text{NO}_3 \cdot 2\text{H}_2\text{O}$; $\text{H}_2[\text{H}_4]\text{L}^2$ behaves as a dianionic ligand resulting in the formation of $[\text{Cu}([\text{H}_4]\text{L}^2)]_2 \cdot 0.4\text{H}_2\text{O}$, via the O,N,N',O'-donor atoms. The complexes also showed high catalytic activities with good-to-excellent selectivity in the oxidation of olefins, benzyl alcohol and ethyl benzene with H_2O_2 in acetonitrile (Figure 1.14b).

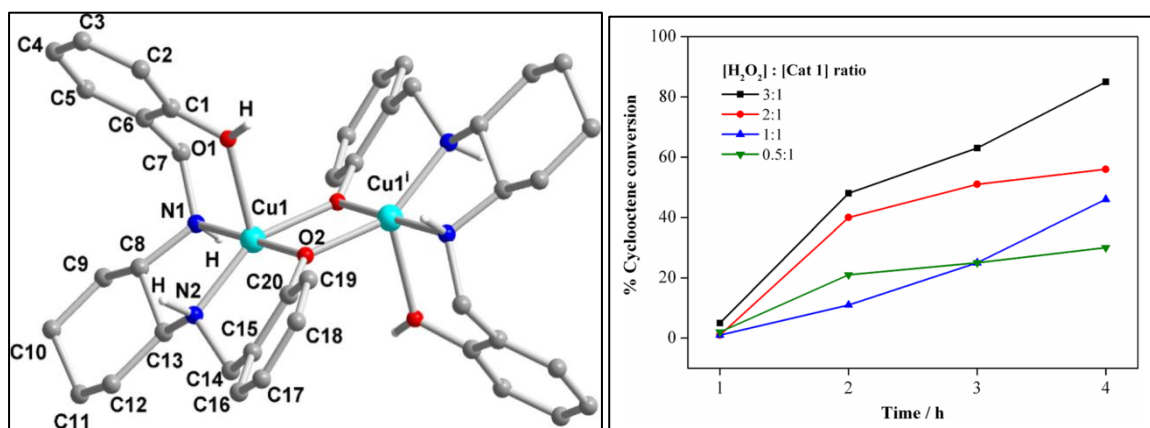


Figure 1.14a

Figure 1.14b

G. Zhang et al.⁶² structurally characterized square planar Cu(II) complexes from salan ligands, *R,R*-**H₂1** (derived from cyclohexylamine and *para*-hydroxymethylbenzoate). This ligand, *R,R*-**H₂1**, was further modified by hydrolysis of the pendant ester to carboxylic acid functionality *R,R*-**H₂2**. 2HCl. Resultant Cu(II) complex of the modified ligand was however a distorted octahedron, where apart from the tetradentate ligand, the Cu(II) center was axially coordinated to the CO₂H carbonyl units. They thus assembled a polymeric copper(II) complex of ligand *R,R*-**H₂2** in a 2D coordination network $[\text{Cu}(\text{R,R-H}_2\mathbf{2})]_n$, where the stacked sheets involved interdigitation of the cyclohexyl domains giving a porous architecture featuring carboxylic acid functionality. Ball-stick

representation of an extended 2D network, stacked 2D sheets and space filling representation of the 3D stacking of sheets in [Cu(R,R-H₂2)] is given in Figure 1.15.

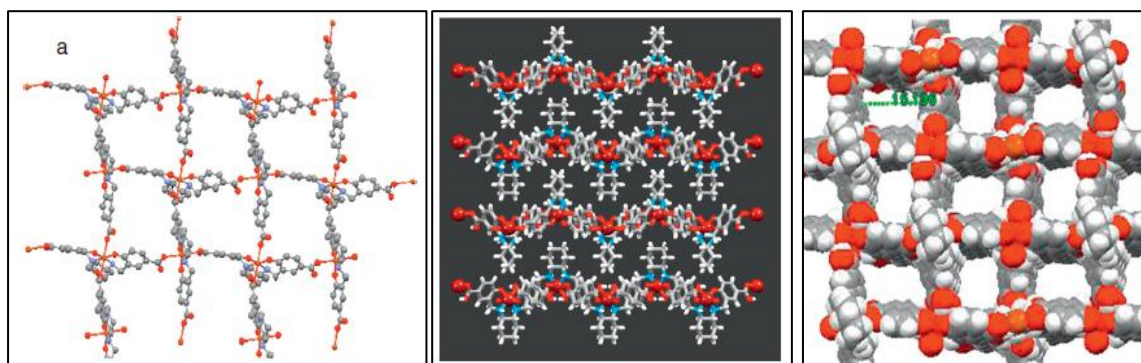
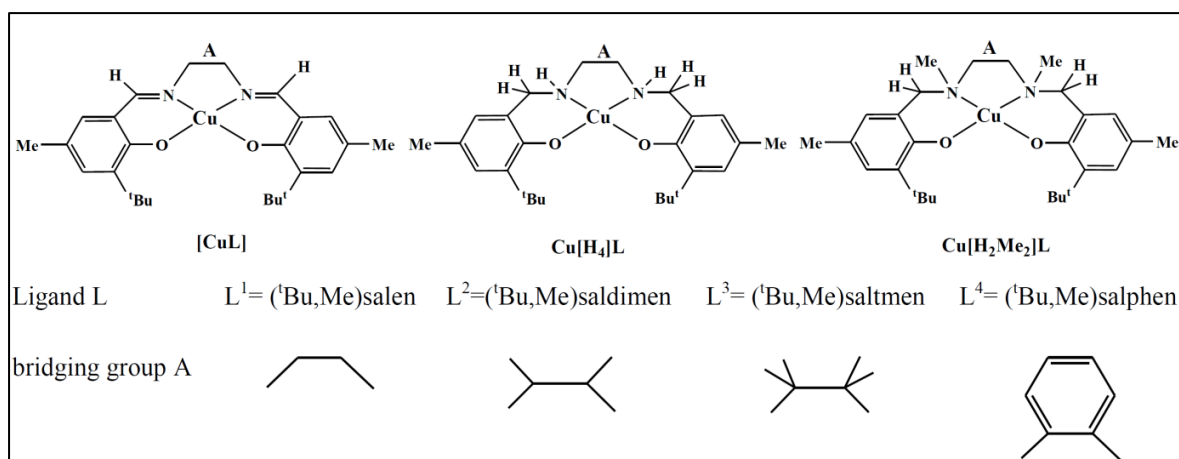


Figure 1.15

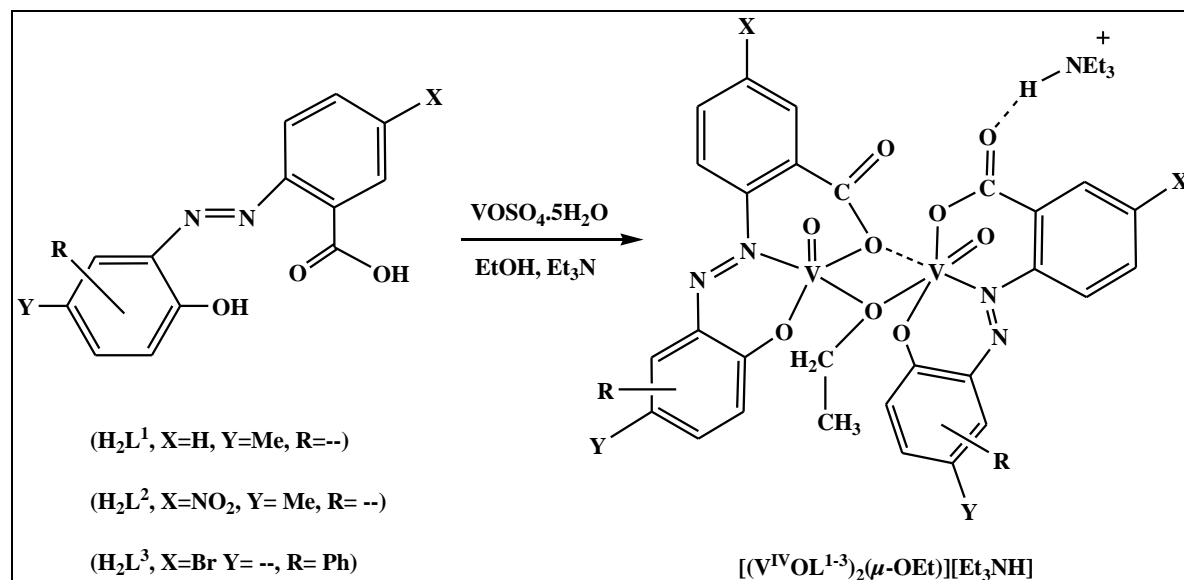
Early investigations in the coordination chemistry of Cu(II) tetrahydro salen derivatives by Valko et al⁶³ revealed that the loss of conjugation in coordinated tetrahydro salens as compared to the salen derivatives, generate interesting electronic and magnetic properties. They observed that while the corresponding tetrahydro salen type complexes, Cu[H₄]L, and *N,N'*-dimethylated tetrahydro salen, Cu[H₂Me₂]L were air-stable at ambient temperature, the complex Cu(^tBu,Me)[H₄]salphen [H₂(^tBu,Me)[H₄], (salphen = *N,N'*-bis(2-hydroxy-3-*tert*-butyl-5-methylbenzyl)-1,2-diaminobenzene) interacts with dioxygen and the ligand is thereby oxidatively dehydrogenated (–CH–NH– → –C=N–) to form Cu(^tBu,Me)[H₂]salphen and finally, in the presence of base, is converted to Cu(^tBu,Me)salphen. It was seen that both factors, planarity and conjugation, are essential for the observation of distant hydrogen shf splitting in CuL. Due to the C=N bond hydrogenation, the coordination polyhedra of the complexes Cu[H₄]L and Cu[H₂Me₂]L is more sensitive and flexible to ligand modification than that of CuL. Schematic representation of their work is presented in Scheme 1.11.



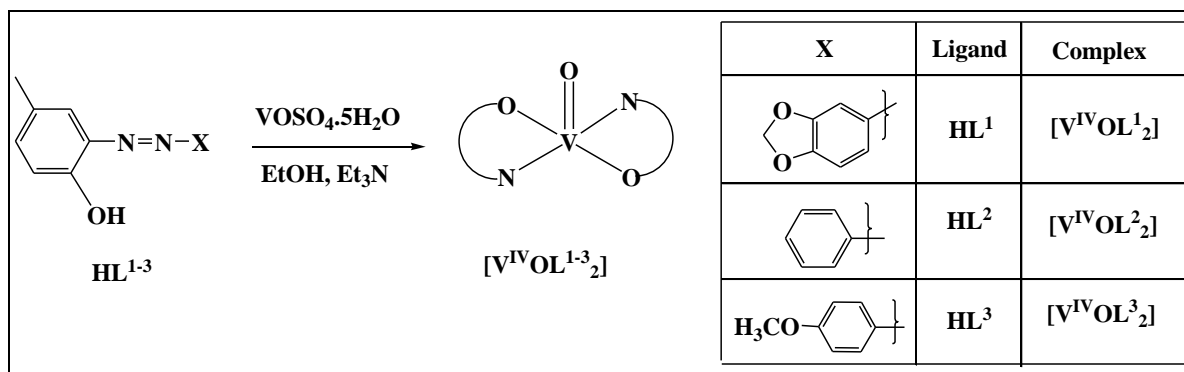
Scheme 1.11

1.3. AIM OF THE PRESENT WORK

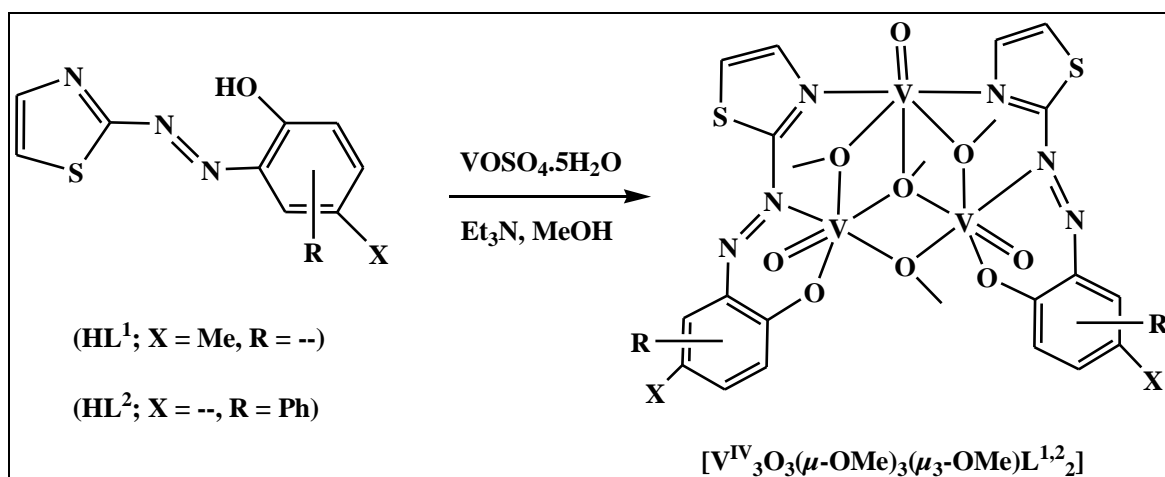
The aim of the present work has been to study the synthesis and chemistry of variable valence V, Ru and Ir arylazo functionalised complexes and Mo and Cu salen complexes. All the synthesized ligand systems and their corresponding metal complexes are collectively summarized below (Scheme I–VI):



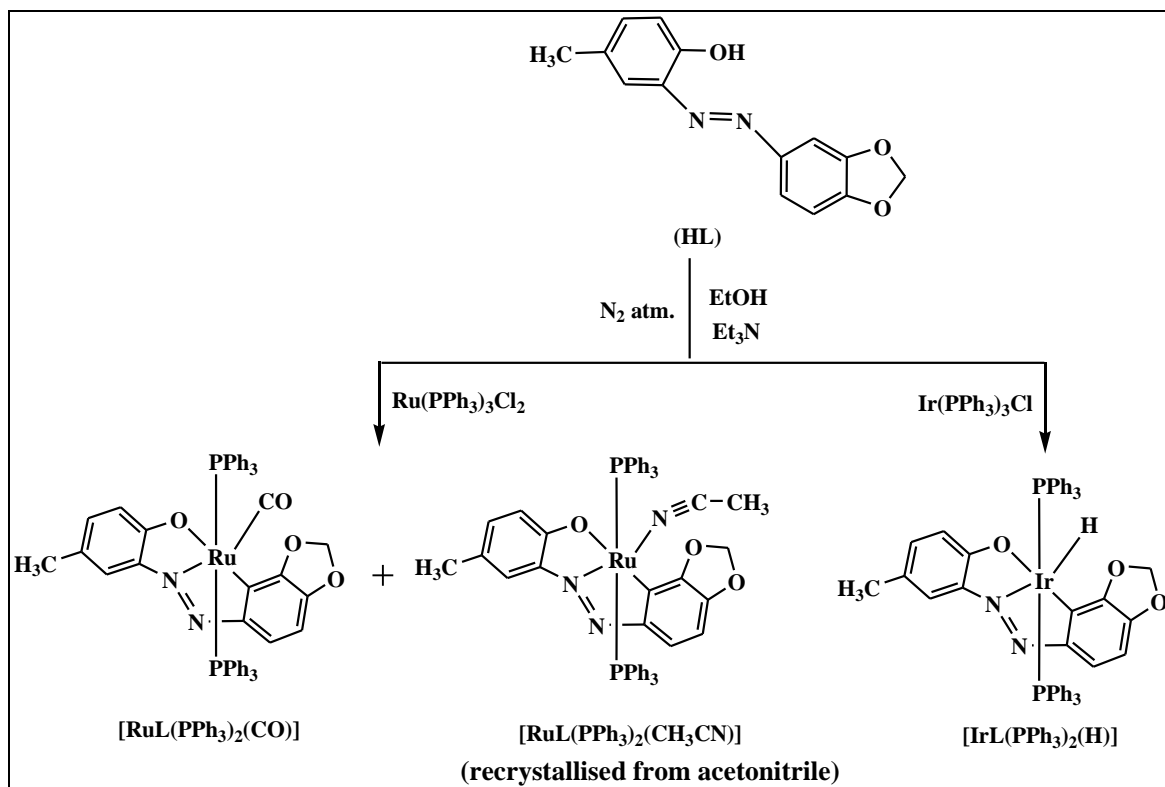
Scheme I



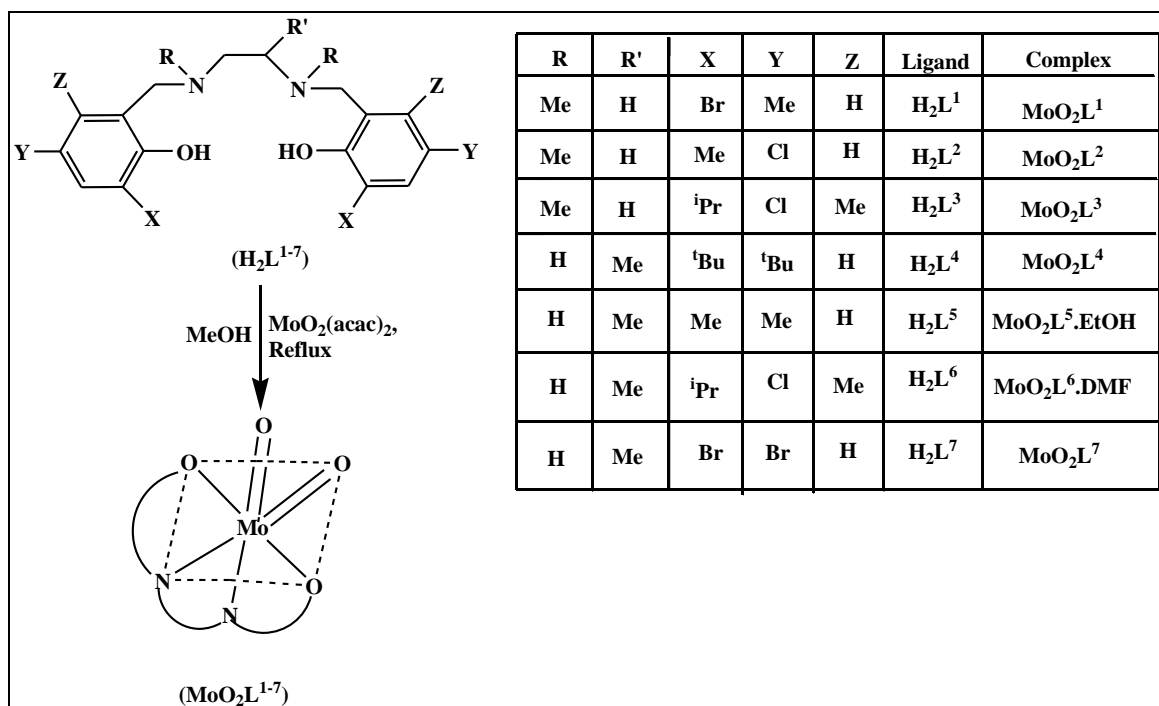
Scheme II



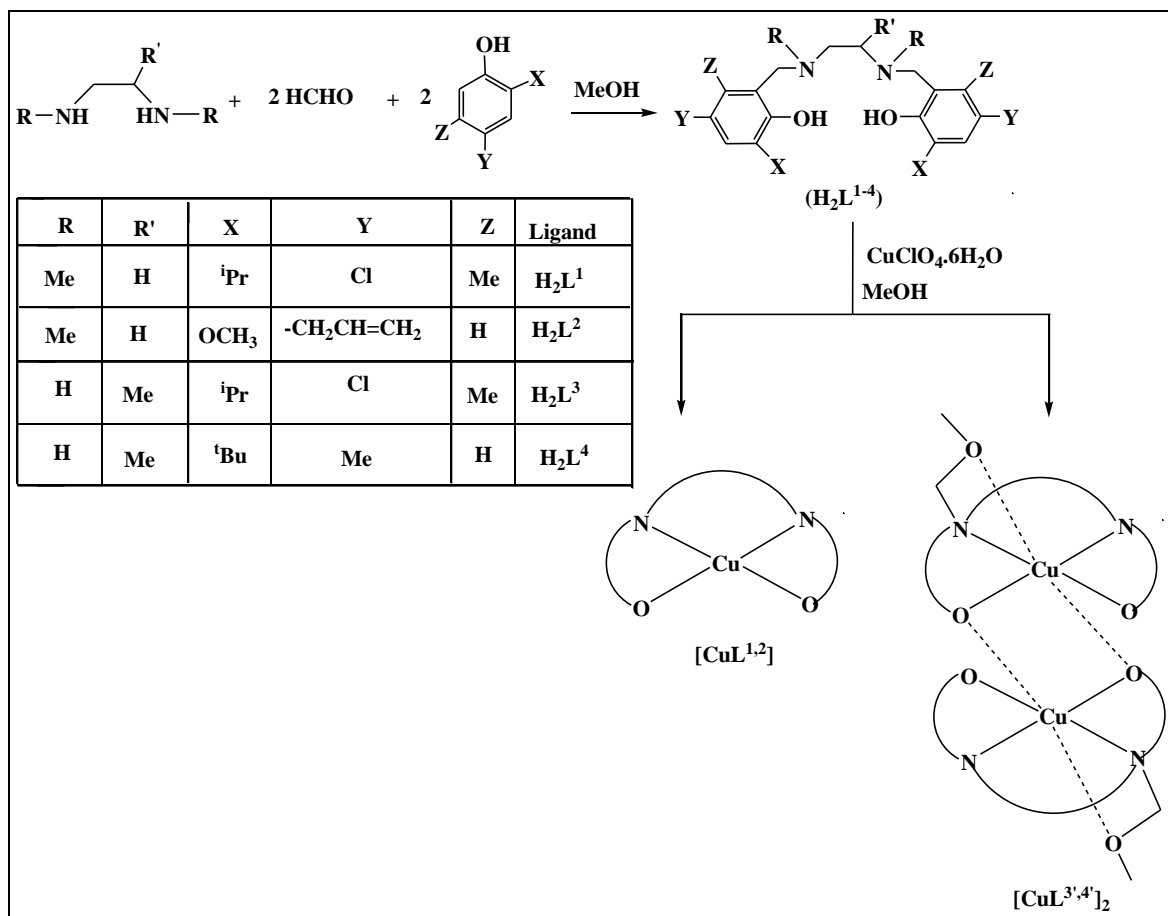
Scheme III



Scheme IV



Scheme V



Scheme VI

1.4. THE MAIN OBJECTIVES OF THE PRESENT STUDY

1. Molecular design and synthesis of several bi- and tridentate ON, ONO and ONN donating arylazo and tetradentate ONNO coordinating salan derivatives, and consequently develop mono and dibasic (O-N- donor) ligand systems.
2. Develop versatile variable valence vanadium, ruthenium and iridium complexes of arylazo functionality as well as some Mo and Cu complexes, employing salan ligands, for use as reagents in some biological reactions, and analyze the magnetic properties of the paramagnetic species. This work uses synthetic and analytical approaches to generate and study the metal complexes, relying upon current mechanistic understanding of their mode of action.

3. Study of spectral and redox behavior of the synthesized metal complexes, solve their X-ray structure and develop the structure–reactivity correlation.
4. Investigate the pharmacological properties (DNA interaction, insulin–mimetic, antiproliferative and superoxide dismutase activity) of the synthesized complexes.
5. Study of the magnetochemical behavior of paramagnetic metal complexes, particularly multinuclear vanadium complexes.
6. Further evaluation of the magnetic properties by density functional theory (DFT) methods.

1.5. REFERENCES

- (1) (a) Kar, S.; Pradhan, B.; Sinha, R. K.; Kundu, T.; Kodgire, P.; Rao, K. K.; Puranic, V. G.; Lahiri, G. K. *Dalton Trans.* **2004**, 1752–1760. (b) Sanyal, A.; Banerjee, P.; Lee, G.; Peng, S. M.; Hung, C. J.; Goswami, S. *Inorg. Chem.* **2004**, *43*, 7456–7462.
- (2) (a) Maiti, N.; Pal, S.; Chattopadhyay, S. *Inorg. Chem.* **2001**, *40*, 2204–2205. (b) Datta, P.; Sardar, D.; Mitra, P.; Sinha, C. *Polyhedron* **2011**, *30*, 1516–1523.
- (3) (a) Sarker, K. K.; Saha, S.; Halder, S. S.; Banerjee, D.; Mondal, T. K.; Paital, A. R.; Nanda, P. K.; Raghavaiah, P.; Sinha, C. *Inorg. Chim. Acta* **2010**, *363*, 2955–2964. (b) Mondal, J. A.; Saha, G.; Sinha, C.; Palit, D. K. *Phys. Chem. Chem. Phys.* **2012**, *14*, 13027–13034. (c) Kawata, S.; Kawata, Y. *Chem. Rev.* **2000**, *100*, 1777–1788.
- (4) (a) Otsuki, J.; Sato, K.; Tsujino, M.; Okuda, N.; Araki, K.; Seno, M. *Chem. Lett.* **1996**, 847–848. (b) Yam, V. W. W.; Lan, V. C. Y.; Cheung, K. K. *J. Chem. Soc., Chem. Commun.* **1995**, 259–261. (c) Marvand, V.; Launay, P. J. *Inorg. Chem.* **1993**, *32*, 1376–1382. (d) Das, A.; Maher, J. P.; McCleverty, J. A.; Badiola, J. A. N.; Ward, M. D. *J. Chem. Soc., Dalton Trans.* **1993**, 681–686.
- (5) (a) Pal, C. K.; Chattopadhyay, S.; Sinha, C.; Chakravorty, A. *Inorg. Chem.* **1994**, *33*, 6140–6147. (b) Pal, C. K.; Chattopadhyay, S.; Sinha, C.; Chakravorty, A. *Inorg. Chem.* **1996**, *35*, 2442–2447 and references therein.
- (6) Sui, K.; Peng, S., -M.; Bhattacharya, S. *Polyhedron* **1999**, *18*, 631–640 and references therein.
- (7) (a) Bag, N.; Lahiri, G. K.; Chakravorty, A. *Inorg. Chem.* **1992**, *31*, 40–45. (b) Lahiri, G. K.; Bhattacharya, S.; Goswami, S.; Chakravorty, A. *J. Chem. Soc., Dalton Trans.* **1990**, 561–565. (c) Mishra, T. K.; Das, D.; Sinha, C.; Ghosh, P.; Pal, C. K. *Inorg. Chem.* **1998**, *37*, 1672–1678.
- (8) (a) Chattopadhyay, S.; Sinha, C.; Basu, P.; Chakravorty, A. *Organometallics* **1991**, *10*, 1135–1139. (b) Pal, C. K.; Chattopadhyay, S.; Sinha, C.; Chakravorty, A. *J. Organomet. Chem.* **1992**, *439*, 91–99 and references therein.
- (9) (a) Sinha, C.; Bandyapadhyay, D.; Chakravorty, A. *Inorg. Chem.* **1988**, *27*, 1173–1178. (b) Mahapatra, A. K.; Bandyapadhyay, D.; Bandyapadhyay, P.; Chakravorty, A. *Inorg. Chem.* **1986**, *25*, 2214–2221. (c) Sinha, C.; Bandyapadhyay, D.; Chakravorty, A. *J. Chem. Soc., Chem. Commun.* **1988**, 468–470.

- (10) Sigel H.; Sigel, A.; Dekker, M. ed., *Vanadium and its Role in Life, Metal Ions in Biological Systems*, New York, 1995, vol. 31.
- (11) Crans, D. C.; Smee, J. J.; Gaidamauskas E.; Yang, L. *Chem. Rev.* **2004**, *104*, 849–902.
- (12) Tracey, A. S.; Willsky G. R.; Takeuchi, E. S. *Vanadium Chemistry, Biochemistry, Pharmacology and Practical Applications*, CRC Press, Boca Raton, 2007.
- (13) Rehder, D. *Bioinorganic Vanadium Chemistry*, John Wiley & Sons, Chichester, 2008.
- (14) Butler A.; Walker, J. V. *Chem. Rev.* **1993**, *93*, 1937–1944.
- (15) Cornman, C. R.; Zovinka E. P.; Meixner, M. H. *Inorg. Chem.* **1995**, *34*, 5099–5100.
- (16) Thompson, K. H.; McNeill J. H.; Orvig, C. *Chem. Rev.* **1999**, *99*, 2561–2571.
- (17) Thompson, K. H.; Liboiron, B. D.; Sun, Y.; Bellman, K. D. D.; Karunaratne, V.; Rawji, G.; Wheeler, J.; Sutton, K.; Bhanot, S.; Cassidy, S. B. C.; McNeill, J. H.; Yuen V. G.; Orvig, C. *J. Biol. Inorg. Chem.* **2003**, *8*, 66–74.
- (18) Yasui, H.; Adachi, Y.; Katoh, A.; Sakurai, H. *J. Biol. Inorg. Chem.* **2007**, *12*, 843–853.
- (19) Shechter, Y.; Goldwasser, I.; Mironchik, M.; Fridkin M.; Gefel, D. *Coord. Chem. Rev.* **2003**, *237*, 3–11.
- (20) Bastos, A. M. B.; Silva, J. G. da; Maia, P. I. S.; Deflon, V. M.; Batista, A. A.; Ferreira, A. V. M.; Botion, L. M.; Niquet E.; Beraldo, H. *Polyhedron*, **2008**, *27*, 1787–1794.
- (21) Eady, R. R. *Coord. Chem. Rev.* **2003**, *237*, 23–30.
- (22) Sasmal, P. K.; Patra, A. K.; Chakravarty, A. R. *J. Inorg. Biochem.* **2008**, *102*, 1463–1472.
- (23) Dutta, S.; Basu, P.; Chakravorty, A. *Inorg. Chem.* **1993**, *32*, 5343–5348.
- (24) Chakravarty, J.; Dutta, S.; Chandra, S. K.; Basu, P.; Chakravorty, A. *Inorg. Chem.* **1993**, *32*, 4249–4255.
- (25) Chakravarty, J.; Chakravorty, A. *J. Chem. Soc., Dalton Trans* **1993**, 1091–1092.
- (26) Sanna, D.; Varnagy, K.; Lihi, N.; Micera, G.; Garribba, E. *Inorg. Chem.* **2013**, *52*, 8202–8213.
- (27) Bhattacharya, S.; Ghosh, T. *Transition Met. Chem.* **2002**, *27*, 89–94.

- (28) Pattanayak P.; Pratihar J. L.; Patra D.; Mitra S.; Bhattacharyya A.; Lee H. M.; Chattopadhyay S. *Dalton Trans.* **2009**, 6220–6230.
- (29) Acharyya, R.; Peng, S. -M.; Lee, G. -H.; Bhattacharya, S. *Inorg. Chem.* **2003**, *42*, 7378–7380.
- (30) Nag, S.; Gupta, P.; Butcher, R. J.; Bhattacharya, S. *Inorg. Chem.* **2004**, *43*, 4814–4816.
- (31) (a) Shivakumar, M.; Pramanik, K.; Ghosh, P.; Chakravorty, A. *Inorg. Chem.* **1998**, *37*, 5968–5969. (b) Misra, T. K.; Das, D.; Sinha, C.; Ghosh, P.; Pal, C. K. *Inorg. Chem.* **1998**, *37*, 1672–1678.
- (32) Ding, F.; Sun, Y.; Verpoort, F. *Eur. J. Inorg. Chem.* **2010**, 1536–1543.
- (33) Deo, C.; Bogliotti, N.; Métivier, R.; Retailleau, P.; Xie, J. *Organometallics* **2015**, *34*, 5775–5784.
- (34) Das, C.; Saha, A.; Hung, C. -H.; Lee, G.-H.; Peng, S. -M.; Goswami, S. *Inorg. Chem.* **2003**, *42*, 198–204.
- (35) Acharyya, R.; Basuli, F.; Wang, R. -Z; Mak, T. C. W.; Bhattacharya, S. *Inorg. Chem.* **2004**, *43*, 704–711.
- (36) Datta, P.; Sardar, D.; Mitra, P.; Sinha, C. *Polyhedron* **2011**, *30*, 1516–1523.
- (37) Panda, M.; Das, C.; Lee, G.-H.; Peng, S.-M.; Goswami, S. *Dalton Trans.* **2004**, 2655–2661.
- (38) (a) Katsuki, T. *Chem. Soc. Rev.* **2004**, *33*, 437–444. (b) Katsuki, T. *Coord. Chem. Rev.* **1995**, *140*, 189–214.
- (39) (a) Sergeeva, E.; Kopilov, J.; Goldberg, I.; Kol, M. *Chem. Commun.* **2009**, 3053–3055. (b) Yeori, A.; Goldberg, I.; Shuster, M.; Kol, M. *J. Am. Chem. Soc.* **2006**, *128*, 13062–13063. (c) Mandal, D.; Ganguly, R.; Chatterjee, P. B.; Endo, A.; Weakley, T. J. R.; Chaudhury, M. *Struct. Chem.* **2007**, *18*, 187–193. (d) Subramanian, P.; Spence, J. T.; Ortega, R.; Enemark, J. H. *Inorg. Chem.* **1984**, *23*, 2564–2572. (e) Hinshaw, C. J.; Peng, G.; Singh, R.; Spence, J. T.; Enemark, J. H.; Bruck, M.; Kristofzski, J.; Merbs, S. L.; Ortega, R. B.; Wexler, P. A. *Inorg. Chem.* **1989**, *28*, 4483–4491.
- (40) Reytman, L.; Braitbard, O.; Tshuva, E. Y. *Dalton Trans.* **2012**, *41*, 5241–5247 and references therein.

- (41) Tunney, J. M.; McMaster, J.; Garner, C. D. in *Comprehensive Coordination Chemistry II* (Eds.: J. A. McCleverty, T. J. Meyer), Elsevier Pergamon, Amsterdam, 2004, vol. 8, pp. 459.
- (42) (a) Holm, R. H. *Coord. Chem. Rev.* **1990**, *100*, 183–221. (b) Holm, R. H.; Berg, J. M. *Acc. Chem. Res.* **1986**, *19*, 363–370. (c) Holm, R. H.; Berg, J. M. *Pure Appl. Chem.* **1984**, *56*, 1645–1657.
- (43) Hille, R.; Mendel, R. *Coord. Chem. Rev.* **2011**, *255*, 991–992.
- (44) Enemark, J. H.; Cooney, J. J. A.; Wang, J. J.; Holm, R. H. *Chem. Rev.* **2004**, *104*, 1175–1200.
- (45) Young, C. G. in *Biomimetic Oxidations Catalyzed by Transition Metals* (Ed.: B. Meunier), Imperial College Press, London, 2004, pp. 415.
- (46) Hille, R. *Chem. Rev.* **1996**, *96*, 2757–2816.
- (47) Sheldon, R. A.; Kochi, J. K. *Metal Catalyzed Oxidation of Organic Compounds*, Academic, New York, **1981**.
- (48) Heinze, K. *Coord. Chem. Rev.* **2015**, *300*, 121–141.
- (49) Bottomley, F.; Sutin, L. *Adv. Organomet. Chem.* **1988**, *28*, 339–396.
- (50) Majumdar, A.; Sarkar, S. *Coord. Chem. Rev.* **2011**, *255*, 1039–1054.
- (51) Yang, H.; Wang, H.; Zhu, C. *J. Org. Chem.* **2007**, *72*, 10029–10034.
- (52) Whiteoak, C. J.; Britovsek, G. J. P.; Gibson, V. C.; White, A. J. P. *Dalton Trans.* **2009**, 2337–2344.
- (53) Lehtonen, A.; Sillanpää, R. *Polyhedron* **2005**, *24*, 257–265.
- (54) Mayilmurugan, R.; Traar, P.; Schachner, J. A.; Volpe, M.; Mösch-Zanetti, N. C. *Eur. J. Inorg. Chem.* **2013**, 3664–3670.
- (55) (a) Kraatz, H. B.; Metzler–Nolte, N. *Concepts and Models in Bioinorganic Chemistry*; Wiley–VCH: Weinheim, Germany, 2006. (b) Lippard, S. J.; Berg, J. M. *Principles of Bioinorganic Chemistry*; University Science Books: Mill Valley, CA, 1994. (c) Frausto da Silva, J. J. R.; Williams, R. J. P. *The Biological Chemistry of the Elements*; Clarendon: Oxford, U. K., 1991.
- (56) Santini, C.; Pellei, M.; Gandin, V.; Porchia, M.; Tisato, F.; Marzano, C. *Chem. Rev.* **2014**, *114*, 815–862 and references therein.
- (57) Bottcher, A.; Elias, H.; Jager, E.-G.; Langfelderova, H.; Mazur, M.; Muller, L.; Paulus, H.; Pelikan, P.; Rudolph, M.; Valko, M. *Inorg. Chem.* **1993**, *32*, 4131–4138.

- (58) Adão, P.; Barroso, S.; Avecilla, F.; Oliveira, M. C.; Pessoa, J. C. *J. Organomet. Chem.* **2014**, *760*, 212–223.
- (59) Xiong, Y.; Wang, F.; Huang, X.; Wen, Y.; Feng, X. *Chem. Eur. J.* **2007**, *13*, 829–833.
- (60) Jia, L.; Xu, J.; Zhao, X.; Shen, S.; Zhou, T.; Xu, Z.; Zhu, T.; Chen, R.; Ma, T.; Xie, J.; Dong, K.; Huang, J. *J. Inorg. Biochem.* **2016**, *159*, 107–119.
- (61) Hosseini-Monfared, H.; Soleymani-Babadi, S.; Sadighian, S.; Pazio, A.; Wozniak, K.; Siczek, M.; Mayer, P. *Transition Met. Chem.* **2015**, *40*, 255–267.
- (62) Zhang, G.; Constable, E. C.; Housecroft, C. E.; Zampese, J. A. *Inorg. Chem. Comm.* **2014**, *43*, 51–55.
- (63) Klement, R.; Stock, F.; Elias, H.; Paulus, H.; Pelikán, P.; Valko, M.; Mazúr, M. *Polyhedron* **1999**, *18*, 3617–3628.

Chapter 2

Magnetic exchange coupling interaction of μ -ethoxido bridged azo functionalized oxidovanadium(IV) dimeric anions: Synthesis, X-ray structure, characterization and cytotoxicity

Chapter 2

Magnetic exchange coupling interaction of μ -ethoxido bridged azo functionalized oxidovanadium(IV) dimeric anions: Synthesis, X-ray structure, characterization and cytotoxicity

ABSTRACT

The synthesis of ethoxido bridged dioxidovanadium(IV/IV) $[(VOL^{1-3})_2(\mu-OEt)][Et_3NH]$ (**1-3**) complexes of three azo dyes, 2-(2'-carboxy-5'-X-phenylazo)-4-methylphenol (H_2L^1 , X = H; H_2L^2 , X = NO_2) and 2-(2'-carboxy-5'-Br-phenylazo)-2-naphthol (H_2L^3), differing in the substituents of the phenyl ring, in order to discern their influence, if any, on their redox potentials, biological activity and magnetochemistry, has been discussed. All the synthesized ligands and the vanadium(IV) complexes have been successfully characterized by various physico-chemical techniques, viz. elemental analysis, IR and UV-vis spectroscopy, ESI-MS and cyclic voltammetry. Molecular structures of $[(VOL^{1,3})_2(\mu-OEt)][Et_3NH]$ (**1** and **3**) have been determined by X-ray crystallography. Antiferromagnetic coupling interaction was observed between the vanadium d^1-d^1 centers of the complexes and this phenomenon was also established theoretically. The complexes were also screened for their *in vitro* cytotoxicity against HeLa and HT-29 cancer cell lines and the results indicated that the synthesized azo functionalized vanadium(IV) complexes were cytotoxic in nature, with **1** being the most potent against HeLa cancer cell line.

2.1. INTRODUCTION

Potential biomedical applications of vanadium compounds with polydentate ligands in biological systems, especially its insulin enhancing action,¹ anticancer efficacy,^{1h,i,2} and more recently *in vitro* antiamoebic activity against *Entamoeba histolytica*³ and antitrypanosomal activity against *Trypanosoma cruzi*⁴ have driven a substantial body of research. Vanadium as an ion occupies the active site metalloenzyme centers in nitrogenases⁵ and haloperoxidases⁶ and controls activation/inhibition of key metabolic enzymes in the biological environment.

After successful accomplishment of phase I clinical trial in humans for the treatment of type 1 and type 2 diabetes mellitus,⁷ vanadium complexes are treated as the emerging class of agents that can show potent antitumor activity.^{7a,8} Therefore, development of new vanadium complexes with improved pharmacological activity is of current interest. Oxidovanadium containing compounds have been reported to suppress growth of malignant cells and the spread of tumors by limiting tumor cell proliferation and triggering apoptosis.⁹⁻¹¹ There are a number of reports which have demonstrated that complexation of a ligand fragment to vanadium(IV) ion remarkably improved their antitumor and antioxidant properties,¹² as in case of flavonoids,¹³ and in some substituted isoniazids.¹⁴ Recently studies are also going on to synthesize new oxidovanadium(IV) complexes that can act as an effective probe for photodynamic therapy (PDT).¹⁵ Despite promising results, a deeper understanding on their mode of action, as well as selectivity towards their biological target, remains the main focus of current research.

In addition to their biological activities, there has been an ongoing interest in the magnetic exchange interactions of bridged di-, tri- and polynuclear vanadium complexes.^{16,17} This has been driven by the desire to design and produce molecular scale magnetic devices.¹⁸⁻²⁰ The magnetic properties of polynuclear transition-metal systems have also aroused substantial interest due to their relevance for the understanding of the function of metalloproteins, as well as their potential applications as magnetic materials.^{21,22} While, most dimeric oxidovanadium(IV) complexes exhibit an antiferromagnetic coupling,^{23,24} a few have also been reported to show strong ferromagnetic interaction.^{25,21a,24f} The contribution of Carrano et al is worth mentioning in this respect, since they presented the first X-ray crystallographic structural information for ligand derived dialkoxo bridged V(IV) dimer, which had then served to clarify the previously disparate

magnetochemistry.^{21a} Further analysis of temperature dependant (2–300 K) magnetic susceptibility measurements of solvent derived alkoxo bridging mixed ligand oxidovanadium(IV) dimers, was provided by Y. Sun et al.²⁴ It is relevant to mention that, despite numerous investigations on the study of the magnetic coupling interaction of oxo and hydroxo bridged divanadium(IV) complexes,²⁵ the magnetochemistry of the corresponding solvent derived alkoxo bridged divanadium(IV) complexes remains inadequately addressed.²⁴ The variation of exchange coupling in hydroxido- and alkoxido-bridged dioxidodivanadium(IV) compounds has also been explained theoretically by Rodríguez-Forteza et al.²⁶ In order to explain this variation in a better way and to overcome the paucity in literature of solvent derived alkoxido bridged dinuclear vanadium(IV) complexes, further probe needs to be done.

On the other hand, the coordination behavior of transition metals with azo (–N=N–) ligands is of interest for their π -acidity, interesting coordination modes and molecular structures, dyes and pigmenting behavior, redox, photo-physical, catalytic and biological properties.²⁷⁻³⁵ These properties are attributed to the low lying π^* orbitals of the azo functionality. Transition metal chelates incorporating arylazooximes,³¹ arylazophenols,³² arylazoimines,³³ alkylthioazobenzenes³⁴ and sulfenylazobenzenes,³⁵ are some of the notable examples. Azo-compounds containing an imidazole moiety have been reported to have the potential to photoregulate biofunctions, such as gene-expression and enzymatic action.

Over the past few years, we have been studying the chemistry of oxido–metal complexes including those of vanadium, in N,O–donor environments³⁶ along with electro-generation of mixed-valence divanadium(IV,V),^{36a,b} and some highly stable nonoxido vanadium(IV) complexes.^{1j,36f} Our group has currently focused on synthesis of variable valence oxido–vanadium complexes that mimic the coordination environment of the metal ions in enzymes, as well as enhances the pharmacological activities.^{36c,d,e,g,h} Herein we have extended our study to the syntheses of three tridentate binegative ONO containing arylazo ligands coordinated to vanadium(IV) metal center, thereby forming complexes of coordination type $[(VOL^{1-3})_2(\mu-OEt)][Et_3NH]$. It is relevant to mention that, although, there are numerous reports on transition metal complexes with azo ligand functionality, but rather limited attention has been focused on the synthesis of vanadium coordinated azo complexes.³⁷ The novelty of our synthesized complexes lies in the fact that these represent

the first examples of structurally characterized fully reduced arylazo containing stable bridged divanadium (IV, IV) complexes. The complexes have been further studied by other spectroscopic techniques (IR, UV-vis and ESI-MS) and their redox properties studied by cyclic voltammetry.

It is noteworthy, that, despite the interesting magnetic properties exhibited by solvent derived bridging divanadium(IV, IV) complexes, there remains a gap in literature concerning the study of the magnetic behavior of similar alkoxido bridged arylazo ligand coordinated vanadium(IV, IV) systems, which needs to be scrutinized further. So, herein we have tried to probe the variable-temperature (2–300 K) magnetic susceptibility measurements of the synthesized ethoxido bridged arylazo V(IV, IV) complexes. Temperature dependent magnetic susceptibility measurements and corresponding theoretical simulations reveal strong antiferromagnetism for complex **1** ($J = -53.4\text{cm}^{-1}$) and **3** ($J = -52.2\text{cm}^{-1}$). The experimental and calculated exchange coupling constants of these complexes are found to be rather similar, with slight differences in antiferromagnetic coupling due to the structural differences of the bridging ethanolate moiety.

In addition, the antiproliferative activity of the dinuclear vanadium(IV) complexes (**1–3**) was probed against human colorectal adenocarcinoma (HT-29) and human cervical cell line (HeLa).

2.2. EXPERIMENTAL SECTION

2.2.1. General Methods and Materials.

Chemicals were purchased from commercial sources and used without further purification. $\text{VOSO}_4 \cdot 5\text{H}_2\text{O}$, *p*-cresol and β -naphthol were purchased from Loba Chemie. Anthranilic acid and its derivatives were purchased from Sigma Aldrich. Dulbecco's Modified Eagle Media (DMEM), Dulbecco's phosphate buffer saline (DPBS), Trypsin EDTA solution, Fetal Bovine Serum (FBS), antibiotic-antimitotic solution and MTT assay kit were purchased from Himedia, Mumbai, India. TRITC-Phalloidin and DAPI were procured from Sigma-Aldrich, India. HeLa and HT-29 cell lines were procured from NCCS, Pune, India. Elemental analyses were performed on a Vario ELcube CHNS Elemental analyzer. IR spectra were recorded on a Perkin-Elmer Spectrum RXI spectrophotometer. ^1H and ^{13}C NMR spectra were recorded on a Bruker Ultrashield 400 MHz spectrometer using SiMe_4 as an internal standard. Electronic spectra were recorded on a Lambda25, PerkinElmer spectrophotometer. ESI-MS were obtained on a SQ-300 MS instrument operating in both positive and negative ion ESI mode. Electrochemical data were collected using a PAR electrochemical analyzer and a PC-controlled Potentiostat/Galvanostat (PAR 273A) at 298 K in a dry nitrogen atmosphere. Cyclic voltammetry experiments were carried out with Pt working and auxiliary electrodes, Ag/AgCl as the reference electrode and TEAP as the supporting electrolyte.

2.2.2. Synthesis of Ligands (H_2L^{1-3}). The 2-(2'-carboxyphenylazo)phenol ligands were prepared by coupling substituted diazotized anthranilic acid with *p*-cresol (H_2L^1 and H_2L^2), or β -naphthol (H_2L^3).³⁸ The resulting red compounds were filtered, washed with ethanol and dried over fused CaCl_2 .

Elemental analysis, NMR (^1H and ^{13}C) and IR data of the ligands confirmed their structures.

H_2L^1 . Yield: 64%. Anal. calcd. for $\text{C}_{14}\text{H}_{12}\text{N}_2\text{O}_3$: C, 65.62; H, 4.72; N, 10.93. Found: C, 65.65; H, 4.72; N, 10.90. IR (KBr pellet, cm^{-1}): 3542 $\nu(\text{O-H})_{\text{b}}$; 1700 $\nu(\text{C=O})$; 1594 $\nu(\text{N=N})$; 1409 $\nu(\text{C-O})_{\text{phenolic}}$. ^1H NMR (400 MHz, CDCl_3): δ (ppm) = 8.24 – 6.97 (m, 7H, aromatic), 2.36 (s, 3H, CH_3). ^{13}C NMR (100 MHz, CDCl_3): δ (ppm) = 168.82 (C=O), 151.96 – 116.27 (12C, aromatic), 20.37 ($-\text{CH}_3$).

H₂L². Yield: 66%. Anal. calcd. for C₁₄H₁₁N₃O₅: C, 55.82; H, 3.68; N, 13.95. Found: C, 55.82; H, 3.66; N, 13.97. IR (KBr pellet, cm⁻¹): 3510 ν(O-H)b; 1699 ν(C=O); 1590 ν(N=N); 1402 ν(C-O)_{phenolic}. ¹H NMR (400 MHz, CDCl₃, ppm): δ 8.67–6.90 (m, 6H, aromatic), 2.39 (s, 3H, CH₃). ¹³C NMR (100 MHz, CDCl₃, ppm): δ 166.39 (C=O), 152.61–118.05 (12C, aromatic), 20.34 (–CH₃).

H₂L³. Yield: 64%. Anal. calcd. for C₁₇H₁₁BrN₂O₃: C, 55.01; H, 2.99; N, 7.55. Found: C, 55.04; H, 3.01; N, 7.55. IR (KBr pellet, cm⁻¹): 3337 ν(O-H)b ;1698 ν(C=O); 1549 ν(N=N); 1402 ν(C-O)_{phenolic}. ¹H NMR (400 MHz, CDCl₃, ppm): δ 11.8 (s, 1H, –COOH), 8.33–7.21 (m, 10H, aromatic). ¹³C NMR (100 MHz, CDCl₃, ppm): δ 169.12 (C=O), 156.40–118.60 (16C, aromatic).

2.2.3. Synthesis of complexes, [(μ-OEt)(V^{IV}OL¹⁻³)₂][Et₃NH] (1–3). Triethylamine (100 mg, 1 mmol) was added to a hot ethanolic solution of H₂L (1 mmol), followed by VOSO₄·5H₂O (253 mg, 1 mmol). After refluxing for 64 h, greenish black X-ray quality crystals of **1** and **3** were obtained directly from the reaction medium. However, X-ray quality crystals of **2** have not been isolated.

[(VOL¹)₂(μ-OEt)][Et₃NH] (**1**). Yield: 62%. Anal. calcd. for C₃₆H₄₁N₅O₉V₂: C, 54.75; H, 5.23; N, 8.86. Found: C, 54.75; H, 5.21; N, 8.82. IR (KBr pellet, cm⁻¹): 1664 ν(C=O); 1493 ν(N=N); 1373 ν(C-O)_{phenolic}; 980, 966 ν(V=O)s; 829 ν(V–O–V). ESI–MS (CH₃CN): *m/z* 811.58 [M – Na]⁺; 827.59 [M + K]⁺.

[(VOL²)₂(μ-OEt)][Et₃NH] (**2**). Yield: 57%. Anal. Calcd. for C₃₆H₄₃N₇O₁₃V₂: C, 48.93; H, 4.90; N, 11.10. Found: C, 49.05; H, 4.86; N, 11.15. IR (KBr pellet, cm⁻¹): 1656 ν(C=O) s; 1589 ν(N=N); 1356 ν(C-O)_{phenolic}; 985, 970 ν(V=O)s; 831 ν(V–O–V). ESI–MS (CH₃CN): *m/z* 859.54 [M – Na][–]; 880.56 [M – 2H][–].

[(VOL³)₂(μ-OEt)][Et₃NH] (**3**). Yield: 66%. Anal. calcd. for C₄₂H₃₉Br₂N₅O₉V₂: C, 49.48; H, 3.85; N, 6.87. Found: C, 49.90; H, 3.87; N, 6.83. IR (KBr pellet, cm⁻¹): 1677 ν(C=O)s; 1502 ν(N=N); 1349 ν(C-O)_{phenolic}; 992, 973 ν(V=O)s; 832 ν(V–O–V). ESI–MS (CH₃CN): *m/z* 1019.60 (75%, [M⁺]); *m/z* 998.35(68%, [M – Na + 4H]⁺).

2.2.4. X-ray Crystallography.

[(VOL¹)₂(μ-OEt)][Et₃NH] (**1**): A suitable single-crystal was selected using a polarizing microscope and mounted on a 50 μm MicroMesh MiTeGen Micromount™ using FROMBLIN Y perfluoropolyether (LVAC 16/6, Aldrich) before centering on a standard Bruker Kappa APEX II CCD-based 4-circle X-ray diffractometer using graphite monochromated Mo Kα radiation ($\lambda = 0.71073 \text{ \AA}$) of a fine focus molybdenum-target X-ray tube operating at 50 kV and 30 mA. Crystal was cooled to 100(2) K with a Kryoflex low temperature device.

Initial unit cell parameters were obtained by least-squares refinement of the xyz centroids of strong reflections harvested from a series of 12 frames in each of three orthogonally related regions of the reciprocal space using the *Evaluate* routine of the APEX software suite.³⁹ Final unit cell parameters were calculated at the end of intensity measurements from xyz centroids of 9664 well-centred reflections of the complete data set. Intensity data were collected via ω - and ϕ -scans in a range up to $2\theta = 56^\circ$ with scan widths of 0.5° and scan speeds of 3 sec/frame at a crystal to detector distance of 40 mm. Collecting strategy was optimized by use of the *Collect* routine of the APEX software suite in order to reach an average data redundancy of 10 or better in about 24 h. Information about crystal mosaicity, as well as its scattering behavior at higher θ values was derived from prescans for unit cell determination. Integrated intensities were obtained with the Bruker SAINT⁴⁰ software package using a narrow-frame algorithm performing spatial corrections of frames, background subtractions, Lorentz and polarization corrections, profile fittings and error analyses. Semi-empirical absorption corrections based on equivalent reflections were made by use of the program SADABS.⁴¹ Details of the data collection parameters applied on the individual crystals are summarized in Table 2.1 with $R_{\text{int}} = \Sigma|F_o^2 - F_o^2(\text{mean})|/\Sigma[F_o^2]$ and $R_{\text{sigma}} = \Sigma[\sigma(F_o^2)]/\Sigma[F_o^2]$.

The centrosymmetric triclinic space group⁴² was determined from *E*-value statistics evaluated by the *examine data* routine of the APEX program suite and confirmed by successful refinement. Structure was solved by Direct Methods and subsequent difference Fourier syntheses of the program SHELXS⁴³ and refined by full-matrix least-squares techniques on F^2 with SHELXL.⁴⁴ Atomic scattering factors were taken from International Tables for Crystallography.⁴⁵ No extinction corrections were applied. Final agreement

indices: $R_1 = \Sigma||F_o| - |F_c||/\Sigma|F_o|$ and $wR_2 = [\Sigma[w(F_o^2 - F_c^2)^2]/\Sigma(wF_o^2)^2]^{1/2}$. Weighting function used: $w = 1/[\sigma^2(F_o^2) + (pP)^2 + qP]$ with $P = (F_o^2 + 2F_c^2)/3$. $Goof = [\Sigma[w(F_o^2 - F_c^2)^2]/(n-p)]^{1/2}$ where n is the number of reflections and p is the total number of parameters refined. All non-hydrogen atoms were refined with anisotropic displacement parameters, hydrogen atoms with common isotropic displacement parameters for chemically related groups of hydrogen atoms.

Although the hydrogen atoms could be localised in difference Fourier syntheses, those of the organic groups were refined in geometrically optimized positions riding on the corresponding carbon atoms with C-H distances of 0.98 Å (–CH₃), 0.99 Å (–CH₂–), 0.95 Å (CH_{arom}) and 0.93 Å (R₃N–H). Further details on the results of structure refinement are summarized in Table 2.1.

Figures were drawn using DIAMOND⁴⁶ and Mercury,⁴⁷ respectively. In the ball- and stick models all atoms are drawn as thermal displacement ellipsoids of the 50% level with exception of the hydrogen atoms which are shown as spheres of arbitrary radii. Hydrogen bridging bonds are drawn in red as dashed sticks.

[(μ–OEt)(V^{IV}OL³)₂][Et₃NH] (**3**): Suitable single crystals were chosen for X-ray diffraction studies. Crystallographic data and details of refinement are given in Table 2.1. Data was collected at 22°C on a Nonius Kappa CCD FR590 single crystal X-ray diffractometer, Mo–radiation. Data collection was 98.9% complete to 25° in θ . A total of 16045 partial and complete reflections were collected covering the indices, $h = -11$ to 11, $k = -23$ to 21, $l = -20$ to 23. The data was integrated and scaled using hkl-SCALEPACK.⁴⁸ This program applies a multiplicative correction factor (S) to the observed intensities (I) and has the following form: $S = (e^{-2B(\sin^2 \theta)/\lambda^2})/\text{scale}$

S was calculated from the scale and the B factor determined for each frame and was then applied to I to give the corrected intensity (I_{corr}). The solution was achieved by direct methods (SHELXS, SIR97⁴⁹) to produce a complete heavy atom phasing model that was consistent with the proposed structure. The structure was completed by difference Fourier synthesis with SHELXL97.^{50,51} Scattering factors were from Waasmair and Kirfel.⁵² Hydrogen atoms were placed in geometrically idealized positions and constrained to ride on their parent atoms with C–H distances in the range 0.95–1.00 Å. Isotropic thermal parameters U_{eq} were fixed such that they were 1.2 U_{eq} of their parent atom U_{eq} for CH's

and $1.5U_{\text{eq}}$ of their parent atom U_{eq} in case of methyl groups. All non-hydrogen atoms were refined anisotropically by full-matrix least-squares.

Table 2.1. Crystal data and refinement details for $[(\text{VOL}^{1,3})_2(\mu\text{-OEt})][\text{Et}_3\text{NH}]$ (**1** and **3**)

| Complex | 1 | 3 |
|--|--|---|
| Formula | $\text{C}_{36}\text{H}_{41}\text{N}_5\text{O}_9\text{V}_2$ | $\text{C}_{42}\text{H}_{39}\text{Br}_2\text{N}_5\text{O}_9\text{V}_2$ |
| M (g mol ⁻¹) | 789.62 | 1019.48 |
| crystal system | Triclinic | Triclinic |
| space group | <i>P</i> -1 | <i>P</i> -1 |
| a (Å) | 11.3507(7) | 11.0675(5) |
| b (Å) | 12.1801(8) | 12.2101(6) |
| c (Å) | 13.2000(8) | 16.9540(8) |
| α (°) | 89.234(3) | 93.516(2)° |
| β (°) | 89.231(3) | 107.485(3)° |
| γ (°) | 89.799(3) | 95.750(2)° |
| V(Å ³) | 1824.6(2) | 2164.12(18) |
| Z | 2 | 2 |
| d_{calc} (gcm ⁻³) | 1.437 | 1.565 |
| absorption coefficient (mm ⁻¹) | 0.573 | 2.338 |
| Θ range for data collection (°) | 2.87 to 28.00 | 2.20 to 25.35° |
| F(000) | 820 | 1028 |
| crystal size (mm ³) | 0.13 x 0.24 x 0.29 | 0.50 x 0.30 x 0.20 |
| max./min. transmittance | 0.9019/0.8648 | 0.9875/ 0.8953 |
| $2\theta_{\text{max}}$ (°) | 28 | 30.5 |
| reflections collected | 168645 | 16045 |
| unique reflections | 8784 [$R_{\text{int}} = 0.0738$] | 7824 [$R_{\text{int}} = 0.0630$] |
| $R_1[I > 2\sigma(I)]$, w R_2 | 0.0308, 0.0783 | 0.0590, 0.1207 |
| $R_1[\text{all data}]$, w R_2 | 0.0362, 0.0814 | 0.1419, 0.1535 |
| S[goodness of fit] | 1.047 | 0.985 |
| peak, hole (e.Å ⁻³) | 0.447, -0.357 | 0.677, -0.653 |

2.2.5. Magnetic Susceptibility Study. Magnetic susceptibilities' data were obtained from powdered samples in gelatin capsules at 1000 Oe and 2000 Oe using a Quantum-Design MPMS-5 SQUID magnetometer equipped with a 5 Tesla magnet in the range from 2 to 300 K. The data is corrected for the sample holder and the diamagnetic moment of the sample. The data was simulated using the MagProp package of DAVE (Data Analysis and Visualization Environment, www.ncnr.nist.gov/dave). For data calculation and graphics OriginPro 8.5 (OriginLab, Northampton, MA) was used.

2.2.6. Computational details. The quantum chemical calculations were performed with the Turbomole package of programs (version 6.6).⁵³ Geometries were taken from the crystallographic structures for which the position of the hydrogen atoms were energy optimized prior to single-point calculations. These optimizations were carried out using the gradient-corrected BP86 functional^{54,55} in combination with single- ζ def2-SVP basis sets⁵⁶ and the resolution of identity (RI) approximation.⁵⁷ The magnetic exchange coupling constants were calculated within the model of a phenomenological Heisenberg-Dirac-van Vleck Hamiltonian $H_{\text{HDVV}} = -J_{12}S_1S_2$ utilizing the broken-symmetry (BS) approach with the spin projection procedure suggested by Yamaguchi.⁵⁸ Within this theory the coupling constant can be derived by Eq. 2.1.

$$J_{12} = \frac{2(E_{\text{BS}} - E_{\text{HS}})}{\langle S_{\text{HS}}^2 \rangle - \langle S_{\text{BS}}^2 \rangle} \quad \text{Eq. 2.1}$$

Single-point calculations for the high-spin (HS) and broken-symmetry (BS) states have been performed with Becke's three-parameter hybrid functional^{54,59} for the exchange part and the correlation functional of Lee-Yang-Parr,⁶⁰ together denoted as B3LYP. Additional BS-DFT calculations were employed with the *meta*-GGA hybrid functional proposed by Tao, Perdew, Staroverov, and Scuseria⁶¹ (denoted as TPSSh). In all calculations the triple- ζ def2-TZVPP basis sets⁵⁶ were used together with a tight SCF energy convergence criterion (10^{-8} a.u.).

2.2.7. Cytotoxicity

Anticancer properties of vanadium(IV) complexes (**1–3**) was tested against two different human cancerous cell lines namely HeLa (cervical cancer) and HT-29 (colon cancer) *in vitro* by MTT assay. Cells cultured in DMEM media with 10% FBS in a humidified (95% humidity) CO₂ incubator (5% CO₂) at 37 °C were harvested by trypsinization and were seeded into a 96-well plate at a concentration of 1 x 10⁴ cells/well. After 12 h of initial seeding, cells were treated with compounds (**1–3**) for 48 h. For this purpose, five different concentrations (250, 100, 50, 10 and 5 µg/ml) of each compound prepared in complete DMEM media were used. Tissue culture plate (TCP) was taken as control. After 48 h, MTT assay was performed using a MTT assay kit following the manufacture's instruction. The relative viability of the cells after treatment was reported in terms of cell viability index as per Eq. 2.2 given below. All the experiments were performed in quadruplets and the data were expressed as mean ± S.D. Statistical significance of the data was evaluated using single variance ANOVA under 95 % confidence interval.

$$\text{Cell viability index} = \frac{\text{Absorbance of the sample at 595 nm}}{\text{Absorbance of the control at 595 nm}} \quad \text{Eq. 2.2}$$

IC₅₀ value of the compounds was calculated from the absorbance-concentration plot following standard procedure.⁶²

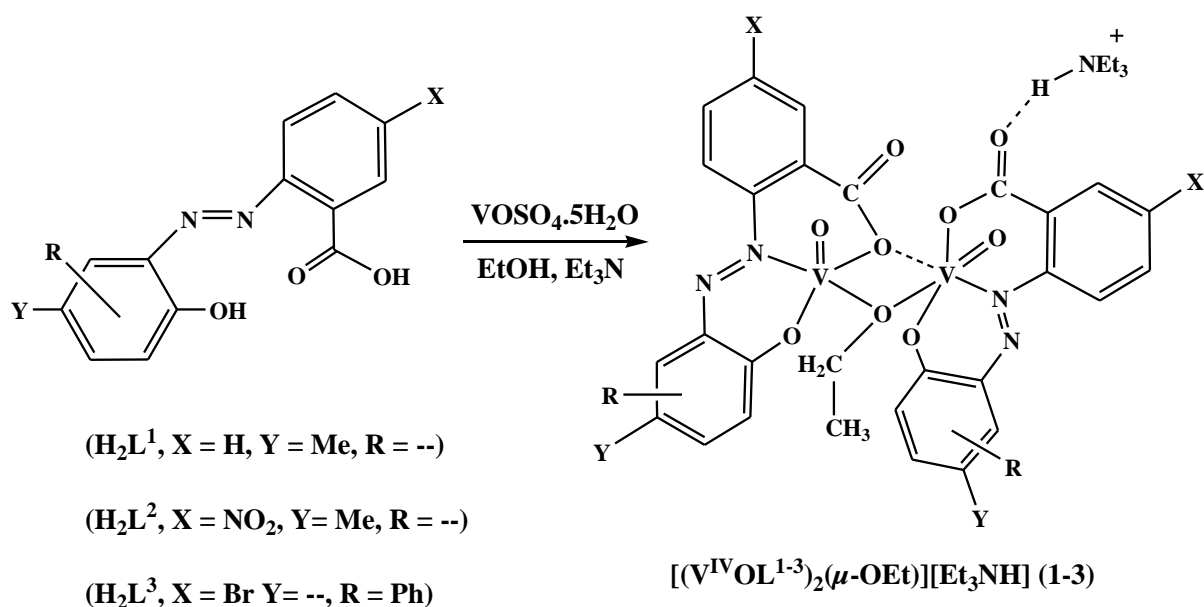
Distribution of F-actin (cytoskeletal organization), shape of the nucleus and its structural integrity were examined using fluorescence microscopy (Olympus). In brief, at the end of the treatment, cells were washed gently with PBS and were fixed with 4% paraformaldehyde for 15 min. Cells were then subjected for permeabilization (0.25% Triton X-100 in PBS, 10 min exposure) and subsequently stained with TRITC-Phalloidin and DAPI.⁶³ For this study, cells were treated with the compounds at a concentration of 100 µg/ml for 36 h.

2.3. RESULTS AND DISCUSSION

2.3.1. Synthesis.

Three 2-(2'-carboxyphenylazo)phenol ligands have been employed in the present study for the synthesis of ethoxido bridged V(IV) dimeric complexes. Reactions of the azo dyes with $\text{VOSO}_4 \cdot 5\text{H}_2\text{O}$ proceeded smoothly in refluxing ethanol, and did not require dried solvents or an inert atmosphere. Complexes **1** and **3** are obtained directly from the reaction medium as greenish black color crystalline compounds in good yields, but single crystals of **2** have not been isolated.

The synthesis of the complexes is summarised in Scheme 2.1. Elemental analysis confirmed the purity of the synthesized complexes. All the three complexes are highly soluble in aprotic solvents, viz. CH_3CN , DMF or DMSO, while complex **1** and **2** are also partially soluble in protic solvents, viz., EtOH, CH_2Cl_2 , and CHCl_3 and sparingly soluble (**1**: 50% , **2**, 40%; **3**: 20%) in H_2O . The complexes are stable in the solid as well as in the solution state for 24 h. The solution state stability was confirmed by time-dependent UV-vis (Figure 2.1) spectroscopy.



Scheme 2.1. Schematic representation for the synthesis of $[(\text{V}^{\text{IV}}\text{OL}^{1-3})_2(\mu\text{-OEt})][\text{Et}_3\text{NH}]$ (1-3).

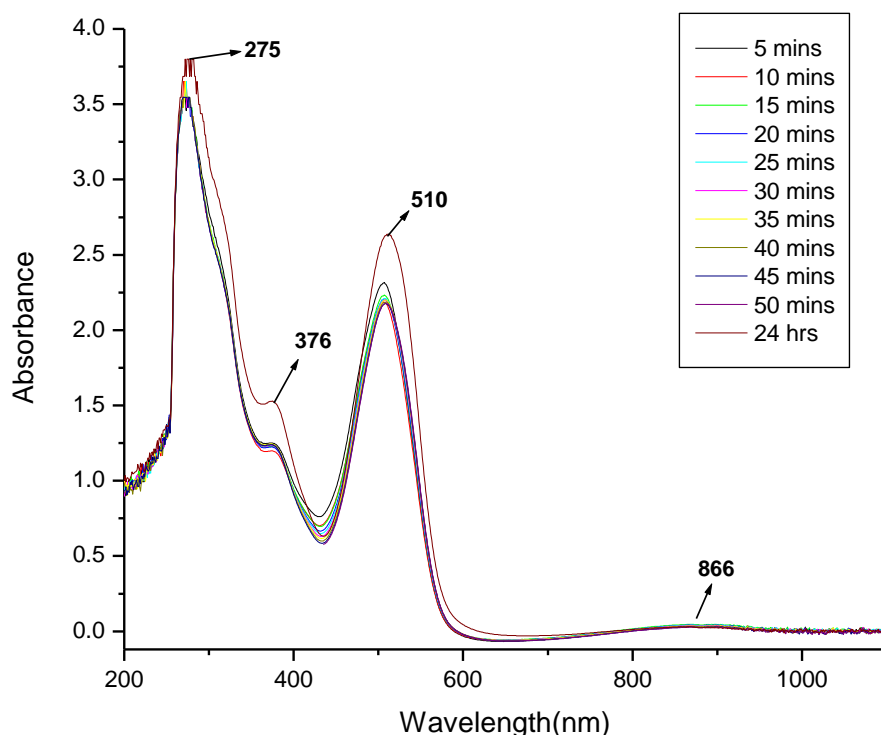


Figure 2.1. Time dependent UV-vis spectra of $[(V^{IV}OL^1)_2(\mu-OEt)][Et_3NH]$ (**1**) in DMSO.

2.3.2. Spectral Characteristics

2.3.2.1. IR Spectroscopy. The IR spectra of complexes (**1–3**) showed similar shift in wavenumbers compared to those of their respective ligands. Three bands are observed at ~ 1700 , ~ 1594 and $\sim 1409\text{ cm}^{-1}$; these bands are attributed to the carboxylate (C=O), azo ($-N=N$) and C–O phenolic fragments, respectively, of the ligands.⁶⁴ The observed shift in $(\nu(C=O)_{\text{carboxylate}})$ of the complexes below 1678 cm^{-1} , as compared to the ligand ($\nu(C=O)_{\text{carboxylate}} > 1697\text{ cm}^{-1}$) is attributed to complexation. The bands shift to lower frequency upon coordination to the metal center. The vanadium complexes show two additional strong and sharp bands of $\nu(V=O)$ in the $992\text{--}966\text{ cm}^{-1}$ region, which suggests presence of two V=O bonds in the complex, while the presence of a bridging O atom is indicated by a $\nu(V-O-V)$ stretching vibration at $\sim 831\text{ cm}^{-1}$ in all the three complexes.^{36a,b,65} The representative FT-IR spectrum of $[(V^{IV}OL^3)_2(\mu-OEt)][Et_3NH]$ (**3**) is elucidated in Figure 2.2.

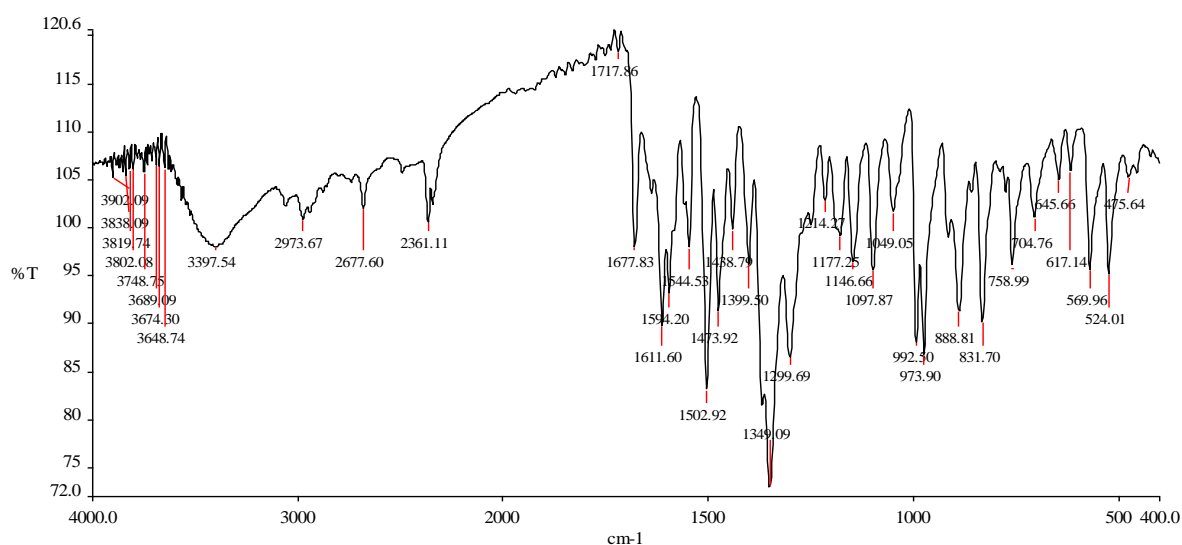


Figure 2.2. IR spectrum of $[(V^{IV}OL^3)_2(\mu-OEt)][Et_3NH]$ (**3**).

2.3.2.2. UV–vis Spectroscopy. Electronic absorption spectra of complexes **1–3** were recorded in DMSO (Table 2.2) and a representative spectrum of **3** is shown in Figure 2.3. Three strong absorptions are observed in the wavelength range of 510–258 nm in the complexes. The lower energy absorption in the visible range, $\lambda_{max} = 510\text{--}503$ nm in the complexes is assigned to ligand to metal charge transfer transitions,^{36b} while the bands in the higher energy UV absorption region (376–258 nm) are likely to be due to ligand centered transitions. The low intensity band in the near IR range (869–828 nm) is assigned to a *d–d* transition in the complexes.

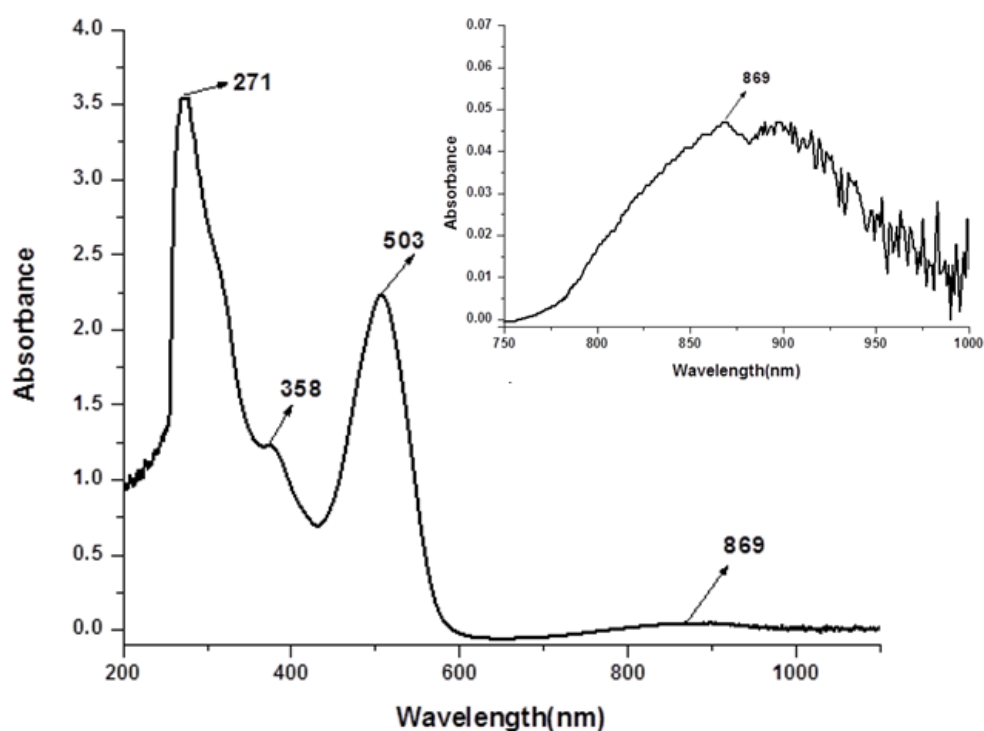


Figure 2.3. UV-vis spectrum of $[(\mu\text{-OEt})(\text{V}^{\text{IV}}\text{OL}^3)_2][\text{Et}_3\text{NH}]$ (**3**), in DMSO.

Table 2.2. UV-vis spectral data for $[(\mu\text{-OEt})(\text{V}^{\text{IV}}\text{OL}^{1-3})_2][\text{Et}_3\text{NH}]$ (**1-3**) in DMSO

| Complex | Wavelength (nm) (ϵ_{max} ($\text{M}^{-1}\text{cm}^{-1}$)) | | | |
|--|--|------------|------------|---------|
| $[(\mu\text{-OEt})(\text{V}^{\text{IV}}\text{OL}^1)_2][\text{Et}_3\text{NH}]$ (1) | 275(11540) | 376(1560) | 510(7650), | 866(72) |
| $[(\mu\text{-OEt})(\text{V}^{\text{IV}}\text{OL}^2)_2][\text{Et}_3\text{NH}]$ (2) | 258(11580) | 356(1582), | 509(7600), | 828(70) |
| $[(\mu\text{-OEt})(\text{V}^{\text{IV}}\text{OL}^3)_2][\text{Et}_3\text{NH}]$ (3) | 271(11531) | 358(1500) | 503(7000) | 869(75) |

2.3.3. ESI-MS. ESI-MS of the complexes (**1-3**) were recorded in acetonitrile solution. ESI-MS of complex **1** shows major peaks at m/z 811.58 $[\text{M} + \text{Na}]^+$ and 827.59 $[\text{M} + \text{K}]^+$ in the positive ion mode. Complex **2** exhibits two prominent peaks at m/z 859.54 $[\text{M} - \text{Na}]^-$ and 880.56 $[\text{M} - 2\text{H}]^-$ whereas complex **3** shows the characteristic molecular ion peak $[\text{M}]^+$ at m/z 1019.60 and another peak at m/z 998.35 $[\text{M} - \text{Na} + 4\text{H}]^+$ in the

negative ion mode. The ESI-MS data are summarized in the Experimental Section. ESI-MS of the complexes (1-3) is depicted in Figure 2.4-2.6.

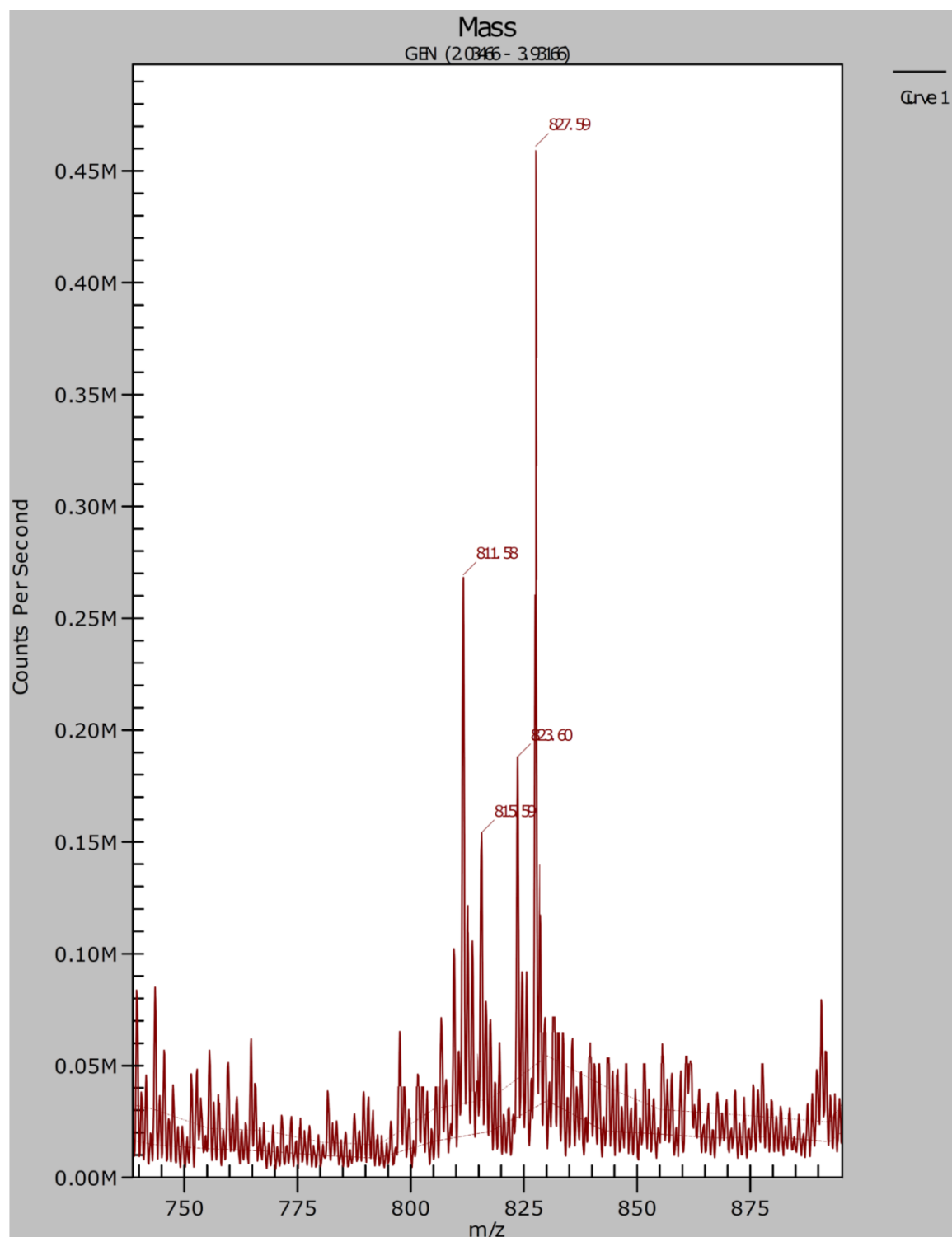


Figure 2.4. ESI-MS of $[(V^{IV}OL^1)_2(\mu-OEt)][Et_3NH]$ (**1**) in CH_3CN .

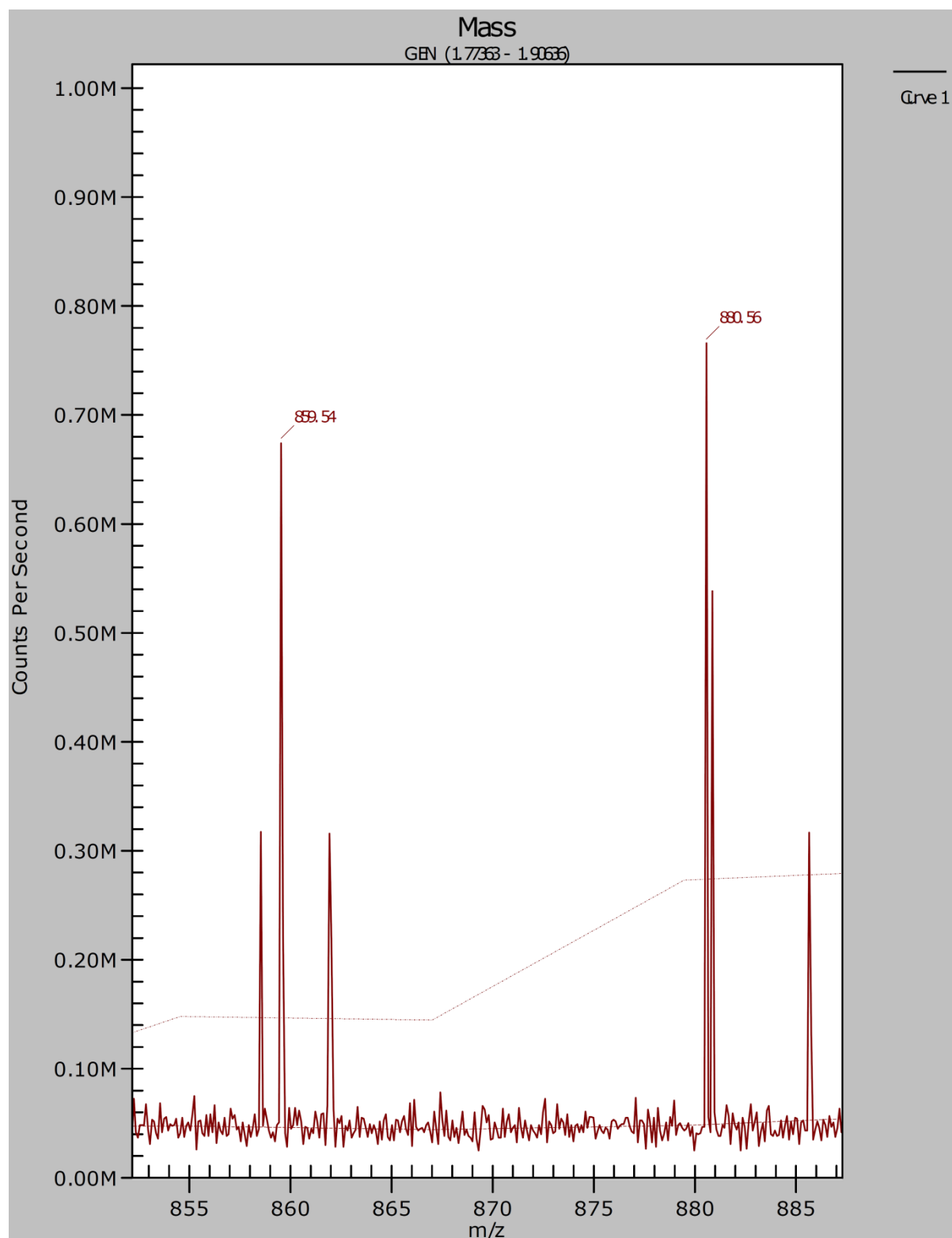


Figure 2.5. ESI-MS of $[(V^{IV}OL^2)_2(\mu-OEt)][Et_3NH]$ (**2**) in CH_3CN .

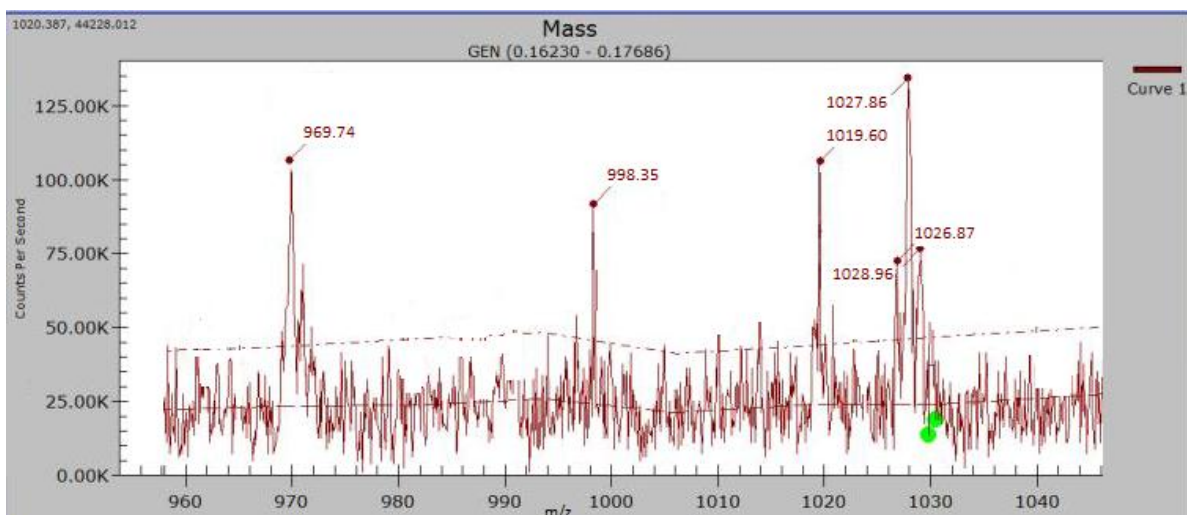


Figure 2.6. ESI-MS of $[(V^{IV}OL^3)_2(\mu-OEt)][Et_3NH]$ (**3**).

2.3.4. Electrochemical Properties. The Cyclic Voltammetry (CV) of **1** and **2** were examined in CH_2Cl_2 solution and that of **3** in DMF (0.1 M TEAP) at a scan rate of 100 mV s^{-1} . The CVs are similar for **1–3**, which include two oxidation and two reduction peaks corresponding to one electron transfer (Table 2.3). A representative CV of **1** is depicted in Figure 2.7. The anodic region of **1** shows one reversible and one quasi-reversible single-electron wave at $E_{1/2}^a$ values 0.46 and 1.09 V, which are assigned to the V(IV)/V(V) oxidation of the individual metal centers.⁶⁶ In the cathodic region each V(IV) is reduced to V(III) showing two quasi-reversible single-electron waves at $E_{1/2}^c$ values -0.59 and -1.36 V.⁶⁷ In the anodic region of Figure 2.7 two quasi-reversible oxidation waves at $E_{1/2}^a$ 1.26 and 0.82 V and a quasi-reversible wave in the cathodic region at $E_{1/2}^c$ -0.94 V were observed due to ligand oxidation and reduction processes, respectively. The corresponding cyclic voltammogram of ligand, H_2L^1 is shown in Figure 2.8.

Table 2.3. Cyclic voltammetric results for $[(V^{IV}OL^{1-3})_2(\mu-OEt)][Et_3NH]$ (**1-3**) at 298 K.^[a]

| Complex | $E_{1/2}^a$ (V) | ΔE_P^a (mV) | $E_{1/2}^c$ (V) | ΔE_P^c (mV) |
|--|-----------------|---------------------|-----------------|---------------------|
| $[(V^{IV}OL^1)_2(\mu-OEt)][Et_3NH]$ (1) | 0.46, 1.09 | 236, 70 | -0.59, -1.36 | 220, 420 |
| $[(V^{IV}OL^2)_2(\mu-OEt)][Et_3NH]$ (2) | 0.42, 1.05 | 240, 71 | -0.56, -1.30 | 222, 418 |
| $[(V^{IV}OL^3)_2(\mu-OEt)][Et_3NH]$ (3) | 0.45, 1.07 | 232, 73 | -0.60, -1.32 | 225, 417 |

^[a]**1** and **2** in CH_2Cl_2 and **3** in DMF at a scan rate of 100 mV s^{-1} . $E_{1/2} = (E_p^a + E_p^c)/2$, where E_p^a and E_p^c are anodic and cathodic peak potentials vs. Ag/AgCl, respectively. $\Delta E_P = E_p^a - E_p^c$.

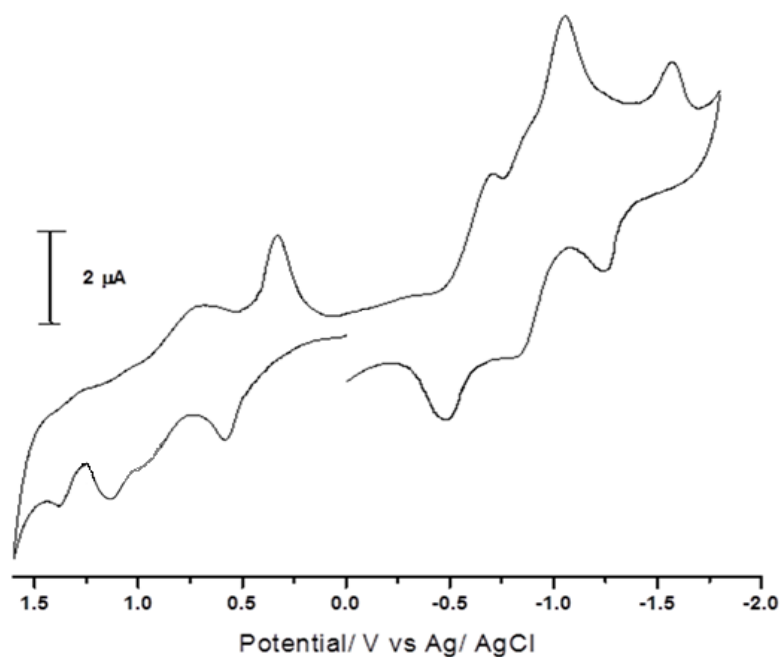


Figure 2.7. Cyclic voltammogram of $[(V^{IV}OL^1)_2(\mu-OEt)][Et_3NH]$ (**1**) in CH_2Cl_2 .

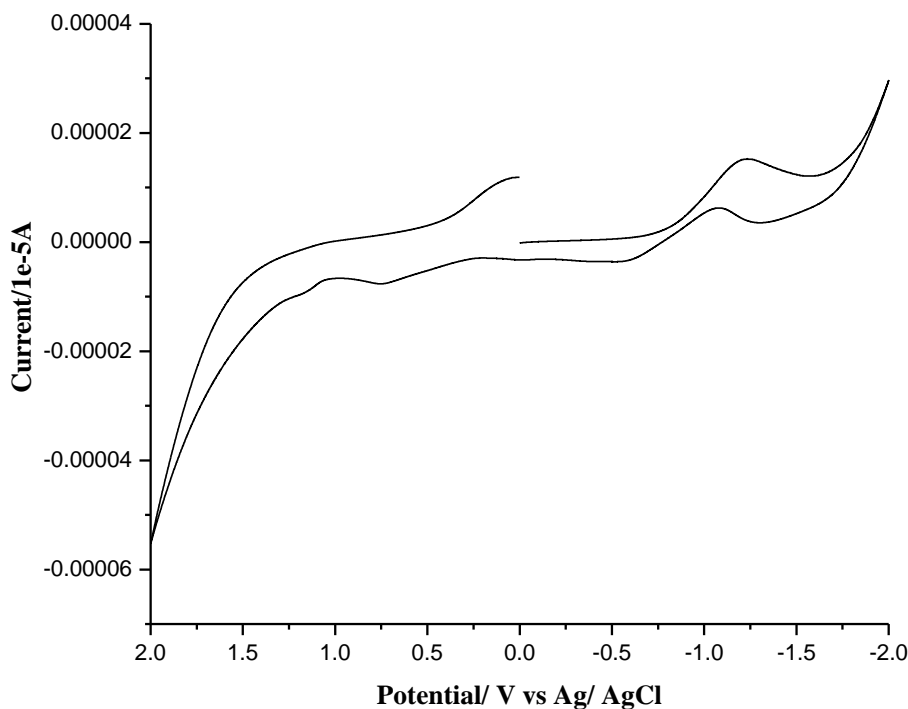


Figure 2.8. Cyclic Voltammogram of H_2L^1 .

2.3.5. Description of X-ray crystallographic structure of $[(\mu-OEt)(V^{IV}OL^{1,3})_2][Et_3NH]$ (**1** and **3**)

Single crystal X-ray structure determinations revealed similar geometry and coordination environments for complexes **1** and **3**. The ball and stick model of **1** and the ORTEP representation with atom numbering schemes of **3** are depicted in Figures 2.9 and 2.10, respectively. The selected bond parameters are given in Table 2.4. The asymmetric unit of both structures comprises of a dinuclear, monovalent anion, the charge of which is being balanced by a triethylammonium cation. The common feature of both anions is the presence of two five-fold coordinated vanadium atoms linked via the oxygen atom O(9) of an ethoxido ligand with bond angles of $104.04(4)^\circ$ for **1** and $108.3(2)^\circ$ for **3**. Asymmetry of this bridge arises from the fact that the corresponding bond lengths fall into two categories: a short one to V2 ($d(V-O) = 1.977(1) \text{ \AA}$, **1**; $1.961(4) \text{ \AA}$, **3**) and a longer one to V1 ($d(V-O) = 2.023(1) \text{ \AA}$, **1**; $2.019(3) \text{ \AA}$, **3**). In each case, the coordination sphere of the vanadium atoms is completed by a tridentate ligand with a 2- charge ([O(1)/O(5) of

carboxyl group, [N(1)/N(3)] of azo group and [O(3)/O(7)] from phenoxido group) and a double bonded [O(4)/O(8)] oxygen atom resulting, to a first extent, in a square-pyramidal ($\tau(V1) = 0.15$, $\tau(V2) = 0.25$, **1**; $\tau(V1) = 0.14$, $\tau(V2) = 0.32$, **3**; with $\tau = 0$ for a square-pyramidal coordinated atom and $\tau = 1$ for a trigonal-bipyramidal coordinated atom,⁶⁸ {VO₄N}-coordination of these metal atoms with the double bonded oxygen atom in an apical position, a typical coordination geometry of vanadium(IV).⁶⁹ While the vanadium oxygen distances to the apical oxygen atoms ($d(V=O) = 1.594(1)/1.597(1)$ Å, **1**; $1.589(4)/1.587(5)$ Å, **3**) correspond to vanadium oxygen double bonds, vanadium bonds to the organic ligand via single bonds of different strength. The strongest (shortest) ones are observed in case of the V(2)–O(7)_{phenoxido} bond ($d(V-O_{phenoxido}) = 1.922(1)$ Å, **1**; $1.919(4)$ Å, **3**) while the corresponding bonds in case of V(1) are significantly longer (weaker) [$d(V-O_{phenoxido}) = 1.945(1)$ Å, **1**; $1.966(5)$ Å, **3**]. In contrast, vanadium-oxygen bonds to the carboxylato groups are of similar length for both vanadium atoms (mean value of $d(V-O)_{carboxylato} = 1.963(6)$ Å) and of similar strength like the V(2)–O_{phenoxido} bonds. With the weakest bonds in the coordination sphere of the vanadium atoms found in case of the coordination of the azo group (N(1)/N(3): $2.050(6)$ Å, **3** – $2.096(1)$ Å, **1**) and taking the vanadium ethoxido bonds into account the following order of bond lengths is realized: $d(V-O_{apical}) < d(V(2)-O_{phenoxido}) < d(V(1)-O_{phenoxido}) \sim d(V-O_{carboxylate}) < d(V-O_{ethoxido}) < d(V-N_{azo})$.

Due to a weak ($d(V\cdots O) = 2.344(1)$ Å, **1**; $2.367(4)$ Å, **3**) bonding interaction (Figure 2.11) of O(5) and V(1), the coordination sphere of V1 is expanded from five, square-pyramidal to six, distorted octahedral, generating a pseudo four-membered, butterfly-shaped (dihedral angle between V(1)–O(9)–O(5) and V(2)–O(9)–O(5) planes: $34.29(4)^\circ$, **1**; $31.1(2)^\circ$, **3**) ring, responsible for the rectangular ($96.20(8)^\circ$, **1**; $85.5(2)^\circ$, **3**) orientation of the two apical oxygen atoms, O(4) and O(8). In case of V2, a similar interaction seems possible to O3, but distance between both atoms is rather long ($d(V\cdots O) = 2.808(1)$ Å, **1**; $3.106(4)$ Å, **3**).

In the solid state, anion and cation are linked via a hydrogen bond between the carboxylate atom O(2) as acceptor and Et₃NH as donor (Figure 2.11 and 2.12). In case of **1**, the corresponding donor acceptor distance of $2.752(2)$ Å and the angle of 173.8° at the hydrogen atom are in good agreement with a hydrogen bond of medium strength. It is interesting to see that these hydrogen bonded ion pairs interact with each other in a way

that the cation moiety of one ion pair is sandwiched in the pocket of the anion of a neighboring ion pair. The anions exist in a V-shaped conformation with the tridentate organic ligands forming both sides of the opening and the vanadium–oxido–ethoxido moiety as linking unit on the opposite side (Figure 2.13). There are, however, no other interactions between neighboring ion pairs than van–der–Waals ones (Figure 2.14).

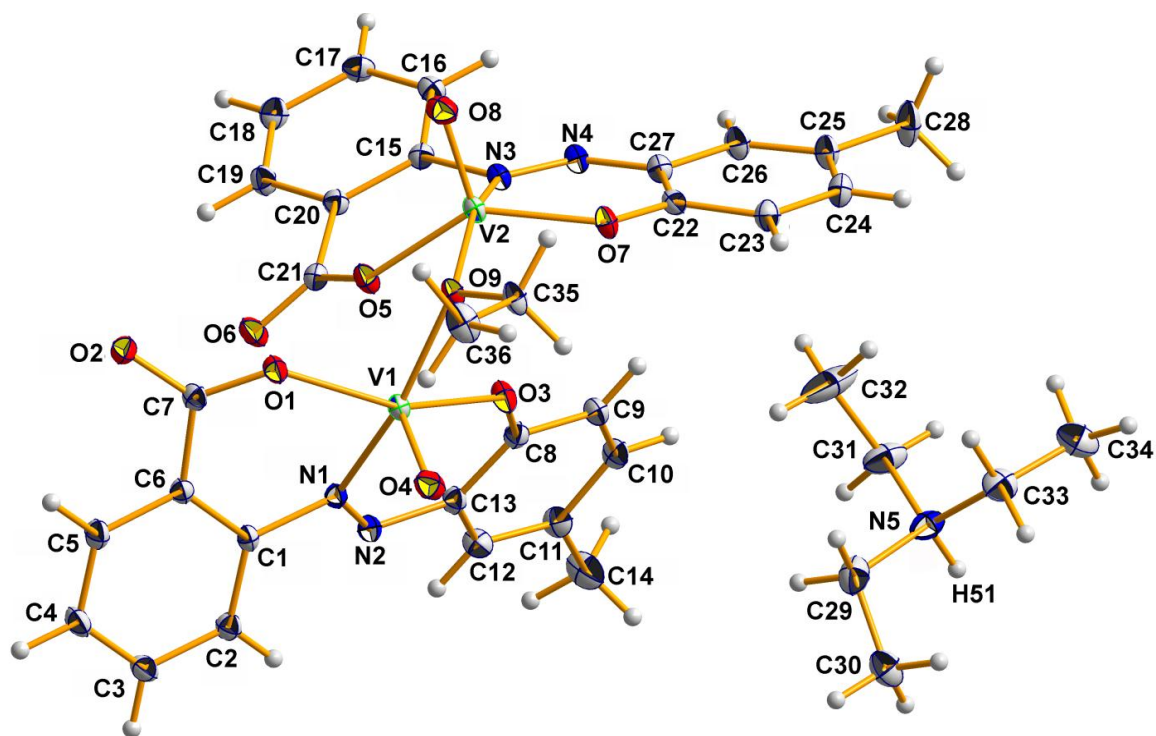


Figure 2.9. Asymmetric unit in the crystal structure of $[(\mu\text{-OEt})(\text{V}^{\text{IV}}\text{OL}^1)_2][\text{Et}_3\text{NH}]$ (**1**) with the atom numbering scheme used.

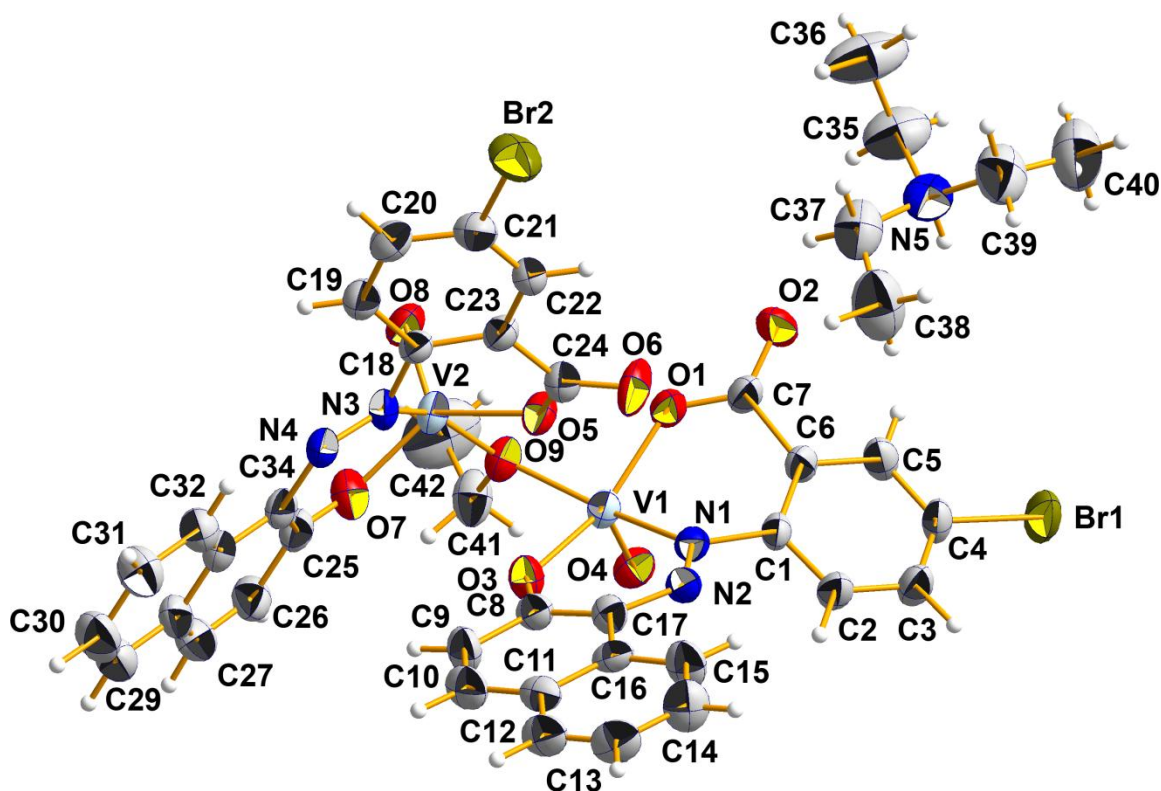


Figure 2.10. ORTEP representation of $[(V^{IV}OL^3)_2(\mu-OEt)][Et_3NH]$ (**3**) with atom numbering.

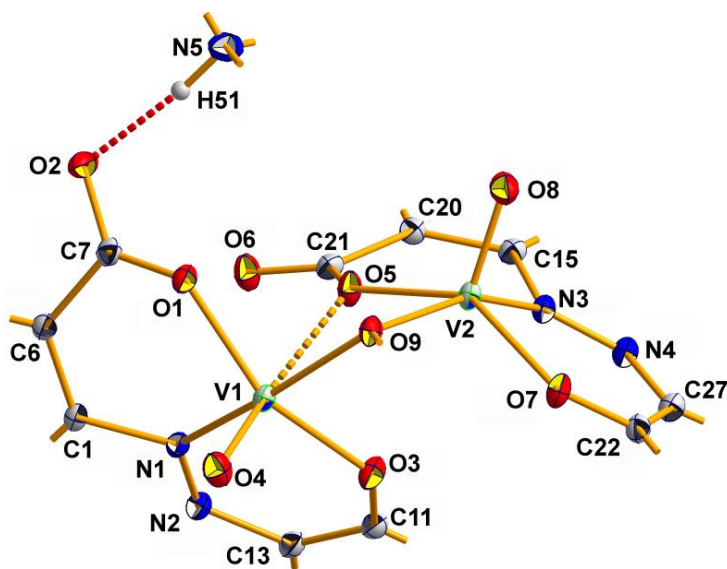


Figure 2.11. Central part of the anion of $[(V^{IV}OL^1)_2(\mu-OEt)][Et_3NH]$ (**1**) visualizing the weak interaction [broken stick] of O(5) with V(1) and the hydrogen bond between O(2) of the anion with the donor function of the ammonium ion [broken, red stick].

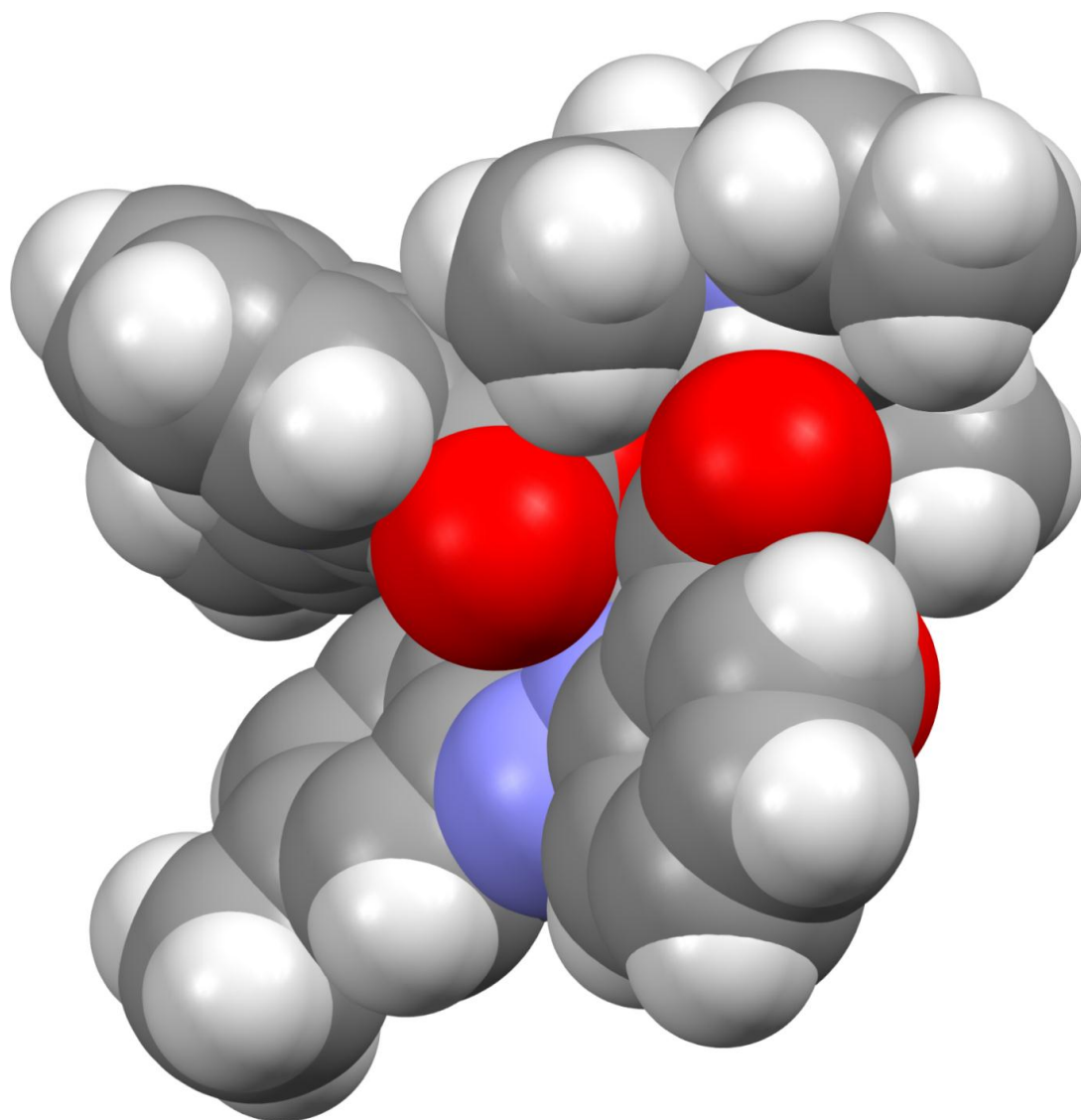


Figure 2.12. Space-filling model of the hydrogen bonded ion-pairs found in the crystal structure of $[(V^{IV}OL^1)_2(\mu-OEt)][Et_3NH]$ (**1**).

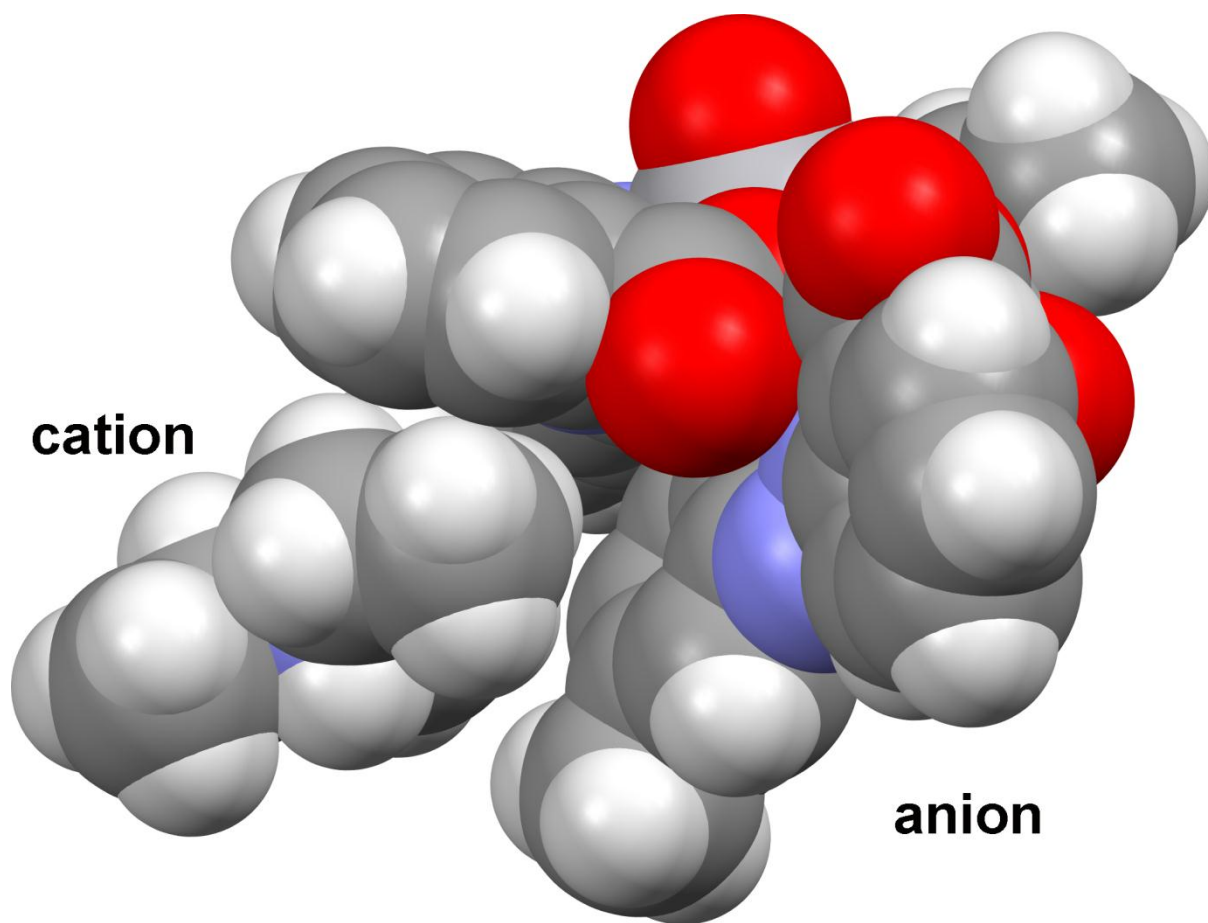


Figure 2.13. Space-filling model representing the anion-cation interaction between two neighboring ion pairs in $[(V^{IV}OL^1)_2(\mu-OEt)][Et_3NH]$ (**1**); only the interacting parts of both ion pairs are shown.

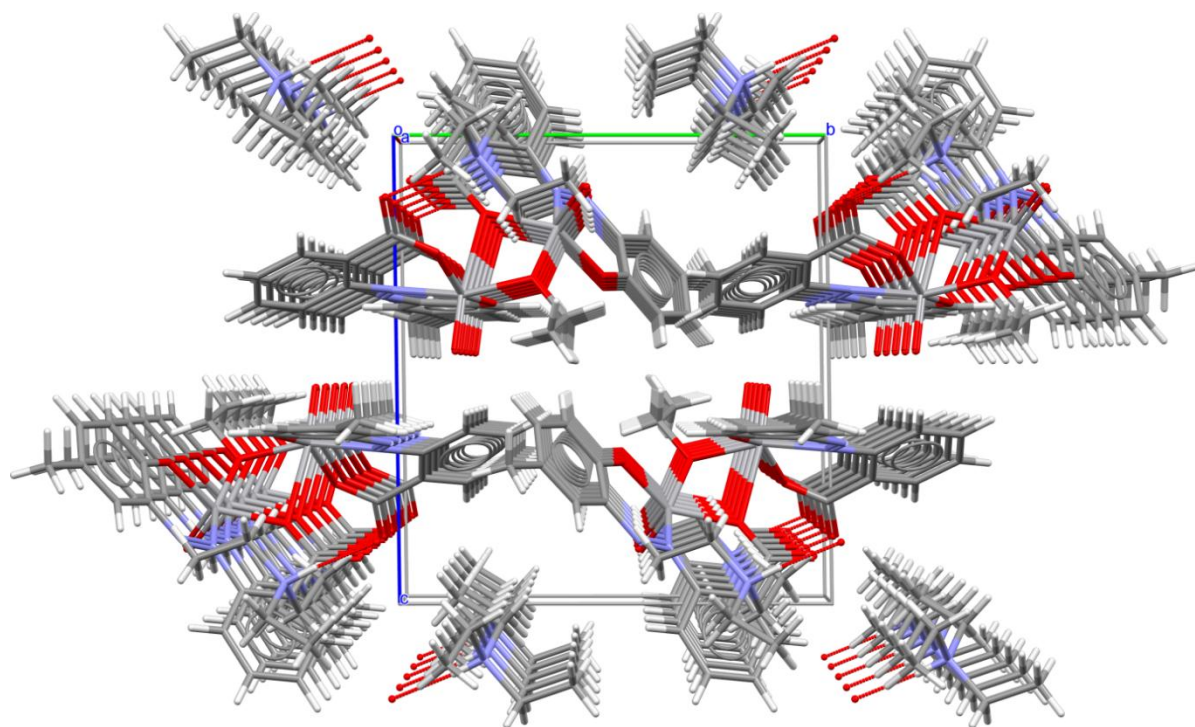
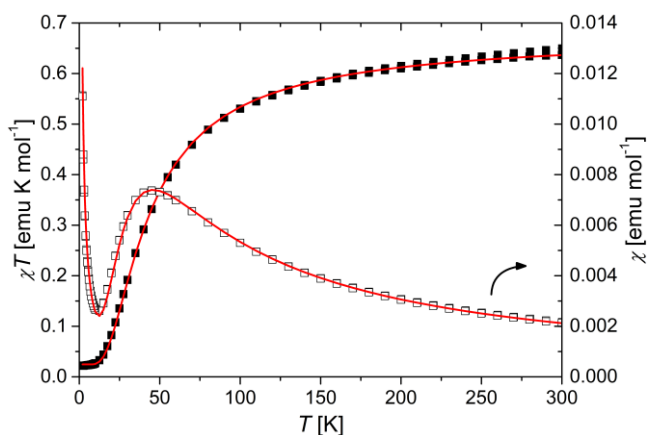


Figure 2.14. Packing of ion pairs in the crystal structure of $[(V^{IV}OL^1)_2(\mu-OEt)][Et_3NH]$
(1) looking down the a axis; for a better understanding some ion pairs are drawn incompletely so that hydrogen bonds between the cation and anion become visible.

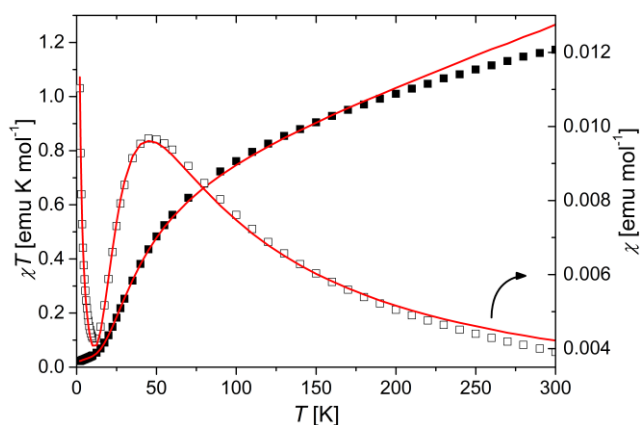
Table 2.4. Selected geometric parameters for $[(V^{IV}OL^{1,3})_2(\mu-OEt)][Et_3NH]$ (**1** and **3**)

| | 1 | 3 |
|-------------------------------|---------------------|-------------------|
| | Bond lengths(Å) | |
| V(1)–O(9)/V(2)–O(9) | 2.023(1)/1.977(1) | 2.019(3)/1.961(4) |
| V(1)–N(1)/V(2)–N(3) | 2.096(1)/2.089(1) | 2.086(4)/2.050(6) |
| V(1)–O(1)/V(2)–O(5) | 1.970(1)/1.959(1) | 1.965(4)/1.957(4) |
| V(1)–O(3)/V(2)–O(7) | 1.945(1)/1.922(1) | 1.966(5)/1.919(4) |
| V(1)–O(4)/V(2)–O(8) | 1.594(1)/1.597(1) | 1.589(4)/1.587(5) |
| O(5)–V(1) | 2.344(1) | 2.367(4) |
| | Bond Angles(°) | |
| V(2)–O(9)–V(1)/V(2)–O(5)–V(1) | 104.04(4)/93.82(4) | 108.3(2)/96.0(2) |
| O(4)–V(1)–O(1)/O(8)–V(2)–O(5) | 103.87(5)/109.86(5) | 101.8(2)/114.4(2) |
| O(4)–V(1)–O(3)/O(8)–V(2)–O(7) | 104.09(5)/110.02(5) | 104.1(2)/110.9(2) |
| O(4)–V(1)–N(1)/O(8)–V(2)–N(3) | 96.36(5)/99.08(5) | 97.1(2)/100.3(2) |
| O(4)–V(1)–O(9)/O(8)–V(2)–O(9) | 102.13(5)/104.72(5) | 99.9(2)/105.3(2) |
| O(1)–V(1)–O(9)/O(5)–V(2)–O(9) | 89.09(4)/79.41(4) | 91.6(2)/79.7(2) |
| O(1)–V(1)–O(3)/O(5)–V(2)–O(7) | 152.02(5)/140.12(5) | 154.0(2)/134.6(2) |
| O(1)–V(1)–N(1)/O(5)–V(2)–N(3) | 89.65(4)/86.27(5) | 88.7(2)/85.0(2) |
| O(3)–V(1)–O(9)/O(7)–V(2)–O(9) | 84.02(4)/90.49(4) | 86.1(2)/90.9(2) |
| O(3)–V(1)–N(1)/O(7)–V(2)–N(3) | 88.37(5)/87.67(5) | 86.2(2)/84.9(2) |
| O(9)–V(1)–N(1)/O(9)–V(2)–N(3) | 161.22(5)/155.25(5) | 162.6(2)/153.8(2) |
| O(1)–V(1)–O(5) | 77.50(4) | 78.5(1) |
| O(4)–V(1)–O(5) | 171.93(5) | 169.2(2) |
| O(3)–V(1)–O(5) | 74.66(5) | 76.5(1) |
| O(9)–V(1)–O(5) | 69.85(4) | 69.3(1) |
| N(1)–V(1)–O(5) | 91.59(4) | 93.7(2) |

2.3.6. Magnetic Susceptibility Study. The magnetic properties of **1** and **3** were measured in the temperature range from 300 to 2 K (Figure 2.15). In case of complex **1** (Figure 2.15(a)), at higher temperatures the χT value reaches $0.65 \text{ emu K mol}^{-1}$, which is slightly lower than the spin only value for two independent $S = 1/2$ species with $g = 2$, as expected for early transition metals with g -values typically smaller than 2. With decreasing temperature the χT value decreases and reaches a plateau below 10 K. The data could be simulated using spin hamiltonian $\hat{H} = -J\hat{S}_1\hat{S}_2$ for two coupled $S = 1/2$ ions with an isotropic $g = 1.935$ and 6.5% of a mononuclear impurity with $S = 1/2$. Refinement of all parameters gives an antiferromagnetic coupling of $J = -53.4 \text{ cm}^{-1}$. While in case of complex **3** (Figure 2.15(b)), at high temperatures the χT still has a constant slope which could be simulated as a temperature independent contribution (*tic*). With decreasing temperature the χT value decreases and reaches a plateau below 10 K. By fitting the data with the same model as for **1** we obtain $g = 1.932$, $J = -52.2 \text{ cm}^{-1}$, 4.9% of a mononuclear impurity with $S = 1/2$ and a $tic = 219 \cdot 10^{-5} \text{ emu/mol}$. However, the magnetic properties of **2** did not give convincing results.



(a)



(b)

Figure 2.15. (a) Magnetic behavior of complex **1**. The data could be simulated with $g = 1.935$, $J = -53.4 \text{ cm}^{-1}$ and 6.5% mononuclear impurity. (b) Magnetic behavior of complex **3**. The data could be simulated with $g = 1.932$, $J = -52.2 \text{ cm}^{-1}$, 4.9% mononuclear impurity and a $t_{ic} = 219 \cdot 10^{-5} \text{ emu/mol}$. In both (a) and (b) black squares: measured data (solid: χT , open: χ), red line: simulation.

2.3.7. Computational studies. Computational studies based on broken-symmetry density functional theory (BS-DFT) were performed to further investigate the magnetic properties of the dinuclear complexes **1** and **3**. The structural parameters used for these calculations were derived from the crystallographic data. In these calculations two common density functionals (B3LYP and TPSSh) were employed, as they are known to reproduce properties of transition metal complexes.⁷⁰ The energies of the high-spin (HS) and

broken-symmetry (BS) states together with their corresponding spin expectation values $\langle S^2 \rangle$ and the exchange coupling constants J_{12} derived from Eq. 2.1 for both complexes **1** and **3** are summarized in Table 2.5. For **1** both BS-DFT calculated coupling constants of -55.1 cm^{-1} (B3LYP) and -55.9 cm^{-1} (TPSSh) are in good agreement with the experimental value of -53.4 cm^{-1} . The situation is different for complex **3**. The coupling constant of **3** derived from BS-DFT/B3LYP calculation is found to be -50.7 cm^{-1} , which is in good accordance to the experimental value of -52.2 cm^{-1} , whereas the calculations with the TPSSh functional gave a value of -41.5 cm^{-1} , which significantly underestimates the experimental coupling constant. The latter result is somewhat unexpected, as the TPSSh density functional is reported to show promising performance in bioinorganic applications, including the prediction of the energy sequence of spin states.⁷¹ However, at least for the cases reported here, the B3LYP functional provides the better description for the energy splitting of the spin states, which might be due to the difference in the amount of exact Hartree-Fock exchange implemented in the B3LYP (20%) and TPSSh (10%) functional. Nevertheless, the experimental trend of a stronger antiferromagnetic coupling in case of **1** compared to **3** is reproduced with both functionals.

Table 2.5. Results of BS-DFT calculations for $[(V^{IV}OL^{1,3})_2(\mu-OEt)][Et_3NH]$ (**1** and **3**)

| Complex | Density Functional | J_{12} (cm^{-1}) | State | Energy (a.u.) | $\langle S^2 \rangle$ |
|----------|--------------------|---------------------------|-------|------------------|-----------------------|
| 1 | B3LYP | -55.1 | HS | -3942.247718 | 2.023310 |
| | | | BS | -3942.247844 | 1.020910 |
| 1 | TPSSh | -55.9 | HS | -3943.673995 | 2.021577 |
| | | | BS | -3943.674123 | 1.018236 |
| 3 | B3LYP | -50.7 | HS | -9317.717246 | 2.023223 |
| | | | BS | -9317.717362 | 1.020538 |
| 3 | TPSSh | -41.5 | HS | -9319.347309 | 2.021780 |
| | | | BS | -9319.347404 | 1.018305 |

The classification of the geometry of the $[VO(\mu-OR)_2VO]^{2+}$ core in dinuclear vanadium(IV) complex, which is based on the orientation of the V=O groups, generally allows at least for a qualitative assignment of the magnetic properties.^{20a} Although this classification was strictly proposed for dinuclear complexes with six-coordinate vanadium centers, it can also be basically applied for dinuclear complexes with five-coordinate metal centers in a square-pyramidal environment.⁷² Interestingly, for the complexes **1** and **3** a mixed situation is observed as one of the centers is six-coordinate (V1) whereas the other shows a square-pyramidal coordination (V2). At first glance it might be tempting to assign for both complexes a twist configuration of the bridging $[VO(\mu-OR)_2VO]^{2+}$ core, which could be expected to lead to an accidental orthogonality of the magnetic orbitals. However, this would clearly disagree with the antiferromagnetic coupling observed for both complexes. In fact, the tilting angles between the two V=O bonds significantly deviate from the accidental orthogonality with values of 59.3° for **1** and 68.0° for **3**. This

is consistent with the spin density distribution calculated for the high-spin states of both complexes depicted in Figure 2.16 and 2.17.

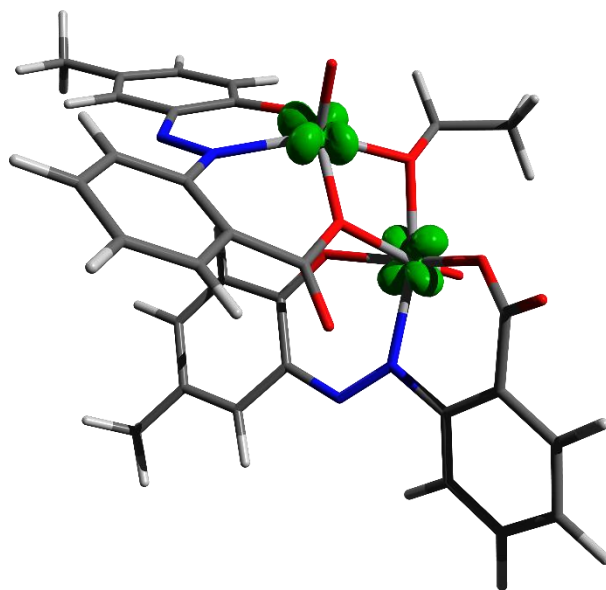


Figure 2.16. Spin density (green surface, iso value = 0.04) of the high-spin state of $[(V^{IV}OL^1)_2(\mu-OEt)][Et_3NH]$ (**1**) obtained with DFT/B3LYP.

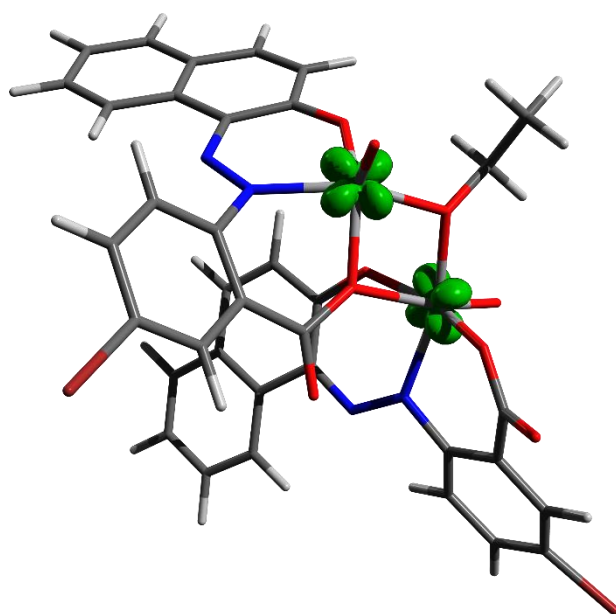


Figure 2.17. Spin density (green surface, iso value = 0.04) of the high-spin state of $[(V^{IV}OL^3)_2(\mu-OEt)][Et_3NH]$ (**3**) obtained with DFT/B3LYP.

On the other hand, a quantitative magneto-structural correlation reported for systems with so-called orthogonal configurations of the bridging $[\text{VO}(\mu\text{-OR})_2\text{VO}]^{2+}$ core ($J = -A \exp(-\varepsilon R)$ with $A = 2.22 \times 10^{-11}$, $\varepsilon = 6.9$ and R given in \AA)⁷³ leads to predicted coupling constants of -79 and -47 cm^{-1} for complexes **1** and **3**, respectively. This is in surprisingly good agreement with the observed experimental values, although a super exchange pathway via the bridging ethanolate oxygen atom is operative in **1** and **3** rather than a direct exchange between the magnetic orbitals at the vanadium centers.

To further investigate the possible exchange mechanism we performed a natural population analysis (NPA)⁷⁴ for complexes **1** and **3**. Selected total density NPA charges of the two vanadium atoms V1 and V2 as well as the bridging ethanolate oxygen atoms O(Et) and O(Bz) can be found in Table 2.6. In addition, the corresponding NPA spin densities for **1** and **3** are summarized in Table 2.7. The following discussion solely refers to the values obtained from the BS-DFT/B3LYP calculations, as their results are in better agreement with the experiment and their counterparts derived from BS-DFT/TPSSh calculations show similar trends. Not surprisingly, in all cases the square-pyramidal coordinated vanadium center V2 shows the higher total charge due to its lower coordination number. For the bridging oxygen atoms O(Et) and O(Bz) no significant differences in total NPA charges are observed between **1** and **3** as well as between HS and BS states. The situation is different as the NPA spin densities for **1** and **3** are compared. For **1** a clear difference in spin density at oxygen atom O(Bz) is observed between HS (0.0079) and BS (-0.0107) states, whereas for the oxygen atom O(Et) rather similar values are found in both states (HS: 0.0092; BS: 0.0102). On the other hand, for **3** a generally larger distribution of spin density onto the bridging oxygen atom O(Et) in both spin states is observed, which goes along with a lower spin density on the vanadium(IV) centers. Moreover, there is an additional considerable increase of spin density at the bridging ethanolate oxygen atom O(Et) in **3** when going from the HS (0.0126) to the BS (0.0337) state, which is accompanied by a significant decrease of spin density at vanadium center V1 (HS: 1.0699; BS: 1.0226). On the contrary, only a slight change in spin density at oxygen atom O(Bz) is observed for **3** when both spin states are compared (HS: 0.0055; BS: -0.0044). Therefore, it is tempting to conclude the presence of a better overlap of the magnetic orbitals at the bridging O(Et) in complex **3**. However, the

experimental and calculated exchange coupling constants of **1** and **3** are rather similar, with a slight trend to a somewhat larger antiferromagnetic coupling in the case of **1**. This might be related to structural differences of the bridging ethanolate moiety in **1** and **3**, i.e. the V1–O(Et)–V2 bonding angle (**1**: 104°; **3**: 108°) and the out-of-plane distortion of the alkyl substituent at the bridging oxygen atom O(Et) (**1**: $\tau = 31.0^\circ$; **3**: $\tau = 4.9^\circ$). Both parameters are known to have a prominent influence on exchange coupling in such dinuclear vanadium(IV) complexes.²⁶ In fact, the larger angle observed for **3** should lead to a decrease of the antiferromagnetic coupling, whereas the smaller out-of-plane distortion found for **3** is expected to result in the opposite trend. Overall, this leads to a situation where both structural effects counterbalance each other.

Table 2.6. Selected total densities derived from natural population analysis (NPA) for $[(V^{IV}OL^{1,3})_2(\mu-OEt)][Et_3NH]$ (**1** and **3**)

| Complex | Density Functional | State | V1 | V2 | O(Bz) | O(Et) |
|----------|--------------------|-------|--------|--------|---------|---------|
| 1 | B3LYP | HS | 1.2708 | 1.3109 | -0.6832 | -0.6926 |
| | | BS | 1.2700 | 1.3097 | -0.6829 | -0.6913 |
| 3 | B3LYP | HS | 1.2636 | 1.3064 | -0.6894 | -0.6963 |
| | | BS | 1.2628 | 1.3053 | -0.6891 | -0.6951 |
| 1 | TPSSh | HS | 1.2165 | 1.2606 | -0.6684 | -0.6770 |
| | | BS | 1.2154 | 1.2592 | -0.6681 | -0.6758 |
| 3 | TPSSh | HS | 1.2104 | 1.2564 | -0.6747 | -0.6801 |
| | | BS | 1.2091 | 1.2551 | -0.6743 | -0.6794 |

Table 2.7. Selected spin densities derived from natural population analysis (NPA) for $[(V^{IV}OL^{1,3})_2(\mu-OEt)][Et_3NH]$ (**1** and **3**)

| Complex | Density Functional | State | V1 | V2 | O(Bz) | O(Et) |
|----------|--------------------|-------|--------|--------|---------|---------|
| 1 | B3LYP | HS | 1.2708 | 1.3109 | -0.6832 | -0.6926 |
| | | BS | 1.2700 | 1.3097 | -0.6829 | -0.6913 |
| 3 | B3LYP | HS | 1.2636 | 1.3064 | -0.6894 | -0.6963 |
| | | BS | 1.2628 | 1.3053 | -0.6891 | -0.6951 |
| 1 | TPSSh | HS | 1.2165 | 1.2606 | -0.6684 | -0.6770 |
| | | BS | 1.2154 | 1.2592 | -0.6681 | -0.6758 |
| 3 | TPSSh | HS | 1.2104 | 1.2564 | -0.6747 | -0.6801 |
| | | BS | 1.2091 | 1.2551 | -0.6743 | -0.6794 |

2.3.8. Cytotoxicity Study

Analysis of the *in vitro* cytotoxicity study clearly showed that all the three complexes are cytotoxic and can kill cancer cells effectively. The ligands and metal precursor showed significantly lower toxicity (IC_{50} values $>100 \mu\text{M}$) in both HeLa and HT-29 cancer cells, as compared to the divanadium(IV) arylazo complexes, **1–3** (IC_{50} values: 1.92–9.39 μM and 25.93–28.77 μM against HeLa and HT-29 cells respectively, Table 2.8), indicating enhanced cytotoxicity upon complexation and the presence of the vanadium (IV) ion. The variation in potency was found prominent at very low concentration of the compound (up to 10 $\mu\text{g/ml}$). At relatively higher concentration of about 50 $\mu\text{g/ml}$, such variation become insignificant and there was 80% cell death with respect to the control for all the treatment sets irrespective of the cell type. No further increase in cell death was observed with an increase in concentration above 50 $\mu\text{g/ml}$. Among the three compounds, **1** showed maximum cytotoxicity (IC_{50} value 1.92 μM) followed by **3** (IC_{50} value 6.57 μM) and **2** (IC_{50} value 9.39 μM) against HeLa cells. In the case of HT-29, although **3** showed highest cytotoxicity but the data was found statistically insignificant. Further analysis revealed that IC_{50} value of each complex was many fold less for HeLa cells in comparison to that of HT-29 cells, which indicates the specificity of a complex towards a particular cell type specific (Table 2.8).

It is already known that during the course of their action on the cell, many of the cytotoxic agents disrupts nuclear integrity and cytoskeletal structure.^{75,76} These includes clinically active compounds like cisplatin⁷⁷ (complexation of nucleic acid), doxorubicin⁷⁸ (intercalate nucleic acid), taxol⁷⁹ (stabilize microtubule), vinblastin⁸⁰ (prevent polymerization of microtubule), and other compounds like Jasplakinolide⁸¹ (enhance polymerization of actin) and cytochalacin⁸² (prevents polymerization of actin). Keeping this perspective in mind cells after treatment were stained with fluorescence dyes specific for nucleus (stained with DAPI, blue colored) and F-actin (stained with TRITC Phalloidin, red colored) and investigated under fluorescence microscope and imaged (Figure 2.18). Preliminary inspection confirmed that for all the treatment sets, cell nuclei remain intact which ruled out the possibility of nuclear defragmentation. However, a critical analysis of the images revealed two very interesting points. In this study, we observed that although under the exposure of the compounds (100 $\mu\text{g/ml}$ for 36 h) individual cells were able to maintain their cytoskeletal integrity, however, both HeLa and

HT-29 cells failed to form a colony. Such variation was more profound in the cells treated with **1** and **3**. So far a number of cytotoxic compounds have been reported which effectively inhibit colony formation.⁸³⁻⁸⁵ On the basis of this aforesaid fact, we hypothesize that these set of compound may possess similar property.

The higher potency of **1** can be explained in terms of relatively high π electron density of **1** in comparison to **2** and **3**. As **2** and **3** both are substituted with an electron withdrawing group ($-\text{NO}_2$ and $-\text{Br}$), it is expected that π electron density will be less for this molecule in comparison to **1** (substituted with $-\text{H}$). It is already well established that π electron density has a very important role in governing the interaction among physiologically relevant biomolecules.⁸⁶ It is assumed that the higher π electron density of **1** is responsible for the greater receptor-ligand interaction and subsequent changes in cell physiology. However, π density factor does not play a role in the cytotoxicity in HT-29 cancer cells.

Commonly used chemotherapeutic drugs like cisplatin, cyclophosphamide, tamoxifen and 5-fluorouridine have shown comparable antiproliferative efficacy under similar conditions, against HT-29 and HeLa cells. The μ -ethoxido dinuclear arylazovanadium(IV) complexes (**1-3**) have shown improved *in vitro* cytotoxicity results as compared to our earlier cytotoxicity reports on vanadium^{36d,e,g,h} and molybdenum hydrazone⁸⁷ and copper thiosemicarbazone complexes⁸⁸ (IC_{50} : 10–40 μM) against HeLa cells. The IC_{50} values of **1-3** are either lower or comparable to photocytotoxic oxidovanadium(IV) complexes of polypyridyl ligands⁸⁹ (IC_{50} 3.9–16.2 μM) and curcuminoids⁹⁰ (IC_{50} 2.4–10.9 μM).

The cytotoxicity results of **1-3** against HT-29 were comparatively lower as compared to the standard drug, cisplatin (IC_{50} 12.2 μM), however their antiproliferative efficacy was better or comparable to other vanadium complexes (>47 μM against HT-29 for $[\text{VO}(\text{sal-L-trypt})(\text{acetyletHTSC})].\text{C}_2\text{H}_5\text{OH}$, $[\text{VO}(\text{sal-L-trypt})(\text{Me-ATSC})]$ and $[\text{VO}(\text{sal-L-trypt})(\text{N-ethhymethohcarbthio})].\text{H}_2\text{O}$).⁹²

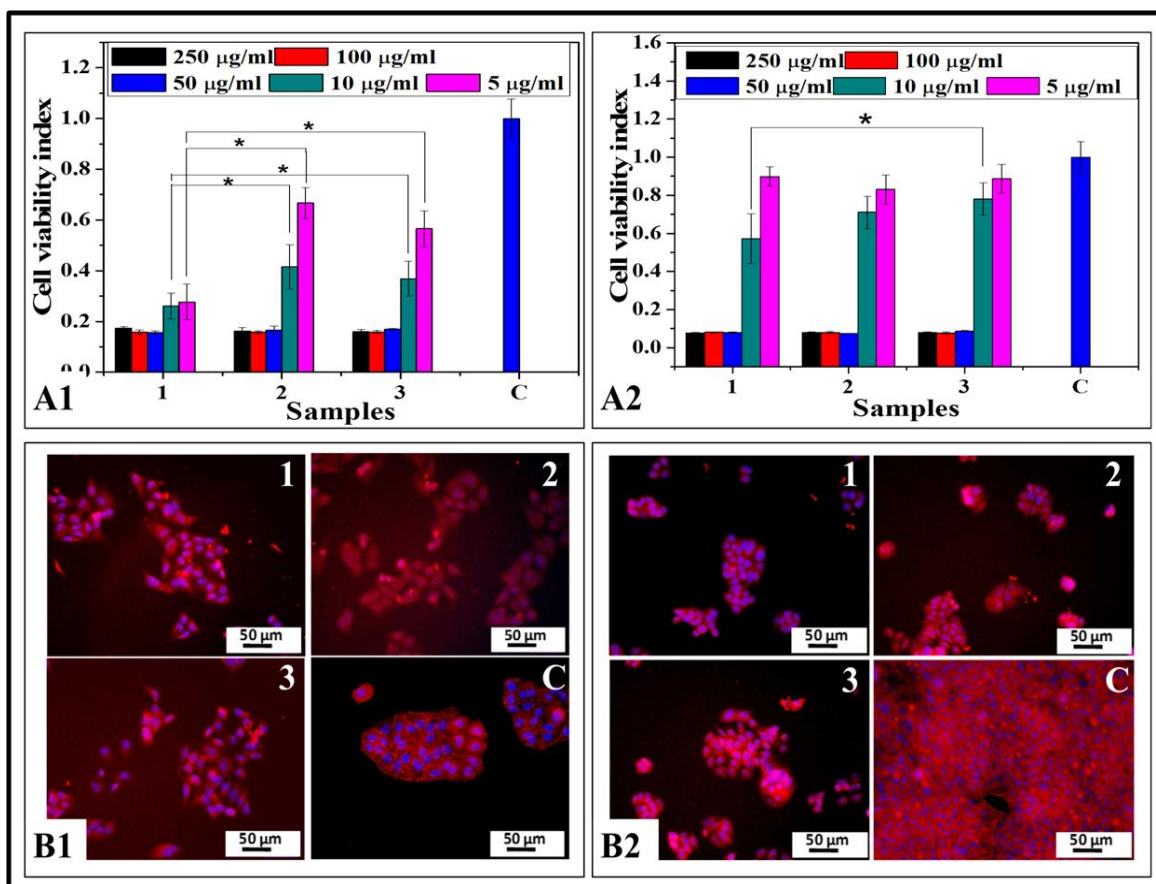


Figure 2.18. Cytotoxicity of $[(V^{IV}OL^{1-3})_2(\mu-OEt)] [Et_3NH]$ (**1–3**) against HeLa (A1) and HT-29 cells (B1) after 48 h exposure. The experiments were performed in quadruplets and the data were expressed as mean \pm S.D. Morphology of HeLa (B1) and HT-29 (B2) cells treated with complexes (**1–3**) for 36 h. Cells were stained with DAPI (Blue color – nucleus) and TRITC Phalloidin (Red color – F-actin) and visualized under fluorescent microscope.

Table 2.8. IC₅₀ values of [(V^{IV}OL¹⁻³)₂(μ-OEt)][Et₃NH] (**1-3**) and some reported drugs against HeLa and HT-29 cell lines

| Complex | IC ₅₀ (μM) | |
|--|-----------------------|--------------|
| | HeLa cells | HT-29 cells |
| [(V ^{IV} OL ¹) ₂ (μ-OEt)][Et ₃ NH] (1) | 1.92 ± 0.26 | 28.77 ± 2.27 |
| [(V ^{IV} OL ²) ₂ (μ-OEt)][Et ₃ NH] (2) | 9.39 ± 0.95 | 27.28 ± 1.91 |
| [(V ^{IV} OL ³) ₂ (μ-OEt)][Et ₃ NH] (3) | 6.57 ± 0.55 | 25.93 ± 1.71 |
| Cisplatin | 70 | 12.2 |
| Cyclophosphamide | 21.5 | 1689 |
| Tamoxifen | 9.3 | 8.82 |
| 5-Fluorouridine | 0.3 | 2.85 |

2.4. CONCLUSION

The following are the salient observations and findings of this work:

- (a) Three ethoxido bridged dimeric V(IV) complexes, $[(V^{IV}OL^{1-3})_2(\mu-OEt)][Et_3NH]$ (**1-3**), employing tridentate azo ligands (H_2L^{1-3}) have been synthesized and characterized by various physicochemical techniques. Single crystal X-ray structures have been solved for **1** and **3**.
- (b) Time dependent UV-vis spectroscopy studies in DMSO showed the presence of d-d transition peak even after 24 h, thus proving the stability of the compounds in the solution state.
- (c) Variable temperature magnetic susceptibility measurements and corresponding theoretical simulations of **1** and **3** show strong antiferromagnetic coupling, which are in good agreement with the theoretical values. However, magnetic properties of **2** did not give convincing results.
- (d) Cytotoxicity studies against human cancer cell lines, HeLa and HT-29, confirmed the antiproliferative effect of the complexes and their specificity over particular cell type. Even though all the complexes were found to be cytotoxic, complex **1** was the most potent amongst them.

2.5. REFERENCES

- (1) (a) Sakurai, H.; Yoshikawa, Y.; Yasui, H. *Chem. Soc. Rev.* **2008**, *37*, 2383–2392. (b) Shechter, Y.; Goldwasser, I.; Mironchik, M.; Fridkin, M.; Gefel, D. *Coord. Chem. Rev.* **2003**, *237*, 3–11. (c) Thompson, K. H.; McNeill, J. H.; Orvig, C. *Chem. Rev.* **1999**, *99*, 2561–2572. (d) Thompson, K. H.; Orvig, C. *Dalton Trans.* **2006**, 761–764. (e) Thompson, K. H.; Lichter, J.; LeBel, C.; Scaife, M. C.; McNeil, J. H.; Orvig, C. *J. Inorg. Biochem.* **2009**, *103*, 554–558. (f) Crans, D. C. *J. Inorg. Biochem.* **2000**, *80*, 123–131. (g) Yamaguchi, M.; Wakasugi, K.; Saito, R.; Adachi, Y.; Yoshikawa, Y.; Sakurai, H.; Katoh, A. *J. Inorg. Biochem.* **2006**, *100*, 260–269. (h) Rehder, D.; Pessoa, J. C.; Geraldes, C. F. G. C.; Castro, M. M. C. A.; Kabanos, T.; Kiss, T.; Meier, B.; Micera, G.; Pettersson, L.; Rangel, M.; Salifoglou, A.; Turel, I.; Wang, D. *J. Biol. Inorg. Chem.* **2002**, *7*, 384–396. (i) Crans, D. C.; Smee, J. J.; Gaidamauskas, E.; Yang, L. *Chem. Rev.* **2004**, *104*, 849–902. (j) Levina, A.; Lay, P. A. *Dalton Trans.* **2011**, *40*, 11675–11686. (k) Rehder, D. *Future Med. Chem.* **2016**, *8*, 325–338. (l) Melchior, M.; Rettig, S. J.; Liboiron, B. D.; Thompson, K. H.; Yuen, V. G.; McNeill, J. H.; Orvig, C. *Inorg. Chem.* **2001**, *40*, 4686–4690.
- (2) (a) Evangelou, A. M. *Crit. Rev. Oncol. Hematol.* **2002**, *42*, 249–265. (b) Louie, A. Y.; Meade, T. J. *Chem. Rev.* **1999**, *99*, 2711–2734. (c) Narla, R. K.; Dong, Y.; Klis, D.; Uckun, F. M. *Clin. Can. Res.* **2001**, 1094–1101. (d) Chohan Z. H.; Sumrra, S. H.; Yousoufi, M. H.; Hadda, T. B. *Eur. J. Med. Chem.* **2010**, *45*, 2739–2747. (e) Naso, L.; Ferrer, G. E.; Butenko, N.; Cavaco, I.; Lezama, L.; Rojo, T.; Etcheverry, B. S.; Williams, M. A. P. *J. Biol. Inorg. Chem.* **2011**, *16*, 653–668.
- (3) (a) Maurya, M. R.; Khurana, S.; Shailendra; A. A.; Zhang, W.; Rehder, D. *Eur. J. Inorg. Chem.* **2003**, *10*, 1966–1973. (b) Maurya, M. R.; Kumar, A.; Bhat, A. R.; Azam, A.; Bader, C.; Rehder, D. *Inorg. Chem.* **2006**, *45*, 1260–1269. (c) Maurya, M. R.; Kumar, A.; Abid, M.; Azam, A. *Inorg. Chim. Acta* **2006**, *359*, 2439–2447. (d) Maurya, M. R.; Agarwal, S.; Abid, M.; Azam, A.; Bader, C.; Ebel, M.; Rehder, D. *Dalton Trans.* **2006**, *7*, 937–947. (e) Maurya, M. R.; Khan, A. A.; Azam, A.; Ranjan, S.; Mondal, N.; Kumar, A.; Pessoa, J. C. *Eur. J. Inorg. Chem.* **2009**, *35*, 5377–5390. (f) Maurya, M. R.; Khan, A. A.; Azam, A.; Ranjan, S.; Mondal, N.; Kumar, A.; Avecilla, F.; Pessoa, J. C. *Dalton Trans.* **2010**, *39*, 1345–1360.
- (4) Benítez, J.; Guggeri, L.; Tomaz, I.; Arrambide, G.; Navarro, M.; Pessoa, J. C.; Garat, B.; Gambino, D. *J. Inorg. Biochem.* **2009**, *103*, 609–616.

- (5) Liang, J.; Madden, M.; Shah, V. K.; Burris, R. H. *Biochemistry* **1990**, *29*, 8577–8581.
- (6) (a) Vilter, H. In *Metal Ions in Biological Systems: Vanadium and its Role in Life*; Sigel, H., Sigel, A., Eds.; Marcel Dekker: New York, NY, 1995; Chapter 10, pp 325–362. (b) Butler, A.; Walker, J. V. *Chem. Rev.* **1993**, *93*, 1937–1944.
- (7) (a) Rehder, D. *Future Med. Chem.* **2012**, *4*, 1823–1837. (b) Thompson, K. H.; Orvig, C. J. *Inorg. Biochem.* **2006**, *100*, 1925–1935.
- (8) Mjos, K. D.; Orvig, C. *Chem. Rev.* **2014**, *114*, 4540–4563.
- (9) Pessoa, J. C.; Etcheverry, S.; Gambino, D. *Coord. Chem. Rev.* **2015**, *301*, 24–28.
- (10) Kioseoglou, E.; Petanidis, S.; Gabriel, C.; Salifoglou, A. *Coord. Chem. Rev.* **2015**, *301–302*, 87–105.
- (11) Naso, L.; Ferrer, G. E.; Lezama, L.; Rojo, T.; Etcheverry, B. S.; Williams, M. A. *P. J. Biol. Inorg. Chem.* **2010**, *15*, 889–902.
- (12) Sartzi, H.; Stoumpos, C. C.; Giouli, M.; Verginadis, I. I.; Karkabounas, C. S.; Cunha-Silva, L.; Escuer, A.; Perlepes, P. S. *Dalton Trans.* **2012**, *41*, 11984–11988 and references therein.
- (13) Naso, L.; Valcarcel, M.; Villacé, P.; Roura-Ferrer, M.; Salado, C.; Ferrer, G. E.; Williams, M. A. P. *New J. Chem.* **2014**, *38*, 2414–2421.
- (14) Liao, X.; Lu, J.; Ying, P.; Zhao, P.; Bai, Y.; Li, W.; Liu, M. *J. Biol. Inorg. Chem.* **2013**, *18*, 975–984.
- (15) Sasmal, P. K.; Saha, S.; Majumdar, R.; Dighe, R. R.; Chakravarty, A. R. *Inorg. Chem.* **2010**, *49*, 849–859.
- (16) Kahn, O. *Nature* **1995**, *378*, 667–668.
- (17) Ferlay, S.; Mallah, T.; Ouahes, R.; Veillet, P.; Verdaguer, M. *Nature* **1995**, *378*, 701–703.
- (18) Kahn, O.; Pei, Y.; Verdaguer, M.; Renard, J. P.; Sletten, J. *J. Am. Chem. Soc.* **1988**, *110*, 782–789.
- (19) (a) *Magneto-Structural Correlations in Exchange Coupled Systems*; Willet, R. D., Gatteschi, D., Kahn, O., Eds.; Riedel: Dordrecht, The Netherlands, 1985. (b) *Magnetic Molecular Materials*; Gatteschi, D., Kahn, O., Miller, J. S., Palacio, F., Eds.; Kluwer: Dordrecht, The Netherlands, 1991; pp 157–169. (c) *Biomimetic Materials Chemistry*; Mann, S., Ed.; VCH Publishers: New York, 1995.

- (20) (a) Plass, W. *Angew. Chem., Int. Ed. Engl.* **1996**, *35*, 627–631. (b) Centrone, A.; Harada, T.; Speakman, S.; Hatton, T. A. *Small* **2010**, *6*, 1598–1602.
- (21) (a) Carrano, C. J.; Nunn, C. M.; Quan, R.; Bonadies, J. A.; Pecoraro, V. L. *Inorg. Chem.* **1990**, *29*, 944–951. (b) Castro, S. L.; Cass, M. E.; Hollander, F. J.; Bartley, S. L. *Inorg. Chem.* **1995**, *34*, 466–472. (c) Mohanta, S.; Nanda, K. K.; Ghosh, S.; Mukherjee, M.; Helliwell, M.; Nag, K. *J. Chem. Soc., Dalton Trans.* **1996**, 4233–4238. (d) Das, R.; Nanda, K. K.; Mukherjee, A. K.; Mukherjee, M.; Helliwell, M.; Nag, K. *J. Chem. Soc., Dalton Trans.* **1993**, 2241–2246.
- (22) (a) Sessoli, R.; Gatteschi, D.; Caneschi, A.; Novak, M. A. *Nature* **1993**, *365*, 141–143. (b) Eppley, H. J.; Tsai, H. -L.; de Vries, N.; Folting, K.; Christou, G.; Hendrickson, D. N. *J. Am. Chem. Soc.* **1995**, *117*, 301–317. (c) Powell, A. K.; Heath, S. L.; Gatteschi, D.; Pardi, L.; Sessoli, R.; Spina, G.; Del Giallo, F.; Pieralli, F. *J. Am. Chem. Soc.* **1995**, *117*, 2491–2502. (d) Goldberg, D. P.; Caneschi, A.; Delfs, C. D.; Sessoli, R.; Lippard, S. J. *J. Am. Chem. Soc.* **1995**, *117*, 5789–5800. (e) Benelli, C.; Parsons, S.; Solan, G. A.; Winpenny, R. E. P. *Angew. Chem., Int. Ed. Engl.* **1996**, *35*, 1825–1828. (f) Tsaramyrsi, M.; Kaliva, M.; Salifoglou, A.; Raptopoulou C. P.; Terzis, A.; Tangoulis, V.; Giapintzakis, J. *Inorg. Chem.* **2001**, *40*, 5772–5779.
- (23) Velayutham, M.; Varghese B.; Subramanian, S. *Inorg. Chem.* **1998**, *37*, 1336–1340.
- (24) Sun, Y; Melchior, M; Summers, D. A.; Thompson, C. R.; Rettig, S. J.; Orvig C. *Inorg. Chem.* **1998**, *37*, 3119–3121.
- (25) (a) Wieghardt, K.; Bossek, U.; Volckmar, K.; Swiridoff, W.; Weiss, J. *Inorg. Chem.* **1984**, *23*, 1387–1389. (b) Dean, N. S.; Bond, M. R.; O'Connor, C. J.; Carrano, C. J. *Inorg. Chem.* **1996**, *35*, 7643–7648.
- (26) Rodríguez-Forteza, A.; Alemany, P.; Alvarez, S.; Ruiz, E. *Eur. J. Inorg. Chem.* **2004**, *1*, 143–153.
- (27) (a) Chanda, N.; Laye, R. H.; Chakraborty, S.; Paul, R. L.; Jeffery, J. C.; Ward, M. D.; Lahiri, G. K. *J. Chem. Soc., Dalton Trans.* **2002**, 3496–3504. (b) Sanyal, A.; Banerjee, P.; Lee, G.; Peng, S. M.; Hung, C. J.; Goswami, S. *Inorg. Chem.* **2004**, *43*, 7456–7462.
- (28) (a) Maiti, N.; Pal, S.; Chattopadhyay, S. *Inorg. Chem.* **2001**, *40*, 2204–2205. (b) Datta, P.; Sardar, D.; Mitra, P.; Sinha, C. *Polyhedron* **2011**, *30*, 1516–1523.

- (29) (a) Sarker, K. K.; Saha, S.; Halder, S. S.; Banerjee, D.; Mondal, T. K.; Paital, A. R.; Nanda, P. K.; Raghavaiah, P.; Sinha, C. *Inorg. Chim. Acta* **2010**, *363*, 2955–2964. (b) Mondal, J. A.; Saha, G.; Sinha, C.; Palit, D. K. *Phys. Chem. Chem. Phys.* **2012**, *14*, 13027–13034. (c) Ire, M. *Chem. Rev.* **2000**, *100*, 1683–1684.
- (30) (a) Otsuki, J.; Sato, K.; Tsujino, M.; Okuda, N.; Araki, K.; Seno, M. *Chem. Lett.* **1996**, 847–848. (b) Yam, V. W. W.; Lan, V. C. Y.; Cheung, K. K. *J. Chem. Soc., Chem. Commun.* **1995**, 259–261. (c) Marvand, V.; Launay, P. J. *Inorg. Chem.* **1993**, *32*, 1376–1382. (d) Das, A.; Maher, J. P.; McCleverty, J. A.; Badiola, J. A. N.; Ward, M. D. *J. Chem. Soc., Dalton Trans.* **1993**, 681–686.
- (31) (a) Pal, C. K.; Chattopadhyay, S.; Sinha, C.; Chakravorty, A. *Inorg. Chem.* **1994**, *33*, 6140–6147. (b) Pal, C. K.; Chattopadhyay, S.; Sinha, C.; Chakravorty, A. *Inorg. Chem.* **1996**, *35*, 2442–2447 and references therein.
- (32) Acharyya, R.; Peng, S.-M.; Lee, G.-H.; Bhattacharya, S. *Inorg. Chem.* **2003**, *42*, 7378–7380 and references therein.
- (33) (a) Bag, N.; Lahiri, G. K.; Chakravorty, A. *Inorg. Chem.* **1992**, *31*, 40–45. (b) Lahiri, G. K.; Bhattacharya, S.; Goswami, S.; Chakravorty, A. *J. Chem. Soc., Dalton Trans.* **1990**, 561–565. (c) Mishra, T. K.; Das, D.; Sinha, C.; Ghosh, P.; Pal, C. K. *Inorg. Chem.* **1998**, *37*, 1672–1678.
- (34) (a) Chattopadhyay, S.; Sinha, C.; Basu, P.; Chakravorty, A. *Organometallics* **1991**, *10*, 1135–1139. (b) Pal, C. K.; Chattopadhyay, S.; Sinha, C.; Chakravorty, A. *J. Organomet. Chem.* **1992**, *439*, 91–99 and references therein.
- (35) (a) Sinha, C.; Bandyapadhyay, D.; Chakravorty, A. *Inorg. Chem.* **1988**, *27*, 1173–1178. (b) Mahapatra, A. K.; Bandyapadhyay, D.; Bandyapadhyay, P.; Chakravorty, A. *Inorg. Chem.* **1986**, *25*, 2214–2221. (c) Sinha, C.; Bandyapadhyay, D.; Chakravorty, A. *J. Chem. Soc., Chem. Commun.* **1988**, 468–470.
- (36) (a) Dinda, R.; Sengupta, P.; Ghosh, S.; Mak, T. C. W. *Inorg. Chem.* **2002**, *41*, 1684–1688. (b) Dinda, R.; Sengupta, P.; Sutradhar, M.; Mak, T. C. W.; Ghosh, S. *Inorg. Chem.* **2008**, *47*, 5634–5640. (c) Dash, S. P.; Pasayat, S.; Bhakat, S.; Dash, H. R.; Das, S.; Butcher, R. J.; Dinda, R. *Polyhedron* **2012**, *31*, 524–529. (d) Dash, S. P.; Panda, A. K.; Pasayat, S.; Dinda, R.; Biswas, A.; Tiekink, E. R. T.; Patil, Y. P.; Nethaji, M.; Kaminsky, W.; Mukhopadhyay, S.; Bhutia, S. *Dalton Trans.* **2014**, *43*, 10139–10156. (e) Dash, S. P.; Panda, A. K.; Pasayat, S.; Dinda, R.; Biswas, A.; Tiekink, E. R. T.; Mukhopadhyay, S.;

- Bhutia, S. K.; Kaminsky, W.; Sinn, E. *RSC Adv.* **2015**, *5*, 51852–51867. (f) Dash, S. P.; Majumder, S.; Banerjee, A.; Carvalho, M. F. N. N.; Adão, P.; Pessoa, J. C.; Brzezinski, K.; Garribba, E.; Reuter, H.; Dinda, R. *Inorg. Chem.* **2016**, *55*, 1165–1182. (g) Dash, S. P.; Pasayat, S.; Saswati; Roy, S.; Dinda, R.; Tiekink, E. R. T.; Mukhopadhyay, S.; Bhutia, S.; Hardikar, M. R.; Joshi, B.; Patil, Y. P.; Nethaji, M. *Inorg. Chem.* **2013**, *52*, 14096–14107. (h) Dash, S. P.; Panda, A. K.; Pasayat, S.; Majumder, S.; Biswas, A.; Kaminsky, W.; Mukhopadhyay, S.; Bhutia, S. K.; Dinda, R. *J. Inorg. Biochem.* **2015**, *144*, 1–12.
- (37) (a) Sanna, D.; Várnagy, K.; Lihi, N.; Micera, G.; Garribba, E. *Inorg. Chem.* **2013**, *52*, 8202–8213. (b) Bhattacharya, S.; Ghosh, T. *Transition Met. Chem.* **2002**, *27*, 89–94. (c) Bhattacharya, S.; Ghosh, T. *J. Indian Chem. Soc.* **1999**, *76*, 373–377. (d) Dutta, S.; Basu, P.; Chakravorty, A. *Inorg. Chem.* **1993**, *32*, 5343–5348. (e) Chakravarty, J.; Dutta, S.; Chandra, S. K.; Basu, P.; Chakravorty, A. *Inorg. Chem.* **1993**, *32*, 4249–4255. (f) Chakravarty, J.; Dutta, S.; Chakravorty, A. *J. Chem. Soc., Chem. Commun.* **1993**, 1091–1092.
- (38) (a) Drew, H. D. K.; Landquist, J. K. *J. Chem. Soc.* **1938**, 292–304. (b) Aleya, A. E.; Malek, A. *Can. J. Chem.* **1975**, 939–944. (c) Bakshi, S.; Acharyya, R.; Dutta, S.; Blake, A. J.; Drew, M. G. B.; Bhattacharya, S. *J. Organomet. Chem.* **2007**, *692*, 1025–1032.
- (39) Bruker, *APEX 2 - Suite of Crystallographic Software*. **2008**: Madison, Wisconsin, USA.
- (40) *SAINT*. 2008, Bruker AXS Inc.: Madison, Wisconsin, USA.
- (41) *SADABS*. 2008, Bruker AXS Inc.: Madison, Wisconsin, USA.
- (42) Hahn, T. ed. *International Tables for Crystallography* 4th ed. Vol. A Space-Group Symmetry. 1996, Kluwer Academic Publishers: Dordrecht.
- (43) Sheldrick, G.M. *A short history of SHELX*. *Acta Cryst.* **2008**, *A34*, 112–122.
- (44) Wilson, A. J. C. ed. *International Tables for Crystallography*. Vol. C. 1992, Kluwer Academic Publishers: Dordrecht.
- (45) Brandenburg, K. *Diamond - Crystal and Molecular Visualization*. 2006, Crystal Impact: Bonn, Germany.
- (46) Macrae, C.F.; Bruno, I.J.; Chisholm, J.A.; Edgington, P.R.; McCabe, P.; Pidcock, E.; Rodriguez-Monge, L.; Taylor, R.; van de Streek, J.; Wood, P.A. *Appl. Crystallogr.* **2008**, *41*, 466–470.

- (47) Otwinowsky, Z.; Minor, W. In: *Methods in Enzymology*; Carter, C. W., Jr., Sweet, R. M., Eds.; Academic Press: New York, 1997, 276, 307–326.
- (48) (a) Altomare, A.; Burla, C.; Camalli M.; Cascarano L.; Giacovazzo C.; Guagliardi A.; Moliterni A. G. G.; Polidori, G.; Spagna, R. *J. Appl. Cryst.* **1999**, 32, 115–119. (b) Altomare, A., Cascarano, G., Giacovazzo, C., Guagliardi, A. *J. Appl. Cryst.* **1993**, 26, 343–350.
- (49) Sheldrick, G. M. SHELXL-97: Program for the Refinement of Crystal Structures **1997** University of Gottingen, Germany.
- (50) Mackay, S.; Edwards, C.; Henderson, A.; Gilmore, C.; Stewart, N.; Shankland, K.; Donald, A.; *MaXus: a computer program for the solution and refinement of crystal structures from diffraction data*. University of Glasgow, Scotland, 1997.
- (51) Farrugia, L. *J. Appl. Cryst.* 1997, 30, 565.
- (52) Waasmaier, D.; Kirfel, A. *Acta Crystallogr. A.* **1995**, 51, 416.
- (53) (a) TURBOMOLE V6.6 2014, a development of University of Karlsruhe and Forschungszentrum Karlsruhe GmbH, 1989–2007, TURBOMOLE GmbH, since 2007; available from <http://www.turbomole.com>. (b) Ahlrichs, R.; Bär, M.; Häser, M.; Horn, H.; Kölmel C. *Chem. Phys. Lett.* **1989**, 162, 165–253.
- (54) Perdew, J. P. *Phys. Rev. B* **1986**, 33, 8822–8824.
- (55) Becke, A. D. *Phys. Rev. A* **1988**, 38, 3098–3100.
- (56) (a) Schäfer, A.; Horn, H.; Ahlrichs, R. *J. Chem. Phys.* **1992**, 97, 2571–2577. (b) Weigend, F.; Häser, M.; Patzelt, H.; Ahlrichs, R. *Chem. Phys. Lett.* **1998**, 294, 143–152. (c) Weigend, F.; Ahlrichs, R. *Phys. Chem. Chem. Phys.* **2005**, 7, 3297–3305.
- (57) (a) Baerends, E.; Ellis D.; Ros, P. *Chem. Phys.* **1973**, 2, 41–51. (b) Whitten, J. L. *J. Chem. Phys.* **1973**, 58, 4496–4501. (c) Dunlap; B. I.; Connolly, J. W. D.; Sabin, J. R. *J. Chem. Phys.* **1979**, 71, 3396–3402. (d) Van Alsenoy, C. *J. Comput. Chem.* **1988**, 9, 620–626.
- (58) Yamaguchi, K.; Tsunekawa, T.; Toyoda, Y.; Fueno, T. *Chem. Phys. Lett.* **1988**, 143, 371–376.
- (59) Becke, A. D. *J. Chem. Phys.* **1993**, 98, 5648–5652.
- (60) Lee, C.; Yang, W.; Parr, R. G. *Phys. Rev. B: Condens. Matter Mater. Phys.* **1988**, 37, 785–789.

- (61) (a) Tao, J.; Perdew, J. P.; Staroverov, V. N.; Scuseria, G. E. *Phys. Rev. Lett.* **2003**, *91*, 146401–146414. (b) V. N. Staroverov, G. E. Scuseria, J. Tao, J. P. Perdew, *J. Chem. Phys.* **2003**, *119*, 12129–12137.
- (62) Serpe, L.; Catalano, M.; Cavalli, R.; Ugazio, E.; Bosco, O.; Canaparo, R.; Muntoni, E.; Frairia, R.; Gasco, M. R.; Eandi, M.; Zara, G. P. *Eur. J. Pharmaceut. Biopharmaceut.* **2004**, *58*, 673–680.
- (63) Wang, X.; Tanaka, M.; Krstin, S.; Peixoto, H. S.; de Melo Moura, C. C.; Wink, M. *Eur. J. Pharmacol.* **2016**, *789*, 265–274.
- (64) Halder, S.; Drew, M. G. B.; Bhattacharya, S. *J. Chem. Sci.* **2008**, *120*, 441–446.
- (65) Li, Y.; Yan, C.; Gua, B.; Liao, D. *Polyhedron* **1997**, *16*, 4379–4384.
- (66) Chatterjee, P. B.; Bhattacharya, S.; Audhya, A.; Ki-Young, C.; Endo, A.; Chaudhury, M. *Inorg. Chem.* **2008**, *47*, 4891–4902.
- (67) Smith, I. K.; Borer, L. L.; Olmstead, M. M. *Inorg. Chem.* **2003**, *42*, 7410–7415.
- (68) Addison, A. W.; Rao, T. N.; Reedijk, J.; van Rijn, J.; Verschoor, G. C. *J. Chem. Soc., Dalton Trans.* **1984**, 1349–1356.
- (69) (a) Tarlton, M. L.; Anderson, A. E.; Weberski Jr. M. P.; Riart-Ferrer, X.; Nelson, B. M.; McLaughlan, C. C. *Inorg. Chim. Acta* **2014**, *420*, 159–165. (b) Raja, K. K.; Lekha, L.; Hariharan, R.; Easwaramoorthy, D.; Rajagopal, G. *J. Mol. Struct.* **2014**, *1075*, 227–233. (c) Sartzi, H.; Stoumpos, C. C.; Giouli, M.; Verginadis, I. I.; Karkabounas, S.; Cunha-Silva, L.; Escuer, A.; Perlepes, S. P. *Dalton Trans.* **2012**, *41*, 11984–11988. (d) Hanninen, M. M.; Peuronen, A.; Damlin, P.; Tyystjarvi, V.; Kivela, H.; Lehtonen, A. *Dalton Trans.* **2014**, *43*, 14022–14028.
- (70) Cramer, C. J.; Truhlar, D. G. *Phys. Chem. Chem. Phys.* **2009**, *11*, 10757–10816.
- (71) Jensen, K. P. *Inorg. Chem.* **2008**, *47*, 10357–10365.
- (72) Plass, W. *Inorg. Chem.* **1997**, *36*, 2200–2205.
- (73) Plass, W. *Z. Anorg. Allg. Chem.* **1997**, *623*, 1290–1298.
- (74) Reed, A. E.; Weinstock, R. B.; Weinhold, F. *J. Chem. Phys.* **1985**, *83*, 735–746.
- (75) El-Awady R. A.; Semreen, M. H.; Saber, M. M.; Cyprian, F.; Menon, V.; Al-Tel, T. H. *DNA repair.* **2016**, *37*, 1–11.
- (76) Jordan M. A; Wilson, L. *Curr. Opin. Cell Biol.* **1998**, *10*, 123–130.
- (77) Siddik, Z. H. *Oncogene* **2003**, *22*, 7265–7279.

- (78) Temperini, C.; Messori, L.; Orioli, P.; Di Bugno, C.; Animati, F.; Ughetto, G. *Nucleic Acids Res.* **2003**, *31*, 1464–1469.
- (79) Wani, M. C.; Taylor, H. L.; Wall, M. E.; Coggon, P.; McPhail, A. T. *J. Am. Chem. Soc.* **1971**, *93*, 2325–2327.
- (80) Jordan, M. A.; Wilson, L. *Nat. Rev. Cancer* **2004**, *4*, 253–265.
- (81) Sasse, F.; Kunze, B.; Gronewold, T. M.; Reichenbach, H. *J. Natl. Cancer Inst.* **1998**, *90*, 1559–1563.
- (82) Filaments, A. *J. Cell Biol.* **1987**, *105*, 1473–1478.
- (83) Lee, E. A.; Keutmann, M. K.; Dowling, M. L.; Harris, E.; Chan, G.; Kao, G. D. *Mol. Cancer Ther.* **2004**, *3*, 661–669.
- (84) Nair, H. K.; Rao, K. V.; Aalinkeel, R.; Mahajan, S.; Chawda, R.; Schwartz, S. A. *Clin. Diagn. Lab. Immunol.* **2004**, *11*, 63–69.
- (85) Stehn, J. R.; Haass, N. K.; Bonello, T.; Desouza, M.; Kottyan, G.; Treutlein, H.; Zeng, J.; Nascimento, P. R.; Sequeira, V. B.; Butler, T. L. *Cancer Res.* **2013**, *73*, 5169–5182.
- (86) Dougherty, D. A. *Science* **1996**, *271*, 63.
- (87) Pasayat, S.; Dash, S. P.; Majumder, S.; Dinda, R.; Sinn, E.; Stoeckli-Evans, H.; Mukhopadhyay, S.; Bhutia, S. K.; Mitra, P. *Polyhedron* **2014**, *80*, 198–205.
- (88) Saswati; Chakraborty, A.; Dash, S. P.; Panda, A. K.; Acharyya, R.; Biswas, A.; Mukhopadhyay, S.; Bhutia, S. K.; Crochet, A.; Patil, Y. P.; Nethaji, M.; Dinda, R. *Dalton Trans.* **2015**, *44*, 6140–6157.
- (89) Banerjee, S.; Hussain, A.; Prasad, P.; Khan, I.; Banik, B.; Kondaiah, P.; Chakravarty, A. R. *Eur. J. Inorg. Chem.* **2012**, 3899–3908.
- (90) Balaji, B.; Balakrishnan, B.; Perumalla, S.; Karande, A. A.; Chakravarty, A. R. *Eur. J. Med. Chem.* **2014**, *85*, 458–467.
- (91) Lewis, N. A.; Liu, F.; Seymour, L.; Magnusen, A.; Erves, T. R.; Arca, J. F.; Beckford, F. A.; Venkatraman, R.; Sarrías, A. G.; Fronczek, F. R.; VanDerveer, D. G.; Seeram, N. P.; Liu, A.; Jarrett W. L.; Holder, A. A. *Eur. J. Inorg. Chem.* **2012**, 664–677.

Chapter 3

*Synthesis, structure and characterization of mono- and trinuclear
oxidovanadium(IV) azo complexes: Study of antiproliferative and
insulin-mimetic activity*

Chapter 3

Synthesis, structure and characterization of mono- and trinuclear oxidovanadium(IV) azo complexes: Study of antiproliferative and insulin-mimetic activity

ABSTRACT

Three monooxidovanadium(IV), $[V^{IV}OL^{1-3}_2]$ (**1-3**), and two alkoxido bridged trioxidovanadium(IV) $[V^{IV}_3O_3(\mu\text{-OMe})_3(\mu_3\text{-OMe})L^{4,5}_2]$ (**4** and **5**), complexes have been reported, which were obtained upon reaction of 2-((2-X)-diazol)-4-methylphenol (where X = benzo[1,3]dioxol-5-yl (HL¹), phenyl (HL²) and 4-methoxyphenyl (HL³)), 1-(2-(thiazol-2-yl)diazenyl)naphthalene-2-ol (HL⁴) and 2-(2-(thiazol-2-yl)diazenyl)-4-methylphenol (HL⁵) with $VOSO_4 \cdot 5H_2O$. The synthesized complexes were successfully characterized by elemental analysis, IR and UV-vis spectroscopy, ESI-MS and their redox properties studied by cyclic voltammetry. Molecular structure of **4** has been determined by single crystal X-ray diffraction study. X-ray structure showed the molecule to be composed of three slightly distorted octahedral vanadium atoms forming an almost butterfly-shaped V_3O_4 unit similar to the well-known 3Fe-4S iron sulfur cluster. The complexes were probed for their *in vitro* insulin-mimetic activity against insulin responsive L6 myoblast cells. The complexes (**1-5**) have been screened for their cytotoxicity in human breast adenocarcinoma cell line, MCF-7. The cytotoxicity of the complex is affected by the functional groups on the arylazo ligand backbone. IC_{50} values of the complexes were found to be comparable with some of the clinically referred chemotherapeutic drugs. The insulin-mimetic activity of **1-5** was probed on rat L6 myoblast cells. The percent glucose uptake of the complexes was found to be significant as compared to insulin, where complex **2** (25 μM) proved to be most potent. In order to further confirm whether these compounds act via insulin signaling pathway, immunoblot analysis for IRS-1 was carried out.

3.1. INTRODUCTION

Vanadium coordination chemistry with O–N oligodentate ligands has aroused continued interest ever since the presence of vanadium was unraveled in certain ascidians, *Amanita* mushrooms,¹ and various enzymes,² in addition to its interesting chemistry.

Over the past few years, vanadium compounds have flourished as potent therapeutic agents for the treatment of malignancies.³ It is established that vanadium inhibits growth and the spread of tumors by suppressing the proliferation of tumor cells and inducing apoptosis, and also by limiting invasion and the metastatic potential of neoplastic cells.⁴ Review of both the chemical and biological traits of the existing vanadoforms triggered the design of vanadium complexes to promote anticancer activity with effectiveness, selectivity and specificity.⁵ The ternary hybrid vanadium-peroxido-betaine species, $\{\text{Na}_2[\text{V}_2\text{O}_2(\text{O}_2)_4\{\text{L}\}_2]\}_n \cdot 4n\text{H}_2\text{O}$, $\text{L} = \text{Me}_3\text{N}(+)\text{-CH}_2\text{-COO}(-)$, has been known to inhibit the Ras signaling pathway in a dose-dependent fashion and the downstream cancer marker MMP-2 in both MCF-7 and A549 cancer cell lines.⁶

Moreover, the potential of inorganic vanadyl and vanadate, as well as some vanadium(IV) and (V) complexes as insulin mimics and possible alternative to insulin in the treatment of diabetes, is continuously being exploited.^{7–20} The discovery of the insulin mimesis of oxidovanadates(V),²¹ the oxidovanadium(IV) precursor, vanadyl sulphate,²² and the much more potent bis(ethylmaltolato)oxovanadium(IV) (BEOV) and bis(maltolato)oxovanadium(IV) (BMOV),²³ which have completed phase II clinical trials,²⁴ also stimulate the search for vanadium complexes which may have application in the treatment of type II diabetes.^{25,26} Attempts have been made to identify more potent and orally active organic vanadium complexes, and also to understand how structural differences in inhibitors for phosphatase translate to functional differences in alleviating the symptoms of diabetes.^{27–30} Although the said complexes have shown pharmacological advantages compared to the uncomplexed $\text{VOSO}_4 \cdot 5\text{H}_2\text{O}$, further improvement in ligand design is needed, focusing on development of new vanadium complexes with increased potency and decreased toxicity.³¹

In this respect, coordinating ligands with azo functionality could be utilized, considering the structural modifiability, the possibility of high environmental stability, and the diversity of electronic properties of azo transition metallic chelates.^{32,33} Furthermore, azo compounds are known to be involved in many biological reactions such as DNA and

RNA inhibition, and protein synthesis,^{34,35} in addition to its utility in the chemical industry.³⁶⁻³⁹ Besides the role of bis-azo compound, FP-21399, as potent anti-human immunodeficiency virus (HIV) agent,⁴⁰ other pharmaceutical application of azo compounds, such as, site-specific drug delivery in colon diseases such as colitis and irritable bowel syndrome⁴¹ and antimicrobial activity against both gram positive and negative bacteria (*Escherichia coli*, *Pseudomonas aeruginosa*, *Proteus vulgaris*, *Staphylococcus aureus* and *Streptococcus pyogenes*) and fungi species (*Candida albicans*)⁴² have also been explored. Interest in the synthesis of thiazole ring containing azo ligands stems from the extensive research of the pharmacological properties exhibited by compounds utilizing this heterocyclic moiety;⁴³ for example, for the treatment of Parkinson's disease and also as anti-Alzheimer⁴⁴ and anticonvulsant drugs.⁴⁵ In addition, thiazole derivatives have also been explored for their antitumor and antidiabetic activities.^{46,47} β -naphthol moieties are yet another important pharmacophoric cores of several anticancer, hypotensive and bradycardiac drugs.⁴⁸ So, the combined effects of thiazole and β -naphthol can be utilized to design new biological complexes of enhanced pharmacological utility. Again, while many azo complexes exhibit good biological activities, their aqueous solubility is still inadequate, which may restrict their application. Hence, synthesis of some new water-soluble transition metal complexes of azophenols appeared to be of interest, which may also have significant pharmacological effects.

Considering the rarity in literature of alkoxido bridged V(IV) clusters using organic ligands, in addition to the possible applicability of vanadium(IV) and azo compounds in biology,¹⁻⁴² as well as a continuation of our ongoing research on the study of pharmacological properties of transition metal complexes,⁵⁰ herein we report the synthesis of some new water soluble vanadium(IV) mono-, $[\text{V}^{\text{IV}}\text{OL}^{1-3}_2]$ (**1-3**), and trinuclear, $[\text{V}^{\text{IV}}_3\text{O}_3(\mu\text{-OMe})_3(\mu_3\text{-OMe})\text{L}^{4,5}_2]$ (**4** and **5**) complexes using bi- and tridentate azo ligands. It is noteworthy to mention that although coordination chemistry of the V^{III} ⁵¹ and mixed valence trinuclear vanadium cluster complexes⁵² are established, reports of structurally characterized homovalent trinuclear V^{IV} complexes remain limited.^{53,54} Though trinuclear V species with inorganic phosphonate and silsesquioxane bridging compounds have been isolated,⁵³ fully reduced examples of such complexes using organic ligands remain scarce.⁵⁴ The mono- and trioxidovanadium(IV) complexes were characterized by spectroscopic techniques, and further structural evidence for the formation of complex **4**

was obtained by X-ray crystallography. The cytotoxicity of the complexes against MCF-7 breast cancer cell line was assessed by the MTT assay. The insulin-mimetic activity of these complexes was investigated on immortalized rat skeletal L6 myoblast cell line and to further confirm whether these compounds act via insulin signaling pathway, the immunoblot analysis for IRS-1 molecule was also carried out.

3.2. EXPERIMENTAL SECTION

3.2.1. General Methods and Materials

Reagent grade solvents were dried and distilled prior to use. All other chemicals were reagent grade, available commercially and used as received. Commercially available TBAP (tetra butyl ammonium perchlorate) was properly dried and used as a supporting electrolyte for recording cyclic voltammograms of the complexes. MCF-7 (human breast adenocarcinoma cell line) was procured from NCCS, Pune. Penicillin, streptomycin, Dulbecco's modified Eagle's medium (DMEM), Fetal Bovine Serum (FBS) and insulin were purchased from Invitrogen (San Diego, CA, USA) and glucose estimation kit from Coral clinical systems. Rat L6 myoblast cell line was procured from NCCS, Pune. Anti- β -actin antibodies, HRP-conjugated secondary antibodies, bicinchoninic acid kit, ECL western blotting detection reagents and autoradiography films (Kodak) were purchased from Sigma. Anti-IRS1 antibody and phosphate buffered saline (PBS) were purchased from Life technologies.

Elemental analyses were performed on a Vario ELcube CHNS Elemental analyzer. IR spectra were recorded on a Perkin–Elmer Spectrum RXI spectrometer. ^1H NMR spectra were recorded with a Bruker Ultrashield 400 MHz spectrometer using SiMe_4 as an internal standard. Electronic spectra were recorded on a Lambda25, PerkinElmer spectrophotometer. ESI–MS were obtained on a SQ–300 MS and Thermo DSQ II instruments operating in both positive and negative ion ESI mode. Electrochemical data were collected using a PAR electrochemical analyzer and a PC–controlled Potentiostat/Galvanostat (PAR 273A) at 298 K in a dry nitrogen atmosphere. Cyclic voltammetry experiments were carried out with a Pt working electrode, Pt counter electrode and Ag/AgCl as reference electrode.

3.2.2. Synthesis of Ligands (HL¹⁻⁵)

Azo ligands were prepared under stirring condition at a temperature below 5 °C by diazo coupling of diazotized aniline or its substituted derivatives with p-cresol (HL¹⁻³) and coupling of diazotised 2-aminothiazole with β -naphthol (HL⁴) or p-cresol (HL⁵).⁵⁵ The resulting compounds were washed with water and dried over fused CaCl_2 . Purified ligands were obtained by slow evaporation of the saturated ethanolic solution of the crude products.

HL¹. Yield: 80%. Anal. Calc. for C₁₄H₁₂N₂O₃ (%): C, 65.62; H, 4.72; N, 10.93. Found: C, 65.64; H, 4.70; N, 10.92. IR (KBr pellet, cm⁻¹): 3542 ν (O-H)_b, 1549 ν (N=N). ¹H NMR (400 MHz, CDCl₃, ppm): δ 12.56 (s, 1H, -OH), 7.70–6.06 (m, 6H, aromatic), 4.23 (s, 2H, -O-CH₂-O), 2.39 (s, 3H, -CH₃). ¹³C NMR (100 MHz, CDCl₃, ppm): δ 153.60–115.88 (12C, aromatic), 101.02(-O-CH₂-O), 24.30(-CH₃).

HL². Yield: 88%. Anal. Calc. for C₁₃H₁₂N₂O (%): C, 73.56; H, 5.70; N, 19.16. Found: C, 54.77; H, 4.16; N, 19.20. IR (KBr pellet, cm⁻¹): 3337 ν (O-H)_b, 1544 ν (N=N). ¹H NMR (400 MHz, CDCl₃, ppm): δ 12.72 (s, 1H, -OH), 7.86–6.90 (m, 8H, aromatic), 2.37 (s, 3H, -CH₃). ¹³C NMR (100 MHz, CDCl₃, ppm): δ 150.63–117.86 (12C, aromatic), 20.32 (-CH₃).

HL³. Yield: 85%. Anal. Calc. for C₁₄H₁₄N₂O₂ (%): C, 69.41; H, 5.82; N, 11.56. Found: C, 69.45; H, 5.83; N, 11.58. IR (KBr pellet, cm⁻¹): 3330 ν (O-H)_b, 1542 ν (N=N). ¹H NMR (400 MHz, CDCl₃, ppm): δ 12.00 (s, 1H, -OH), 7.80–6.95 (m, 7H, aromatic), 2.50 (s, 3H, -OCH₃), 2.32 (s, 3H, -CH₃). ¹³C NMR (100 MHz, CDCl₃, ppm): δ 162.90–115.88 (12C, aromatic), 55.00 (-OCH₃), 19.91 (-CH₃).

HL⁴. Yield: 88%. Anal. calc. for C₁₃H₉N₃OS: C, 61.16; H, 3.55; N, 16.46. Found: C, 61.18; H, 3.58; N, 16.48. IR (KBr pellet, cm⁻¹): 3510 ν (O-H)_b; 1504 ν (N=N); 1412 ν (C-O)_{phenolic}. ¹H NMR (400 MHz, CDCl₃, ppm): δ 14.87 (s, 1H, OH), 8.55–6.97 (m, 8H, aromatic). ¹³C NMR (100 MHz, CDCl₃, ppm): δ 172.82–109.50 (13C, aromatic).

HL⁵. Yield: 70%. Anal. calc. for C₁₀H₉N₃OS: C, 54.78; H, 4.14; N, 19.16. Found: C, 54.77; H, 4.16; N, 19.15. IR (KBr pellet, cm⁻¹): 3337 ν (O-H)_b, 1532 ν (N=N); 1419 ν (C-O)_{phenolic}. ¹H NMR (400 MHz, CDCl₃, ppm): δ 10.50 (s, 1H, OH), 8.05–6.97 (m, 5H, aromatic), 2.23 (s, 3H, -CH₃). ¹³C NMR (100 MHz, CDCl₃, ppm): δ 155.06–118.95 (9C, aromatic), 20.34 (-CH₃).

3.2.3. Synthesis of the complexes (1–5)

[VOL¹₂] (1): Triethylamine (100 mg, 1 mmol) was added to 15 ml methanolic solution of the ligand, HL¹ (156 mg, 1 mmol) under refluxing condition. The reddish yellow turbid solution became clear upon addition of base, triethylamine. 1 mmol VOSO₄·5H₂O (252 mg, 1 mmol) was then added to the refluxing solution. The color changed to greenish

black after an hour of reflux. Reflux continued for 68 h. Greenish black amorphous residue was isolated upon filtration. Yield: 62%. Elemental analyses are satisfactory with the general formula $C_{28}H_{22}N_4O_7V$. Anal. Calc. for $C_{28}H_{22}N_4O_7V$ (%): C, 58.24; H, 3.84; N, 9.70. Found: C, 58.23; H, 3.83; N, 9.71. IR (KBr pellet, cm^{-1}): 1472 $\nu(N=N)$; 972 $\nu(V=O)$. ESI-MS (CH_3CN): m/z 577.52 $[M]^+$.

$[VOL^2_2]$ (**2**): This complex was obtained as a greenish black amorphous residue, following the same reaction conditions as adopted for **1** using ligand, HL^2 (212 mg, 1 mmol). Yield: 60%. Elemental analyses are satisfactory with the general formula $C_{26}H_{22}N_4O_3V$. Anal. Calc. for $C_{26}H_{22}N_4O_3V$ (%): C, 63.81; H, 4.53; N, 11.45. Found: C, 63.80; H, 4.54; N, 11.44. IR (KBr pellet, cm^{-1}): 1481 $\nu(N=N)$; 980 $\nu(V=O)$. ESI-MS (CH_3CN): m/z 489.11 $[M]^+$.

$[VOL^3_2]$ (**3**): This complex was obtained as greenish black amorphous product following the procedure adopted for **1** using ligand, HL^3 (242 mg, 1 mmol). Yield: 58%. Elemental analyses are satisfactory with the general formula $C_{28}H_{26}N_4O_5V$. Anal. Calc. for $C_{28}H_{26}N_4O_5V$ (%): C, 61.20; H, 4.77; N, 10.20. Found: C, 61.21; H, 4.78; N, 10.21. IR (KBr pellet, cm^{-1}): 1482 $\nu(N=N)$; 984 $\nu(V=O)$. ESI-MS (CH_3CN): m/z 549.51 $[M]^+$.

$[V^{IV}_3O_3(\mu-O Me)_3(\mu_3-O Me)L^4_2]$ (**4**): Dirty green crystalline residue was isolated upon filtration, following the procedure adopted for **1** using ligand, HL^4 (255 mg, 1 mmol). Yield: 65%. Elemental analyses are satisfactory with the general formula $C_{30}H_{28}N_6O_9S_2V_3$. Anal. calc. for $C_{30}H_{28}N_6O_9S_2V_3$: C, 43.23; H, 3.39; N, 10.08. Found: C, 43.26; H, 3.46; N, 10.02. IR (KBr pellet, cm^{-1}): 1494 $\nu(N=N)$; 935, 916 $\nu(V=O)$, 837 $\nu(V-O-V)$. ESI-MS (CH_3CN): m/z 832.87 $[M-H]^+$.

$[V^{IV}_3O_3(\mu-O Me)_3(\mu_3-O Me)L^5_2]$ (**5**): This complex was obtained as black amorphous product following the same synthetic procedure adopted for **1** using ligand, HL^2 (1 mmol, 219 mg). Yield: 61%. Elemental analyses are satisfactory with the general formula $C_{20}H_{16}N_6O_6S_2V_2$. Anal. calc. for $C_{24}H_{28}N_6O_9S_2V_3$: C, 37.86; H, 3.71; N, 11.04. Found: C, 37.93; H, 3.79; N, 11.09. IR (KBr pellet, cm^{-1}): 1485 $\nu(N=N)$; 972, 933 $\nu(V=O)$; 854 $\nu(V-O-V)$. ESI-MS (CH_3CN): m/z 763.11 $[M+2H]^+$.

3.2.4. X-Ray Crystallography

A black prism of complex **4** measuring 0.04 x 0.02 x 0.02 mm³, was mounted on a loop with oil. Data was collected at -173°C on a Bruker APEX II single crystal X-ray diffractometer, Mo-radiation.

Crystal-to-detector distance was 40 mm and exposure time was 180 seconds per frame for all sets. The scan width was 0.5°. Data collection was 100 % complete to 25° in θ . A total of 38402 reflections were collected covering the indices, $-21 \leq h \leq 21$, $-27 \leq k \leq 27$, $-10 \leq l \leq 10$. 6100 reflections were symmetry independent and the $R_{\text{int}} = 0.1879$ reflects the small sample size. Indexing and unit cell refinement indicated a primitive monoclinic lattice. The space group was found to be P 2₁/c (No. 14).

The data was integrated and scaled using SAINT, SADABS within the APEX2 software package by Bruker.⁵⁶

Solution by direct methods (SHELXS, SIR97)⁵⁷ produced a complete heavy atom phasing model consistent with the proposed structure. The structure was completed by difference Fourier synthesis with SHELXL97.^{58,59} Scattering factors are from Waasmair and Kirfel.⁶⁰ Hydrogen atoms were placed in geometrically idealised positions and constrained to ride on their parent atoms with C---H distances in the range 0.95–1.00 Angstrom. Isotropic thermal parameters U_{eq} were fixed such that they were 1.2 U_{eq} of their parent atom U_{eq} for CH's and 1.5 U_{eq} of their parent atom U_{eq} in case of methyl groups. All non-hydrogen atoms were refined anisotropically by full-matrix least-squares. Table 3.1 summarizes the data collection details.

Table 3.1. Crystal data and refinement details for $[V^{IV}_3O_3(\mu\text{-OMe})_3(\mu_3\text{-OMe})L^4_2]$ (**4**)

| Complex | 4 |
|-----------------------------------|---|
| Empirical formula | $C_{30}H_{28}N_6O_9S_2V_3$ |
| Formula weight | 833.52 |
| Temperature | 100(2) K |
| Wavelength | 0.71073 Å |
| Crystal system | Monoclinic |
| Space group | P 21/c |
| a (Å) | 17.723(2) Å |
| b (Å) | 22.825(3) Å |
| c (Å) | 8.3250(12) Å |
| α (°) | 90° |
| β (°) | 100.411(10)° |
| γ (°) | 90° |
| Volume | 3312.2(7) Å ³ |
| Z | 4 |
| Density (calculated) | 1.671 Mg/m ³ |
| Absorption coefficient | 1.019 mm ⁻¹ |
| F(000) | 1692 |
| Crystal size | 0.04 x 0.02 x 0.02 mm ³ |
| Theta range for data collection | 1.47 to 25.49° |
| Index ranges | -21 ≤ h ≤ 21, -27 ≤ k ≤ 27, -10 ≤ l ≤ 10 |
| Reflections collected | 38402 |
| Independent reflections | 6100 [R(int) = 0.1879] |
| Completeness to theta = 25.00° | 100.0 % |
| Max. and min. transmission | 0.9799 and 0.9604 |
| Refinement method | Full-matrix least-squares on F ² |
| Data / restraints / parameters | 6100 / 0 / 455 |
| Goodness-of-fit on F ² | 1.008 |
| Final R indices [I > 2σ(I)] | R1 = 0.0790, wR2 = 0.1517 |

R indices (all data)

R1 = 0.1834, wR2 = 0.1898

Largest diff. peak and hole

0.964 and -0.430 e.Å⁻³

3.2.5. Cytotoxicity studies

3.2.5.1. MTT assay

MCF-7 cells were cultured in DMEM containing 10% FBS and penicillin (100 U/ml) and streptomycin (100 µg/ml) in a humidified 5% CO₂ incubator at 37 °C. The cytotoxicity was assayed by determining the viability of MCF-7 cells after treatment by MTT assay. Briefly, MCF-7 cells (10⁵ cells/well) were seeded in 96-well plates in DMEM containing 10% FBS. After cells reached confluency, treatment was given with varying concentrations (5, 10, 25 and 50 µM) of the vanadium compounds. The compounds were dissolved in DMSO and working solutions were prepared by diluting the stock of 5 mM of each compound with plain DMEM. Final working concentration of DMSO in assay was less than 2%. Untreated cells were taken as 100% survival. After the treatment, medium was removed and cells were incubated with MTT (5 mg/ml) for 4 h. The crystals formed were dissolved in DMSO and absorbance was noted at 595 nm. IC₅₀ was calculated for each compound by treating the cells for 48 h.

3.2.5.2. Nuclear Morphology study using DAPI Staining

DAPI (4',6-diamidino-2-phenylindole dihydrochloride) staining was performed to see the morphology of the nuclei after treatment. The cells were grown in the 96-well plate. After reaching approximately 90% confluency, the cells were treated with vanadium complexes at different concentrations (5, 10, 25 and 50 µM) and were incubated for 48 h. The cells were washed with PBS and fixed in 3.7% of formaldehyde for 15 min. Then the cells were treated with 0.2% triton-X 100 and 2% BSA in PBS for 30 s. The cells were stained with DAPI for 30 min in dark and imaged under fluorescence microscope (FLoid, Life technologies).

3.2.6. *In Vitro* Insulin-Mimetic Activity

L6 myoblast were cultured in DMEM containing 10% FBS and penicillin (100 U/ml) and streptomycin (100 $\mu\text{g/ml}$) in a humidified 5% CO_2 incubator at 37 °C. To differentiate myotubes, the myoblast cells (5×10^4) were seeded in 24 well plates in DMEM containing 2% FBS. The myoblast cells (5×10^4) were grown for 11 days in 0.4 ml of 2% FBS/DMEM to allow the formation of myotubes. The medium was changed in every 2 days. On the 10th day cells were washed and incubated with plain DMEM containing 25 mM glucose overnight to induce hyperglycemia.⁶¹ On the 11th day, cells were incubated in Kreb's bicarbonate buffer (KRBB) for 2 h. Myotubes were further cultured in KRBB along with 25 mM glucose and 10, 25 and 50 μM of vanadium compounds (1–5) and $\text{VOSO}_4 \cdot 5\text{H}_2\text{O}$ for 4 h. The insulin (100 nM) was taken as positive control.⁶² The buffer aliquots were collected at time 0 and 240 min. The residual glucose in the buffer aliquots remaining in each well after 4 h was estimated using glucose estimation kit (Coral systems, GOD/POD method).

3.2.7. Immunoblot analysis

3.2.7.1. Analysis of accumulation of IRS-1 in L6 myotubes in presence of vanadium complexes

To confirm that the vanadium complexes exert their effect via activation of insulin signaling pathway, the immunoblot for IRS-1 was carried out in the cells. Briefly, L6 myotubes were treated with 25 μM of **2**, 10 μM of **5** or 100 nM insulin in presence of glucose. The cells were harvested at 0, 30, 60, 120, 180 and 240 min. After each time point, L6 myotubes were harvested and lysed in a lysis buffer (10 mM Tris-HCl pH 7.4, 150 mM NaCl, 1% Triton X-100, 0.5% sodium deoxycholate, 0.1% sodium dodecyl sulfate (SDS), 0.5 mM dithiothreitol, 1 mM PMSF) for 30 min at 4°C. The lysates were then sonicated for 10 s and centrifuged at 12,000 g for 15 min at 4°C. The protein concentrations of the supernatants were estimated using BCA assay and further used for immunoblotting.

3.2.7.2. Immunoblot analysis for IRS-1

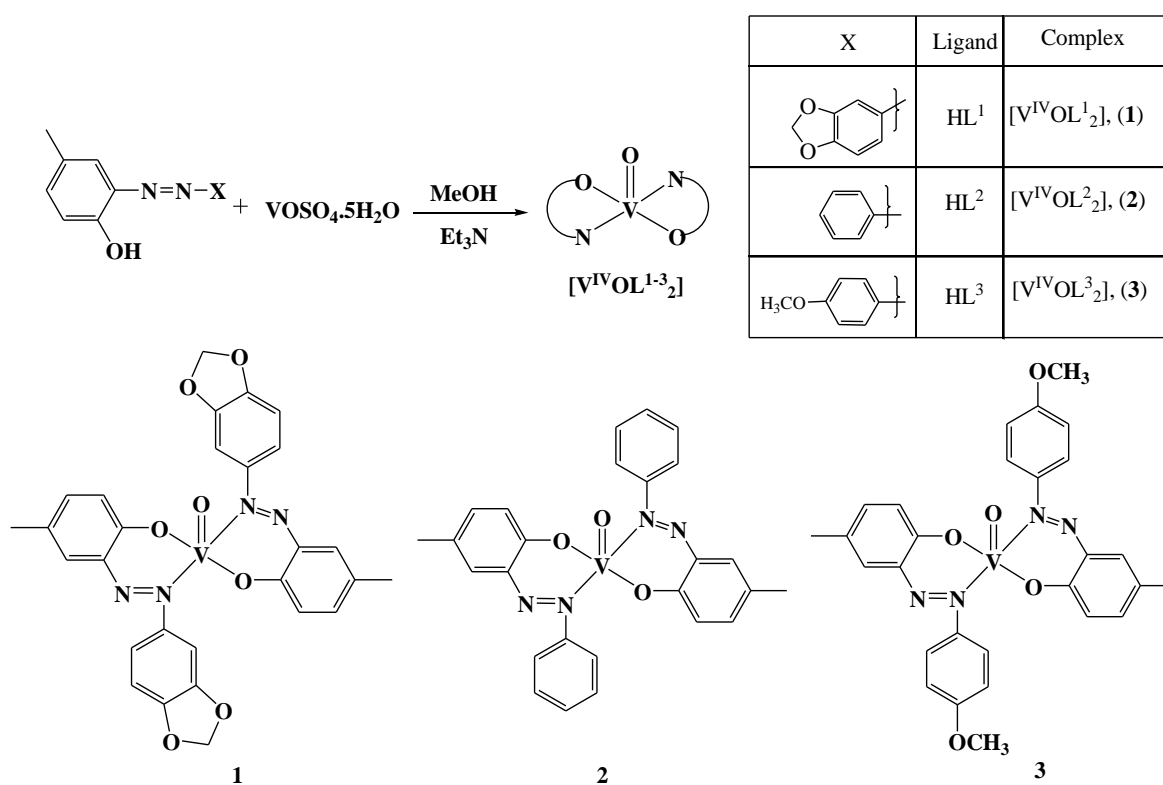
Equal amounts of protein (25 $\mu\text{g/lane}$) and pre-stained molecular weight markers (life technologies) were separated onto 12% SDS-PAGE and transferred to nitrocellulose

membranes. The membranes were then incubated for blocking in 1% BSA in phosphate-buffered saline (PBS) for 1 h. After the incubation, the membranes were washed in PBS containing 0.1% Tween-20 and incubated with anti-IRS-1 or anti-actin antibodies overnight at 4°C respectively. The membranes were then washed in PBS containing 0.1% (v/v) Tween-20 for three times and incubated with horseradish-peroxidase-conjugated anti-rabbit IgG antibodies at a dilution of 1:5000 for 1 h at room temperature. Immunoreactive bands were visualized using ECL Plus™ Western blotting detection reagents.

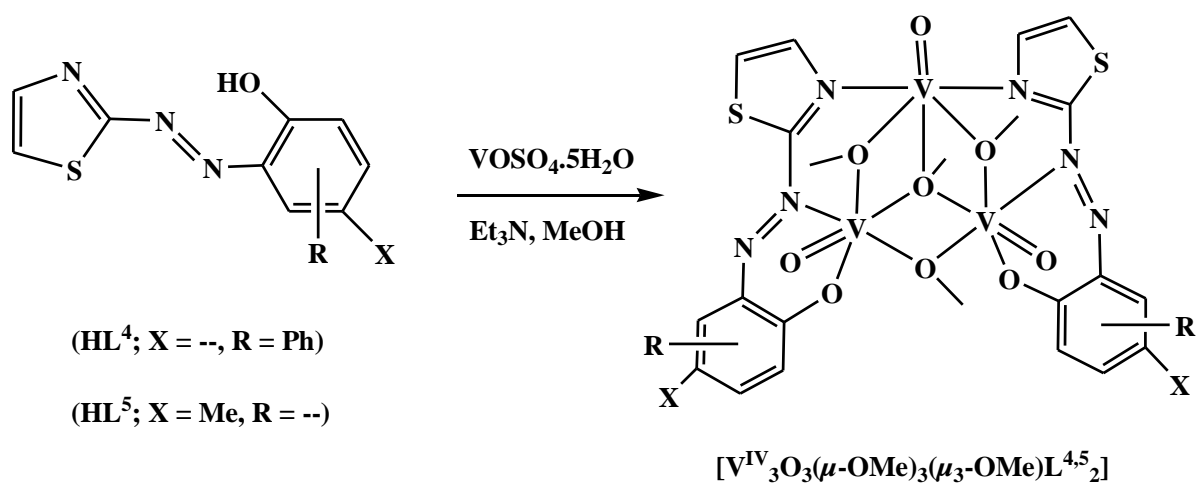
3.3. RESULTS AND DISCUSSION

3.3.1. Synthesis.

Herein we have reported the synthesis of three monooxidovanadium(IV) complexes (**1–3**) and two discrete μ -OCH₃ bridged trivanadium(IV) complexes (**4** and **5**) synthesized by the reaction of 2-((2-X)-diazo)-4-methylphenol (where X = benzo[1,3]dioxol-5-yl (HL¹), phenyl (HL²) and 4-methoxyphenyl (HL³), 1-(2-(thiazol-2-yl)diazenyl)naphthalene-2-ol (HL⁴) and 2-(2-(thiazol-2-yl)diazenyl)-4-methylphenol (HL⁵) with VOSO₄·5H₂O in equimolar ratios in methanolic medium. Schematic representation for the synthesis of the complexes is shown in Scheme 3.1 and 3.2. The compounds are soluble in CH₃CN, DMF and DMSO and partially soluble in water, MeOH and EtOH. The structural formula of the complexes is based on elemental analyses, IR and UV-vis spectroscopy and ESI-MS, and single crystal X-ray diffraction analyses of **4**. Complexes **1** and **3–5** (**1**, 45%; **3**, 60%; **4**, 30% and **5**, 80% H₂O–DMSO solution) were moderately soluble in H₂O, while complex **2** was completely soluble. All the complexes were stable in both solid and solution phases. The solution phase stability of the complexes was confirmed by electronic absorption study. Time-dependent UV-vis study of the complexes showed them to be stable in the solvent medium over a period of 72 h. The representative time-dependent electronic spectrum of (d–d transition peak) of **5** in CH₃CN is given in Figure 3.1.



Scheme 3.1. Schematic diagram of the synthesis of monooxidovanadium(IV) complexes, [V^{IV}OL¹⁻³]₂ (1–3).



Scheme 3.2. Schematic diagram of the synthesis of [V^{IV}₃O₃(μ-O)₃(μ₃-OMe)L^{4,5}]₂ (4 and 5)

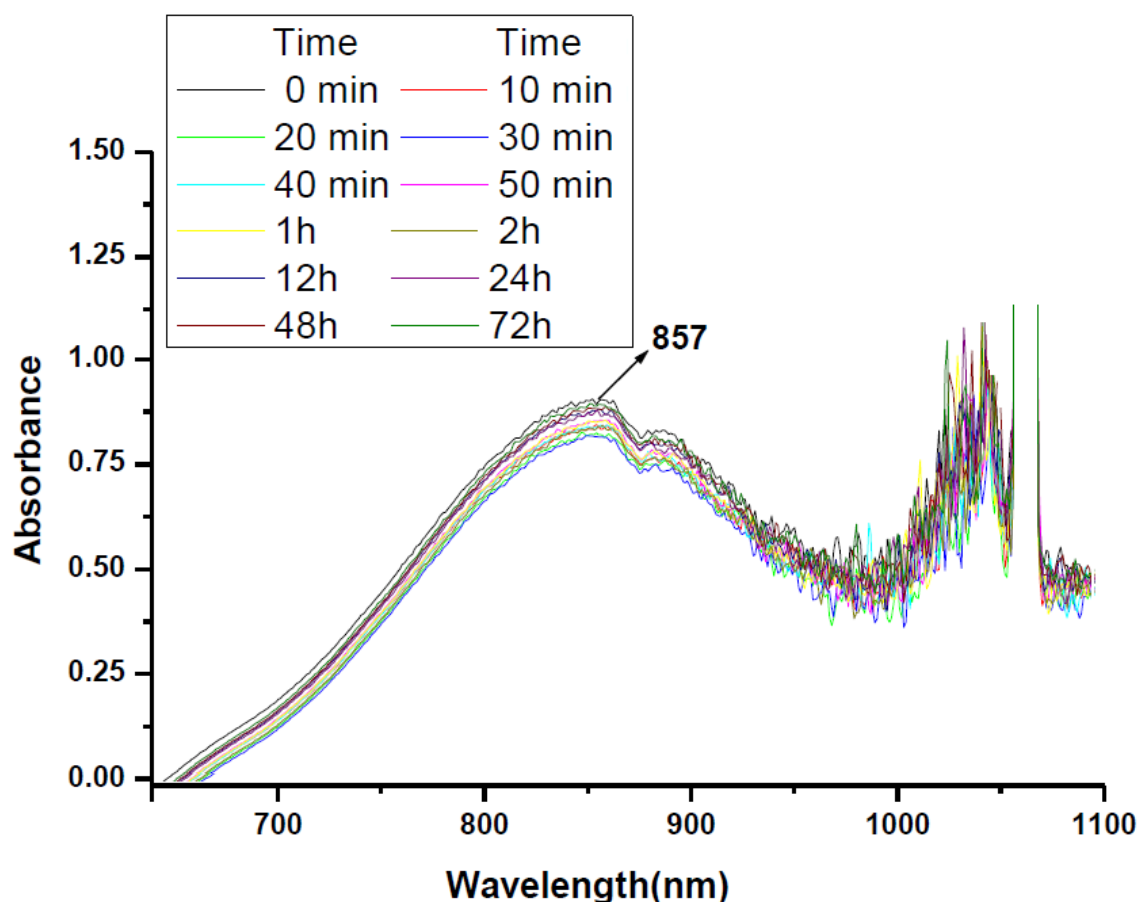


Figure 3.1. Time-dependent UV-vis spectra (d-d transition peak) of $[V^{IV}OL^1_2]$ (**1**) in CH_3CN solution.

3.3.2. Spectral Characteristics

3.3.2.1. IR spectroscopy. IR stretching frequencies of the ligands observed in the range of $1549\text{--}1504\text{cm}^{-1}$ is attributed to the presence of the azo($N=N$) functional group,^{32,33} which shifts to a lower frequency range of $1494\text{--}1472\text{cm}^{-1}$ upon complexation (**1–5**). The presence of a strong band in the range $984\text{--}972\text{cm}^{-1}$ for complexes **1–3** is attributed to $V=O$ stretching which implies formation of a monooxidovanadium complex,⁴ while the presence of two strong and sharp peaks in the IR spectrum of **4** and **5** in the range $972\text{--}916\text{cm}^{-1}$ are consistent with a typical $V=O$ stretching frequency, which indicates presence of symmetry in the molecule.^{50b-e} A medium intensity stretching peak $854\text{--}837\text{cm}^{-1}$ in the IR spectra of **4** and **5** could possibly be due to the $V\text{--}O\text{--}V$ stretching in these complexes.⁶³ Representative IR spectrum of **4** is presented in Figure 3.2.

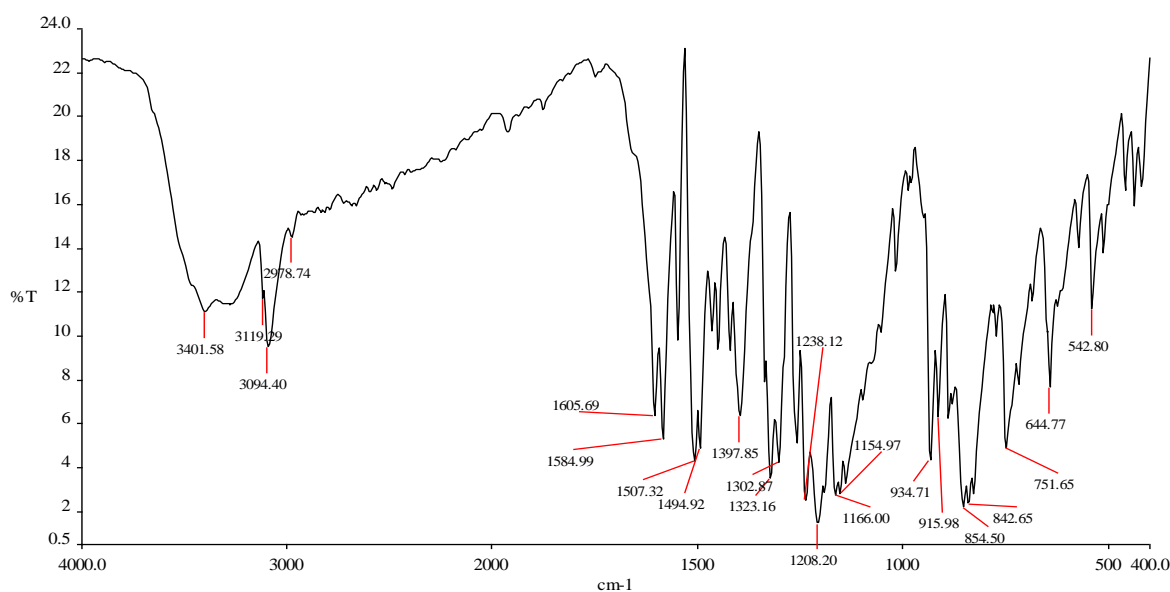


Figure 3.2. IR spectrum of $[\text{V}^{\text{IV}}_3\text{O}_3(\mu\text{-OMe})_3(\mu_3\text{-OMe})\text{L}_4]$ (**4**).

3.3.2.2. UV-vis spectroscopy. The electronic spectra of the complexes were recorded in CH_3CN medium. The main features of all the spectra are quite similar. The spectral data are summarized in Table 3.2 and the representative spectrum of **3** is shown in Figure 3.3. Three strong absorptions are observed in the wavelength range 378–216 nm. The lower energy absorption in this range are possibly due to ligand to metal charge transfer (LMCT) transitions⁶⁴ whereas the higher energy absorptions are likely to be ligand centered transitions.⁶⁵ Low intensity peaks observed in the higher wavelength region, 872–635 nm, are due to d–d transition in the complexes.⁶⁴

Table 3.2. UV–vis spectral data for complex **1–5** in CH_3CN solution.

| Complex | λ_{max} (nm) (ϵ_{max} ($\text{M}^{-1}\text{cm}^{-1}$)) | | | |
|---|--|------------|-----------|------------|
| $[\text{V}^{\text{IV}}\text{OL}^1_2]$ (1) | 253(11540) | 281(9853) | 365(8542) | 866(823) |
| $[\text{V}^{\text{IV}}\text{OL}^2_2]$ (2) | 259(11531) | 284(10120) | 380(9580) | 864(767) |
| $[\text{V}^{\text{IV}}\text{OL}^3_2]$ (3) | 216(15030) | 244(10420) | 378(9920) | 862(694) |
| $[\text{V}^{\text{IV}}_3\text{O}_3(\mu\text{-OMe})_3(\mu_3\text{-OMe})\text{L}^4_2]$ (4) | 260(11580) | 390(7600) | 635(700) | 872(1582) |
| $[\text{V}^{\text{IV}}_3\text{O}_3(\mu\text{-OMe})_3(\mu_3\text{-OMe})\text{L}^5_2]$ (5) | 255(11531) | 384(7500) | 645(705) | 857 (1500) |

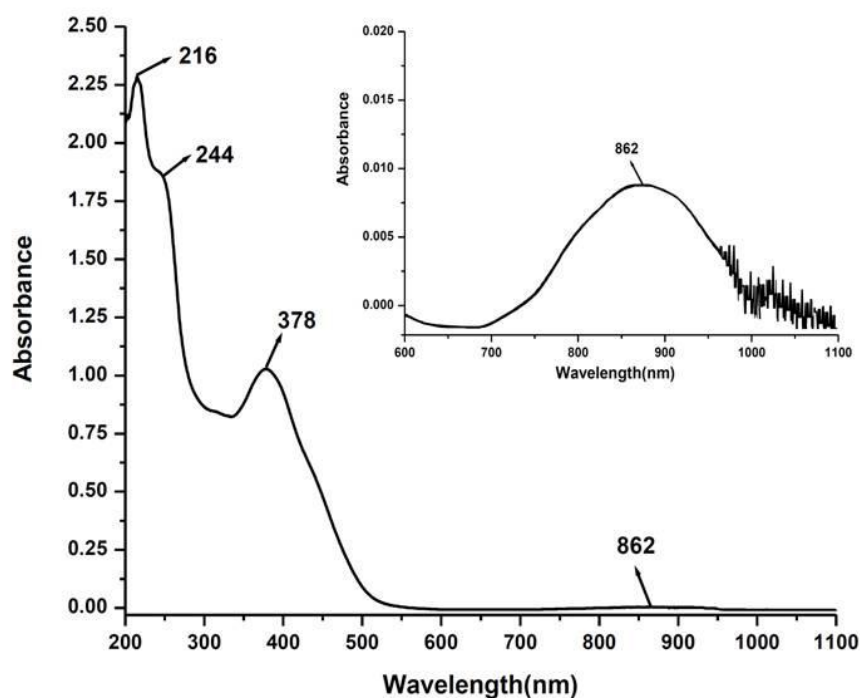
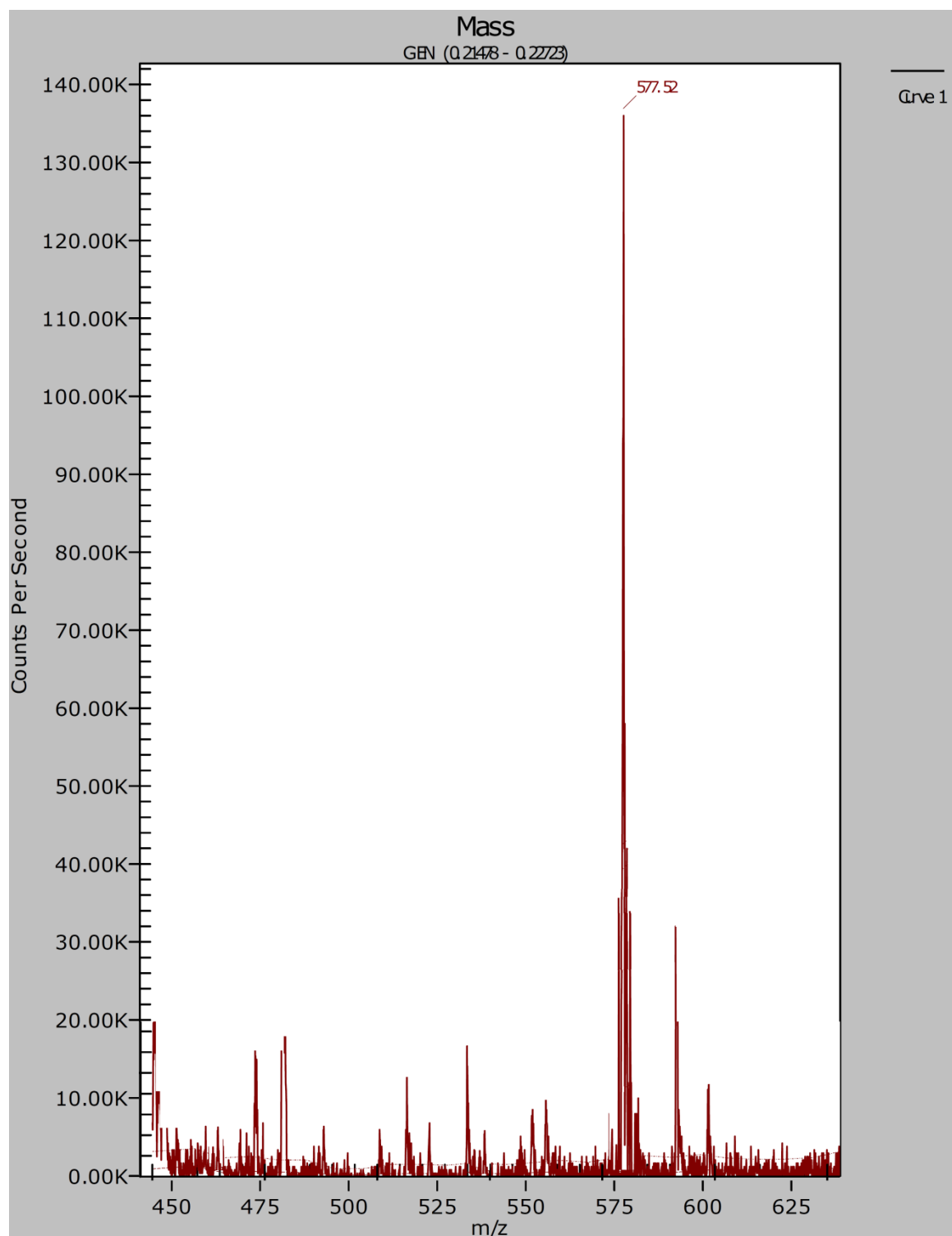


Figure 3.3. UV-vis spectrum of $[V^{IV}OL^3_2]$ (**3**) in CH_3CN solution.

3.3.3. ESI-MS

ESI-MS of complexes **1–5** have been recorded in acetonitrile solution in the positive ion mode. The base peak observed in the ESI-MS of **1**, **2** and **3** is the characteristic molecular ion peak ($[M]^+$) at m/z 577.52, 489.11 and 549.51 respectively. Mass spectral analysis for **4** and **5**, shows predominant peaks at m/z 832.87 and 763.11, which correspond to $[4 - H]^+$ and $[5 + 2H]^+$ respectively. Results of mass spectrometry give strong evidence in favor of the formation of monooxidovanadium(IV) arylazo (**1–3**) and μ -methoxido bridged trivanadium(IV) azo species (**4** and **5**), as proposed in Scheme 3.1 and 3.2. ESI-MS data are summarized in the ‘Materials and Methods’ section. ESI-MS of complexes **1–5** are shown in Figures 3.4–3.7 respectively and their corresponding data are summarized in the Experimental Section.



0

Figure 3.4. ESI-MS of $[V^{IV}OL^1_2]$ (1) in CH_3CN : m/z 577.52 (100%, $[M]^+$, MW = 577.44).

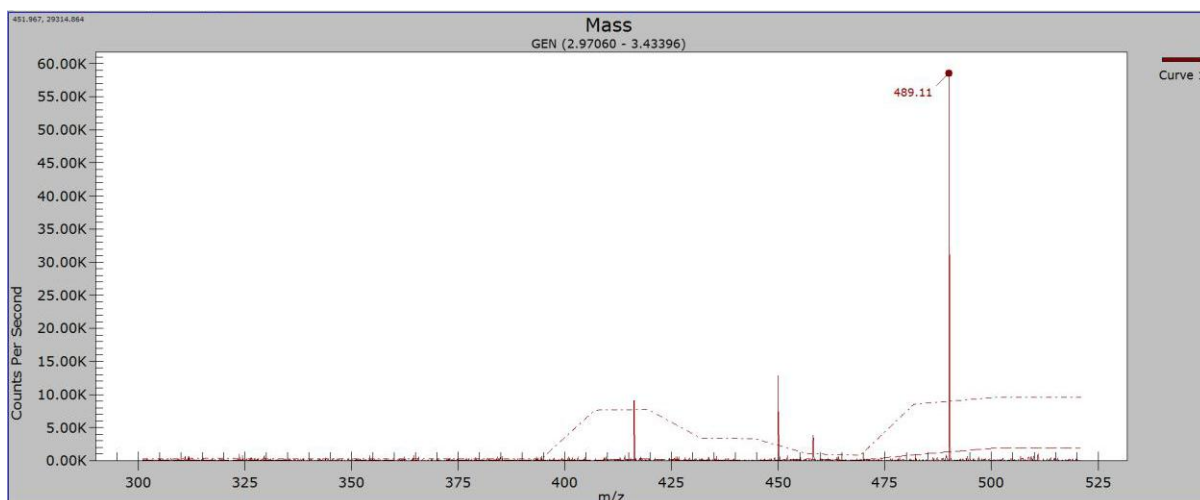


Figure 3.5. ESI-MS of $[V^{IV}OL_2]$ (**2**) in CH_3CN : m/z 489.11 (100%, $[M]^+$, MW = 489.42).

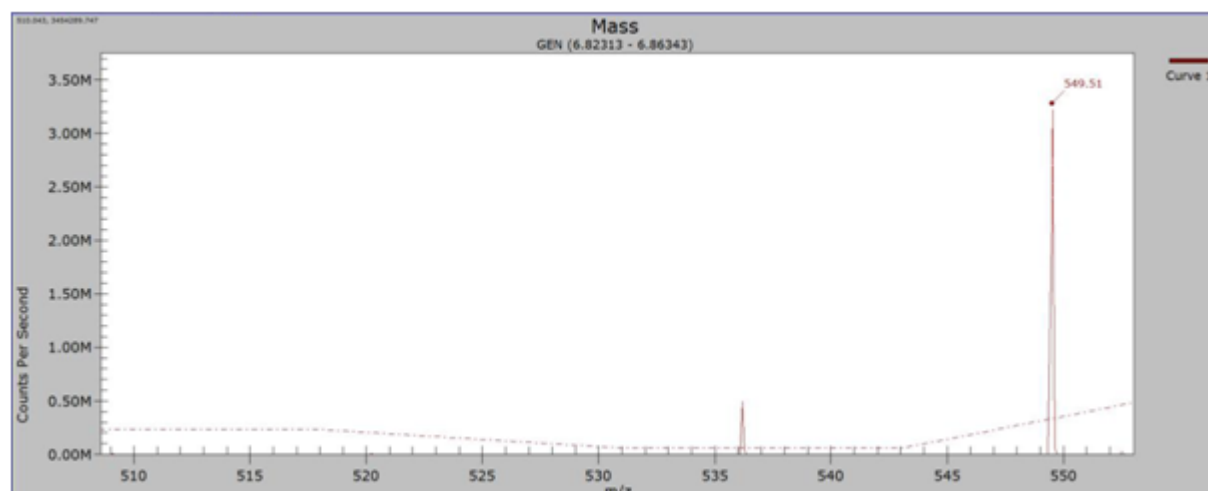


Figure 3.6. ESI-MS of $[V^{IV}OL_3]$ (**3**) in CH_3CN : m/z 549.51 (100%, $[M]^+$, MW = 549.47).

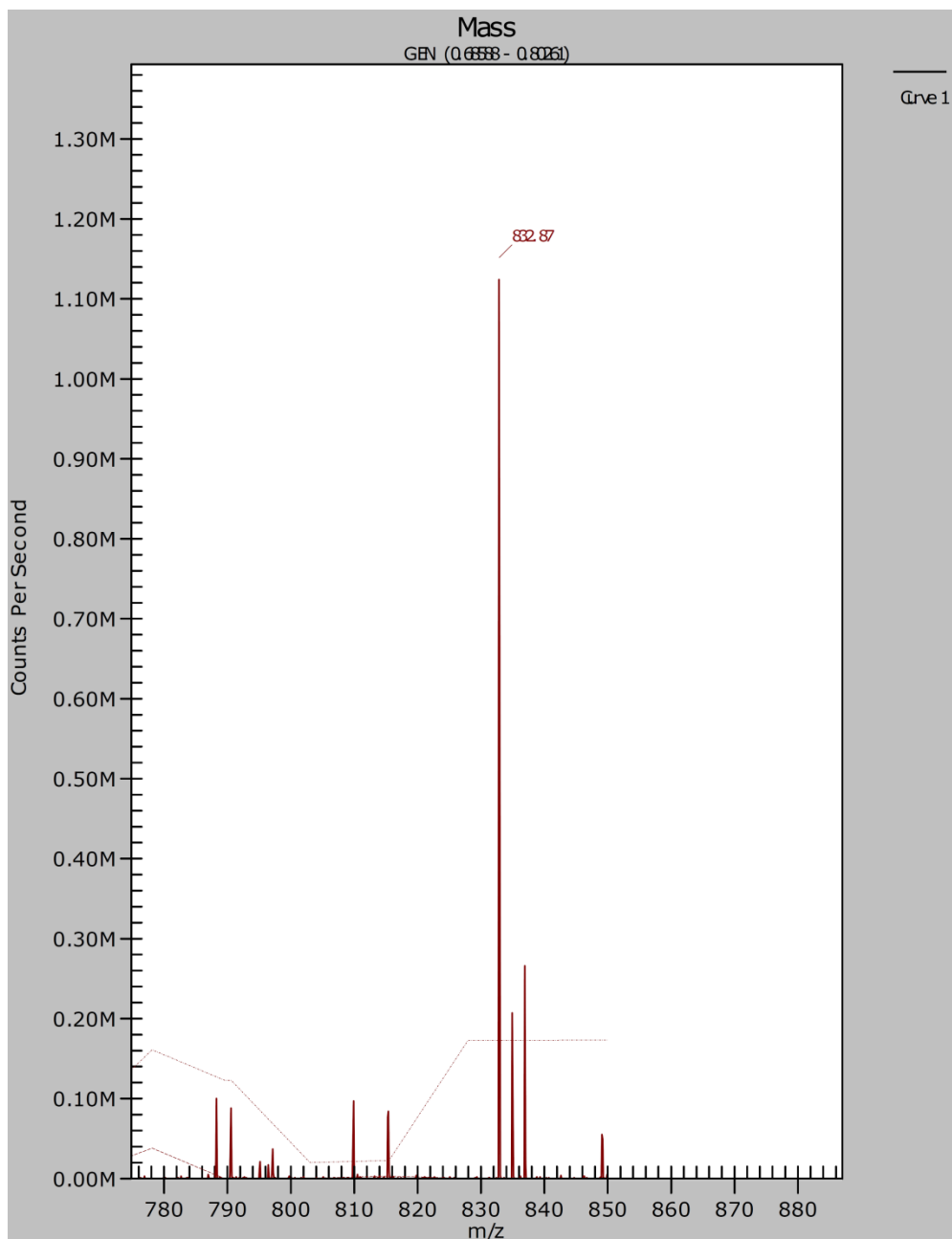


Figure 3.7. ESI-MS of $[\text{V}^{\text{IV}}_3\text{O}_3(\mu\text{-OMe})_3(\mu_3\text{-OMe})\text{L}_2]$ (**4**) in CH_3CN : m/z 832.87 (100%, $[\text{M} - \text{H}]^+$, MW = 833.52).

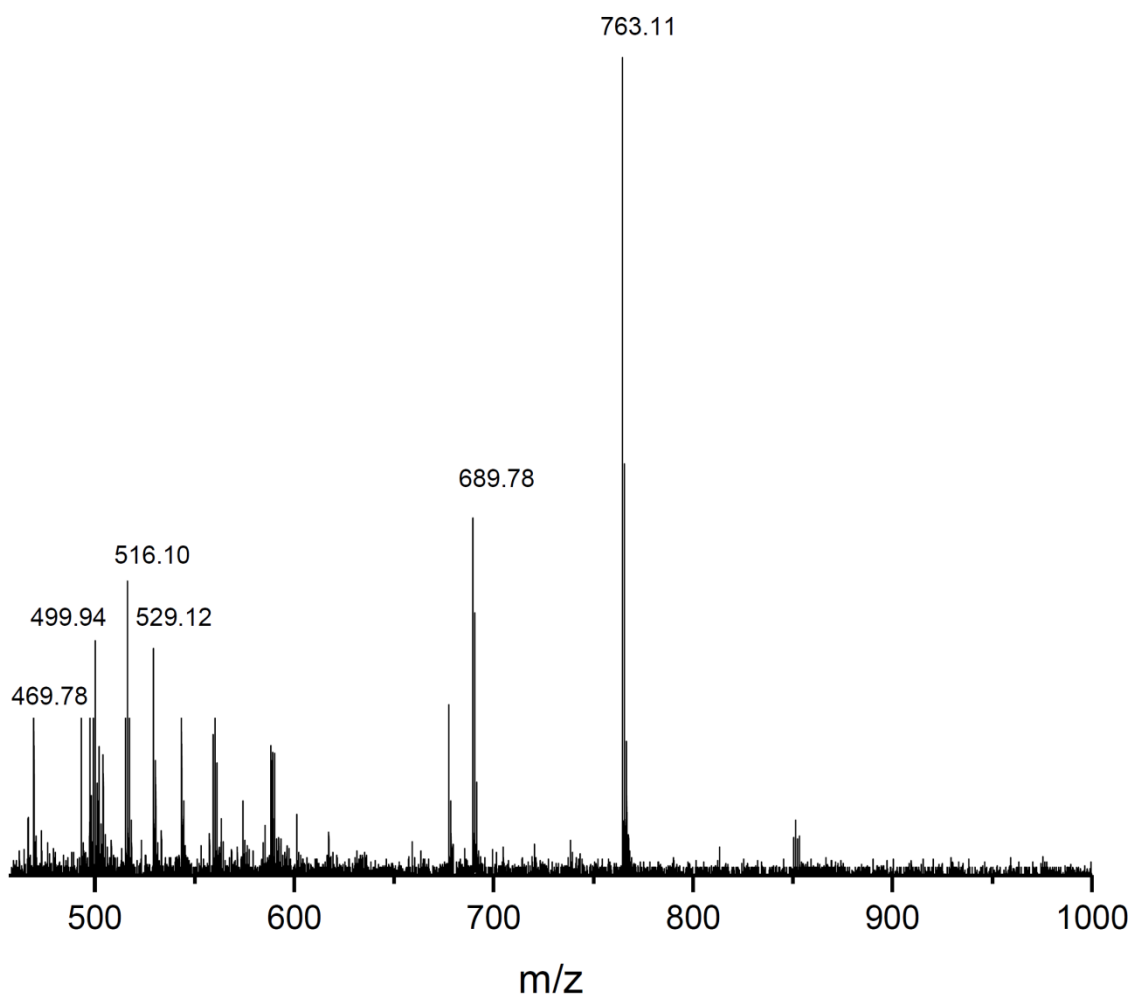
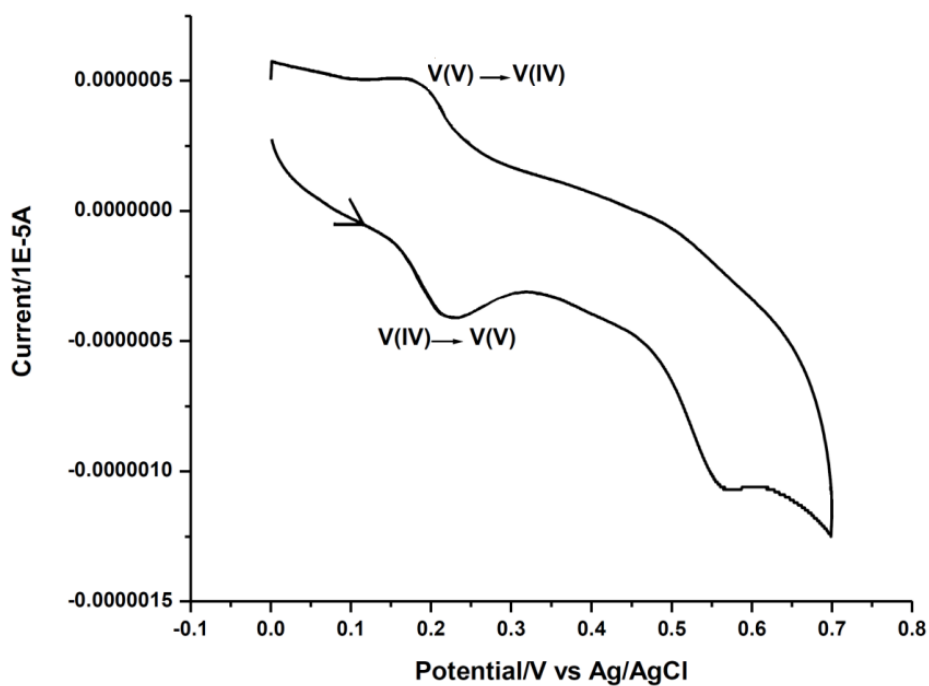


Figure 3.8. ESI-MS of $[\text{V}^{\text{IV}}_3\text{O}_3(\mu\text{-OMe})_3(\mu_3\text{-OMe})\text{L}^5_2]$ (**5**) in CH_3CN : m/z 763.11 (100%, $[\text{M} + 2\text{H}]^+$, MW = 761.47).

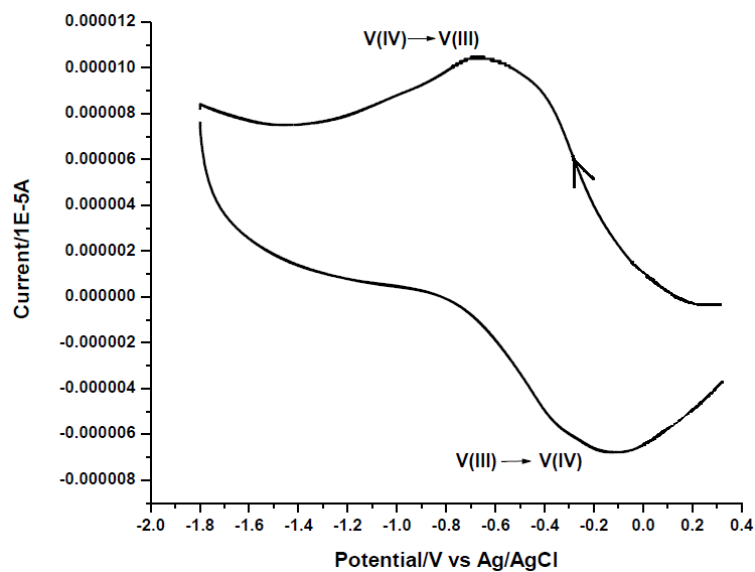
3.3.4. Electrochemical properties

The cyclic voltammetry of **1–3** were recorded in CH_3CN solution and that of **4** and **5** were performed in DMF solution (0.1 M TBAP) at a scan rate of 50 mV s^{-1} for **1–3** and 100 mV s^{-1} for **4** and **5**. The voltammogram pattern is similar for **1–3**, which exhibits a single electron transfer reversible oxidation wave (V(IV)/V(V)) in the anodic region in the $E^a_{1/2}$ range $+0.21$ to $+0.18 \text{ V}^{66}$ and one quasi-reversible reduction wave in the cathodic region at $E^c_{1/2} = -0.31$ to -0.34 V ((V(IV)/V(III)).⁶⁷ The CVs for **4** and **5** are similar, which include the three different redox couple corresponding to single-electron transfer in the three vanadium centers of the trinuclear complexes. The anodic region of **4** and **5** show

one quasi-reversible oxidation wave at $E_{1/2}^a$ value 0.26 and 0.22 V, respectively, which is assigned to the V(IV)/V(V) redox couple of one of the metal centers, while the cathodic region depicts one quasi-reversible and another reversible V(IV)/V(III) couple at $E_{1/2}^c$ – 0.62 V and –1.50 V respectively.⁶⁸ An irreversible oxidation wave for all the complexes is located in the +0.58 to +0.55 V range, which is attributed to a ligand centered process. The representative voltammogram of **1** and **4** are depicted in Figure 3.9 and 3.10 respectively. The results are summarized in Table 3.3. The one–electron nature of this oxidation was verified by comparing its current height with that of the standard ferrocene–ferrocenium couple under identical experimental conditions.



(a)



(b)

Figure 3.9. Cyclic voltammogram of $[V^{IV}OL_2]$ (**1**) showing (a) oxidation ($V(IV) \rightarrow V(V)$) and (b) reduction ($V(IV) \rightarrow V(III)$) of the vanadium(IV) centre.

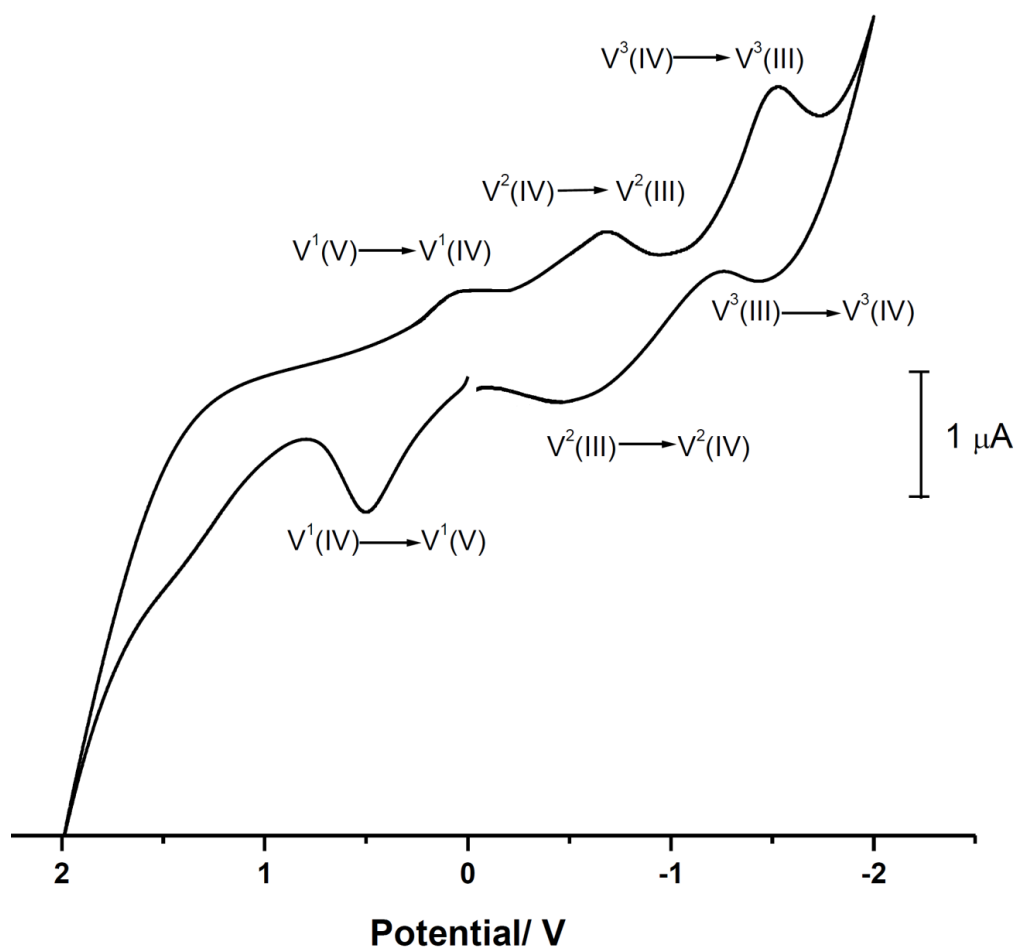


Figure 3.10. Cyclic voltammogram of $[V^{IV}_3O_3(\mu\text{-OMe})_3(\mu_3\text{-OMe})L_2]$ (4) showing three redox couples for oxidation ($V(IV) \rightarrow V(V)$) and reduction ($V(IV) \rightarrow V(III)$) of the three vanadium(IV) centre.

Table 3.3. Cyclic voltammetric results for oxidovanadium(IV) complexes (**1–5**) at 298 K.^[a]

| Complex | $E_{1/2}^a$ (V) | ΔE_p^a (mV) | $E_{1/2}^c$ (V) | ΔE_p^c (mV) |
|---|-----------------|---------------------|-----------------|---------------------|
| $[\text{V}^{\text{IV}}\text{OL}^1_2]$ (1) | 0.20 | 60 | -0.34 | 110 |
| $[\text{V}^{\text{IV}}\text{OL}^2_2]$ (2) | 0.18 | 70 | -0.34 | 160 |
| $[\text{V}^{\text{IV}}\text{OL}]_2$ (3) | 0.21 | 50 | -0.31 | 120 |
| $[\text{V}^{\text{IV}}_3\text{O}_3(\mu\text{-OMe})_3(\mu_3\text{-OMe})\text{L}^4_2]$ (4) | 0.26 | 470 | -0.62, -1.50 | 134, 64 |
| $[\text{V}^{\text{IV}}_3\text{O}_3(\mu\text{-OMe})_3(\mu_3\text{-OMe})\text{L}^5_2]$ (5) | 0.22 | 468 | -0.63, -1.52 | 135, 65 |

^[a]**1–3** in CH_3CN at a scan rate of 50 mV s^{-1} , **4** and **5** in DMF at a scan rate of 100 mV s^{-1} . $E_{1/2} = (E_p^a + E_p^c)/2$, where E_p^a and E_p^c are anodic and cathodic peak potentials vs. Ag/AgCl, respectively. $\Delta E_p = E_p^a - E_p^c$.

3.3.5. Description of X-ray crystallographic structure of $[\text{V}^{\text{IV}}_3\text{O}_3(\mu\text{-OMe})_3(\mu_3\text{-OMe})\text{L}^4_2]$ (**4**)

The trimeric structure of $[\text{V}^{\text{IV}}_3\text{O}_3(\mu\text{-OMe})_3(\mu_3\text{-OMe})\text{L}^4_2]$ (**4**) has been demonstrated by X-ray diffraction analysis. The selected bond lengths and angles of **4** are enlisted in Table 3.4 and an ORTEP plot⁶⁹ of the complex is shown in Figure 3.11. The molecule is composed of three slightly distorted octahedral vanadium atoms forming an almost butterfly-shaped V_3O_4 unit similar to the well-known 3Fe-4S iron sulfur cluster⁷⁰ (Figure 3.12a) where four alternate corners are occupied by four oxygen atoms of the ligands and other three alternate corners are occupied by the three V(IV) atoms (Scheme 3.12b). The linkage between the three vanadium atoms is obtained by four bridging methoxido groups. Three methoxides work as conventional three-center bridged ($\mu\text{-OMe}$) ligands with oxygen donor atom bonding two metal centers. The V–O distances formed with the apical and basal vanadium atoms are rather similar (ranging from 1.958(5) to 2.001(5) Å) and compare well with those observed earlier. The remaining methoxido group adopted a "tridentate" bonding mode ($\mu_3\text{-OMe}$) with the oxygen atom bridging the three metal centers [$\text{V1-O4} = 2.124(5)$ Å, $\text{V2-O4} = 2.192(5)$ Å and $\text{V3-O4} = 2.206(5)$ Å].

All three vanadium atoms contain an oxido oxygen atom with an average V=O bond distance of 1.605 Å. The coordination of the apical vanadium atom (V1) is fulfilled by two iminyl nitrogen atoms (N1 and N4) of the two ligands, apart from the oxygen atoms of the oxido (O1) and bridging methoxido (O4, O5 and O7) groups, whereas for the terminal vanadium atoms (V2 and V3), the coordination is completed by the phenolic oxygen (O9/O8) and the azo nitrogen atoms (N5/N2) of each ligand separately (average V–N distance 2.084 Å). The large bite angle of the bridging methoxido groups results in a basal to apical vanadium-vanadium (V1⋯V2 and V1⋯V3) distance of ~ 3.191(3) Å and basal to basal vanadium-vanadium (V2⋯V3) distance of ~ 3.303(3) Å, outside of the range for any possible metal-metal bonding.

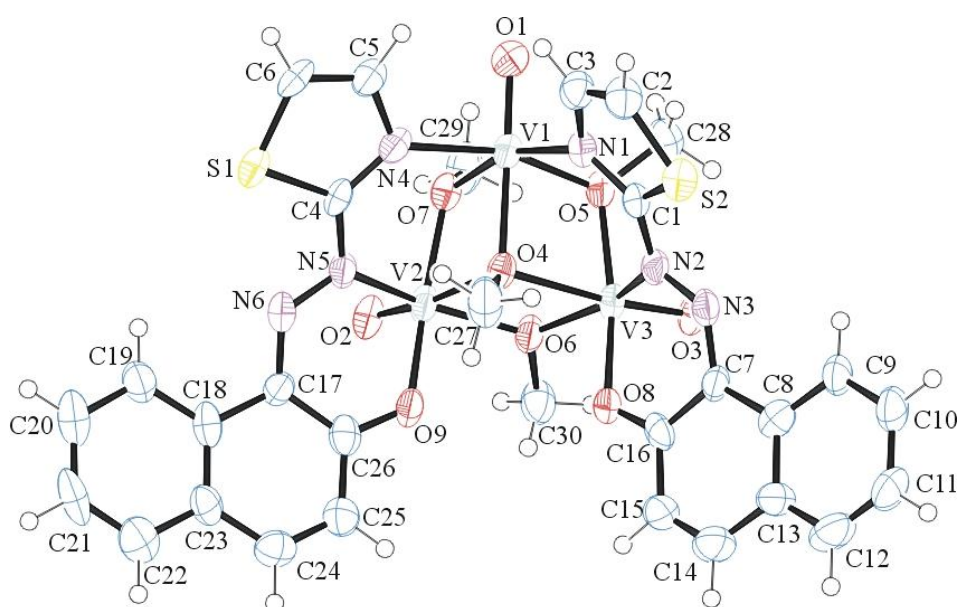


Figure 3.11. ORTEP diagram of $[V^{IV}_3O_3(\mu\text{-OMe})_3(\mu_3\text{-OMe})L^4]$ (**4**) with atom numbering scheme.

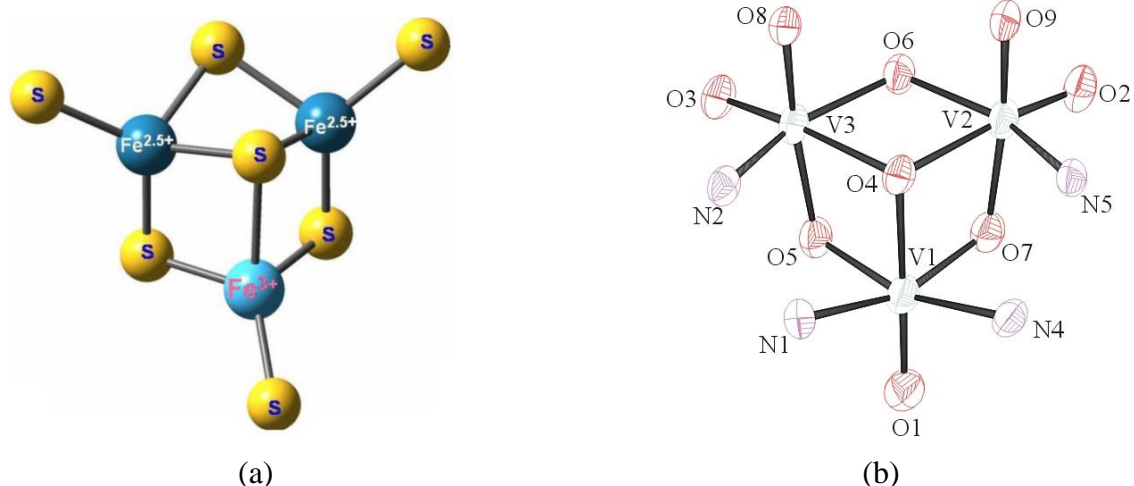


Figure 3.12. Core structure of (a) 3Fe-4S cluster and (b) V₃O₄ unit of [V^{IV}₃O₃(μ -OMe)₃(μ_3 -OMe)L⁴]₂ (**4**).

Table 3.4. Selected bond parameters of [V^{IV}₃O₃(μ -OMe)₃(μ_3 -OMe)L⁴]₂ (**4**)

| Bond lengths (Å) | | | |
|------------------|----------|----------------|----------|
| N(1)-V(1) | 2.147(6) | O(6)-V(3) | 2.004(5) |
| N(2)-V(3) | 2.080(7) | O(7)-V(1) | 1.958(5) |
| N(4)-V(1) | 2.154(6) | O(7)-V(2) | 2.000(5) |
| N(5)-V(2) | 2.088(6) | O(8)-V(3) | 2.002(5) |
| O(4)-V(2) | 2.192(5) | O(9)-V(2) | 1.996(5) |
| O(4)-V(3) | 2.206(5) | O(1)-V(1) | 1.602(5) |
| O(5)-V(1) | 1.970(5) | O(2)-V(2) | 1.600(5) |
| O(5)-V(3) | 2.001(5) | O(3)-V(3) | 1.602(5) |
| O(6)-V(2) | 1.992(5) | O(4)-V(1) | 2.124(5) |
| Bond angles (°) | | | |
| O(1)-V(1)-O(4) | 172.5(3) | O(7)-V(1)-O(4) | 79.6(2) |
| O(5)-V(1)-O(4) | 80.2(2) | O(1)-V(1)-N(1) | 93.4(3) |
| O(7)-V(1)-N(1) | 160.0(2) | O(5)-V(1)-N(1) | 84.3(2) |
| O(4)-V(1)-N(1) | 81.1(2) | O(1)-V(1)-N(4) | 92.0(3) |

| | | | |
|----------------|-----------|----------------|-----------|
| O(7)-V(1)-N(4) | 82.7(2) | O(5)-V(1)-N(4) | 162.6(2) |
| O(4)-V(1)-N(4) | 84.0(2) | N(1)-V(1)-N(4) | 100.6(2) |
| O(2)-V(2)-O(6) | 104.8(2) | O(2)-V(2)-O(9) | 97.5(3) |
| O(6)-V(2)-O(9) | 90.9(2) | O(2)-V(2)-O(7) | 95.8(2) |
| O(6)-V(2)-O(7) | 91.1(2) | O(9)-V(2)-O(7) | 165.5(2) |
| O(2)-V(2)-N(5) | 100.3(2) | O(6)-V(2)-N(5) | 154.7(2) |
| O(9)-V(2)-N(5) | 82.6(2) | O(7)-V(2)-N(5) | 89.5(2) |
| O(2)-V(2)-O(4) | 172.9(2) | O(6)-V(2)-O(4) | 75.73(19) |
| O(9)-V(2)-O(4) | 89.5(2) | O(7)-V(2)-O(4) | 77.1(2) |
| N(5)-V(2)-O(4) | 79.8(2) | O(3)-V(3)-O(5) | 96.1(2) |
| O(3)-V(3)-O(8) | 97.2(2) | O(5)-V(3)-O(8) | 165.2(2) |
| O(3)-V(3)-O(6) | 105.3(2) | O(5)-V(3)-O(6) | 92.3(2) |
| O(8)-V(3)-O(6) | 90.4(2) | O(3)-V(3)-N(2) | 99.5(3) |
| O(5)-V(3)-N(2) | 88.6(2) | O(8)-V(3)-N(2) | 82.9(2) |
| O(6)-V(3)-N(2) | 155.0(2) | O(3)-V(3)-O(4) | 173.7(2) |
| O(5)-V(3)-O(4) | 77.57(19) | O(8)-V(3)-O(4) | 89.0(2) |
| O(6)-V(3)-O(4) | 75.2(2) | N(2)-V(3)-O(4) | 80.6(2) |

3.3.6. Cytotoxicity studies

3.3.6.1. MTT assay

In the present study, antiproliferative efficacy of vanadium complexes with ON and ONN coordinating azo ligands (**1–5**) was assayed by determining the viability of MCF-7 cells using the MTT assay. The ligands HL^{1–5} and VOSO₄·5H₂O gave high IC₅₀ values of >200 μM, whereas corresponding complexes **1–5** gave values in the range of ~51–14 μM after 48 h of incubation period (Table 3.5). The standard anticancer drug, cisplatin, has been reported to have an IC₅₀ value of 7.8 μM against MCF-7 cell line under similar conditions.^{4,71} The significant decrease in the inhibitory concentration for the ligands compared to the metal complexes clearly indicates that incorporation of vanadium in the

ligand environment has a marked effect on cytotoxicity. A possible explanation is that by coordination, the polarity of the ligand and the central metal ion are reduced through charge equilibration, which favors permeation of the complexes through the lipid layer of the cell membrane.^{72,73} The present results are consistent with the observation that metal complexes can exhibit greater biological activities than the free ligands.⁷⁴

Table 3.5. IC₅₀ (μM) values of **1–5** and clinically referred drugs.

| Complex | IC ₅₀ (μM) 48h |
|---|------------------------------|
| [V ^{IV} OL ¹ ₂] (1) | 50.64 ± 2.45 |
| [V ^{IV} OL ² ₂] (2) | 13.82 ± 1.32 |
| [V ^{IV} OL ³ ₂] (3) | 29.89 ± 1.94 |
| [V ^{IV} ₃ O ₃ (μ-OMe) ₃ (μ ₃ -OMe)L ⁴ ₂] (4) | 13.90 ± 3.44 |
| [V ^{IV} ₃ O ₃ (μ-OMe) ₃ (μ ₃ -OMe)L ⁵ ₂] (5) | 22.85 ± 2.48 |
| Cisplatin | 7.8 |

The cytotoxic activity of the three complexes (**1–5**) follows the order **2** ≈ **4** > **5** > **3** > **1**, which is reflected from their IC₅₀ values (48 h) with dose dependency as illustrated in Figure 3.13. The graphical representation showing the percent cell viability of MCF-7 cells after 24 h of treatment with increasing concentrations (5, 10, 25 and 50 μM) of vanadium complexes (**1–5**) is shown in Figure 3.14. The lower IC₅₀ values of **2** as compared to the other complexes after 48 h may be attributed to its higher solubility in aqueous medium.⁷⁵

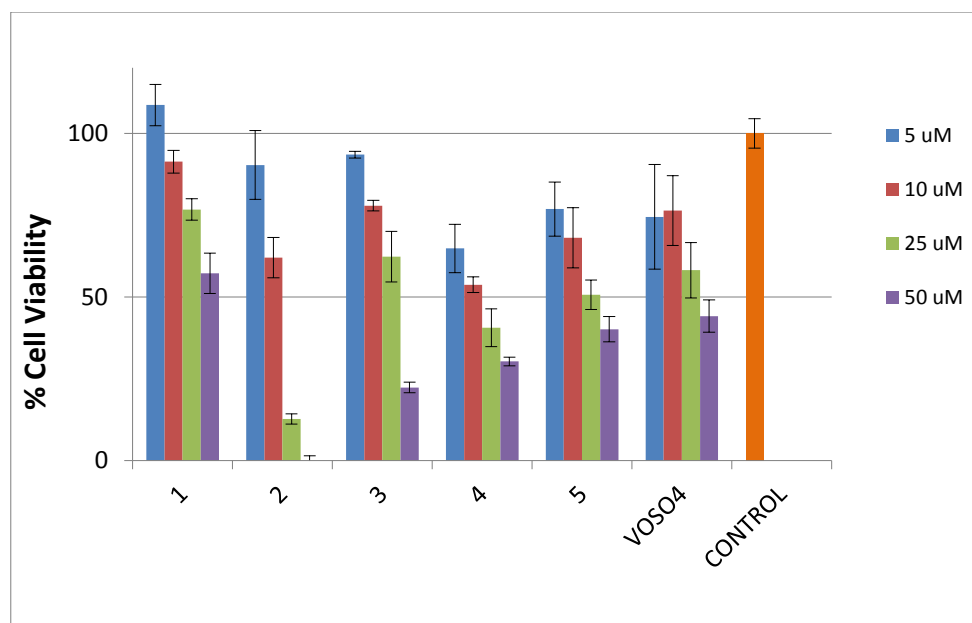


Figure 3.13. Graph showing the percent cell viability of MCF-7 cells after 48 h of treatment with increasing concentrations (5, 10, 25 and 50 μM) of vanadium complexes (1–5).

The IC_{50} values for complexes 2–5 were smaller against MCF-7 cell lines as compared to some other oxidovanadium(IV) complexes reported ($>50 \mu\text{M}$ against MCF-7 for [VO(sal-Gly)(bipy)], [VO(sal-Gly)(phen)], [VO(sal-L-Phe)(H₂O)], [VO(sal-LPhe)(bipy)] and [VO(sal-L-Phe)(phen)],⁶⁷ [VO(pyphen)(acac)](ClO₄) reported in both light and dark conditions⁷⁵ and vanadium complexes of di-2-pyridyl ketones.⁷⁶ The solution stability of complexes 1–5 is of interest considering recent exploration by Reytmann et. al. on HT-29, ovarian OVCAR-1 cell, A2780 and A2780cis cell lines wherein they showed the high cytotoxicity of hydrolytically stable oxidovanadium compounds with ON donor ligands.^{77,78}

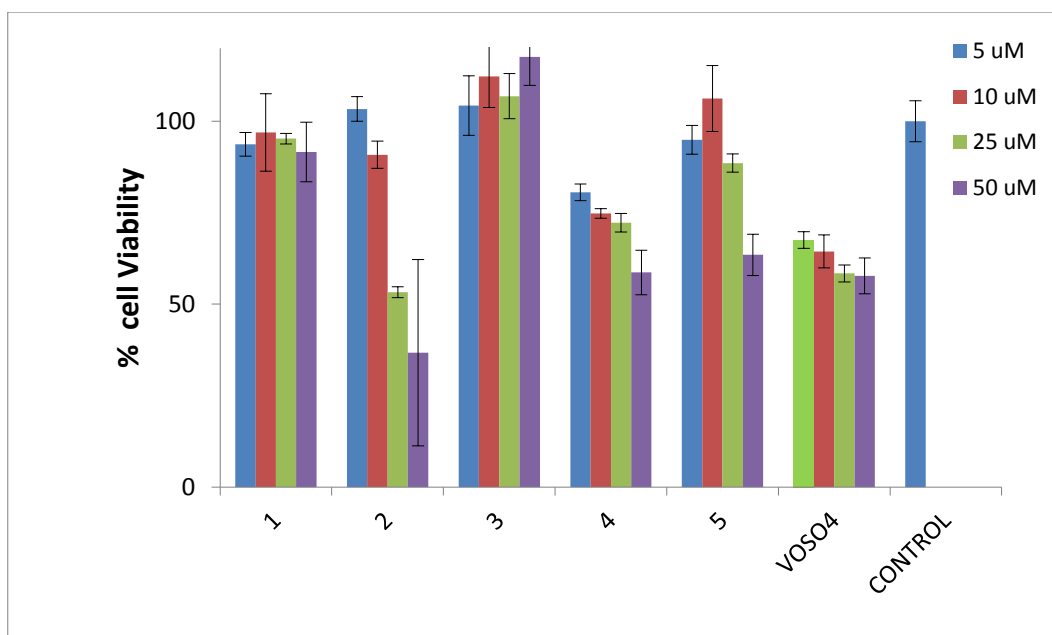


Figure. 3.14. Graph showing the percent cell viability of MCF-7 cells after 24 h of treatment with increasing concentrations (5, 10, 25 and 50 μM) of vanadium complexes (1–5) and $\text{VOSO}_4 \cdot 5\text{H}_2\text{O}$, in comparison to control.

3.3.6.2. Nuclear Morphology study using DAPI Staining

The effect of complexes on the nuclear morphology of MCF-7 cells was determined by staining dying cells with DAPI. The density of the DAPI stained nuclei was used to check the live cells in different treatment groups. Figures 3.15 and 3.16 show images taken after DAPI staining in blue fluorescence at different concentrations of **2** and **4**. It can be seen from Figures 3.15 and 3.16 that the number of DAPI stained nuclei was reduced in treated wells with increasing concentrations of the complexes indicating the dose dependent cell death. Control cells hardly showed any sort of condensation in comparison to the test compounds' activity (as shown in Figure 3.17) when the cells were examined under a fluorescent microscope, with a DAPI filter. Figures 3.15 and 3.16 also show the grey scale images at 48 h of the representative complex **2** and **4**, respectively, after the treatment with increasing concentrations of the complexes. All images clearly demonstrate the brightly condensed chromatin bodies and the nuclear blebbings (indicated by arrows in Figures 3.15 and 3.16) in treated cells compared to control cells. Besides showing nuclear

changes, the drug treated groups also revealed a shrinking morphology, which is another important hallmark of apoptosis.

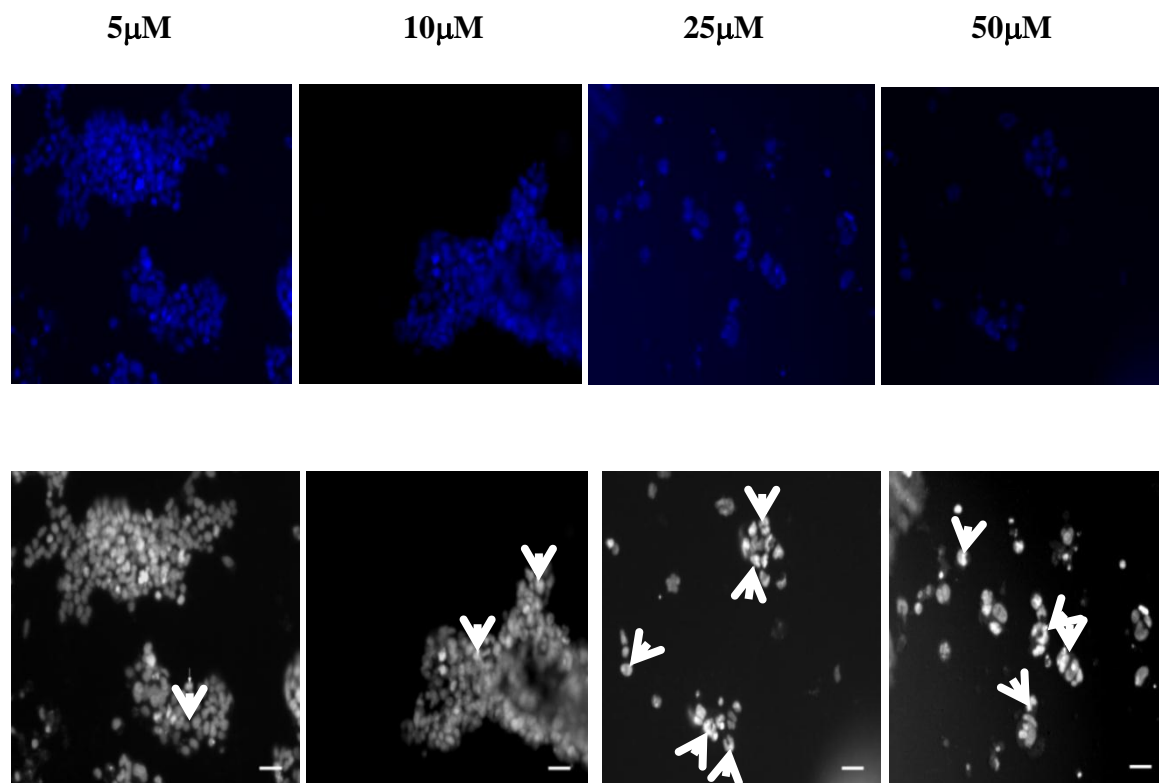


Figure 3.15. Images taken after DAPI staining in blue fluorescence and the corresponding grey scale images at 48 h at different concentrations of $[V^{IV}OL_2]$ (**2**). Arrows showing the morphological changes in nuclei of MCF-7 cells observed on applying increasing concentrations (5, 10, 25 and 50 μM) of $[V^{IV}OL_2]$ (**2**) in comparison to control.

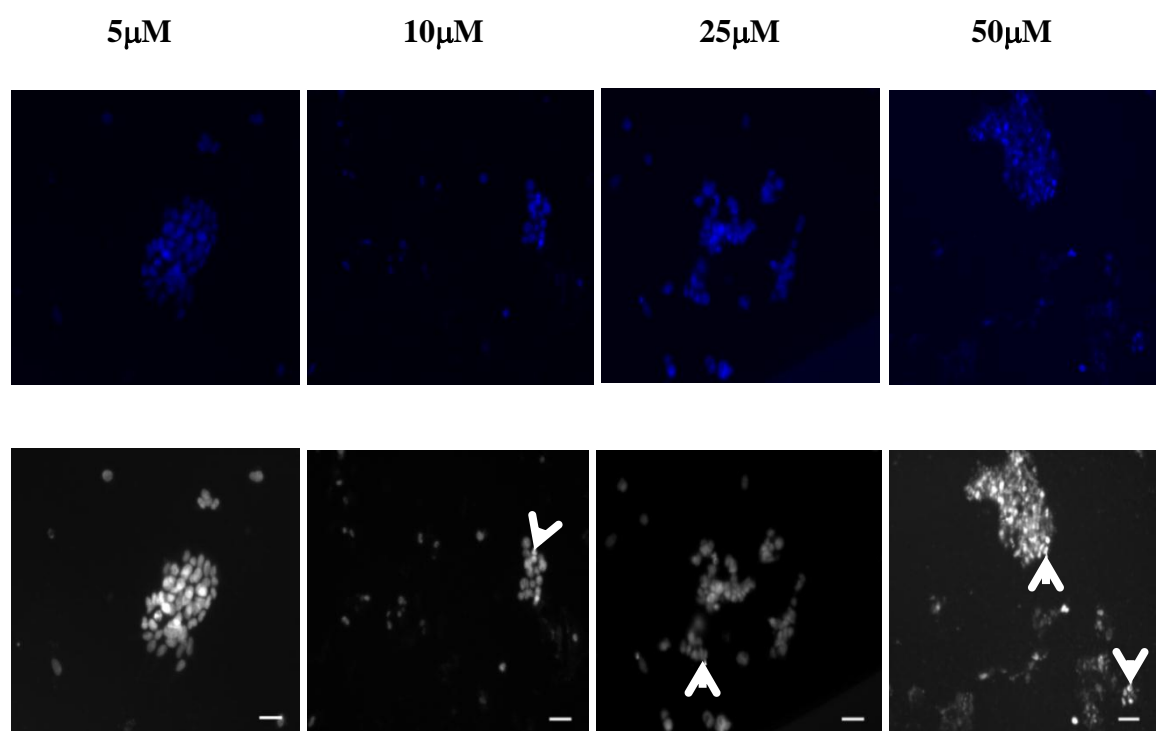


Figure 3.16. Images taken after DAPI staining in blue fluorescence and the corresponding grey scale images at 48 h at different concentrations of $[V^{IV}_3O_3(\mu\text{-OMe})_3(\mu_3\text{-OMe})L^4_2]$ (**4**). Arrows showing the morphological changes in nuclei of MCF-7 cells observed on applying increasing concentrations (5, 10, 25 and 50 μM) of **4** in comparison to control.

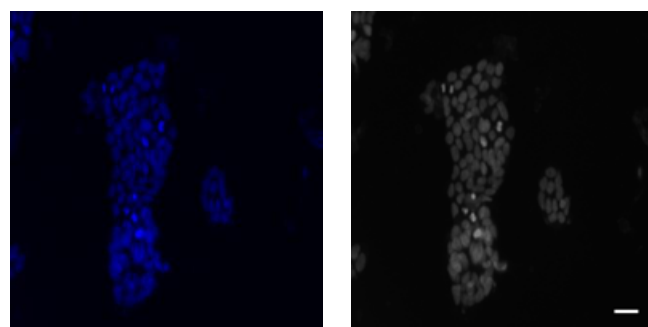


Figure 3.17. Images taken after DAPI staining in blue fluorescence and the corresponding grey scale image at 48 h after the treatment with control.

3.3.7. *In Vitro* Insulin-Mimetic Activity

In this study, **1–5** were tested for their insulin-mimetic potential in an *in vitro* glucose uptake assay. In L6 myotubes, a cell line of skeletal muscle origin, glucose uptake in response to insulin stimulation plays a key role in whole body glucose homeostasis. GLUT4 is the major glucose transporter of muscle exquisitely regulated by insulin through post-translational events.⁷⁹ The L6 myotubes differentiated from the L6 myoblast have the ability to respond to insulin via insulin receptor signaling and translocation of GLUT4 to the plasma membrane.

In the present study, the hyperglycemic condition was created in cell culture by incubating the cells in 25 mM glucose. Table 3.6 summarizes the percent glucose uptake at 10, 25 and 50 μM concentrations of **1–5** while the graphical presentation is shown in Figure 3.18. The glucose uptake induced by insulin (100 nM) was considered as 100%. Complex **2** (25 μM) was found to have considerable insulin-mimetic activity (256.14%). The 10 μM concentrations of all the complexes showed insulin-mimetic activity comparable to that of insulin taken as positive control (**1**: 122.10%; **2**:132.63%; **3**:167.36%, **4**: 135.44%; **5**: 197.89%; $\text{VOSO}_4 \cdot 5\text{H}_2\text{O}$: 138.94%). Therefore it can be concluded that all the compounds have good insulin-mimetic property at 10 μM concentration. D. Rehder et al. have also reported some ON ligated vanadium compounds which are as effective as or more potent than insulin at concentrations of 10 μM and below.⁹ It has also been observed in the case of **1**, **3–5** and VOSO_4 , that with increasing complex concentration (10 to 50 μM), there is a decrease in percent glucose uptake, while in case of **2** it increases from 10 to 25 μM but again decreases upon increasing the concentration to 50 μM . There are literature evidences wherein it has been reported that in many species the linearity of percent glucose uptake is not maintained with increasing concentration.⁸⁰ In the case of **2** and **5** at 25 μM concentration, the enhancement of the insulin-mimetic activity with respect to the other synthesized complexes might be related to their different structural characteristics and extent of solubility in aqueous medium. The mechanism of insulin-mimetic activity of the complexes has to be determined further. However, for vanadium it has been proposed that it can enhance insulin signaling most likely closely to its potent inhibition of PTPases of the insulin regulatory cascade. It has been reported that the exposure of cells to VOSO_4 resulted in an increase in glucose uptake, insulin receptor (IR) and protein kinase B (Akt) phosphorylation and intracellular ROS generation.⁸¹

Our observed results are comparable or better than some of the recent reports on *in vitro* antidiabetic results of vanadium(IV) complexes.⁸² The glucose uptake activity of our reported complexes are comparable to bis(maltolato)vanadium(III)-polypyridyl complexes¹⁴ and also the nonoxidovanadium(IV) aroylhydrazone complexes^{50a} reported earlier. The difference in values may be attributed to the nature of compounds synthesized with different ligands. Thus it can be concluded that the reported vanadium complexes (**1–5**) have profound insulin-mimetic activity and can be considered as a possible treatment option for diabetes.

Table 3.6. Percent glucose uptake at concentrations (10, 25 and 50 μM) of **1–5**, $\text{VO}_2\text{SO}_4 \cdot 5\text{H}_2\text{O}$ and Control as compared to 100% glucose uptake of insulin (100 nm).

| Complex | Glucose Uptake (%) | | |
|---|--------------------|-------------------|-------------------|
| | 10 μM | 25 μM | 50 μM |
| $[\text{V}^{\text{IV}}\text{OL}^1_2]$ (1) | 122.10 \pm 0 | 111.58 \pm 7.27 | 76.49 \pm 3.94 |
| $[\text{V}^{\text{IV}}\text{OL}^2_2]$ (2) | 132.63 \pm 7.87 | 256.14 \pm 1.88 | 73.68 \pm 0.90 |
| $[\text{V}^{\text{IV}}\text{OL}^3_2]$ (3) | 167.36 \pm 9.54 | 119.30 \pm 0.30 | 112.28 \pm 1.36 |
| $[\text{V}^{\text{IV}}_3\text{O}_3(\mu\text{-OMe})_3(\mu_3\text{-OMe})\text{L}^4_2]$ (4) | 135.44 \pm 2.81 | 72.98 \pm 4.65 | 55.79 \pm 1.96 |
| $[\text{V}^{\text{IV}}_3\text{O}_3(\mu\text{-OMe})_3(\mu_3\text{-OMe})\text{L}^5_2]$ (5) | 197.89 \pm 4.54 | 86.31 \pm 2.11 | 67.37 \pm 4.51 |
| $\text{VO}_2\text{SO}_4 \cdot 5\text{H}_2\text{O}$ | 138.94 \pm 5.50 | 126.32 \pm 2.42 | 20.34 \pm 3.21 |
| Control | 7.02 \pm 10.29 | | |

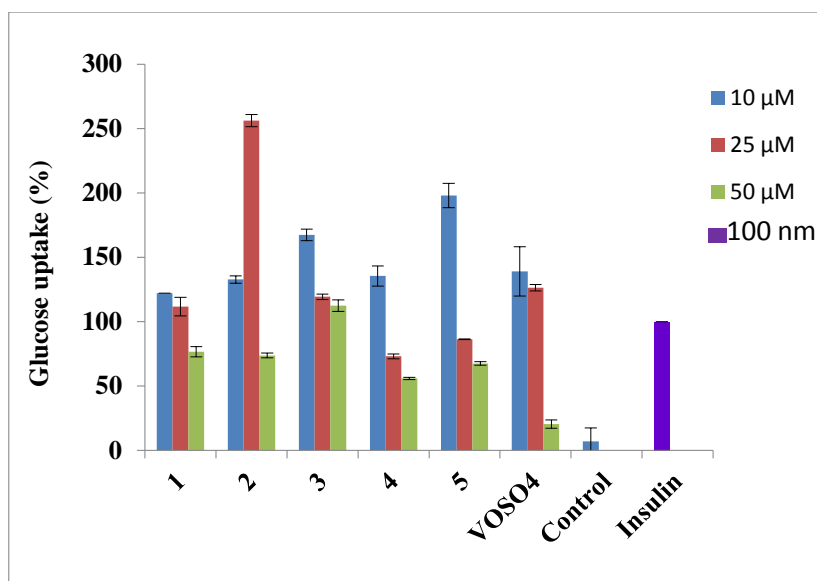


Figure 3.18. Effect of vanadium complexes on glucose uptake in cultured L6 myotubes under high glucose conditions (25 mM Glucose). Three concentrations 10, 25 and 50 μM were tested for each complex. The data is represented as mean \pm SD (n = 3).

3.3.8. Immunoblot analysis

From the glucose uptake study, it was found that complexes **2** (25 μM) and **5** (10 μM) have considerable hypoglycemic activity. Further the mechanism of action of **2** and **5** was studied in differentiated L6 myotubes. Thus to determine whether these compounds act via insulin signaling pathway, immunoblot analysis for Insulin receptor substrate-1 (IRS-1) was carried out. IRS-1 is a cytoplasmic substrate molecule which is phosphorylated by insulin receptor when activated by insulin or insulin like molecules. It may mediate the control of various cellular processes by insulin. There was an increase in IRS-1 protein after the treatment with insulin as revealed by immunoblot. In presence of **2** and **5**, it was found that IRS-1 accumulation was maintained at a constant level in the cytoplasm even after 240 min of treatment. The data indicates that complex **2** (25 μM) and **5** (10 μM) exerts their effect via the activation of insulin receptor. Thus, the immunoblot analysis shows that complexes **2** and **5** have considerable insulin-mimetic activity. Figure 3.19 depicts the immunoblot analysis of IRS-1 after the treatment of differentiated L6 myotubes with **2** (25 μM), **5** (10 μM) and insulin (100 nM).

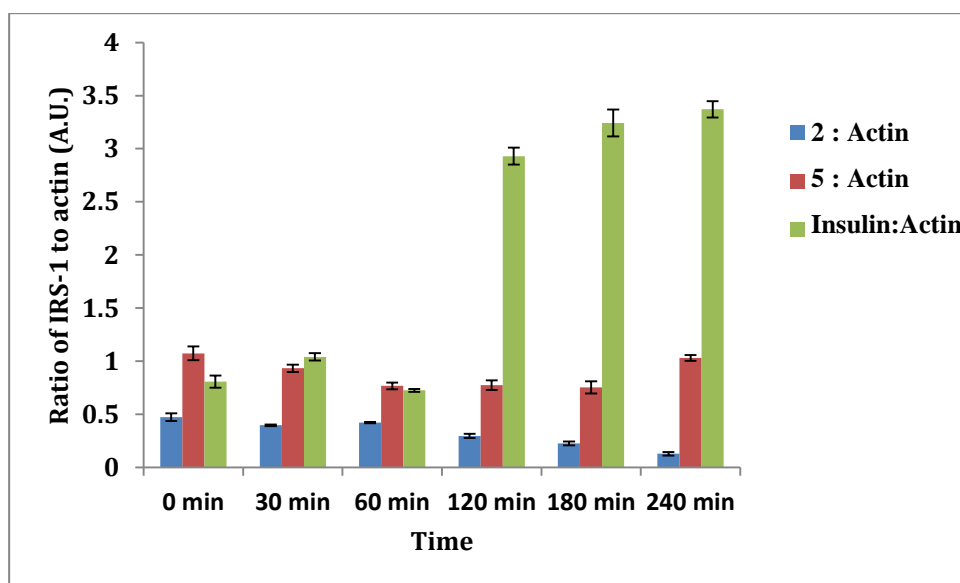
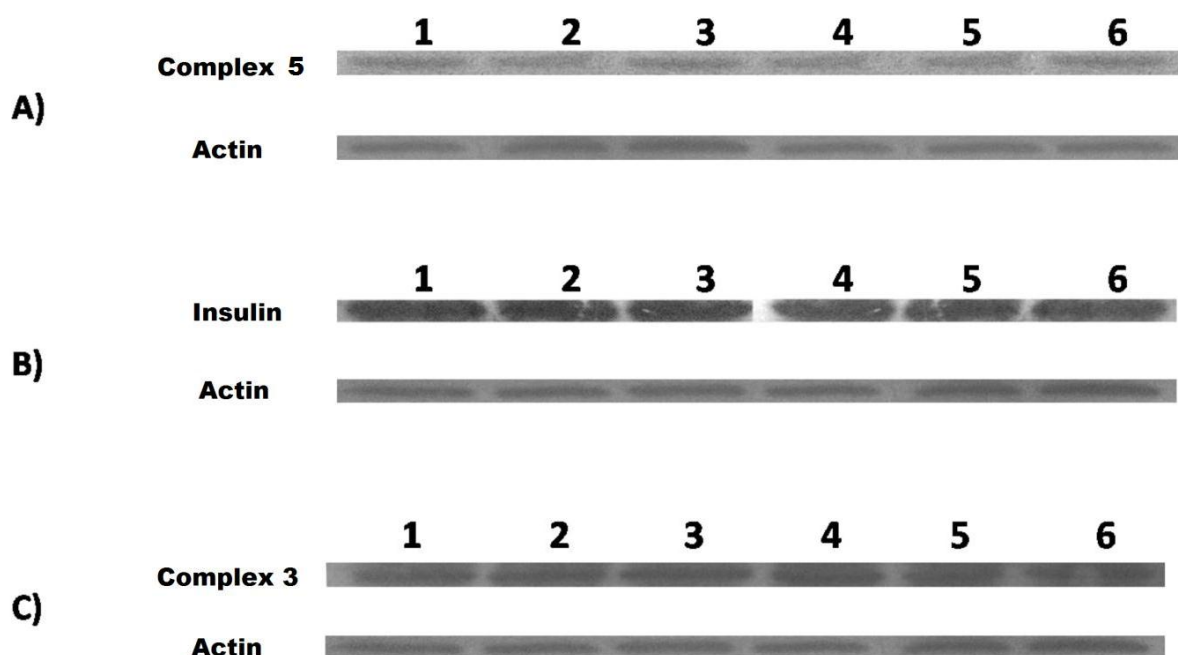


Figure 3.19. Effect of vanadium complexes treatment on IRS-1 accumulation. The immunoblot analysis of IRS-1 after the treatment of differentiated L6 myotubes with A) Complex 5 (25 μ M); B) Insulin (100 nM); and C) Complex 3 (10 μ M). Lanes 1–6 show IRS-1 accumulations at 0, 30, 60, 120, 180 and 240 min after compound or insulin treatment respectively.

3.4. CONCLUSION

Synthetic approach to monooxidovanadium(IV), $[V^{IV}OL^{1-3}]_2$ (**1–3**) and trinuclear alkoxido bridged vanadium(IV), $[V^{IV}_3O_3(\mu\text{-OMe})_3(\mu_3\text{-OMe})L^{4,5}]_2$ (**4** and **5**) complexes using azo ligands have been presented. The synthesized complexes were fully characterized by elemental analysis, IR and UV-vis spectroscopy and cyclic voltammetry. Further support for the formation of the trinuclear species was obtained from single crystal X-ray diffraction study, which revealed the molecule to be composed of three slightly distorted octahedral vanadium atoms forming an almost butterfly-shaped V_3O_4 unit similar to the well-known 3Fe-4S iron sulfur cluster. The *in vitro* antiproliferative activity of the complexes against MCF-7 cancer cell line was assayed. The cytotoxicity of the complexes is affected by varying the substituent of the ligands, whereby **2** and **4** was particularly potent against the cells tested. The cytotoxicity of the complexes is affected by the functional groups attached to the thiazolylazo derivative. The results reported herein will inspire further work on oxidovanadium(IV)–azo complexes for the development of metal-based anti-cancer agents and future drugs for diabetes. IC_{50} values of the complexes were found to be comparable with some of the clinically referred chemotherapeutic drugs. In addition, the complexes were probed for their *in vitro* insulin-mimetic activity against insulin responsive L6 myoblast cells. The percent glucose uptake of the complexes was found to be significant as compared to insulin, where complex **2** (25 μM) and **5** (10 μM) proved to be more potent, possibly due to their greater aqueous solubility. Considering the high values of glucose uptake, the insulin signaling mechanism of **2** and **5** was studied by immunoblot analysis for IRS-1 molecule. Our observed results are comparable or better than some of the recent reports on *in vitro* antidiabetic results of vanadium(IV) complexes.

3.5. REFERENCES

- (1) (a) Kiss, T.; Jakusch, T.; Pessoa, J. C.; Tomaz, I. *Coord. Chem. Rev.* **2003**, *237*, 123–133. (b) Rehder, D. *Dalton Trans.* **2013**, *42*, 11749–11761. (c) Meisch, H. U.; Bielig, H. J. *Basic Res. Cardiol.* **1980**, *75*, 413–417. (d) Baran, E. J. *Adv. Plant Physiol.* **2008**, *10*, 357–372. (e) Anke, M. *Anales de la Real Academia Nacional de Farmacia* **2004**, *70*, 961–999.
- (2) (a) Rehder, D.; Santonin, G.; Licini, G. M.; Schulzke, C.; Meier, B. *Coord. Chem. Rev.* **2003**, *237*, 53–63. (b) Plass, W. *Coord. Chem. Rev.* **2003**, *237*, 205–212. (c) Thompson, K. H.; Orvig, C. *Coord. Chem. Rev.* **2001**, *219*, 1033–1053. (d) Butler, A. *Coord. Chem. Rev.* **1999**, *187*, 17–35. (e) Frausto da Silva, J. J. R.; Williams, R. J. P. *The Biological Chemistry of the Elements*, 2nd ed.; Oxford University Press: Oxford, U.K., 2001. (f) Kaim, W.; Schwederski, B. *Bioinorganic Chemistry: Inorganic Elements in the Chemistry of Life*; John Wiley & Sons: Chichester, U. K., 1994. (g) Eady, R. R. *Coord. Chem. Rev.* **2003**, *237*, 23–30. (h) Pecoraro, V. L.; Slebodnick, C.; Hamstra, B. In: Crans DC, Tracy AS (Ed.) *Vanadium Compounds: Chemistry, Biochemistry and Therapeutic Applications*, ACS Symposium Series; American Chemical Society: Washington DC, Chapter 12, 1998. (i) Butler, A. in: Reedijk, J.; Bouwman, E. (Ed.), *Bioinorganic Catalysis*. Marcel Dekker: New York, Chapter 4, 1999. (j) Maurya, M. R. *Coord. Chem. Rev.* **2003**, *237*, 163–181. (k) Sakurai, H.; Kojima, Y.; Yoshikawa, Y.; Kawabe, K.; Yasui, H. *Coord. Chem. Rev.* **2002**, *226*, 187–192.
- (3) Kioseoglou, E.; Petanidis, S.; Gabriel, C.; Salifoglou, A. *Coord. Chem. Rev.* **2015**, *301*, 87–105.
- (4) Mohamadi, M.; Yousef, E. S.; Torkzadeh-Mahani, M.; Foro, S.; Akbari, A. *RSC Adv.* **2015**, *5*, 101063–101075.
- (5) Kremer, L. E.; McLeod, A. I.; Aitken, J. B.; Levina, A.; Lay, P. A. *J. Inorg. Biochem.* **2015**, *147*, 227–234.
- (6) Petanidis, S.; Kioseoglou, E.; Hadzopoulou-Cladaras, M.; Salifoglou, A. *Cancer Lett.* **2013**, *335*, 387–396.
- (7) Wei, Y.; Zhang, C.; Zhao, P.; Yang, X.; Wang, K. *J. Inorg. Biochem.* **2011**, *105*, 1081–1085.
- (8) Pelletier, J.; Domingues, N.; Castro, M. M. C. A.; Östenson, C.-G. *J. Inorg. Biochem.* **2016**, *154*, 29–34.

- (9) Rehder, D.; Pessoa, J. C.; Geraldés, C. F. G. C.; Kabanos, T.; Kiss, T.; Meier, B.; Micera, G.; Pettersson, L.; Rangel, M.; Salifoglou, A.; Turel, I.; Wang, D. *J. Biol. Inorg. Chem.* **2002**, *7*, 384–396.
- (10) Saltiel, A. R.; Khan, C. R. *Nature* **2001**, *414*, 799–806.
- (11) Noblía, P.; Baran, Enrique J.; Otero, L.; Draper, P.; Cerecetto, H.; González, M.; Piro, Oscar E.; Castellano, Eduardo E.; Inohara, T.; Adachi, Y.; Sakurai, H.; Gambino, D. *Eur. J. Inorg. Chem.* **2004**, *2*, 322–328.
- (12) Nilsson, J.; Shteinman, A. A.; Degerman, E.; Enyedy, E. A.; Kiss, T.; Behrens, U.; Rehder, D.; Nordlander, E. *J. Inorg. Biochem.* **2011**, *105*, 1795–1800.
- (13) Willsky, G. R.; Chi, L.-H.; Godzala Iii, M.; Kostyniak, P. J.; Smees, J. J.; Trujillo, A. M.; Alfano, J. A.; Ding, W.; Hu, Z.; Crans, D. C. *Coord. Chem. Rev.* **2011**, *255*, 2258–2269.
- (14) Islam, M. N.; Kumbhar, A. A.; Kumbhar, A. S.; Zeller, M.; Butcher, R. J.; Dusane, M. B.; Joshi, B. N. *Inorg. Chem.* **2010**, *49*, 8237–8246.
- (15) Pillai, S. I.; Subramanian, S. P.; Kandaswamy, M. *Eur. J. Med. Chem.* **2013**, *63*, 109–117.
- (16) Sostarecz, A. G.; Gaidamauskas, E.; Distin, S.; Bonetti, S. J.; Levinger, N. E.; Crans, D. C. *Chem. Eur. J.* **2014**, *20*, 5149–5159.
- (17) Crans, D. C. *J. Org. Chem.* **2015**, *80*, 11899–11915.
- (18) E. Baran. *J. Inorg. Biochem.* **2000**, *80*, 1–10.
- (19) S. Karmaker, T. K. Saha, Y. Yoshikawa, H. Yasui, H. Sakurai. *J. Inorg. Biochem.* **2006**, *100*, 1535–1546.
- (20) Levina, A.; McLeod, A. I.; Gasparini, S. J.; Nguyen, A.; De Silva, W. G. M.; Aitken, J. B.; Harris, H. H.; Glover, C.; Johannessen, B.; Lay, P. A. *Inorg. Chem.* **2015**, *54*, 7753–7766.
- (21) Melchior, M.; Thompson, K. H.; Jong, J. M.; Rettig, S. J.; Shuter, E.; Yuen, V. G.; Zhou, Y.; McNeill, J. H.; Orvig, C. *Inorg. Chem.* **1999**, *38*, 2288–2293.
- (22) Cohen, N.; Halberstam, M.; Shlimovich, P.; Chang, C. J.; Shamoon, H.; Rossetti, L. *J. Clin. Invest.* **1995**, *95*, 2501–2509.
- (23) McNeill, J. H.; Yuen, V. G.; Hoveyda, H. R.; Orvig, C. *J. Med. Chem.* **1992**, *35*, 1489–1491.

- (24) (a) Thompson, K. H.; Orvig, C. *J. Inorg. Biochem.* **2006**, *100*, 1925–1935. (b) Thompson, K. H.; Lichter, J.; LeBel, C.; M C. Scaife, J. H. McNeill, C. Orvig. *J. Inorg. Biochem.* **2009**, *103*, 554–558.
- (25) Schechter, Y.; Meyerovitch, J.; Farfel, Z.; Sack, J.; Bar-Meir, S.; Amir, S.; Degani, H.; Karlsh, S. J. D. *Vanadium in Biological Systems*. pp 129–142, Kluwer Academic Publishers, Norwell, MA, 1990.
- (26) Thompson, K. H.; McNeill, J. H.; C. Orvig (Eds.) *Topics in Biological Chemistry: Metallopharmaceuticals*. pp. 139–158, Springer-Verlag, Heidelberg (1999).
- (27) Sakurai, H.; Fugono, J.; Yasui, H. *Mini-Rev. Med. Chem.* **2004**, *4*, 41–48.
- (28) Adachi, Y.; Yoshida, J.; Kodera, Y.; Katoh, A.; Takada, J.; Sakurai, H. *J. Med. Chem.* **2006**, *49*, 3251–3256.
- (29) Hooft van Huijsduijnen, R.; Sauer, W. H. B.; Bombrun, A.; Swinnen, D. *J. Med. Chem.* **2004**, *47*, 4142–4146.
- (30) Yamaguchi, M.; Wakasugi, K.; Saito, R.; Adachi, Y.; Yoshikawa, Y.; Sakurai, H.; Katoh, A. *J. Inorg. Biochem.* **2006**, *100*, 260–269.
- (31) Thompson, K. H.; Liboiron, B. D.; Sun, Y.; Bellman, K. D. D.; Setyawati, I. A.; Patrick, B. O.; Karunaratne, V.; Rawji, G.; Wheeler, J.; Sutton, K.; Bhanot, S.; Cassidy, C.; McNeill, J. H.; Yuen, V. G.; Orvig, C. *J. Biol. Inorg. Chem.* **2003**, *8*, 66–74.
- (32) Kar, S.; Pradhan, B.; Sinha, R. K.; Kundu, T.; Kodgire, P.; Rao, K. K.; Puranic, V. G.; Lahiri, G. K. *Dalton Trans.* **2004**, 1752–1760.
- (33) Sanyal, A.; Banerjee, P.; Lee, G.; Peng, S. M.; Hung, C. J.; Goswami, S. *Inorg. Chem.* **2004**, *43*, 7456–7462.
- (34) Karipcin, F.; Dede, B.; Percin-Ozkorucuklu, S.; Kabalcilar, E. *Dyes Pigm.* **2010**, *84*, 14–18.
- (35) Dougan, S. J.; Habtemariam, M. M. A.; Parsons, S.; Sadler, P. J. *Inorg. Chem.* **2006**, *45*, 10882–10894.
- (36) Khedr, A. M.; Gaber, M.; Issa, R. M.; Erten, H. *Dyes Pigm.* **2005**, *67*, 117–124.
- (37) Khanmohammadi, H.; Rezaeian, K.; Amini, M. M.; Ng, S. W. *Dyes Pigm.* **2013**, *98*, 557–564.
- (38) Satam, M. A.; Raut, R. K.; Telore, R. D.; Sekar, N. *Dyes Pigm.* **2013**, *97*, 32–42.
- (39) Delaire, J. A.; Nakatani, K. *Chem. Rev.* **2000**, *100*, 1817–1845.

- (40) Ono, M.; Wada, Y.; Wu, Y.; Nemori, R.; Jinbo, Y.; Wang, H.; Lo, K. M.; Yamaguchi, N.; Brunkhorst, B.; Otomo, H.; Wesolowski, J.; Way, J. C.; Itoh, I.; Gillies, S.; Chen, L. B. *Nature Biotechnol.* **1997**, *15*, 343–348.
- (41) Roldo, M.; Barbu, E.; Brown, J. F.; Laight, D. W.; Smart, J. D.; Tsibouklis, J. *Expert Opin. Drug. Deliv.* **2007**, *4*, 547–560.
- (42) Moanta, A.; Radu, S. *Rev. Roum. Chem.* **2009**, *54*, 151–156.
- (43) (a) Jimonet, P.; Audiau, F.; Barreau, M.; Blanchard, J. -C.; Boireau, A.; Bour, Y.; Coléno, M. -A.; Doble, A.; Doerflinger, G.; Do Huu, C.; Donat, M. -H.; Duchesne, J. M.; Ganil, P.; Guérémy, C.; Honoré, E.; Just, B.; Kerphirique, R.; Gontier, S.; Hubert, P.; Laduron, P. M.; Le Blevet, J.; Meunier, M.; Miquet, J. -M.; Nemecek, C.; Pasquet, M.; Piot, O.; Pratt, J.; Rataud, J.; Reibaud, M.; Stutzmann, J.-M.; Mignani, S. *J. Med. Chem.* **1999**, *42*, 2828–2843. (b) Collins, I.; Moyes, C.; Davey, W. B.; Rowley, M.; Bromidge, F. A.; Quirk, K.; Atack, J. R.; McKernan, R. M.; Thompson, S.-A.; Wafford, K.; Dawson, G. R.; Pike, A.; Sohal, B.; Tsou, N. N.; Ball, R. G.; Castro, J. L. *J. Med. Chem.* **2002**, *45*, 1887–1900. (c) Andreani, S. Burnelli, M. Granaiola, M. Guardigli, A. Leoni, A. Locatelli, R. Morigi, M. Rambaldi, A.; Rizzoli, M.; Varoli, L.; Roda, A. *Eur. J. Med. Chem.* **2008**, *43*, 657–661. (d) A. Alanine, A. Flohr, A. K. Miller, R. D. Norcross, K. Riemer, US 2006/0003986A1.
- (44) (a) Lee, Y. S.; Kim, H.; Kim, Y. H.; Roh, E. J.; Han, H.; Shin, K. J.; *Bioorg. Med. Chem.* **2012**, *22*, 7555–7561. (b) Lagoja, I.; Pannecouque, C.; Griffioen, G.; Wera, S.; Rojasdelaparra, V. M.; Aerschot, A. V. *Eur. J. Pharm. Sci.* **2011**, *43*, 386–392. (b) Shiradkar, M. R.; Akula, K. C.; Dasari, V.; Baru, V.; Chiningiri, B.; Gandhi, S.; Kaur, R. *Bioorg. Med. Chem.* **2007**, *15*, 2601–2610.
- (45) (a) Andurkar, S. V.; Guin, C. B.; Stables, J. P.; Kohn, H. *J. Med. Chem.* **2001**, *44*, 1475–1478. (b) Désaubry, L.; Wermuth, C. G.; Boehrer, A.; Marescaux, C.; Bourguignon, J.-J. *Bioorg. Med. Chem. Lett.* **1995**, *5*, 139–144.
- (46) (a) El-Subbagh, H. I.; Al-Obaid, A. M. *Eur. J. Med. Chem.* **1996**, *31*, 1017–1021. (b) Lombardo, L. J.; Lee, F. Y.; Chen, P.; Norris, D.; Barrish, J. C.; Behnia, K.; Castaneda, S.; Cornelius, L. A. M.; Das, J.; Doweiko, A. M.; Fairchild, C.; Hunt, J. T.; Inigo, I.; Johnston, K.; Kamath, A.; Kan, D.; Klei, H.; Marathe, P.; Pang, S.; Peterson, R.; Pitt, S.; Schieven, G. L.; Schmidt, R. J.; Tokarski, J.; Wen, M.-L.; Wityak, J.; Borzilleri, R. M. *J. Med. Chem.* **2004**, *47*, 6658–6661.

- (47) Vu, C. B.; Bemis, J. E.; Disch, J. S.; Ng, P. Y.; Nunes, J. J.; Milne, J. C.; Carney, D. P.; Lynch, A. V.; Smith, J. J.; Lavu, S.; Lambert, P. D.; Gagne, D. J.; Jirousek, M. R.; Schenk, S.; Olefsky, J. M.; Perni, R. B. *J. Med. Chem.* **2009**, *52*, 1275–1283.
- (48) (a) Das, B.; Reddy, C. R.; Kashanna, J.; Mamidyala, S. K.; Kumar, C. G. *Med. Chem. Res.* **2012**, *21*, 3321–3325. (b) Shen, A. Y.; Tsai, C. T.; Chen, C. L. *Eur. J. Med. Chem.* **1999**, *34*, 877–882. (c) Shaterian, H. R.; Yarahmadi, H.; Ghashang, M. *Bioorg. Med. Chem. Lett.* **2008**, *18*, 788–792.
- (49) Crans, D. C.; Smee, J. J.; Gaidamauskas, E.; Yang, L. *Chem. Rev.* **2004**, *104*, 849–902.
- (50) (a) Dash, S. P.; Pasayat, S.; Saswati; Roy, S.; Dinda, R.; Tiekink, E. R. T.; Mukhopadhyay, S.; Bhutia, S.; Hardikar, M. R.; Joshi, B.; Patil, Y. P.; Nethaji, M. *Inorg. Chem.* **2013**, *52*, 4096–4107. (b) Dash, S. P.; Pasayat, S.; Bhakat, S.; Dash, H. R.; Das, S.; Butcher, R. J.; Dinda, R. *Polyhedron* **2012**, *31*, 524–529. (c) Dash, S. P.; Panda, A. K.; Pasayat, S.; Dinda, R.; Biswas, A.; Tiekink, E. R. T.; Patil, Y. P.; Nethaji, M.; Kaminsky, W.; Mukhopadhyay, S.; Bhutia, S. *Dalton Trans.* **2014**, *43*, 10139–10156. (d) Dash, S. P.; Panda, A. K.; Pasayat, S.; Dinda, R.; Biswas, A.; Tiekink, E. R. T.; Mukhopadhyay, S.; Bhutia, S. K.; Kaminsky, W.; Sinn, E. *RSC Adv.* **2015**, *5*, 51852–51867. (e) Dash, S. P.; Panda, A. K.; Pasayat, S.; Majumder, S.; Biswas, A.; Kaminsky, W.; Mukhopadhyay, S.; Bhutia, S. K.; Dinda, R. *J. Inorg. Biochem.* **2015**, *144*, 1–12.
- (51) (a) Sanudo, E. C.; Smith, A. A.; Mason, P. V.; Helliwell, M.; Aromi, G.; Winpenny, R. E. P. *Dalton Trans.* **2006**, 1981–1987. (b) Castro, S. L.; Sun, Z.; Grant, C. M.; Bollinger, J. C.; Hendrickson, D. N.; Christou, G. *J. Am. Chem. Soc.* **1998**, *120*, 2365–2375. (c) Laye, R. H.; Murrie, M.; Ochsenein, S.; Bell, A. R.; Teat, S. J.; Raftery, J.; Güdel, H. -U.; McInnes, E. J. L. *Chem. Eur. J.* **2003**, *9*, 6215–6220. (d) Ting, C.; Hammer, M. S.; Baenziger, N. C.; Messerle, L.; Deak, J.; Li, S.; McElfresh, M. *Organometallics* **1997**, *16*, 1816–1818. (e) Castro, S. L.; Streib, W. E.; Sun, J.-S.; Christou, G. *Inorg. Chem.* **1996**, *35*, 4462–4468. (f) Batchelor, L. J.; Fitzgerald, E.; Wolowska, J.; McDouall, J. J. W.; McInnes, E. J. L. *Chem. Eur. J.* **2010**, *16*, 11082–11088.
- (52) (a) Daniel, C.; Hartl, H. *J. Am. Chem. Soc.* **2005**, *127*, 13978–13987. (b) Tidmarsh, I. S.; Laye, R. H.; Brearley, P. R.; Shanmugam, M.; Sañudo, E. C.; Sorace, L.; Caneschi, A.; McInnes, E. J. L. *Chem. Eur. J.* **2007**, *13*, 6329 – 6338

- (53) (a) Ohde, C.; Limberg, C.; Stoesser, R.; Demeshko, S. *Inorg. Chem.* **2010**, *49*, 2479–2485. (b) Sahoo, D.; Suriyanarayanan, R.; Chandrasekhar, V. *Dalton Trans.* **2014**, *43*, 10898–10909. (c) Maass, J. S.; Chen, Z.; Zeller, M.; Tuna, F.; Winpenny, R. E. P.; Luck, R. L. *Inorg. Chem.* **2012**, *51*, 2766–2776.
- (54) Zhu, H.; Liu, Q.; Deng, Y.; Wen, T.; Chen, C.; Wu, D. *Inorg. Chim. Acta* **1999**, *286*, 7–13.
- (55) Baksi, S.; Acharyya, R.; Dutta, S.; Blake, A. J.; Drew, M. G. B.; Bhattacharya, S. *J. Organomet. Chem.* **2007**, *692*, 1025–1032 and references therein.
- (56) Bruker (2007) APEX2 (Version 2.1-4), SAINT (version 7.34A), SADABS (version 2007/4), BrukerAXS Inc, Madison, Wisconsin, USA.
- (57) (a) Altomare, A., Burla, C., Camalli, M., Cascarano, G. L., Giacovazzo, C.; Guagliardi, A.; Moliterni, A. G. G.; Polidori, G.; Spagna, R. *J. Appl. Cryst.* **1999**, *32*, 115–119. (b) Altomare A, Cascarano G L, Giacovazzo C, Guagliardi A. *J. Appl. Cryst.* **1993**, *26*, 343–350.
- (58) (a) Sheldrick G. M. SHELXL-97, Program for the Refinement of Crystal Structures. University of Göttingen, Germany, 1997. (b) Sheldrick G. M. (2013) Crystal structure refinement with SHELXL. *Acta Cryst.* **2015**, *C71*, 3–8.
- (59) Mackay, S.; Edwards, C.; Henderson, A.; Gilmore, C.; Stewart, N.; Shankland, K.; Donald, A. (1997) *MaXus: a computer program for the solution and refinement of crystal structures from diffraction data*. University of Glasgow, Scotland.
- (60) Waasmaier, D.; Kirfel, A. *Acta Cryst. A* **1995**, *51*, 416–430.
- (61) Ha, B. G.; Nagaoka, M.; Yonezawa, T.; Tanabe, R.; Woo, J. T.; Kato, H.; Chung, U.-I.; Yagasaki, K. *J. Nutr. Biochem.* **2012**, *23*, 501–509.
- (62) Galante, P.; Mosthaf, L.; Kellerer, M.; Berti, L.; Tippmer, S.; Bossenmaier, B.; Häring, H. U. *Diabetes* **1995**, *44*, 646–651.
- (63) Dutta, S.; Basu, P.; Chakravorty, A. *Inorg. Chem.* **1993**, *32*, 5343–5348.
- (64) Das, C.; Adak, P.; Mondal, S.; Sekiya, R.; Kuroda, R.; Gorelsky, S. I.; Chattopadhyay, S. K. *Inorg. Chem.* **2014**, *53*, 11426–11437.
- (65) Li, Y.-T.; Yan, C.-W.; Guo, B.-R.; Liao, D.-Z. *Polyhedron* **1997**, *16*, 4379–4384
- (66) Maurya, M. R.; Haldar, C.; Khan, A. A.; Azam, A.; Salahuddin, A.; Kumar, A.; Costa Pessoa, J. *Eur. J. Inorg. Chem.* **2012**, 2560–2577.

- (67) Nakai, M.; Obata, M.; Sekiguchi, F.; Kato, M.; Shiro, M.; Ichimura, A.; Kinoshita, I.; Mikuriya, M.; Inohara, T.; Kawabe, K.; Sakurai, H.; Orvig, C.; Yano, S. *J. Inorg. Biochem.* **2004**, *98*, 105–112.
- (68) Pessoa, J. C.; Cavaco, I.; Correia, I.; Duarte, M. T.; Gillard, R. D.; Henriques, R. T.; Higes, F. J.; Madeira, C.; Tomaz, I. *Inorg. Chim. Acta.* **1999**, *293*, 1–11.
- (69) Farrugia L. J. Ortep-3 for Windows. *J. Appl. Cryst.* **1997**, *30*, 565
- (70) S. J. Lippard, J. M. Berg “Principles of Bioinorganic Chemistry” University Science Books: Mill Valley, CA; 1994.
- (71) Zhang, L.; Ren, W.; Wang, X.; Zhang, J.; Liu, J.; Zhao, L.; Zhang, X. *Eur. J. Med. Chem.* **2017**, *126*, 1071.
- (72) Ramadan, A. M. *J. Inorg. Biochem.* **1997**, *65*, 183–189.
- (73) Avaji, P. G.; Kumar, C. H. V.; Patil, S. A.; Shivananda, K. N.; Nagaraju, C. *Eur. J. Med. Chem.* **2009**, *44*, 3552–3559
- (74) Rosu, T.; Pahontu, E.; Pasculescu, S.; Georgescu, R.; Stanica, N.; Curaj, A.; Popescu, A.; Leabu, M. *Eur. J. Med. Chem.* **2010**, *45*, 1627–1634.
- (75) (a) Saswati; Chakraborty, A.; Dash, S. P.; Panda, A. K.; Acharyya, R.; Biswas, A.; Mukhopadhyay, S.; Bhutia, S. K.; Crochet, A.; Patil, Y. P.; Nethaji, M.; Dinda, R. *Dalton Trans.* **2015**, *44*, 6140–6157. (b) Kilpin, K. J.; Dyson, P. J. *Chem. Sci.* **2013**, *4*, 1410–1419. (c) Liu, Y.; Li, F.; Wu, L.; Wang, W.; Zhu, H.; Zhang, Q.; Zhou, H.; Yan, B. *Bioorg. Med. Chem. Lett.* **2015**, *25*, 1971–1975. (d) Lammer, A. D.; Cook, M. E.; Sessler, J. L. *J. Porphyrins Phthalocyanines* **2015**, *19*, 1–8.
- (76) Sartzi, H.; Stoumpos, C. C.; Giouli, M.; Verginadis, I. I.; Karkabounas, S. C.; Cunha-Silva, L.; Escuer, A.; Perlepes, S. P. *Dalton Trans.* **2012**, *41*, 11984–11988.
- (77) Reytman, L.; Braitbard, O.; Hochman, J.; Tshuva, E. Y. *Inorg. Chem.* **2016**, *55*, 610–618.
- (78) Reytman, L.; Braitbard, O.; Tshuva, E. Y. *Dalton Trans.* **2012**, *41*, 5241–5247.
- (79) Ishiki, M.; Klip, A. *Endocrinology* **2005**, *146*, 5071–5078.
- (80) (a) Strobel, P.; Allard, C.; Perez-Acle, T.; Calderon, R.; Aldunate, R.; Leighton, F. *Biochem. J.* **2005**, *386*, 471–478. (b) Sinha, S. K.; Ahmed, I.; Gayathri, M. *Int. J. Drug Dev. & Res.* **2013**, *5*, 187–193.
- (81) Gruzewska, K.; Michno, A.; Pawelczyk, T.; Bielarczyk, H. *J. Physiol. Pharmacol.* **2014**, *65*, 603–611.

(82) (a) Gundhla, I. Z.; Walmsley, R. S.; Ugirinema, V.; Mnonopi, N. O.; Hosten, E.; Betz, R.; Frost, C. L.; Tshentu, Z. R. *J. Inorg. Biochem.* **2015**, *145*, 11–18. (b) Y. Yoshikawa, H. Sakurai, D. C. Crans, G. Micerad, E. Garribba. *Dalton Trans.* **2014**, *43*, 6965–6972. (c) Pelletier, J.; Domingues, N.; Castro, M. M. C. A.; Östenson, C. *J. Inorg. Biochem.* **2016**, *154*, 29–34. (d) Zhao, Q.; Chena, D.; Liu, P.; Wei, T.; Zhanga, F.; Ding, W. *J. Inorg. Biochem.* **2015**, *149*, 39–44.

Chapter 4

Synthesis, characterization and study of reactivity of Ru and Ir complexes of 2-arylazophenols: Solvent assisted CO insertion and formation of metal (Ru, Ir)–carbon bond

Chapter 4

Synthesis, characterization and study of reactivity of Ru and Ir complexes of 2-arylazophenols: Solvent assisted CO insertion and formation of metal (Ru, Ir)–carbon bond

ABSTRACT

Reaction of 2-(arylazo)phenols (HL) with $[\text{Ru}(\text{PPh}_3)_3\text{Cl}_2]$ in ethanolic medium under basic conditions affords two organometallic Ru(II) complexes, $[\text{Ru}(\text{PPh}_3)_2\text{L}(\text{CO})]$ (**1**) and $[\text{Ru}(\text{PPh}_3)_2\text{L}(\text{CH}_3\text{CN})]$ (**2**). A similar reaction of HL with $[\text{Ir}(\text{PPh}_3)_3\text{Cl}]$ results in formation of the organometallic Ir(III) complex, $[\text{IrL}(\text{PPh}_3)_2(\text{H})]$ (**3**). The 2-(arylazo)phenolate ligand is coordinated to the metal center in each complex (**1–3**) as a tridentate C, N, O-donor via C–H activation of the ligand. The sixth coordination site in the equatorial plane of **1–3** is occupied by CO, CH₃CN and H⁺, respectively. The plausible solvent assisted mechanistic pathway for the unprecedented CO coordination to the Ru(II) center in the case of **1** has been explained. The synthesized complexes have been characterized by various spectroscopic techniques (viz., IR, UV-vis and NMR spectroscopy), ESI-MS and their electrochemical behavior studied by cyclic voltammetry. Molecular structures of **1–3** have been determined by X-ray crystallography.

4.1. INTRODUCTION

Azo group is one of the most versatile active units, which depending on the chemical constitution in the molecule might be photochromic,¹ proton-responsive,² and redox active. Azo functionalized metal complexes have been designed, targeted at adjusting the properties by external stimuli to which the azo function responds.³ Being highly selective and sensitive toward the incorporation of various metal ions, the azo-type ligand is one of the most flexible ligands studied in coordination chemistry.

Azo complexes of platinum group metals have largely been explored.⁴ The platinum group metal complexes of 2-(aryloxy)pyridine ligand system have been the subject of substantial interest because of their rich redox and spectroscopic behavior, catalytic activities and isomerization reactions.^{5,6,7} Among the platinum group metals, ruthenium demonstrates versatile chemistry, considering the largest range of oxidation states from -II to +VIII shown by Ru, with most of the inorganic chemistry taking place in the +II and +III states.⁸ Ruthenium-based catalytic systems are found to be effective in the hydrogenation of ketones for the synthesis of chiral alcohols.⁹ Studies by Noyori and coworkers have shown that the transfer hydrogenation of prochiral ketones can be attained in high enantiomeric excess by tailoring the chiral ruthenium catalysts.¹⁰ On the other hand, complexes of iridium are also widely studied due to their application in different fields, viz. photocatalysis, photo-electrochemistry, biological labeling and electroluminescence (EL).¹¹

C-H and C-C activation of ligands is an interesting feature observed in case of platinum group metal complexes.¹² The C-H activation of 2-aryloxyphenols by Wilkinson's catalyst, encouraged chemists to explore more platinum group metal azo complexes.¹³ Therefore, in order to have further insight into the chemistry of aryloxy complexes, we have herein reported the synthesis of some azo functionalized organoruthenium(II) (**1** and **2**) and iridium(III) (**3**) complexes and characterized them using several physico-chemical techniques (elemental analyses, IR, NMR and UV-vis spectroscopy, ESI-MS and cyclic voltammetry), including single crystal X-ray diffraction study and have also compared their varying chemistry. Ru(II) complexes, **1** and **2**, represent the major and minor products respectively, obtained from the same reaction. In addition to the C-H activation in **1**, another interesting feature is the unprecedented CO coordination to the Ru center. A suitable mechanism based on the decomposition of Grubbs metathesis catalysts and

alcohol dehydrogenation¹⁴ is proposed to understand the formation of the carbonyl coordinated bivalent ruthenium complexes as a major product. The source of CO group in previous literature evidences on CO coordinated Ru(II) arylazo complexes, was either the CO contained in the metal precursor,^{12d,15} or that obtained by the oxidation of the substituted alkyl groups.¹⁶ However to the best of our knowledge, there are no proposed mechanistic reports of organometallic CO coordinated arylazo ruthenium products wherein the CO generation could have been attributed to Ru(II) assisted solvent oxidation.

4.2. EXPERIMENTAL SECTION

4.2.1. General Methods and Materials. Chemicals were purchased from commercial sources and used without further purification. Ruthenium trichloride and iridium trichloride was obtained from Arora Matthey, Kolkata, India. $[\text{Ru}(\text{PPh}_3)_3\text{Cl}_2]$ ¹⁷ and $[\text{Ir}(\text{PPh}_3)_3\text{Cl}]$ ^{4a} were synthesized according to previously reported procedure. The synthesis of the ligand is reported as HL¹ in Section. 3.2.2. Reagent grade solvents were dried and distilled prior to use. Elemental analyses were performed on a Vario ELcube CHNS Elemental analyzer. IR spectra were recorded on a Perkin-Elmer Spectrum RXI spectrophotometer. ¹H and ³¹P NMR spectra were recorded on a Bruker Ultrashield 400 MHz spectrometer using SiMe₄ as an internal standard. Electronic spectra were recorded on a Lamda25, PerkinElmer spectrophotometer. Mass spectra were obtained on a SQ-300 MS instrument operating in positive ion ESI mode. A CH-Instruments (Model No. CHI6003E) electrochemical analyzer was used for cyclic voltammetric experiments with CH₃CN solutions of the complexes containing TBAP (tetra butyl ammonium perchlorate) as the supporting electrolyte. The three electrode measurements were carried out at 298 K with a platinum working electrode, platinum auxiliary electrode and SCE as a reference electrode. **Caution:** Although no problems were encountered during the course of this work, attention is drawn to the potentially explosive nature of perchlorates.

4.2.2. Synthesis of complexes (1–3)

Synthesis of $[\text{RuL}(\text{PPh}_3)_2(\text{CO})]$ and $[\text{RuL}(\text{PPh}_3)_2(\text{CH}_3\text{CN})]$ (1 and 2)

2-((2-benzo[1,3]dioxol-5-yl)-diazo)-4-methylphenol (100 mg, 0.1 mmol) was dissolved in ethanol (50 mL) and refluxed for 10 min, followed by addition of triethylamine (22 mg, 0.22 mmol) and $[\text{Ru}(\text{PPh}_3)_3\text{Cl}_2]$ (100 mg, 0.1 mmol). The resulting solution was refluxed in a nitrogen atmosphere for 24 h to yield a brown solution. The solvent was evaporated, and the solid mass, thus obtained, was subjected to purification by thin-layer chromatography on a silica plate. With 10:1.5 benzene-acetonitrile as the eluent, two prominent bands, a dark green and a brown band separated, and the corresponding materials were extracted separately with acetonitrile. Evaporation of these acetonitrile extracts gave $[\text{RuL}(\text{PPh}_3)_2(\text{CO})]$ (**1**) and $[\text{RuL}(\text{PPh}_3)_2(\text{CH}_3\text{CN})]$ (**2**) as green and brown colored crystalline solids respectively.

[RuL(PPh₃)₂CO] (**1**): Yield: 40%. Anal. calc. for: C, 66.30; H, 4.58; N, 4.55. Found: C, 66.36; H, 4.53; N, 4.61. Main IR peaks (KBr, ν/cm^{-1}): 1936 $\nu(\text{CO})$; 1478 $\nu(\text{N}=\text{N})$; 1238 $\nu(\text{C}-\text{O})_{\text{phenolic}}$, 750, 691, 519 $\nu(3\text{P}-\text{Ph})$. ¹H NMR (CDCl₃, 400 MHz) δ (ppm): 7.71 and 7.15–6.91 (m, 5H, Ar–H); 7.36–7.18 (2PPh₃); 6.09 (s, 2H, O–CH₂–O); 2.39 (s, 3H, ArCH₃). ³¹P NMR (CDCl₃) δ (ppm): 33.97.

[RuL(PPh₃)₂(CH₃CN)] (**2**): Yield: 20%. Anal. calc. for: C, 67.82; H, 4.71; N, 4.56. Found: C, 67.78; H, 4.73; N, 4.51. Main IR peaks (KBr, ν/cm^{-1}): 2212 $\nu(\text{CH}_3\text{CN})$; 1487 $\nu(\text{N}=\text{N})$; 1245 $\nu(\text{C}-\text{O})_{\text{phenolic}}$; 749, 690, 516 $\nu(3\text{P}-\text{Ph})$. ¹H NMR (CDCl₃, 400 MHz) δ (ppm): 7.59–6.81 (m, 35H, aromatic); 5.90 (s, 2H, O–CH₂–O); 2.35 (s, 3H, ArCH₃); 1.96 (s, 3H, CH₃CN). ³¹P NMR, δ (ppm): 33.93.

Synthesis of [IrL(PPh₃)₂(H)] (**3**)

2-[(2-benzo[1,3]dioxol-5-yl)-diazo]-4-methylphenol (100mg, 0.1 mmol) was dissolved in ethanol (50 mL) and refluxed for 10 min, followed by addition of triethylamine (22 mg, 0.22 mol) and [Ir(PPh₃)₃Cl] (100 mg, 0.1 mmol). The resulting solution was refluxed in a nitrogen atmosphere for 32 h to yield a green solution. The solvent was evaporated, and the solid mass, thus obtained, was subjected to purification by thin-layer chromatography on a silica plate. With 1:1 benzene-toluene as the eluent, a dark blue band separated, and the corresponding material was extracted separately with acetonitrile. Evaporation of this acetonitrile extract gave [IrL(PPh₃)₂(H)] (**3**), as blue crystalline solid.

[IrL(PPh₃)₂(H)] (**2**): Yield: 45%. Anal. calc. for: C, 61.78; H, 4.25; N, 2.88. Found: C, 61.73; H, 4.20; N, 2.93. Main IR peaks (KBr, ν/cm^{-1}): 2050 $\nu(\text{Ir}-\text{H})$; 1480 $\nu(\text{N}=\text{N})$; 1237 $\nu(\text{C}-\text{O})_{\text{phenolic}}$; 746, 694, 515 $\nu(3\text{P}-\text{Ph})$. ¹H NMR (DMSO-*d*₆, 400 MHz) δ (ppm): 7.36–7.23 (m, 15H, PPh₃); 6.79–5.95 (m, 5H, Ar–H); 1.88 (s, 3H, ArCH₃); -12.54 (t, hydride, Ir–H). ³¹P NMR, δ (ppm): 11.90, 9.89.

4.2.3. X-ray Crystallography.

Single crystals of complexes were mounted on a Bruker Smart Apex CCD diffractometer equipped with a graphite monochromator and a Mo K α radiator (λ) 0.71073 Å. Crystallographic data and details of refinement are given in Table 4.1. The unit cell

dimensions and intensity data were measured at 293(2) K for **1** and **3** and 297(2) K for **2**. Integrated intensities were obtained with the Bruker SAINT¹⁸ software package using a narrow frame logarithm. The intensity data were corrected for Lorentz, polarization and absorption effects. Absorption corrections were applied using SADABS¹⁹ and the structures were solved by direct methods using the program SHELXS-97²⁰ and refined using least squares with the SHELXL-97²⁰ software program. Hydrogens were either found or placed in calculated positions and isotropically refined using a riding model. The non-hydrogen atoms were refined anisotropically. Figures were drawn using DIAMOND and MERCURY. In the ball-and-stick models all atoms are drawn as thermal displacement ellipsoids of the 40% level with exception of the hydrogen atoms which are shown as spheres of arbitrary radii.

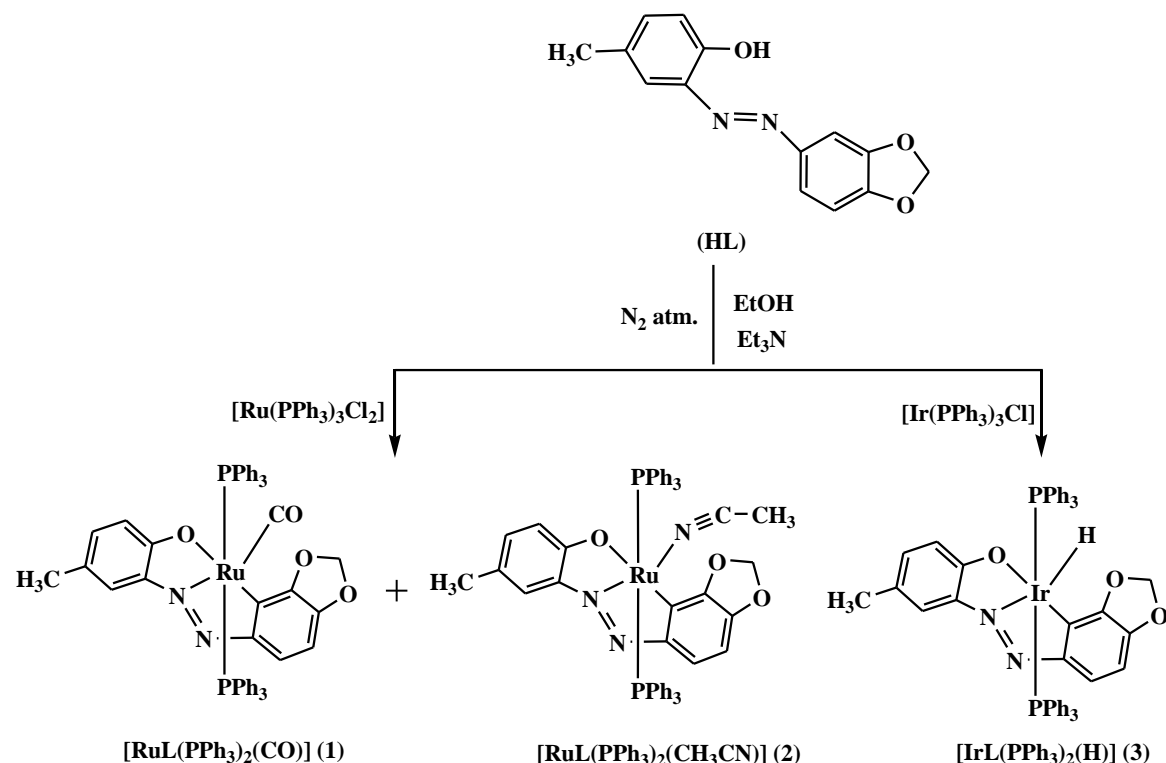
Table 4.1. Crystal data and refinement details for **1–3**

| Complex | 1·CH₃CN | 2 | 3 |
|---------------------------------|--|--|--|
| Empirical formula | C ₅₃ H ₄₂ N ₃ O ₄ P ₂ Ru | C ₅₂ H ₄₃ N ₃ O ₃ P ₂ Ru | C ₅₀ H ₄₁ IrN ₂ O ₃ P ₂ |
| Formula weight | 947.90 | 920.90 | 971.99 |
| Temperature | 293(2) K | 297(2) | 297(2) K |
| Radiation | MoK α | MoK α | MoK α |
| Crystal system | monoclinic | monoclinic | triclinic |
| Space group | <i>C1m1</i> | <i>P 21/n</i> | <i>P-1</i> |
| Unit cell dimensions | a = 18.2828(2) Å b = 14.6228(2) Å c = 9.68930(10) Å $\alpha = 90^\circ$ $\beta = 120.7910(4)^\circ$ $\gamma = 90^\circ$ | a = 12.0619(2) Å b = 17.3951(2) Å c = 20.5496(3) Å $\alpha = 90^\circ$ $\beta = 96.0240(6)$ $\gamma = 90^\circ$ | a = 11.1808(2) Å b = 12.0131(3) Å c = 19.2103(4) Å $\alpha = 101.2930(7)^\circ$ $\beta = 90.9690(7)^\circ$ $\gamma = 111.4660(6)^\circ$ |
| Volume | 2225.25(5) Å ³ | 4287.87(11) | 2343.66(9) Å ³ |
| Z | 2 | 4 | 2 |
| Density (calculated) | 1.415 g/cm ³ | 1.427 g/cm ³ | 1.377 g/cm ³ |
| Absorption coefficient | 0.475 mm ⁻¹ | 0.489 mm ⁻¹ | 2.958 mm ⁻¹ |
| F(000) | 974 | 1896 | 972 |
| Crystal size | 0.250 x 0.350 x 0.600 mm | 0.025 x 0.100 x 0.200 mm | 0.050 x 0.080 x 0.150 mm |
| Theta range for data collection | 1.90 to 28.34° | 1.876 to 28.346° | 1.95 to 30.77° |
| Reflections collected | 32606 | 104119 | 71547 |
| Reflections unique | 5305 | 10676 | 14045 |
| Final R1/wR2 [I>2sigma(I)] | R1 = 0.0233, wR2 = 0.0550 | R1 = 0.0456, wR2 = 0.0954 | R1 = 0.0319, wR2 = 0.0991 |

4.3. RESULTS AND DISCUSSION

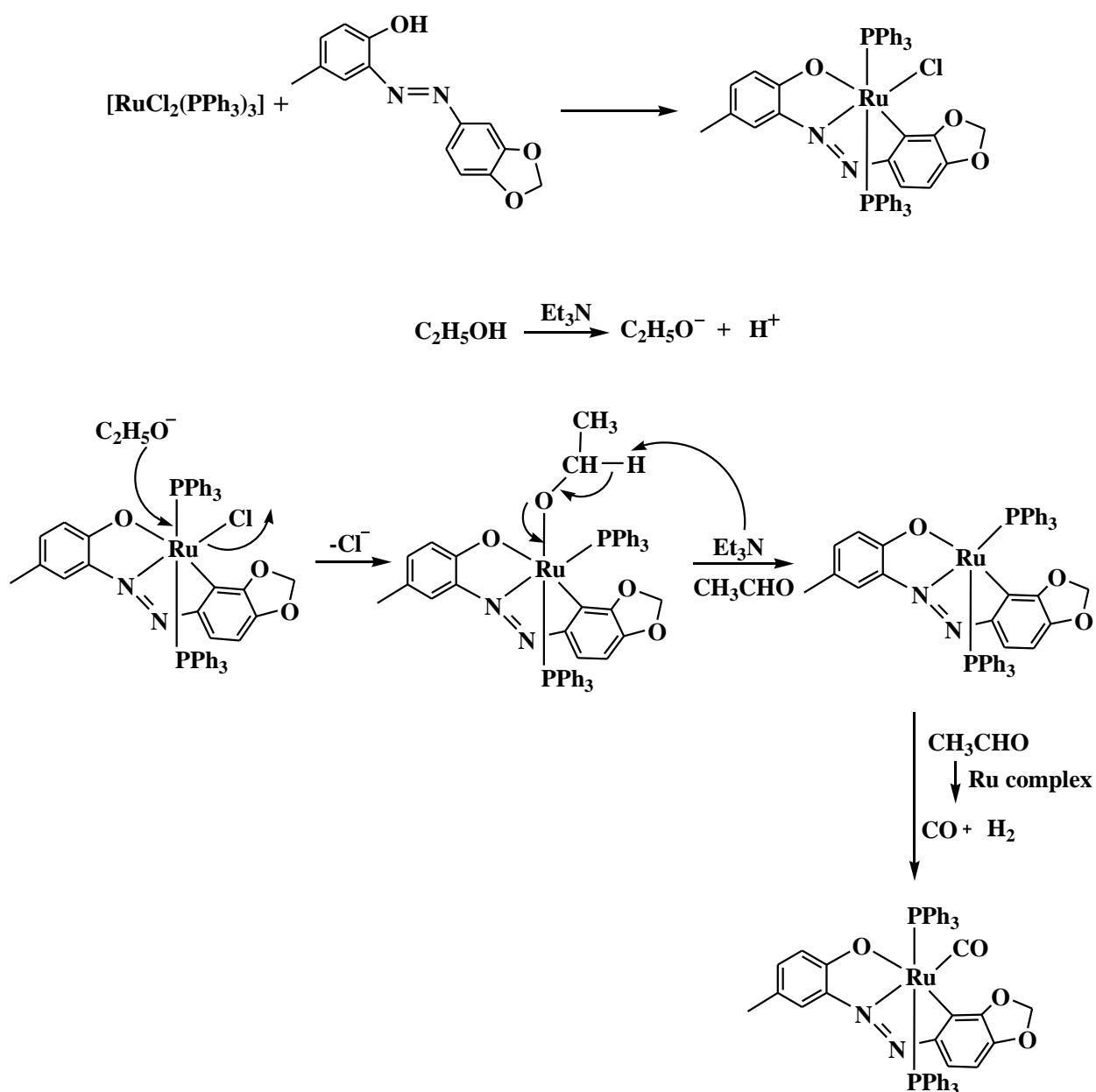
4.3.1. Synthesis of complexes (1–3)

Reaction of equimolar mixture of 2-(aryloxy)phenol, HL, with $[\text{Ru}(\text{PPh}_3)_2\text{Cl}_2]$ in ethanol medium under basic condition, afforded two types of complexes under refluxing conditions in a nitrogen atmosphere, with distinctly different colors, viz. green and brown, having the stoichiometry, $[\text{RuL}(\text{PPh}_3)_2(\text{CO})]$ (1) and $[\text{RuL}(\text{PPh}_3)_2(\text{CH}_3\text{CN})]$ (2), respectively, while under the same condition, reaction of HL with $[\text{Ir}(\text{PPh}_3)_3\text{Cl}]$ resulted in the formation of blue crystalline compound of $[\text{IrL}(\text{PPh}_3)_2(\text{H})]$ (3). The synthetic methodology of 1–3 is illustrated in Scheme 4.1. Elemental analyses, IR and NMR spectra and ESI-MS of 1–3 gave some idea about their compositions, but could not point to a definite formulation. For an unambiguous identification of the complexes, their X-ray structures were solved, which was consistent with their preliminary characterization. The complexes were slightly soluble in ethanol and methanol, but completely soluble in other protic and aprotic solvents.



Scheme 4.1. Schematic representation of the synthesis of $[\text{RuL}(\text{PPh}_3)_2(\text{CO})]$ (1), $[\text{RuL}(\text{PPh}_3)_2(\text{CH}_3\text{CN})]$ (2) and $[\text{IrL}(\text{PPh}_3)_2(\text{H})]$ (3).

The ligand coordinates to the metal center in the case of all the three complexes as a tridentate C, N, O-donor via metal assisted C–H activation, which is well documented in literature.^{4a,12d,f-h,15a,16} In the case of $[\text{RuL}(\text{PPh}_3)_2(\text{CH}_3\text{CN})]$ (**2**), the acetonitrile used for extraction, coordinates to the Ru center at the sixth coordination site, while the hydride generated from C–H activation of the ligand coordinates at the sixth coordination site, in $[\text{IrL}(\text{PPh}_3)_2(\text{H})]$ (**3**). But, the coordination of a carbonyl group to the Ru(II) center in the case of $[\text{RuL}(\text{PPh}_3)_2(\text{CO})]$ (**1**) was unexpected since the metal precursor, $[\text{Ru}(\text{PPh}_3)_3\text{Cl}_2]$, used for synthesis of **1** cannot serve as a source of CO. Earlier reports on unprecedented CO coordination in the case of arylazo ruthenium(II) complexes in ethanolic medium was rationalized by the migration of an alkyl group in the ligand backbone and its subsequent oxidation to CO, resulting in ligand modification.¹⁶ However in the case of complex **1**, similar explanation was not possible since the substituted methyl group in the ligand remained intact even after complex formation. The formation of Ru–CO complexes, by heating Ru(II) and Ru(III) compounds in the presence of primary alcohols, has earlier been established by C. Yi et al. and Jayanthi et al.^{14a} Taking these literature reports into consideration, the source of CO was assumed to be the solvent (ethanol) used for synthesis. In order to ascertain whether ethanol served as the source of CO, reaction of HL with $[\text{Ru}(\text{PPh}_3)_3\text{Cl}_2]$ was carried out in toluene and acetonitrile, in basic medium. However, preliminary characterization (IR) of the products obtained from toluene and acetonitrile did not show any trace of CO generation in the reaction medium, thereby clearly indicating EtOH as the source of CO. A. Chakravorty et al. had previously reported the synthesis of Os and Ru complexes, wherein decarbonylation of the diformylphenol Schiff base ligand had occurred resulting in the formation of CO coordinated organometallic complexes.²¹ In their case however the CO coordination was indifferent to the variation of solvent. Based on the above discussion, a mechanistic scheme for the formation of **1** is exemplified in Scheme 4.2.



Scheme 4.2. Proposed mechanism for the formation of $[\text{RuL}(\text{PPh}_3)_2(\text{CO})]$ (1).

4.3.2. Spectral Characteristics

4.3.2.1. IR spectroscopy. A broad band at $\sim 3450 \text{ cm}^{-1}$ was observed for HL, which disappears upon complex formation of 1–3. IR stretching frequency of HL observed at 1549 cm^{-1} is attributed to the presence of the azo(N=N) functional group.²² The

corresponding peak shifts to a lower frequency range of $\sim 1481\text{ cm}^{-1}$ upon complexation (**1–3**). The presence of a coordinated CO in the case of **1** is evident from the characteristic peak of CO, observed at 1936 cm^{-1} ,¹⁶ while an extra peak at 2212 cm^{-1} in the IR spectra of **2**, as compared to the ligand, could be attributed to the CN stretching frequency in the complex. Besides the difference in the CO and CN stretch, the infrared spectrum of **1** and **2** are very similar. The presence of three strong absorption bands ($\sim 515, 694, 746\text{ cm}^{-1}$) in **1, 2** and **3** is due to the coordinated PPh_3 ligands to the metal centers and the peak at 2050 cm^{-1} is assigned to the Ir–H stretching frequency.^{12g} Figures 4.1 and 4.2 represent the IR spectra of **1** and **3** respectively.

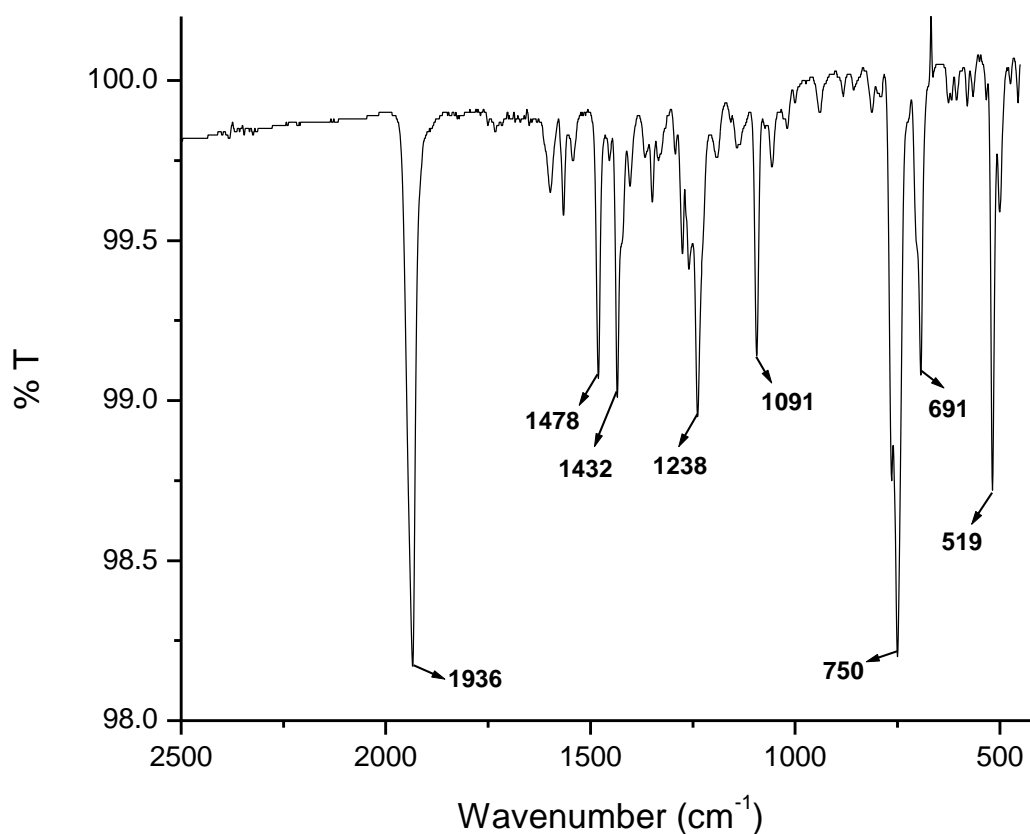


Figure 4.1. IR spectra of $[\text{RuL}(\text{PPh}_3)_2(\text{CO})]$ (**1**).

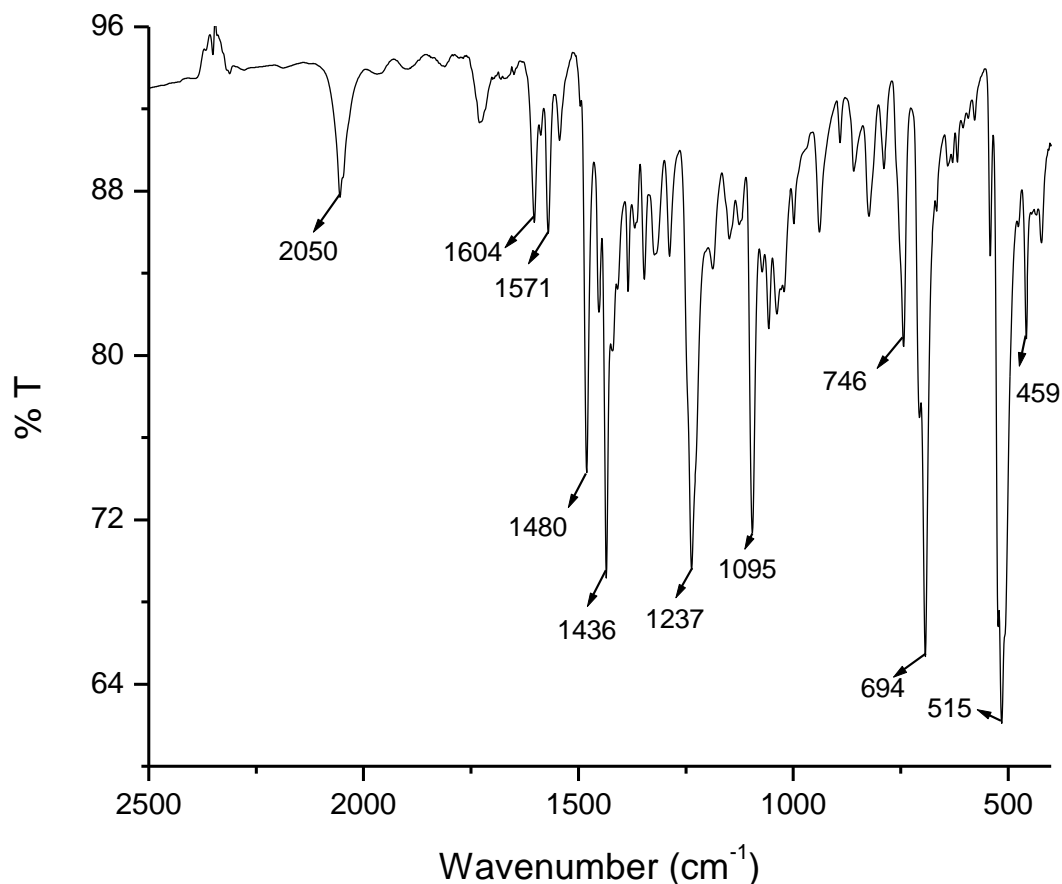


Figure 4.2. IR spectra of $[\text{IrL}(\text{PPh}_3)_2(\text{H})]$ (**3**).

4.3.2.2. UV-vis spectroscopy. The electronic spectra of $[\text{RuL}(\text{PPh}_3)_2(\text{CO})]$ (**1**), $[\text{RuL}(\text{PPh}_3)_2(\text{CH}_3\text{CN})]$ (**2**) and $[\text{IrL}(\text{PPh}_3)_2(\text{H})]$ (**3**) was recorded in dichloromethane solution. The strong transitions in the UV region of **1**, **2** and **3** are attributable to intra-ligand charge transfer transitions whereas the transitions of higher intensities in the lower energy region of the spectra are presumably due to metal to ligand charge transfer transition (MLCT).²³ The weaker absorption tails exhibited by the $[\text{IrL}(\text{PPh}_3)_2(\text{H})]$, **3**, in the lower energy region may be ascribed to forbidden MLCT ($d\pi(\text{Ir})-\pi^*(\text{ligand})$) transitions.²⁴ Representative UV-vis spectra of **1** and **3** is given in Figures 4.3 and 4.4 respectively and the values are tabulated in Table 4.2.

Table 4.2. Electronic spectra for complexes **1–3** in dichloromethane solution.

| Complex | $\lambda_{\text{max}}/\text{nm}$ ($\epsilon_{\text{max}}/\text{M}^{-1} \text{cm}^{-1}$) |
|---|---|
| [RuL(PPh ₃) ₂ (CO)] (1) | 207 (26533), 224 (16000), 262 (5000), 348 (1666), 449 (1333), 642 (1200) |
| [RuL(PPh ₃) ₂ (CH ₃ CN)] (2) | 278 (45121), 230 (25000), 258 (8500), 385 (27637), 457 (9500), 668 (1400) |
| [IrL(PPh ₃) ₂ (H)] (3) | 210 (26666), 258 (10133), 336 (2333), 433 (1466), 598 (2533) |

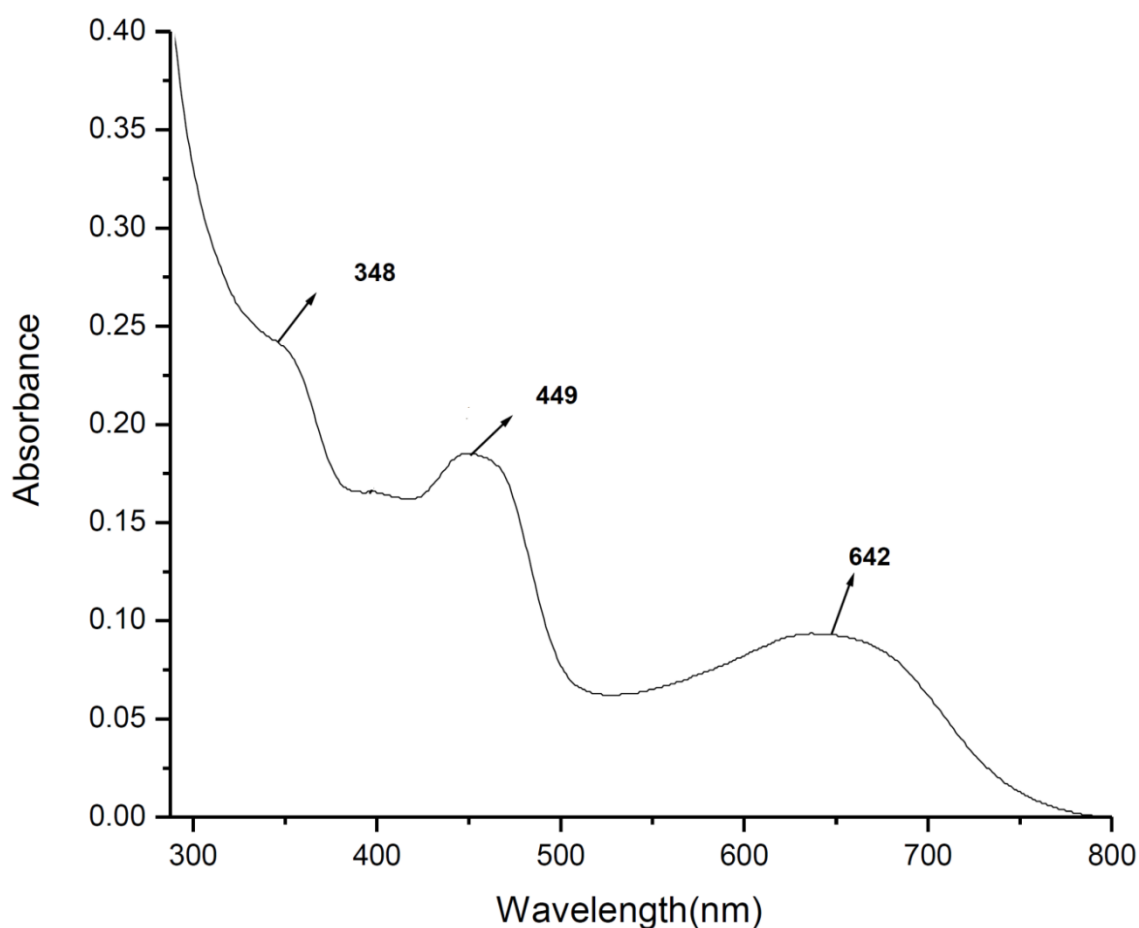


Figure 4.3. UV-vis spectrum of [RuL(PPh₃)₂(CO)] (**1**).

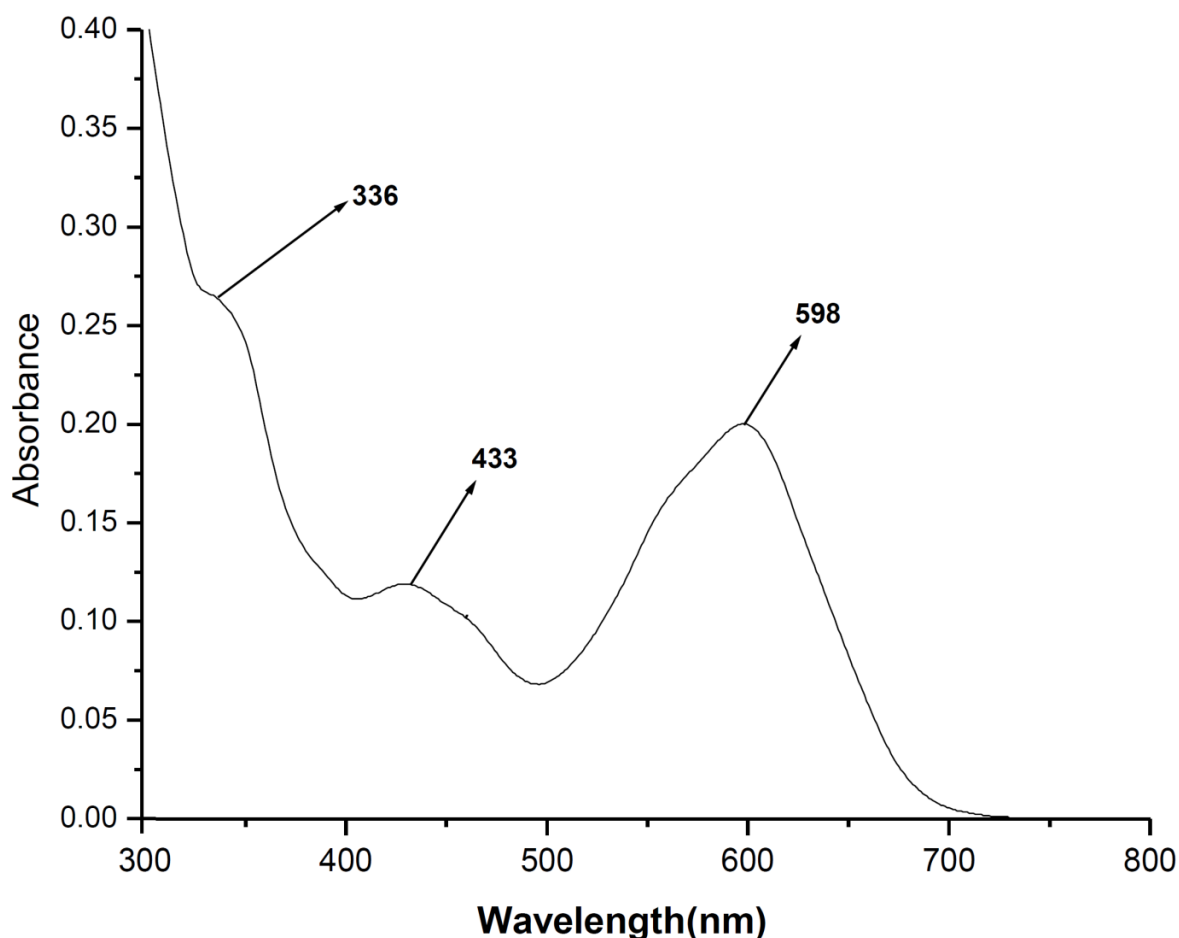


Figure 4.4. UV-vis spectrum of [IrL(PPh₃)₂(H)] (**3**).

4.3.2.3. NMR spectroscopy. The complexes [RuL(PPh₃)₂(CO)] (**1**), [RuL(PPh₃)₂(CH₃CN)] (**2**) and [IrL(PPh₃)₂(H)] (**3**) are diamagnetic, which corresponds to +2 oxidation state of **1** and **2** and +3 oxidation state of **3** (low spin d⁶, S = 0). ¹H NMR spectra of **1** and **2** have been recorded in CDCl₃, while that of **3** in DMSO-*d*₆. The ¹H NMR spectra of **1** and **2** are qualitatively similar. ¹H NMR spectra of **1** shows broad signals in the range 7.36–7.18 ppm for the two coordinated PPh₃ ligands. The signals for the other aromatic protons in the ligand moiety of complex **1** are observed in the range 7.15–6.91 and 7.71 ppm. The expected signals from the aromatic protons of the coordinated 2-(aryloxy)phenolate ligand of complex **2** could not be identified separately because of their overlap with the PPh₃ signals. A singlet is observed at ~5.99 ppm for the CH₂ group (O–CH₂–O) in the ligand fragment for complex **1** and **2**. The signals for the methyl protons of the phenolate fragment of 2-(aryloxy)phenolate ligand in **1** and **2** is

observed at ~ 2.37 ppm, while an extra three proton singlet is observed in **2** due to the methyl group of the coordinated CH_3CN . The protons of the coordinated PPh_3 in complex **3** resonate at ~ 7.36 – 7.23 ppm. The signals for the aromatic protons of the coordinated 2-(aryloxy)phenolate ligand of **3** was observed in the ~ 6.79 – 5.95 ppm range while the peak for the CH_2 group ($\text{O}-\text{CH}_2-\text{O}$) is observed at 5.68 ppm. The methyl protons of complex **3** resonate in the upfield region of ~ 1.88 ppm. In addition ^1H NMR spectrum of the complex **3** show a hydride signal near ~ -12.54 ppm.

^{31}P NMR spectra of **1** and **2** show a single resonance within 33.97–33.93 ppm, as expected, while two resonating signals are observed for **3**, at 11.90 and 9.89 ppm for the two coordinated PPh_3 ligands. The NMR spectral data of **1**, **2** and **3** are therefore in agreement with their respective composition and stereochemistry. Representative ^1H and ^{31}P NMR spectra of **1** and **3** are given in Figures 4.5–4.7, respectively.

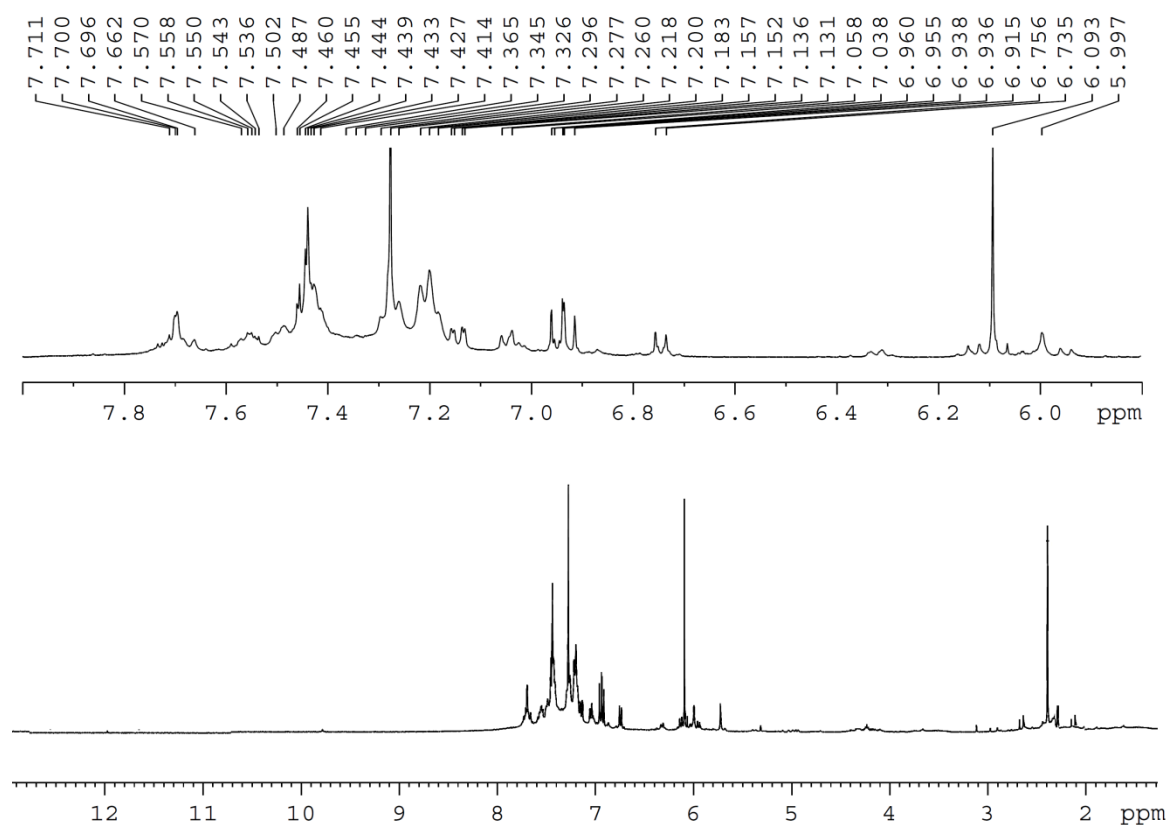


Figure 4.5. ^1H NMR spectrum of $[\text{RuL}(\text{PPh}_3)_2(\text{CO})]$ (**1**).

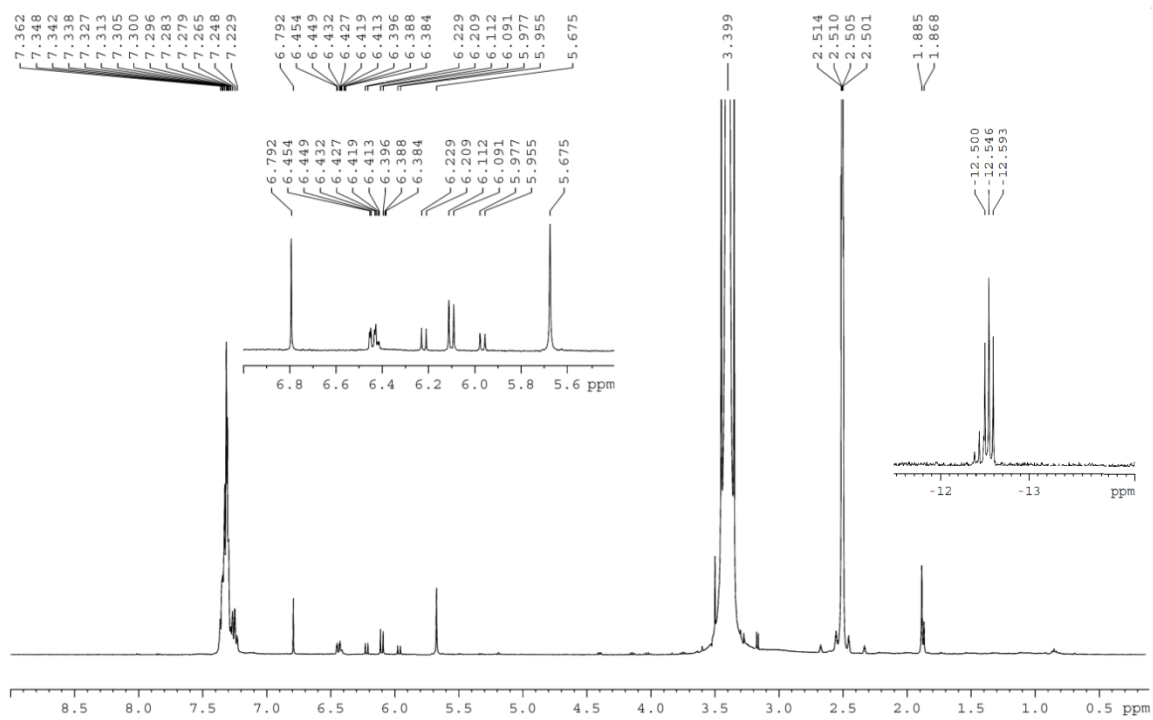


Figure 4.6. ^1H NMR spectrum of $[\text{IrL}(\text{PPh}_3)_2(\text{H})]$ (**3**).

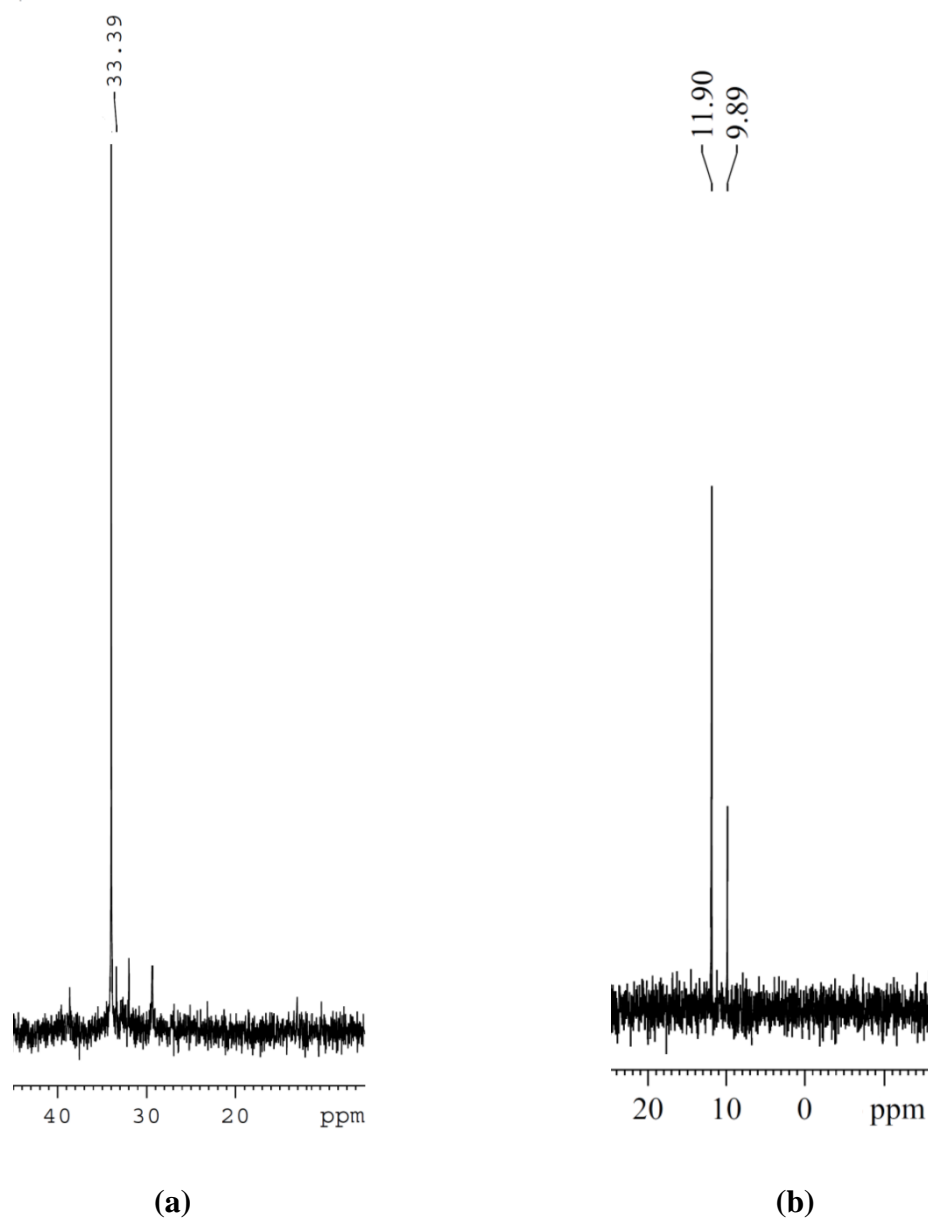


Figure 4.7. ^{31}P NMR spectrum of (a) $[\text{RuL}(\text{PPh}_3)_2(\text{CO})]$ (**1**) in CDCl_3 and $[\text{IrL}(\text{PPh}_3)_2(\text{H})]$ (**3**) in $\text{DMSO-}d_6$.

4.3.3. ESI-MS.

ESI-MS of **1–3** have been recorded in acetonitrile solution. ESI-MS of **1** shows a peak for $[\text{M} + 2\text{H} - \text{CH}_3\text{CN}]^+$ at m/z 908.70, whereas the ESI-MS for **2** and **3** displays molecular ion peaks, $[\text{M}]^+$, at m/z 921.10 and 972.77 respectively. Figures 4.8 and 4.9 depict the representative ESI-MS spectra of **1** and **3** respectively.

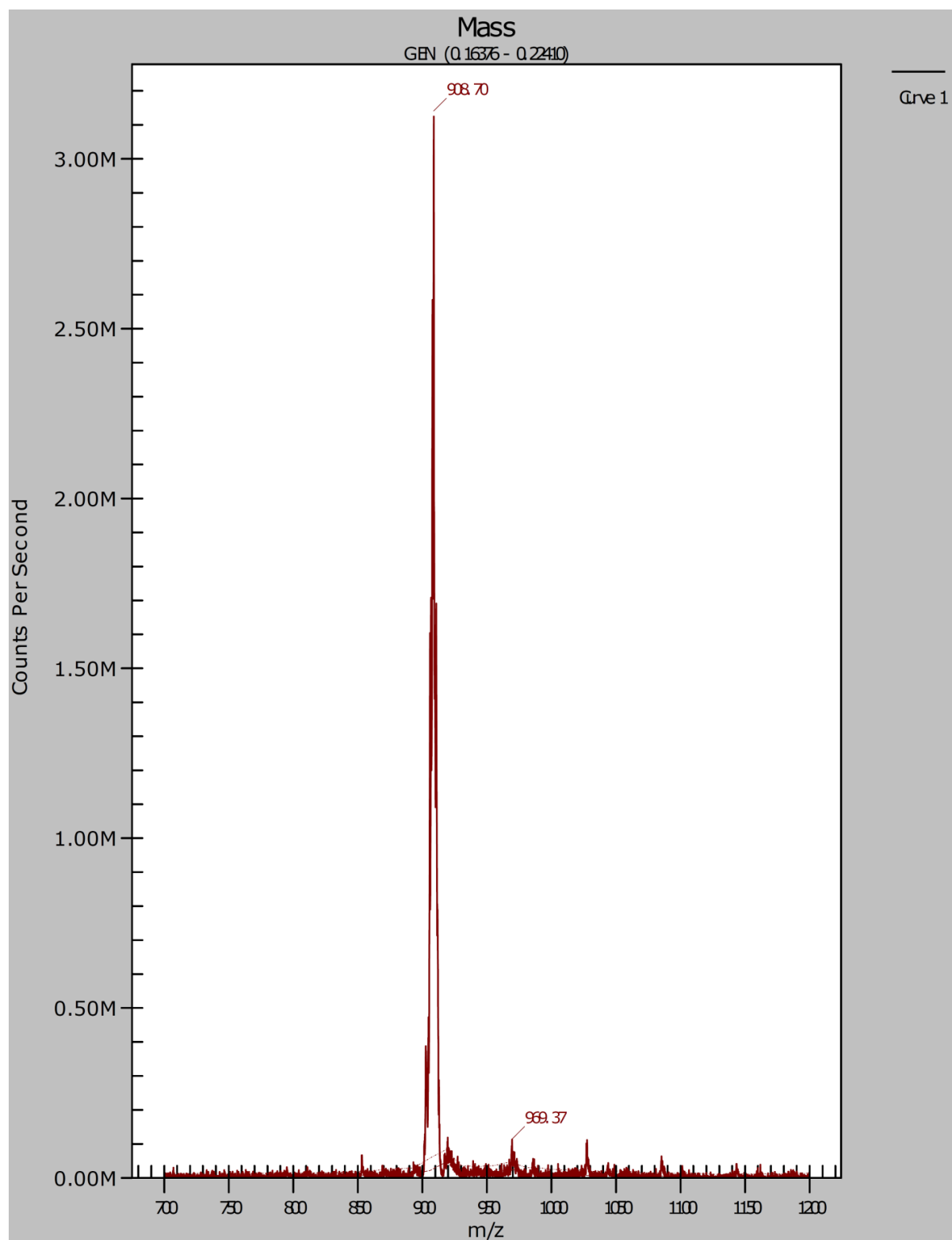


Figure 4.8. ESI-MS of [RuL(PPh₃)₂(CO)] (1) in CH₃CN.

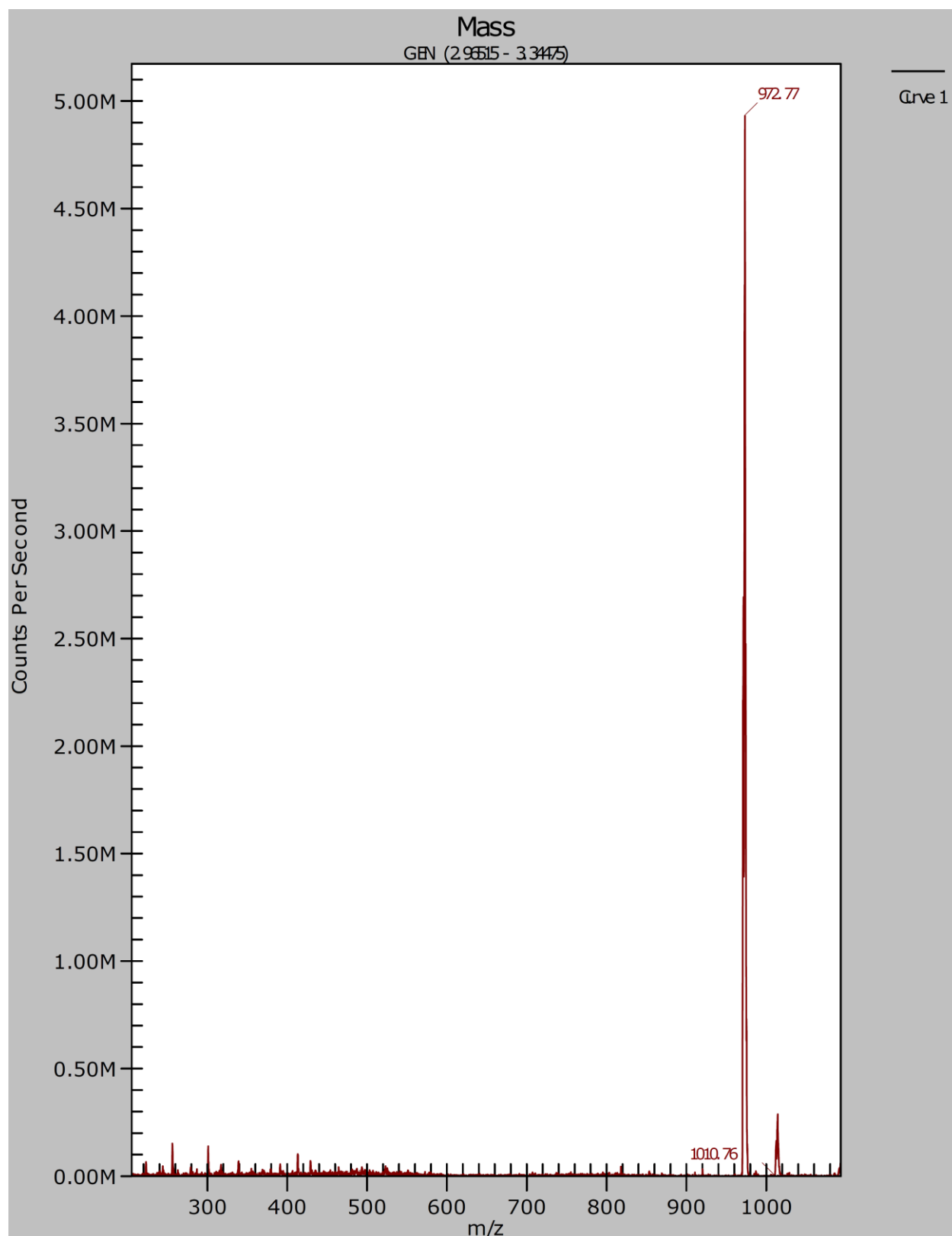


Figure 4.9. ESI-MS of $[\text{IrL}(\text{PPh}_3)_2(\text{H})]$ (**3**).

4.3.4. Electrochemical Properties. The potential data of **1–3** is tabulated in Table 4.2 and the representative cyclic voltammogram of **1** and **3** is given in Figures 4.10 and 4.11, respectively. The cyclic voltammogram pattern of **1** and **2** are similar; each exhibits a single electron transfer quasi-reversible oxidative wave Ru(II)/Ru(III) in the anodic region at $E_{1/2}^a$ value of +0.54 and +0.52 V, respectively, while **3** shows a reversible redox couple for (Ir(III)/Ir(IV)) at +0.50 V respectively. An irreversible ligand centered oxidation and reduction peak is observed at +1.25V and –1.4V in the anodic and cathodic region respectively. The one–electron nature of this oxidation was verified by comparing its current height with that of the standard ferrocene–ferrocenium couple under identical experimental conditions.

Table 4.2. Cyclic voltammetric results for **1–3** at 298 K.^[a]

| Complex | $E_{1/2}$ (V) | ΔE_p (mV) |
|---|---------------|-------------------|
| [Ru(PPh ₃) ₂ L(CO)] (1) | 0.54 | 110 |
| [Ru(PPh ₃) ₂ L(CH ₃ CN)] (2) | 0.52 | 100 |
| [Ir(PPh ₃) ₂ L(H)] (3) | 0.50 | 90 |

^[a] **1–3** in CH₃CN solution at a scan rate of 100 mV s⁻¹. $E_{1/2} = \frac{1}{2}(E_p^a + E_p^c)$, $\Delta E_p = E_p^a - E_p^c$ (E_p^a = anodic peak potential, E_p^c = cathodic peak potential).

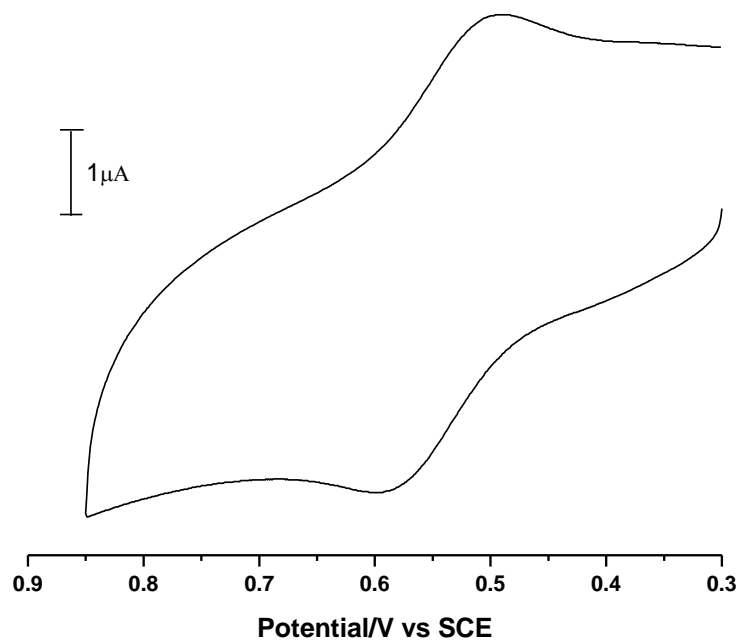


Figure 4.11. Cyclic Voltammogram of $[\text{RuL}(\text{PPh}_3)_2(\text{CO})]$ (**1**).

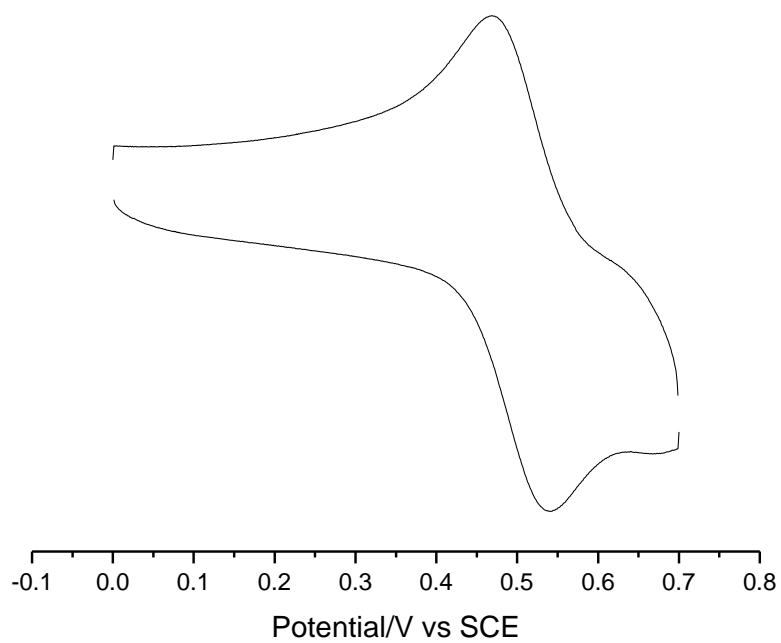


Figure 4.12. Cyclic Voltammogram of $[\text{IrL}(\text{PPh}_3)_2(\text{H})]$ (**3**).

4.3.5. Description of X-ray Structure of [RuL(PPh₃)₂CO] (1), [RuL(PPh₃)₂(CH₃CN)] (2) and [IrL(PPh₃)₂(H)] (3)

[RuL(PPh₃)₂CO] (1): The molecular structure and the atom numbering scheme for [RuL(PPh₃)₂CO] (1) is shown in Figure 4.12 and the relevant bond parameters are collected in Table 4.3. Structure of **1** shows that in this complex the 2-(aryloxy)phenol is coordinated to the metal (via loss of the phenolic proton as well as another proton from one ortho position of the phenyl ring in the arylazo fragment) as a tridentate C, N, O-donor, resulting in a distorted octahedral coordination geometry of **1**. The remaining three coordination sites are occupied by two triphenylphosphines and a carbon monoxide molecule. The coordinated 2-(aryloxy)phenolate ligand and CO share an equatorial plane with Ru at the center, where the CO is trans to the coordinated azo-nitrogen(N1). The PPh₃ ligands occupy the axial positions and the Ru–PPh₃ [Ru(1)–P(1) = 2.3716(6) Å] distances are comparable to those found in similar complexes.^{12d} A CH₃CN molecule is also present as the solvent of crystallisation in the crystal lattice of **1** (not shown in Figure below).

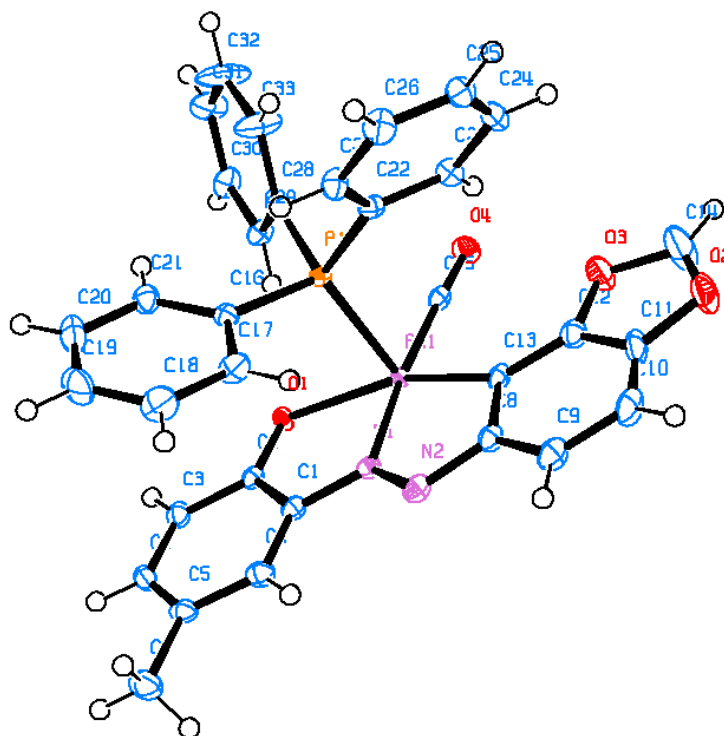


Figure 4.12. ORTEP diagram of the asymmetric unit of [RuL(PPh₃)₂CO] (1).

Table 4.3. Selected geometric parameters for [RuL(PPh₃)₂CO] (**1**)

| Bond Distances(Å) | | | |
|-------------------|-----------|------------------|----------|
| Ru(1)–C(15) | 1.862(4) | Ru(1)–C(13) | 2.042(5) |
| Ru(1)–N(1) | 2.045(3) | Ru(1)–O(1) | 2.195(3) |
| Ru(1)–P(1) | 2.3716(6) | | |
| Bond Angles(°) | | | |
| C(15)–Ru(1)–C(13) | 95.5(2) | C(15)–Ru(1)–N(1) | 172.4(2) |
| C(13)–Ru(1)–N(1) | 76.9(2) | C(15)–Ru(1)–O(1) | 109.6(2) |
| C(13)–Ru(1)–O(1) | 154.9(1) | N(1)–Ru(1)–O(1) | 77.9(1) |
| C(15)–Ru(1)–P(1) | 89.0(2) | C(13)–Ru(1)–P(1) | 96.3(1) |
| N(1)–Ru(1)–P(1) | 91.8(1) | O(1)–Ru(1)–P(1) | 84.44(8) |
| P(1)–Ru(1)–P(1) | 167.36(3) | | |

[RuL(PPh₃)₂(CH₃CN)] (**2**): The molecular structure and the atom numbering scheme for [RuL(PPh₃)₂(CH₃CN)] (**2**) is shown in Figure 4.13 and the relevant bond parameters are tabulated in Table 4.4. The ligand is coordinated to the Ru center as a tridentate dianionic C, N, O donor as in the case of **1**; however in **2** the fourth coordination site in the equatorial plane is occupied by CH₃CN group instead of CO. Two five membered chelate rings define the equatorial plane with bite angles 77.0(1)° [C(13)–Ru(1)–N(1)] and 79.47(9)° [O(1)–Ru(1)–N(1)]. The two triphenylphosphines are placed mutually trans to each other in the axial plane, the bond angle P(1)–Ru(1)–P(2), being 176.38(3)°. In case of [RuL(PPh₃)₂(CH₃CN)] (**2**), there is a slight difference in the bond distance between Ru(1)–P(1) (2.3610(6) Å) and Ru(1)–P(2) (2.3834(8) Å), resulting in the formation of a distorted octahedral geometry, as compared to [RuL(PPh₃)₂(CO)] (**1**), where both the Ru(1)–P(1) bonds are equidistant. Notably, the Ru(1)–N(1) distance (1.989(2) Å) in **2** is shortened as compared to Ru(1)–N(1) distance (2.045(3) Å) of **1** due to the lesser trans effect of CH₃CN (in **2**) than CO (in **1**).

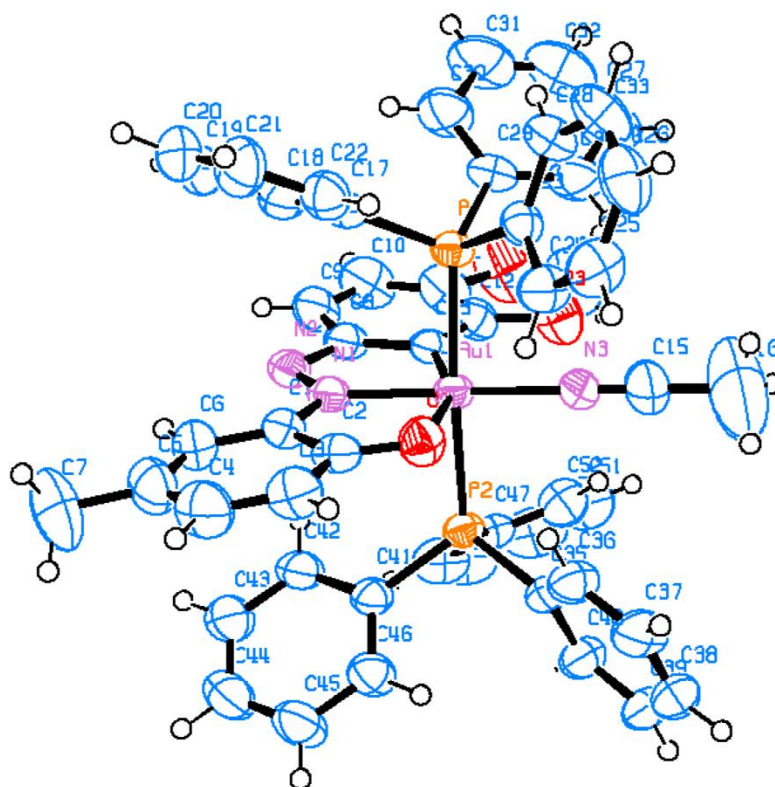


Figure 4.13. ORTEP diagram of $[\text{RuL}(\text{PPh}_3)_2(\text{CH}_3\text{CN})]$ (**2**).

Table 4.4. Selected geometric parameters for $[\text{RuL}(\text{PPh}_3)_2(\text{CH}_3\text{CN})]$ (**2**)

| Bond Distances (Å) | | | |
|--------------------|-----------|------------------|-----------|
| Ru(1)–C(13) | 2.026(3) | Ru(1)–N(3) | 1.997(3) |
| Ru(1)–N(1) | 1.989(2) | Ru(1)–O(1) | 2.160(2) |
| Ru(1)–P(1) | 2.3640(8) | Ru(1)–P(2) | 2.3834(8) |
| Bond Angles (°) | | | |
| P(1)–Ru(1)–P(2) | 176.38(3) | P(2)–Ru(1)–N(3) | 88.43(9) |
| P(1)–Ru(1)–O(1) | 91.14(6) | P(2)–Ru(1)–C(13) | 92.19(8) |
| P(1)–Ru(1)–N(1) | 91.98(7) | O(1)–Ru(1)–N(1) | 79.47(9) |
| P(1)–Ru(1)–N(3) | 87.96(9) | O(1)–Ru(1)–N(3) | 99.3(1) |
| P(1)–Ru(1)–C(13) | 88.43(8) | O(1)–Ru(1)–C(13) | 156.4(1) |
| P(2)–Ru(1)–O(1) | 89.73(6) | N(1)–Ru(1)–N(3) | 178.7(1) |
| P(2)–Ru(1)–N(1) | 91.64(7) | N(1)–Ru(1)–C(13) | 77.0(1) |
| N(3)–Ru(1)–C(13) | 104.3(1) | | |

[IrL(PPh₃)₂(H)] (**3**): The structure of the Ir(III) complex [IrL(PPh₃)₂H] (**3**) is illustrated in Figure 4.14 and selected bond parameters are tabulated in Table 4.5. Bond parameters reflect the distortion of the coordination geometry of the cyclometallated organometallic complex (**3**) from an ideal octahedron. The bond distances, Ir(1)–C(1), Ir(1)–N(1), Ir(1)–O(1), Ir(1)–H(1), Ir(1)–P(1) and Ir(1)–P(2) within the C, N, O-chelated fragment of **3** are normal and comparable to previous evidences.^{4a} The equatorial plane in the complex is defined by two five membered rings formed by the coordination of the ligand as a tridentate C, N, O donor with bite angles of 77.91(8)° [C(1)–Ir(1)–N(1)] and 78.88(7)° [N(1)–Ir(1)–O(1)]. In addition, a hydride occupies the equatorial plane positioned trans to the N1 atom, while two PPh₃ groups occupy the axial positions in complex **3**.

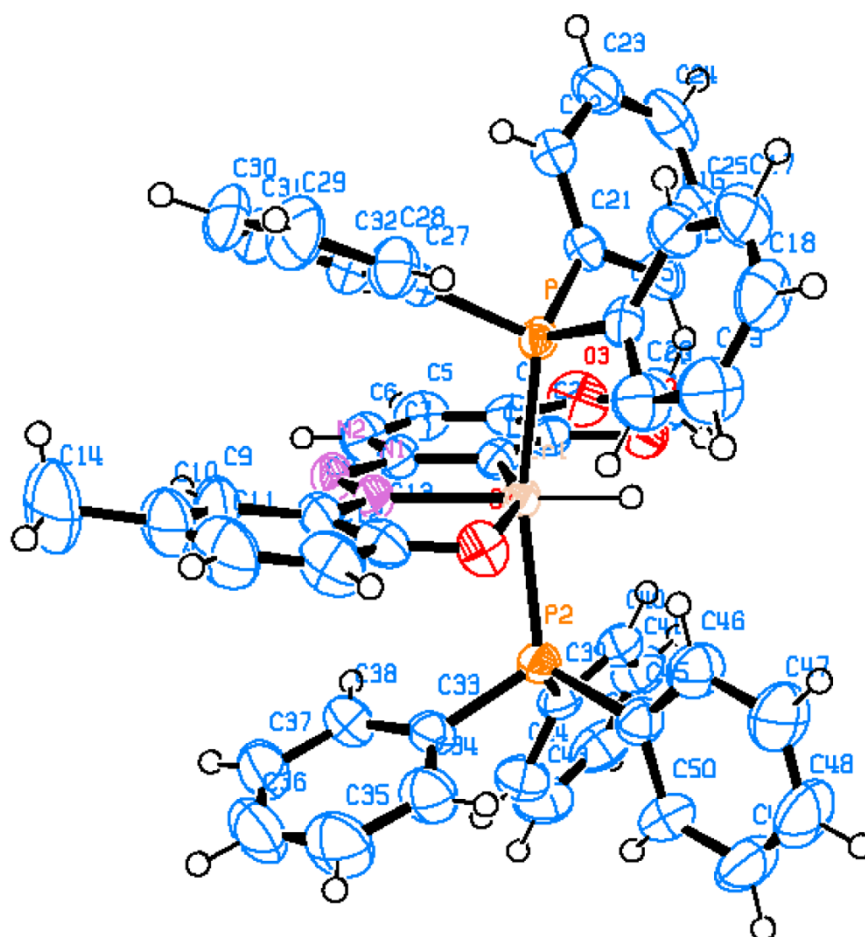


Figure 4.14. ORTEP diagram of [IrL(PPh₃)₂(H)] (**3**).

Table 4.5. Selected geometric parameters for [IrL(PPh₃)₂H] (**3**)

| Bond lengths (Å) | | | |
|-------------------|-----------|-------------------|-----------|
| Ir(1)–C(1) | 2.023(2) | Ir(1)–N(1) | 2.033(2) |
| Ir(1)–O(1) | 2.180(2) | Ir(1)–P(1) | 2.3142(6) |
| Ir(1)–P(2) | 2.3219(6) | Ir(1)–H(101) | 1.51(2) |
| Bond angles (°) | | | |
| C(1)–Ir(1)–N(1) | 77.91(8) | C(1)–Ir(1)–O(1) | 156.68(8) |
| N(1)–Ir(1)–O(1) | 78.88(7) | C(1)–Ir(1)–P(1) | 95.47(6) |
| N(1)–Ir(1)–P(1) | 96.16(5) | O(1)–Ir(1)–P(1) | 89.21(5) |
| C(1)–Ir(1)–P(2) | 97.50(6) | N(1)–Ir(1)–P(2) | 96.10(5) |
| O(1)–Ir(1)–P(2) | 82.74(5) | P(1)–Ir(1)–P(2) | 163.75(2) |
| C(1)–Ir(1)–H(101) | 99.4(9) | N(1)–Ir(1)–H(101) | 177.3(9) |
| O(1)–Ir(1)–H(101) | 103.8(3) | P(1)–Ir(1)–H(101) | 84.0(9) |
| P(2)–Ir(1)–H(101) | 84.3(9) | | |

4.4. CONCLUSION

The chemistry of some new ruthenium(II) (**1** and **2**) and iridium(III) arylazo (**3**) complexes have been reported. The complexes (**1–3**) were characterized by various analytical techniques (IR, UV-vis, ^1H and ^{31}P NMR spectroscopy, ESI-MS and cyclic voltammetry). The molecular structures of **1–3** were also solved by single crystal X-ray diffraction analysis. The complexes have a distorted octahedral geometry. The two PPh_3 groups occupy the axial position and the sixth coordination site in the equatorial plane is occupied by the CO, CH_3CN and H^- in **1**, **2** and **3** respectively. Metal (Ru and Ir) mediated C–H activation of the ligand occurs in all the three complexes, resulting in coordination of the ligand as a tridentate binegative C, N, O-donor. In order to rationalize the unprecedented CO coordination to the Ru(II) center in the case **1**, a suitable mechanism via alcohol dehydrogenation has been proposed.

The ruthenium carbonyl complex, $[\text{RuL}(\text{PPh}_3)_2\text{CO}]$ can act as a CO reservoir and may be utilized for hydroformylation reaction or as a catalyst precursor for the reduction of CO_2 or the water gas shift reaction. There is thus scope for further research in this regard.

4.5. REFERENCES

- (1) Rau, H. In *Studies in Organic Chemistry 40: Photochromism, Molecules and Systems*; Dürr, H.; Bouas-Laurent, H., Eds.; Elsevier: Amsterdam, 1990; pp 165–192. (b) Feringa, B. L.; Jager, W. F.; de Lange, B. *Tetrahedron* **1993**, *49*, 8267–8310. (c) Willner, I.; Rubin, S. *Angew. Chem., Int. Ed. Engl.* **1996**, *35*, 367–385. (d) Makita, S.; Saito, A.; Hayashi, M.; Yamada, S.; Yoda, K.; Otsuki, J.; Takido, T.; Seno, M. *Bull. Chem. Soc. Jpn.* **2000**, *73*, 1525–1533.
- (2) Ueno, A.; Kuwabara, T.; Nakamura, A.; Toda, F. *Nature* **1992**, *356*, 136–137.
- (3) Screen, T. E. O.; Blake, I. M.; Rees, L. H.; Clegg, W.; Borwick, S. J.; Anderson, H. L. *J. Chem. Soc., Perkin Trans.* **2002**, *1*, 320–329. (b) Hunter, C. A.; Sarson, L. D. *Tetrahedron Lett.* **1996**, *37*, 699–702. (c) Autret, M.; LePlouzennec, M.; Moinet, C.; Simonneaux, G. *J. Chem. Soc., Chem. Commun.* **1994**, 1169–1170. (d) Tsuchiya, S. *J. Am. Chem. Soc.* **1999**, *121*, 48–53. (e) Neuman, K. H.; Vögtle, F. *J. Chem. Soc., Chem. Commun.* **1988**, 520–522. (f) Reddy, D. R.; Maiya, B. G. *Chem. Commun.* **2001**, 117–118.
- (4) (a) Acharyya, R.; Basuli, F.; Wang, R.-Z.; Mak, T. C. W.; Bhattacharya, S. *Inorg. Chem.* **2004**, *43*, 704–711. (b) Maiti, N.; Pal, S.; Chattopadhyay, S. *Inorg. Chem.* **2001**, *40*, 2204–2205. (c) Datta, P.; Sardar, D.; Saha, R.; Mondal, T. K.; Sinha, C. *Polyhedron* **2013**, *53*, 193–201.
- (5) Krause, R. A.; Krause, K. *Inorg. Chem.* **1980**, *19*, 2600–2603.
- (6) (a) Ghosh, P.; Pramanik, A.; Bag, N.; Chakravorty, A. *J. Chem. Soc., Dalton Trans.* **1992**, 1883–1886. (b) Lahiri, G. K.; Bhattacharya, S.; Goswami, S.; Chakravorty, A. *J. Chem. Soc., Dalton Trans.* **1990**, 561–565. (c) Ghosh, B. K.; Chakravorty, A. *Coord. Chem. Rev.* **1989**, *95*, 239–294. (d) Wolfgang, S.; Streckas, T. C.; Gafney, H. D.; Krause, A. R.; Krause, K. *Inorg. Chem.* **1984**, *23*, 2650–2655. (e) Goswami, S.; Mukherjee, R. N.; Chakravorty, A. *Inorg. Chem.* **1983**, *22*, 2825–2832. (f) Goswami, S.; Chakravarty, A. R.; Chakravorty, A. *Inorg. Chem.* **1983**, *22*, 602–609.
- (7) (a) Ghosh, A. K.; Majumdar, P.; Falvello, L. R.; Mostafa, G.; Goswami, S. *Organometallics* **1999**, *18*, 5086–5090. (b) Lahiri, G. K.; Goswami, S.; Falvello, L. R.; Chakravorty, A. *Inorg. Chem.* **1987**, *26*, 3365–3370. (c) Goswami, S.; Chakravarty, A. R.; Chakravorty, A. *J. Chem. Soc., Chem. Commun.* **1982**, 1288–1289. (d) Goswami, S.; Chakravarty, A. R.; Chakravorty, A. *Inorg. Chem.* **1982**, *21*, 2737–2742.

- (8) Sabo-Etienne, S.; Grellier, M. Ruthenium: Inorganic & Coordination Chemistry, *Encyclopedia of Inorganic Chemistry* [Online] John Wiley & Sons, Ltd, 2006.
- (9) Touge, T.; Hakamata, T.; Nara, H.; Kobayashi, T.; Sayo, N.; Saito, T.; Kayaki, Y.; Ikariya, T. *J. Am. Chem. Soc.* **2011**, *133*, 14960–14963.
- (10) Ohkuma, T.; Ooka, H.; Hashiguchi, S.; Ikariya, T.; Noyori, R. *J. Am. Chem. Soc.* **1995**, *117*, 2675–2676.
- (11) (a) Lo, K. K.; Chung, C. K.; Lee T. K.; Lui, L. H.; Tsang, K. H.; Zhu, N. *Inorg Chem.* **2003**, *42*, 6886–6897. (b) Lo, K. K. -W.; Chung, C. -K.; N. Zhu, *Chem. Eur. J.* **2003**, *9*, 475–483.
- (12) (a) Arockiam, P. B.; Bruneau, C.; Dixneuf, P. H. *Chem. Rev.* **2012**, *112*, 5879–5918. (b) Park, Y.; Heo, Joon; Baik, Mu-Hyun; Chang, Sukbok, *J. Am. Chem. Soc.* **2016**, *138*, 14020–14029. (c) Labinger, J. A. *Chem. Rev.* **2016** DOI: 10.1021/acs.chemrev.6b00583. (d) Gupta, P.; Dutta, S.; Basuli, F.; Peng, S. -M.; Lee, G. -H.; Bhattacharya, S. *Inorg. Chem.* **2006**, *45*, 460–467. (e) Pratihari, J. L.; Maiti, N.; Chattopadhyay, S. *Inorg. Chem.* **2005**, *44*, 6111–6114. (f) Mandal, S.; Samanta, S.; Mondal, T. K.; Goswami S. *Organometallics* **2012**, *31*, 5282–5293. (g) Acharyya, R.; Basuli, F.; Peng, S. -M.; Lee, G.-H.; Wang, R. -Z.; Mak, T. C. W.; Bhattacharya, S. *J. Organomet. Chem.* **2005**, *690*, 3908–3917. (h) Acharyya, R.; Peng, S. -M.; Lee, G.-H.; Bhattacharya, S. *J. Chem. Sci.* **2009**, *121*, 387–395. (i) Ghosh, P.; Bag, N.; Chakravorty, A. *Organometallics* **1996**, *15*, 3042–3047.
- (13) Colby, D. A.; Bergman, R. G.; Ellman, J. A. *Chem. Rev.* **2010**, *110*, 624–655.
- (14) (a) Jayanthi, E.; S. Kalaiselvi, V. V. Padma, N. S. P. Bhuvanesh, N. Dharmaraj, *Dalton Trans.* **2016**, *45*, 1693–1707 and references therein. (b) Dinger, M. B.; Mol, J. C. *Organometallics* **2003**, *22*, 1089–1095.
- (15) (a) Nag, S.; Gupta, P.; Butcher, R. J.; Bhattacharya, S. *Inorg. Chem.* **2004**, *43*, 4814–4816. (b) Sarkar, S. K.; Jana, M. S.; Mondal, T. K.; Sinha, C. *J. Organomet. Chem.* **2012**, *716*, 129–137.
- (16) Acharyya, R.; Peng, S. -M.; Lee, G. H.; Bhattacharya, S. *Inorg. Chem.* **2003**, *42*, 7378–7380.
- (17) Hallman, P. S.; Stephenson, T. A.; Wilkinson, G., Tetrakis(triphenylphosphine)dichlororuthenium(II) and

Tris(triphenylphosphine)dichlororuthenium(II). In *Inorganic Syntheses*, John Wiley & Sons, Inc.: 2007; pp 237–240.

(18) *SAINT*. 2008, Bruker AXS Inc.: Madison, Wisconsin, USA.

(19) *SADABS*. 2008, Bruker AXS Inc.: Madison, Wisconsin, USA.

(20) Sheldrick, G. M.: *SHELXS-97: Programs for Structure Determination*, University of Göttingen, Göttingen, Germany 1997.

(21) (a) Ghosh, P.; Bag, N.; Chakravorty, A. *Organometallics* **1996**, *15*, 3042–3047.

(b) Bag, N.; Choudhury, S. B.; Pramanik, A.; Lahiri, G. K.; Chakravorty, A. *Inorg. Chem.* **1990**, *29*, 5013–5014.

(22) Halder, S.; Drew, M. G. B.; Bhattacharya, S. *J. Chem. Sci.* **2008**, *120*, 441–446.

(23) Panda, M.; Paul, N. D.; Joy, S.; Hung, C. -H.; Goswami, S. *Inorg. Chim. Acta* **2011**, *372*, 168–174.

(24) Lo, K. K. -W. Chung, C. -K. Zhu, N. *Chem. Eur. J.* **2003**, *9*, 475.

Chapter 5

Synthesis, structure, DNA interaction and cytotoxicity of a series of dioxidomolybdenum(VI) complexes featuring salan ligands

Chapter 5

Synthesis, structure, DNA interaction and cytotoxicity of a series of dioxidomolybdenum(VI) complexes featuring salan ligands

ABSTRACT

Seven hexacoordinated *cis*-dioxidomolybdenum(VI) complexes $[\text{MoO}_2\text{L}^{1-7}]$ (**1–7**) derived from various substituted tetradentate diamino bis(phenolato) “salan” ligands, *N,N'*-dimethyl-*N,N'*-bis-(2-hydroxy-3-X-5-Y-6-Z-benzyl)-1,2-diaminoethane {(X = Br, Y = Me, Z = H (H_2L^1); X = Me, Y = Cl, Z = H (H_2L^2); X = ⁱPr, Y = Cl, Z = Me (H_2L^3)} and *N,N'*-bis-(2-hydroxy-3-X-5-Y-6-Z-benzyl)-1,2-diaminopropane {(X = Y = ^tBu, Z = H (H_2L^4); X = Y = Me, Z = H (H_2L^5); X = ⁱPr, Y = Cl, Z = Me (H_2L^6); X = Y = Br, Z = H (H_2L^7)} containing O–N donor atoms, have been isolated and structurally characterized. The formation of *cis*-dioxidomolybdenum(VI) complexes was confirmed by elemental analysis, IR, UV-vis and NMR spectroscopy, ESI-MS and cyclic voltammetry measurements. X-ray crystallography showed the O_2N_2 donor set to define an octahedral geometry in each case. The asymmetric unit of all the complexes consists of a complete formula unit with the exception of **2**, which belongs to point group C_2 . $[\text{MoO}_2\text{L}^{1-7}]$ (**1–7**) showed moderate DNA binding propensity with binding constants ranging from 10^4 – 10^5 M^{-1} . The experimental results showed that the complexes **1–7** effectively interact with CT-DNA by both minor and major groove binding mode, while complex **2** additionally interacts by partial intercalative mode of binding. The dioxidomolybdenum (VI) complexes (**1–3**) showed moderate photo-induced cleavage of pUC19 supercoiled plasmid DNA. All the complexes (**1–7**) were tested for their *in vitro* antiproliferative activity against HT-29 and HeLa cell lines. IC_{50} values of the complexes in HT-29 follow the order **6** < **7** << **1** < **2** < **5** << **3** < **4** while the order is **6** < **7** < **5** < **1** << **3** < **4** < **2** in HeLa cells. Some of the complexes proved to be as active as the clinical referred drugs, and the greater potency of **6** and **7** (IC_{50} values of **6** are 2.62 and 10.74 μM and that of **7** is 11.79 and 30.48 μM in HT-29 and HeLa cells, respectively) may be dependent on the substituents in the salan ligand environment coordinated to the metal.

5.1. INTRODUCTION

Metals, in particular transition metals provide potential advantages over the more common organic-based drugs, including a broad range of coordination numbers and geometries, accessible redox states, kinetics of ligand substitution and ‘tune-ability’ of the thermodynamics, and a wide structural diversity.¹⁻¹³ It was the discovery of cisplatin that gave momentum to metal-based drug research.¹⁴ Despite its tremendous success as an anticancer drug, its use is restricted due to serious side-effects, general toxicity, and acquired drug resistance.¹⁵ In order to overcome the challenges set forth by platinum based drugs, researchers in the field of medicinal inorganic chemistry are developing non-platinum based chemotherapeutic agents that exhibit enhanced selectivity and non-covalent DNA binding interaction modes.^{16,17} Investigation of DNA binding interactions with metal complexes have gained profound interest due to its medical applications and genomic research.^{16,17}

As compared to other transition metals, molybdenum gains advantages due to its low toxicity and its extensive and labile chemistry.¹⁸ Lack of molybdenum in nutrition may cause increased risk of developing esophageal cancer.¹⁹ Again, exploitation of molybdenum(VI) complexes seems relevant, due to its already proven versatility in biology,²⁰⁻²³ such as the presence of molybdenum(VI) center at the active centers of oxotransfer molybdoenzymes, nitrogen fixing enzymes - the nitrogenases²¹ as well as several oxotransferase enzymes like xanthine oxidase, sulphite oxidase and DMSO reductase.^{20,22,23}

Among the diverse class of molybdenum complexes utilized for their pharmaceutical applicability, their anti-cancer activities gained special attention.²⁴⁻²⁷ Significant anti-tumoral effect of Mo(II) complexes was observed in organometallic complexes Cp_2MoX_2 (X= Cl, Br, acido ligand) which presented favorable drug like characteristics.^{24k,1} Researchers have further investigated the toxicity and specificity of other molybdocene complexes, for example in $[CpMo(2,2'-biimidazole)_2(CO)_2](BF_4)$, $[Mo(\eta^3-C_3H_5)X(CO)_2(N-N)]$ (N-N= 1,10-phenanthroline or 2,2'-bipyridyl and X = CF_3-SO_3 , Br, Cl) etc., on variable cancer cell lines.²⁵ Remarkable cell-growth inhibition of various polyoxidomolybdates was observed in a dose dependent manner selectively on specific carcinoma cells.²⁶ Most promising cytotoxicity results of molybdenum complexes

obtained so far have been with the Mo centre in +II oxidation state, but reports on similar potency of Mo(VI) complexes against cancer cells remain scarce.²⁷ Anticancer activities of Mo(VI) complexes against human cancer cells, was shown to decrease with increasing chelation and this *in vitro* structure-cytotoxicity relationship have also been rationalized by theoretical calculations.^{27c}

On the other hand, use of the salen ligand (Schiff bases (SB)) framework in transition-metal chemistry is well-documented, especially in the area of asymmetric catalysis.²⁸ Less common is the related salan (hydrogenated analogue of SB) complexes, which often display different structural conformation, due to greater flexibility as a consequence of C=N bond hydrogenation and increased N-basicity, which leads to different reactivity and selectivity.²⁹ In contrast to the salen complexes, where the imine moiety is prone to decomposition in the presence of water, the higher resistance to hydrolytic decomposition of reduced SB compounds deserves special mention.³⁰ It is noteworthy that though catalytic efficiency of metal complexes of tetradentate salan ligands have largely been investigated,³¹ their utility for the treatment of malignancies have only been exploited in the recent past.^{32, 33} Promising cytotoxicity results as compared to cisplatin, both *in vitro* and *in vivo* have been obtained for titanium(IV)^{33a-h} and vanadium(V)^{29a,30,33j} complexes, by tuning the steric and electronic effects of the salan ligand backbone. Though the synthesis, characterization and catalytic activity of analogues Mo(VI)-salan complexes have been reported previously,^{29c-h} however, to the best of our knowledge, these complexes have never been probed for their antitumor activity, and thus demand further investigation.

Recent reports from our laboratory have shown that variable valence nonoxido- and oxidovanadium complexes with varying aroylhydrazone ligands³⁴ and some copper(I/II)-thiosemicarbazone complexes³⁵ are cytotoxic against the human cervical cancer cell line (HeLa) with IC₅₀ values ranging from 9.90–44.96 μM .^{34,35} It is noteworthy that evaluation of cell cytotoxicity of vanadium³⁶ and copper³⁷ have been studied extensively, but there are rather limited reports in the related field for *cis*-dioxidomolybdenum(VI) complexes.^{38,39a,b} Considering these facts and as a continuation of our ongoing research on the study of Mo(VI) complexes with multidentate ligands,³⁹ especially those with pharmacological utility,^{39a,b} we have herein reported the synthesis of a series of *cis*-dioxidomolybdenum(VI) complexes with various substituted tetradentate salan ligands.

These complexes were fully characterized by IR, UV-vis and NMR spectroscopy, ESI-MS, cyclic voltammetry and X-ray crystallography. Furthermore, the DNA binding and cleavage activity of the complexes were probed and their cytotoxicity was surveyed by the MTT assay against the HeLa and HT-29 cell line.

5.2. EXPERIMENTAL SECTION

5.2.1. General Methods and Materials

[MoO₂(acac)₂] was prepared as described in the literature.⁴⁰ Reagent grade solvents were dried and distilled prior to use. All other chemicals were reagent grade, available commercially and used as received. Dulbecco's Modified Eagle Media (DMEM), Dulbecco's phosphate buffer saline (DPBS), Trypsin EDTA solution, Fetal Bovine Serum (FBS), antibiotic-antimitotic solution and MTT assay kit were purchased from Himedia, Mumbai, India. TRITC-Phalloidin and DAPI were procured from Sigma-Aldrich, India. HeLa and HT-29 cell lines were procured from NCCS, Pune, India. The supercoiled (SC) pUC19 DNA from *E. coli* DH5a cells was purified by using GeneJET Plasmid Isolation Kit (Thermo Scientific, USA). Calf thymus (CT) DNA (biochemistry grade) and agarose (molecular biology grade) were purchased from SRL (India) and Sigma Aldrich (USA), respectively.

Elemental analyses were performed on a VarioELcube CHNS Elemental analyzer. IR spectra were recorded on a Perkin-Elmer Spectrum RXI spectrometer. NMR spectra were recorded with a BrukerUltraShield 400 MHz spectrometer at 298 K room temperature using SiMe₄ (¹H and ¹³C) as an internal. Electronic spectra were recorded on a Lamda25, PerkinElmer spectrophotometer. Mass spectra were recorded on a SQ-300 MS instrument operating in positive ESI mode. Magnetic susceptibility was measured with a Sherwood Scientific AUTOMSB sample magnetometer. Conductivity was measured using Eutech CON 700 conductivity meter. A CH-Instruments (Model No. CHI6003E) electrochemical analyzer was used for cyclic voltammetric experiments with CH₃CN solutions of the complexes containing TBAP (tetra butyl ammonium perchlorate) as the supporting electrolyte. The three electrode measurements were carried out at 298 K with a glassy carbon working electrode, platinum auxiliary electrode and SCE as a reference electrode. **Caution:** Although no problems were encountered during the course of this work, attention is drawn to the potentially explosive nature of perchlorates.

5.2.2. Synthesis of ligands (H_2L^{1-7})

Salan ligands, H_2L^{1-7} , were prepared by the one pot Mannich condensation of substituted phenols, formaldehyde and substituted amines in methanol medium following a standard procedure.⁴¹ The resulting white compounds were filtered, washed with ethanol and dried over fused CaCl_2 .

H_2L^1 : Yield: 0.13 g (65%). Anal. Calcd for $\text{C}_{20}\text{H}_{26}\text{N}_2\text{O}_2\text{Br}_2$: C, 49.40; H, 5.39; N, 5.76. Found: C, 49.45; H, 5.40; N, 5.79%. Selected IR peaks with proposed assignments (KBr, $\nu_{\text{max}}/\text{cm}^{-1}$): 2942 $\nu(\text{O-H})_{\text{H-bonded}}$. ^1H NMR (400 MHz, CDCl_3): δ (ppm) = 10.54 (s, 1H, OH), 7.25–6.72 (2H, aromatic), 3.68 (s, 2H, ArCH_2), 2.71 (s, 2H, NCH_2), 2.31 (s, 3H, ArCH_3), 2.23 (s, 3H, NCH_3). ^{13}C NMR (100 MHz, $\text{DMSO-}d_6$): δ (ppm) = 152.02, 132.44, 129.57, 128.30, 122.23, 109.76, 61.57, 54.31, 41.84, 20.18.

H_2L^2 : Yield: 0.20 g (72%). Anal. Calcd for $\text{C}_{20}\text{H}_{26}\text{N}_2\text{O}_2\text{Cl}_2$: C, 60.46; H, 6.60; N, 7.05. Found: C, 60.42; H, 6.61; N, 7.05%. Selected IR peaks with proposed assignments (KBr, $\nu_{\text{max}}/\text{cm}^{-1}$): 2900 $\nu(\text{O-H})_{\text{H-bonded}}$. ^1H NMR (400 MHz, CDCl_3): δ (ppm) = 10.87 (s, 1H, OH), 7.04–6.8 (m, 2H, aromatic), 3.64 (s, 2H, ArCH_2), 2.65 (s, 2H, NCH_2), 2.28 (s, 3H, ArCH_3), 2.19 (s, 3H, NCH_3). ^{13}C NMR (100 MHz, $\text{DMSO-}d_6$): δ (ppm) = 154.48, 129.66, 126.97, 125.69, 123.03, 122.12, 61.34, 53.78, 41.57, 15.62.

H_2L^3 : Yield: 0.15 g (66%). Anal. Calcd for $\text{C}_{26}\text{H}_{38}\text{N}_2\text{O}_2\text{Cl}_2$: C, 64.86; H, 7.95; N, 5.82. Found: C, 64.86; H, 7.97; N, 5.81%. Selected IR peaks with proposed assignments (KBr, $\nu_{\text{max}}/\text{cm}^{-1}$): 2956 $\nu(\text{O-H})_{\text{H-bonded}}$. ^1H NMR (400 MHz, $\text{DMSO-}d_6$): δ (ppm) = 11.47 (s, 1H, OH), 7.11 (m, 1H, aromatic), 3.75 (s, 2H, ArCH_2), 3.26 (heptet, 1H, ArCH), 3.21 (s, 2H, NCH_2), 2.64 (s, 3H, ArCH_3), 2.27 (3H, NCH_3), 1.95 (m, 6H, $\text{CH}(\text{CH}_3)_2$). ^{13}C NMR (100 MHz, $\text{DMSO-}d_6$): δ (ppm) = 154.19, 134.84, 130.76, 125.94, 124.56, 120.71, 58.18, 53.53, 41.50, 41.49, 26.47, 22.46, 16.10.

H_2L^4 : Yield: 0.18 g (70%). Anal. Calcd for $\text{C}_{33}\text{H}_{54}\text{N}_2\text{O}_2$: C, 77.60; H, 10.66; N, 5.48. Found: C, 77.65; H, 10.67; N, 5.44%. Selected IR peaks with proposed assignments (KBr, $\nu_{\text{max}}/\text{cm}^{-1}$): 2957 $\nu(\text{O-H}/\text{N-H})_{\text{H-bonded}}$. ^1H NMR (400 MHz, $\text{DMSO-}d_6$): δ (ppm) = 10.64 (s, 2H, OH), 7.23–6.83 (m, 4H, aromatic), 4.19–3.45 (m, 6H, 3CH_2), 3.03 (sextet, 1H,

CHCH₃), 2.19 (s, 3H, CHCH₃), 1.44–1.28 (m, 36H, 4C(CH₃)₃). ¹³C NMR (100 MHz, DMSO-*d*₆): δ (ppm) = 154.07, 153.98, 140.71, 140.67, 135.69, 135.64, 123.26, 123.22, 123.11, 123.05, 121.03, 120.71, 74.59, 59.77, 59.71, 59.42, 59.36, 59.18, 59.01, 58.02, 34.88, 34.43, 34.14, 33.95, 31.66, 31.52, 30.96, 30.90, 29.60, 29.21, 29.10, 18.55, 15.01.

H₂L⁵: Yield: 0.13 g (65%). Anal. Calcd for C₂₁H₃₀N₂O₂: C, 73.65; H, 8.83; N, 8.18. Found: C, 73.61; H, 8.80; N, 8.18%. Selected IR peaks with proposed assignments (KBr, $\nu_{\max}/\text{cm}^{-1}$): 2957 $\nu(\text{O-H/ N-H})_{\text{H-bonded}}$. ¹H NMR (400 MHz, DMSO-*d*₆): δ (ppm) = 10.80 (s, 2H, OH), 6.93–6.52 (m, 4H, aromatic), 4.98–4.88 (m, 4H, ArCH₂), 4.12–4.09 (sextet, 1H, CHCH₃), 3.24–3.20 (d, 2H, NCH₂), 2.26 (s, 6H, *p*-ArCH₃), 2.25 (s, 6H, *o*-ArCH₃), 1.00 (d, 3H, CHCH₃). ¹³C NMR (100 MHz, DMSO-*d*₆): δ (ppm) = 153.33, 149.22, 131.60, 131.35, 130.87, 129.85, 129.64, 129.13, 128.38, 124.08, 120.83, 114.76, 59.36, 53.09, 50.47, 48.77, 20.52, 20.38, 16.05, 15.57, 15.42.

H₂L⁶: Yield: 0.12g (58%). Anal. Calcd for C₂₅H₃₆N₂O₂Cl₂: C, 64.23; H, 7.76; N, 5.99. Found: C, 64.23; H, 7.71; N, 5.96%. Selected IR peaks with proposed assignments (KBr, $\nu_{\max}/\text{cm}^{-1}$): 2966 $\nu(\text{O-H/ N-H})_{\text{H-bonded}}$. ¹H NMR (400 MHz, DMSO-*d*₆): δ (ppm) = 11.23 (s, 2H, OH), 7.12–7.11 (m, 2H, aromatic), 3.93–3.37 (m, 4H, ArCH₂), 3.32 (d, 2H, NCH₂), 3.28–3.01 (m, 2H, 2CH(CH₃)), 2.47 (q, 1H, CHCH₃), 2.29–2.28 (m, 6H, 2ArCH₃), 1.33 (d, 3H, CH(CH₃)), 1.23–1.20 (m, 12H, 2CH(CH₃)₂). ¹³C NMR (100 MHz, DMSO-*d*₆): δ (ppm) = 153.96, 153.79, 134.91, 134.85, 130.60, 130.55, 126.13, 126.07, 124.86, 124.79, 120.71, 120.33, 74.72, 74.24, 59.70, 59.57, 54.41, 53.25, 26.51, 26.46, 22.54, 22.39, 18.33, 16.17, 16.14 .

H₂L⁷: Yield: 0.13 g (65%). Anal. Calcd for C₁₇H₁₈N₂O₂Br₄: C, 33.92; H, 3.01; N, 4.65. Found: C, 33.91; H, 3.05; N, 4.60%. Selected IR peaks with proposed assignments (KBr, $\nu_{\max}/\text{cm}^{-1}$): 2964 $\nu(\text{O-H/ N-H})_{\text{H-bonded}}$. ¹H NMR (400 MHz, DMSO-*d*₆): δ (ppm) = 10.71 (s, 2H, OH), 6.85–6.62 (m, 4H, aromatic), 3.68–3.33 (s, 4H, ArCH₂), 2.71 (m, 2H, NCH₂) 2.62 (q, 1H, CHCH₃), 1.41 (d, 3H, CH(CH₃)). ¹³C NMR (100 MHz, DMSO-*d*₆): δ (ppm) = 154.09, 153.97, 135.79, 135.70, 127.25, 127.23, 126.86, 126.78, 126.67, 126.60, 122.62, 122.30, 73.57, 59.25, 58.86, 57.73, 56.71, 34.74, 29.80, 20.85, 19.09.

5.2.3. Synthesis of complexes [MoO₂L¹⁻⁷] (1-7)

Triethylamine (1.0 mmol) was added to the methanolic solution of the ligand H₂L¹⁻⁷ (1.0 mmol) and the resulting solution was refluxed for 0.5 h, followed by the addition of MoO₂(acac)₂ (1.0 mmol). Reflux was continued for 3 h. Yellow residue of complexes **1-4**, **6** and orange residue of complexes **5** and **7** were obtained immediately upon MoO₂(acac)₂ addition. Crystals suitable for X-ray analysis were isolated for [MoO₂L²⁻⁴] (**2-4**) directly from the reaction medium. X-ray quality crystals of [MoO₂L¹] (**1**) were obtained by layer diffusion of DCM:n-hexane, [MoO₂L⁵] (**5**) by recrystallizing in EtOH while that of [MoO₂L⁶] (**6**) by layer diffusion in DMF:EtOEt.

[MoO₂L¹] (1): Yield: 57%. Anal. Calcd for C₂₀H₂₄N₂O₄Br₂Mo: C, 39.24; H, 3.95; N, 4.58. Found: C, 39.22; H, 3.98; N, 4.60%. Selected IR peaks with proposed assignments (KBr, $\nu_{\max}/\text{cm}^{-1}$): 923, 907 $\nu(\text{Mo}=\text{O})$. ¹H NMR (400 MHz, CDCl₃): δ (ppm) = 7.34–6.80 (m, 4H, aromatic), 3.56–3.51 (m, 4H, 2PhCH₂), 3.02–3.00 (4H, 2NCH₂), 2.74 (6H, 2PhCH₃), 2.27 (s, 6H, 2NCH₃). ¹³C (100 MHz, CDCl₃): δ (ppm) = 153.81, 153.21, 133.22, 133.21, 131.06, 131.16, 129.32, 129.31, 122.93, 122.91, 113.43, 113.41, 64.83, 64.77, 51.83, 51.82, 48.12, 48.10, 29.71, 20.23. ESI-MS: m/z 621.58 [M – CH₃ + Na]⁺, 612.94 [M]⁺, 533.81 [M – Br]⁺.

[MoO₂L²] (2): Yield: 65%. Anal. Calcd for C₂₀H₂₄N₂O₄Cl₂Mo: C, 45.91; H, 4.62; N, 5.35. Found: C, 45.92; H, 4.60; N, 5.38%. Selected IR peaks with proposed assignments (KBr, $\nu_{\max}/\text{cm}^{-1}$): 919, 897 $\nu(\text{Mo}=\text{O})$. ¹H NMR (400 MHz, CDCl₃): δ (ppm) = 7.21–7.07 (m, 2H, aromatic), 3.82–3.78 (d, 2H, ArCH₂), 2.78 (s, 2H, NCH₂), 2.50 (s, 3H, ArCH₃), 2.11 (s, 3H, NCH₃). ¹³C NMR (100 MHz, CDCl₃): δ (ppm) = 156.93, 129.82, 128.94, 127.33, 124.41, 123.72, 63.12, 52.06, 47.71, 16.44. ESI-MS: m/z 523.31 [M]⁺.

[MoO₂L³] (3): Yield: 60%. Anal. Calcd for C₂₆H₃₆N₂O₄Cl₂Mo: C, 51.41; H, 5.97; N, 4.61. Found: C, 51.41; H, 5.99; N, 4.59%. Selected IR peaks with proposed assignments (KBr, $\nu_{\max}/\text{cm}^{-1}$): 913, 901 $\nu(\text{Mo}=\text{O})$. ¹H NMR (400 MHz, DMSO-*d*₆): δ (ppm) = 7.17 (s, 2H, aromatic), 3.34–3.32 (m, 4H, 2ArCH₂), 3.21–3.17 (m, 2H, 2ArCH), 2.80–2.78 (m, 4H, 2NCH₂), 2.54–2.49 (m, 6H, 2Ar-CH₃), 2.29 (m, 6H, 2NCH₃), 1.16–1.10 (m, 12H,

2CH(CH₃)₂). ¹³C NMR (100 MHz, CDCl₃): δ (ppm) = 156.31, 155.98, 136.17, 136.48, 131.92, 131.86, 128.42, 127.93, 125.54, 125.01, 123.29, 122.86, 60.51, 60.22, 48.34, 48.12, 40.19, 39.98, 26.76, 26.73, 23.59, 23.51, 22.66, 22.62, 16.59, 16.40. ESI-MS: *m/z* 607.42 [M]⁺.

[MoO₂L⁴] (4): Yield: 62%. Anal. Calcd for C₃₃H₅₂N₂O₄Mo: C, 62.25; H, 8.23; N, 4.40. Found: C, 62.21; H, 8.24; N, 4.43%. Selected IR peaks with proposed assignments (KBr, *v*_{max}/cm⁻¹): 918, 905 *v*(Mo=O). ¹H NMR (400 MHz, DMSO-*d*₆): δ (ppm) = 7.14–6.84 (m, 4H, aromatic), 4.10–3.36 (m, 6H, 3CH₂), 3.55 (m, 1H, CHCH₃), 2.83 (s, 3H, CHCH₃), 1.35–1.19 (m, 36H, 4C(CH₃)₃). ¹³C NMR (100 MHz, DMSO-*d*₆): δ (ppm) = 154.01, 153.98, 141.41, 140.25, 134.98, 133.41, 123.56, 123.34, 122.52, 122.91, 121.63, 121.42, 75.41, 59.26, 58.96, 57.23, 40.57, 40.36, 35.25, 35.33, 34.86, 34.38, 34.33, 34.21, 33.50, 31.96, 31.92, 30.48, 30.33, 29.88, 29.86, 18.96, 14.74. ESI-MS: *m/z* 636.72 [M]⁺.

[MoO₂L⁵]·EtOH (5): Yield: 70%. Anal. Calcd for C₂₃H₃₄N₂O₅Mo: C, 53.70; H, 6.66; N, 5.45. Found: C, 53.71; H, 6.68; N, 5.41%. Selected IR peaks with proposed assignments (KBr, *v*_{max}/cm⁻¹): 920, 892 *v*(Mo=O). ¹H NMR (400 MHz, CDCl₃): δ (ppm) = 6.92–6.70 (m, 4H, aromatic), 4.16–3.96 (s, 4H, 2ArCH₂), 2.90–2.83 (m, 1H, CHCH₃), 2.54–2.48 (m, 2H, NCH₂), 2.25–2.20 (m, 12H, 4ArCH₃), 1.16 (d, 3H, CHCH₃). ¹³C NMR (100 MHz, CDCl₃): δ (ppm) = 156.81, 156.67, 130.18, 129.85, 128.23, 128.19, 127.98, 127.82, 127.71, 126.39, 121.29, 121.19, 53.05, 52.89, 50.24, 49.84, 49.05, 20.58, 20.55, 17.31, 17.25, 14.20. ESI-MS: *m/z* 468.46 [M – EtOH]⁺.

[MoO₂L⁶]·DMF (6): Yield: 70%. Anal. Calcd for C₂₈H₄₁Cl₂MoN₃O₅: C, 50.46; H, 6.20; N, 6.30. Found: C, 50.41; H, 6.24; N, 6.33%. Selected IR peaks with proposed assignments (KBr, *v*_{max}/cm⁻¹): 904, 882 *v*(Mo=O). ¹H NMR (400 MHz, DMSO-*d*₆): δ (ppm) = 7.17–6.90 (m, 2H, aromatic), 4.25–3.93 (m, 4H, 2PhCH₂), 3.57 (m, 1H, CHCH₃), 3.20–3.15 (m, 2H, 2ArCH), 2.77 (d, 2H, NCH₂), 2.31–2.09 (m, 6H, 2ArCH₃), 1.23–1.12 (m, 12H, 2CH(CH₃)₂), 1.10 (d, 3H, NCHCH₃). ¹³C NMR (100 MHz, DMSO-*d*₆): δ (ppm) = 157.32, 156.86, 136.91, 136.84, 131.25, 131.09, 126.39, 126.37, 125.52, 125.07, 120.23, 120.05, 53.64, 51.41, 50.92, 50.40, 47.51, 27.42, 22.72, 22.60, 22.48, 22.42, 16.30, 16.23, 16.09. ESI-MS: *m/z* 592.48 [M – DMF – H]⁺.

[MoO₂L⁷] (**7**): Yield: 68%. Anal. Calcd for C₁₇H₁₆N₂O₄Br₄Mo: C, 28.05; H, 2.22; N, 3.85. Found: C, 28.05; H, 2.24; N, 3.87%. Selected IR peaks with proposed assignments (KBr, $\nu_{\max}/\text{cm}^{-1}$): 931, 833 $\nu(\text{Mo}=\text{O})$. ¹H NMR (400 MHz, DMSO-*d*₆): δ (ppm) = 7.24–7.00 (m, 4H, aromatic), 3.82–3.81 (m, 4H, ArCH₂), 3.03 (m, 1H, CHCH₃), 2.76 (d, 2H, NCH₂), 1.47 (d, 3H, CH(CH₃)). ¹³C NMR (100 MHz, DMSO-*d*₆): δ (ppm) = 156.80, 156.65, 130.18, 129.84, 128.23, 128.33, 128.19, 127.99, 127.71, 126.39, 121.29, 121.19, 56.48, 52.88, 49.83, 17.27, 14.19. ESI-MS: m/z 727.12 [M]⁺.

5.2.4. X-ray crystallography

General handling and description of equipment

Suitable single-crystals were either gathered from solution or selected from solid samples. Inherent impurities of other crystals were removed carefully and appropriate size was achieved by cutting. Therefore, crystal shape and size given in the table of crystallographic data only approximate the properties of the crystal measured and not of the naturally grown crystals. The data for complex **1** was collected on SuperNova AS2 using high intensity of SuperNova microfocus Cu source ($\lambda = 1.54184 \text{ \AA}$) and a highly sensitive Atlas CCD detector at ~ 100 K. Single crystals of **2** were mounted on a Bruker Smart Apex CCD diffractometer, equipped with a graphite monochromator and a Mo K α radiator ($\lambda = 0.71073 \text{ \AA}$) at 150 K. Crystals of complexes (**3** – **6** · DMSO) were mounted on a 50 μm MicroMeshMiTeGenMicromountTM using FROMBLIN Y perfluoropolyether (LVAC 16/6, Aldrich) before they were centred on a Bruker Kappa APEX II CCD-based 4-circle X-ray diffractometer using graphite monochromated Mo K α radiation ($\lambda = 0.71073 \text{ \AA}$) of a fine focus molybdenum-target X-ray tube operating at 50 kV and 30 mA. In case crystals were cooled this was achieved with a Kryoflex low temperature device.

Data collection and handling

Integrated intensities were obtained with the Bruker SAINT⁴² software package using a narrow-frame algorithm performing spatial corrections of frames, background subtractions, Lorentz and polarization corrections, profile fittings and error analyses. Semi-empirical absorption corrections based on equivalent reflections were made by use of the program SADABS.⁴³ Details on the data collection parameters applied on the individual crystals are summarized in Table 5.1 with $R_{\text{int}} = \Sigma|F_o^2 - F_o^2(\text{mean})|/\Sigma[F_o^2]$ and

$R_{\text{sigma}} = \Sigma[\sigma(F_o^2)]/\Sigma[F_o^2]$. Space groups⁴⁴ were determined from systematic absences and E-value statistics evaluated by the *examine data* routine of the APEX program suite.

General information on structure solution and refinement

Structures were solved by direct methods or Patterson methods and subsequent difference Fourier syntheses of the program SHELXS⁴⁵ and refined by full-matrix least-squares techniques on F^2 with SHELXL,⁴⁵ applying anisotropic displacement factors for all non-hydrogen atoms. Atomic scattering factors were taken from International Tables for Crystallography.⁴⁶ No extinction corrections were applied.

In all cases, final agreement indices were defined as following: $R_1 = \Sigma||F_o| - |F_c||/\Sigma|F_o|$ and $wR_2 = [\Sigma[w(F_o^2 - F_c^2)^2]/\Sigma(F_o^2)^2]^{1/2}$. Weighting function used: $w = 1/[\sigma^2(F_o^2) + (pP)^2 + qP]$ with $P = (F_o^2 + 2F_c^2)/3$. $\text{Goof} = [\Sigma[w(F_o^2 - F_c^2)^2]/(n-p)]^{1/2}$ where n is the number of reflections and p is the total number of parameters refined. All non-hydrogen atoms were refined with anisotropic displacement parameters and hydrogen atoms with common isotropic displacement parameters for chemically related groups of hydrogen atoms.

Although most of the hydrogen atoms could be localised in difference Fourier syntheses, those of the organic groups were refined in geometrically optimized positions riding on the corresponding carbon atoms with C-H distances of 0.98 Å (-CH₃), 0.99 Å (-CH₂-), 1.00 Å (-CH=) and 0.95 Å (CH_{arom}). Hydrogen atoms bonded to oxygen were refined with respect to a common O-H distance of 0.96 Å before they were fixed and allowed to ride on the corresponding oxygen atoms. Further details on the results of structure refinement are summarized in Table 5.1.

With the exception of complex **2** all other compounds crystallize in centrosymmetric space groups. Complex **2** crystallizes in the non-centrosymmetric space group *Fdd2* with a Flack-Parameter of 0.020(9).

Disorder was only observed in case of one t-butyl group of complex **4**, the methyl groups of which adopt two different positions of occupancy 0.646/0.354. The positions of these carbon atoms were refined without constraints in contrast to the anisotropic displacement parameters which were set equal for neighboring atoms.

Figures were drawn using DIAMOND⁴⁷ and Mercury,⁴⁸ respectively. In the ball-and stick models all atoms are drawn as thermal displacement ellipsoids of the 40% level with exception of the hydrogen atoms which are shown as spheres of arbitrary radii. Hydrogen bonds are drawn in red as dashed sticks.

Table 5.1. Crystal data and refinement details for [MoO₂L¹⁻⁶] (**1-6**)

| Complex | 1 | 2 | 3 | 4 | 5 | 6 |
|--------------------------|--|--|--|---|---|--|
| Empirical formula | C ₂₀ H ₂₄ Br ₂ MoN ₂ O ₄ | C ₂₀ H ₂₄ Cl ₂ MoN ₂ O ₄ | C ₂₆ H ₃₆ Cl ₂ MoN ₂ O ₄ | C ₃₃ H ₅₂ Mo N ₂ O ₄ | C ₂₃ H ₃₄ Mo N ₂ O ₅ | C ₂₈ H ₄₁ Cl ₂ MoN ₃ O ₅ |
| Formula weight | 612.17 | 523.25 | 607.41 | 636.71 | 514.46 | 666.48 |
| Temperature | 293(2) K | 150(2) K | 200(2) K | 100(2) K | 100(2) K | 100(2) K |
| Radiation | CuK α | MoK α | MoK α | MoK α | MoK α | MoK α |
| Crystal system | triclinic | orthorhombic | orthorhombic | orthorhombic | monoclinic | monoclinic |
| Space group | <i>P</i> -1 | <i>Fdd</i> 2 | <i>Pbca</i> | <i>Pbca</i> | <i>P</i> 2 ₁ / <i>c</i> | <i>P</i> 2 ₁ / <i>n</i> |
| Unit cell dimensions | a = 7.2058(2) Å | a = 35.1333(8) Å | a = 13.6828(6) Å | a = 12.4692(3) Å | a = 8.0902(3) Å | a = 14.9920(5) Å |
| | b = 7.6148(3) Å | b = 10.1735(2) Å | b = 11.2862(5) Å | b = 15.6244(5) Å | b = 11.3676(4) Å | b = 8.5462(3) Å |
| | c = 20.9813 (7) Å | c = 11.8528 (3) Å | c = 34.5755 (14) Å | c = 34.2618 (9) Å | c = 26.5906 (9) Å | c = 23.5139 (8) Å |
| | α = 92.634(3)° | α = 90° | α = 90° | α = 90° | α = 90° | α = 90° |
| | β = 90.386(2)° | β = 90° | β = 90° | β = 90° | β = 95.336(2)° | β = 92.040(2)° |
| | γ = 111.985 (3)° | γ = 90° | γ = 90° | γ = 90° | γ = 90° | γ = 90° |
| Volume (Å ³) | 1066.1(1) | 4236.5(2) | 5339.4(4) | 6675.0(3) | 2434.8(2) | 3010.8(2) |
| Z | 2 | 8 | 8 | 8 | 4 | 4 |
| Density (calculated) | 1.907 Mg/m ³ | 1.641 Mg/m ³ | 1.511 Mg/m ³ | 1.267 Mg/m ³ | 1.403 Mg/m ³ | 1.470 Mg/m ³ |
| Absorption coefficient | 9.676 mm ⁻¹ | 0.901 mm ⁻¹ | 0.726 mm ⁻¹ | 0.429 mm ⁻¹ | 0.573 mm ⁻¹ | 0.654 mm ⁻¹ |
| F(000) | 604 | 2128 | 2512 | 2704 | 1072 | 1384 |
| Crystal size | 0.794 x 0.1196 x 0.1486 mm | 0.60 x 0.60 x 0.15 mm | 0.34 x 0.08 x 0.05 mm | 0.24 x 0.15 x 0.11 mm | 0.29 x 0.29 x 0.18 mm | 0.22 x 0.15 x 0.12 mm |
| Theta | 4.22° to | 2.32° to | 2.79° to | 2.67° to | 2.53° to | 2.74° to |

| | | | | | | |
|---------------------------|------------|------------|------------|------------|-----------|------------|
| range for data collection | 67.00° | 30.03° | 28.00° | 28.00° | 28.00° | 28.00° |
| Reflections collected | 5531 | 15517 | 91268 | 264860 | 89947 | 120330 |
| Reflections unique | 3424 | 2334 | 6403 | 8062 | 5826 | 7243 |
| Final R1/wR2 | 0.0315/0.0 | 0.0152/0.0 | 0.0393/0.0 | 0.0324/0.0 | 0.0507/0. | 0.0472/0.1 |
| [I>2sigma(I)] | 828 | 427 | 717 | 717 | 1127 | 019 |

5.2.5. DNA binding experiments

Absorption spectral studies The binding of the dioxidomolybdenum (VI) complexes to calf thymus DNA (CT-DNA) was carried out using a Perkin-Elmer Lambda35 spectrophotometer as described previously.^{34b,d} UV-vis spectroscopy was used to perform the titration experiments with variable CT-DNA concentrations ranging from 0 to 70 μM against a fixed concentration of dioxidomolybdenum (VI) complex (25 μM) in 10 mM Tris-HCl buffer (pH 8.0) containing 1% DMF. Binding of the ligands to CT-DNA was also studied with the aid of UV-vis spectroscopy. For this, the concentration of ligand was fixed at 25 μM and was titrated with variable CT-DNA concentration ranging from 0 to 70 μM in 10 mM Tris-HCl buffer (pH 8.0) containing 1% DMF. For both complexes and ligands, the spectra were recorded after each addition of CT-DNA (5 μM). The data obtained from the titration experiments were then fit to Eq. 5.1 to obtain binding constant K_b .^{34b,d}

$$\frac{[\text{DNA}]}{\varepsilon_a - \varepsilon_f} = \frac{[\text{DNA}]}{\varepsilon_b - \varepsilon_f} + \frac{1}{K_b(\varepsilon_b - \varepsilon_f)} \quad \text{Eq. 5.1}$$

where [DNA] is the concentration of DNA base pairs, ε_a , ε_f , and ε_b correspond to apparent extinction coefficient for the complex *i.e.* Abs/[complex] in the presence of DNA, in absence of DNA and to fully bound DNA, respectively. A plot of [DNA]/($\varepsilon_a - \varepsilon_f$) vs [DNA] gave a slope and intercept equal to $1/(\varepsilon_b - \varepsilon_f)$ and $1/K_b(\varepsilon_b - \varepsilon_f)$, respectively; K_b is calculated from the ratio of the slope to the intercept.

Thermal denaturation studies Thermal denaturation studies were carried out in absorbance mode using a Chirascan CD spectropolarimeter (Applied Photophysics, UK) equipped with a peltier temperature controller. The thermal denaturation of 100 μM CT-DNA in the absence and presence of 25 μM complexes were carried out by monitoring the absorbance at 260 nm in the temperature range of 30–90 $^{\circ}\text{C}$ in 10 mM Tris-HCl buffer (pH 8.0) containing 1% DMF. The ramp rate for each of the denaturation experiment was 0.50 $^{\circ}\text{C}/\text{min}$. The melting temperature (T_m) was calculated from the derivative plot (dA_{260}/dT vs T) of the melting profile.⁴⁹

Circular dichroism studies. Chirascan CD spectropolarimeter (Applied Photophysics, UK) equipped with a peltier temperature controller was used to perform the circular dichroism (CD) spectroscopic studies. All the CD studies were done at 25 $^{\circ}\text{C}$. The CD spectra of 100 μM CT-DNA in the absence and presence of 25 μM complexes were obtained in the wavelength range of 240–400 nm in 10 mM Tris-HCl buffer (pH 8.0) containing 1% DMF using quartz cell with 10 mm path length.^{34b,d}

Competitive DNA binding fluorescence measurements The competitive binding experiments were done as described previously.³⁵ Briefly, each of the DNA binding probe i.e. 4',6-diamidino-2-phenylindole (DAPI), methyl green (MG) and ethidium bromide (EB), 2 μM each, was separately incubated with 50 μM of CT-DNA for 1 h at 25 $^{\circ}\text{C}$. Thereafter, the competitive binding of the dioxidomolybdenum (VI) complex (**1–7**) with DAPI, MG and EB bound CT-DNA was studied by measuring the fluorescence intensities of the DAPI, MG and EB bound CT-DNA with increasing concentration of the complexes (0–90 μM). The fluorescence emission intensities of DAPI, MG and EB at 455 nm (excitation 358 nm), 672 nm (excitation 633 nm) and 597 nm (excitation 510 nm) respectively, was monitored with the aid of Fluoromax 4P spectrofluorimeter (Horiba Jobin Mayer, USA).

5.2.6. DNA cleavage experiments

For DNA cleavage experiments, 300 ng supercoiled (SC) pUC19 DNA was used and all experiments were carried out in 50 mM Tris-HCl buffer (pH 8.0) containing 1% DMF.

Chemical-induced DNA cleavage. For chemical nuclease studies, the cleavage experiments were carried out in dark using 0.5 mM hydrogen peroxide as the oxidising

agent in the absence and presence of 1–100 μM complexes. The reactions were incubated at 37 °C for 3 h and analysed for DNA cleaved products by agarose gel electrophoresis.

Photo-induced DNA cleavage. The photo-induced DNA cleavage studies were done as described previously.^{34b,d} Briefly, the photolytic DNA cleavage experiments were carried out on supercoiled (SC) pUC19 DNA (300 ng) with varying concentration from 1 to 100 μM of complexes in 50 mM Tris HCl buffer (pH 8.0) containing 1% DMF. The extent of DNA cleavage was measured from the intensities of the bands using the UVP Gel Documentation System (Gel Doc It²). The observed error in measuring the band intensities ranged between 2–5%. The mechanistic aspect behind the DNA cleavage was studied using four different additives: two singlet oxygen quenchers (sodium azide and L-histidine) and other two hydroxyl radical quenchers (KI and D-mannitol). These additives were added to the reaction mixture prior to the addition of the complex. The concentration of each additive was 0.5 mM.

5.2.7. Cytotoxic Activity

Cytotoxicity of dioxidomolybdenum(VI) complexes (**1–7**) was evaluated *in vitro* against two different human cancerous cell lines namely HeLa (cervical cancer) and HT-29 (colon cancer) by MTT assay. Prior to the experiment, cells were maintained in DMEM with 10% FBS in a humidified (95% humidity) CO₂ incubator (5% CO₂) at 37 °C with regular passages at 70–80 % cell confluence. For the cytotoxicity study, cells were seeded into 96 well plate at a concentration of 1×10^4 cells/ well. Aqueous suspensions of the compounds (**1–7**) of four different concentrations (100, 50, 10 and 5 $\mu\text{g/ml}$) were prepared in complete DMEM media. After 12 h of initial seeding, cells were treated with compounds (**1–7**) for 48h. Tissue culture plate (TCP) was taken as controls. After 48 h, MTT assay was performed using a MTT assay kit following the manufacturer's instruction. The absorbance of the final product was measured at 595 nm. The experiment was performed in quadruplets. The cytotoxicity index of the compounds was calculated using the equation Eq. 5.2 given below, expressed as mean \pm S.D. Statistical significance of the data was evaluated using single variance ANOVA under 95 % confidence interval.

$$\text{Cytotoxicity Index} = \frac{\text{Absorbance of sample at 595 nm}}{\text{Absorbance of the control at 595 nm}} \quad \text{Eq. 5.2}$$

IC₅₀ value of the compounds was calculated from the absorbance-concentration plot following standard procedure.⁵⁰

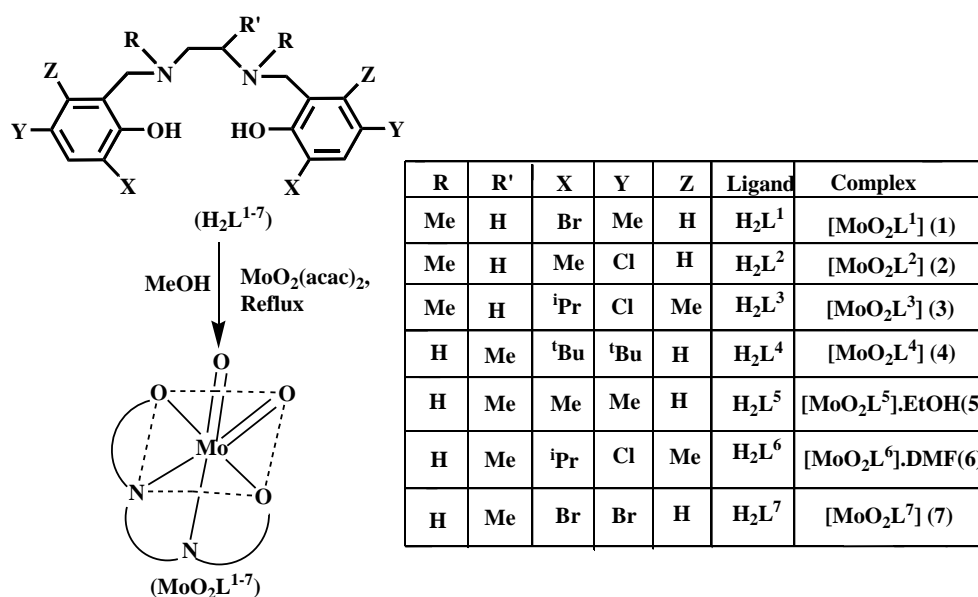
Cytoskeletal organization and the integrity of the nucleus were examined using fluorescence microscopy (Olympus). For this purpose, cells were fixed with 4 % paraformaldehyde for 15 min, permeabilized for 10 min with 0.25% Triton X-100 in PBS and stained with TRITC-Phalloidin and DAPI.⁵¹ For this study, cells were treated with the compounds at a concentration of 100 µg/ml for 36 h.

5.3. RESULTS AND DISCUSSION

5.3.1. Synthesis.

The synthetic methods of all the complexes are illustrated in Scheme 5.1. Reaction of $\text{MoO}_2(\text{acac})_2$ with tetradentate diamino bis(phenolato) (ONNO) “salan” ligands (H_2L^{1-7}) in the molar ratio of 1:1 in MeOH formed a yellow for **1–4** and **6** and an orange precipitate for **5** and **7**, of stoichiometry $[\text{MoO}_2\text{L}^{1-7}]$. The purity of these compounds was further confirmed by elemental analyses. NMR spectra and ESI-MS were consistent with the X-ray structures. The complexes were soluble in aprotic solvents, DMF and DMSO, and sparingly soluble in protic solvents. It was determined that the complexes are diamagnetic, indicating the presence of molybdenum in the +VI oxidation state and are non-conducting in solution.

All the complexes were stable in both solid and solution phases. The solution phase stability of the complexes was confirmed by NMR spectral studies (Figure 5.1).



Scheme 5.1. Schematic representation of ligands (H_2L^{1-7}) and synthesis of complexes, $[\text{MoO}_2\text{L}^{1-7}]$ (**1–7**)

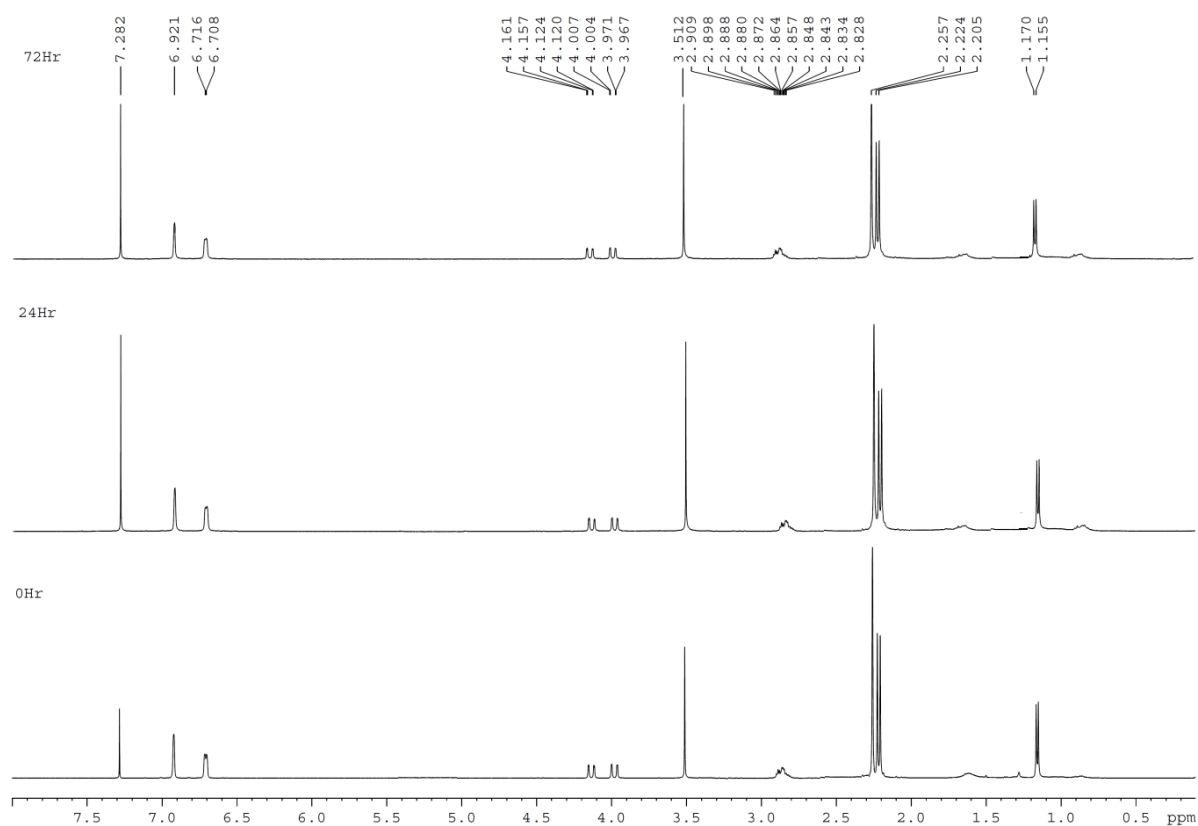


Figure 5.1. Time dependent ^1H NMR spectrum of $\text{MoO}_2\text{L}^5 \cdot \text{EtOH}$ (**5**) in CDCl_3 .

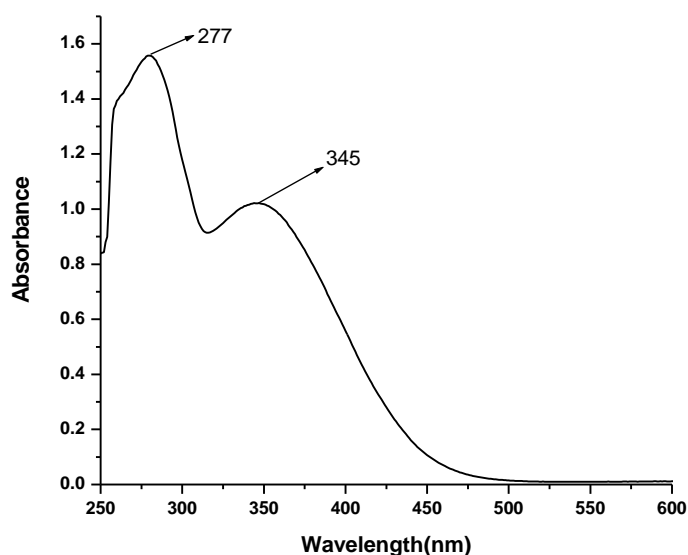
5.3.2. Spectral characteristics

Infrared spectra of these complexes in the $940\text{--}833\text{ cm}^{-1}$ region display a strong two-band pattern characteristic of a *cis*-dioxidomolybdenum(VI) center.³⁹ Their IR spectra also contain all the characteristic bands of the coordinated tetradentate ligands. Absence of a broad peak in the $3600\text{--}3400\text{ cm}^{-1}$ range as compared to the ligand indicates the deprotonation of the two phenolic --OH groups of the ligand.

The electronic spectra of all the complexes (Table 5.2) were recorded in DMF solutions. Two strong absorptions are observed in the wavelength range $388\text{--}275\text{ nm}$. The lower energy medium intensity absorptions at around $388\text{--}330\text{ nm}$ are ascribable to $\text{L} \rightarrow \text{Mo}(\text{d}\pi)$ LMCT transitions whereas the higher energy absorptions are likely to be due to ligand centered transitions.³⁹ A representative spectrum of **1** is shown in Figure 5.2.

Table 5.2. Electronic spectra for complexes $[\text{MoO}_2\text{L}^{1-7}]$ (**1–7**) in DMF solution.

| Complex | $\lambda_{\text{max}}/\text{nm}$ ($\epsilon_{\text{max}}/\text{M}^{-1}\text{cm}^{-1}$) |
|---|--|
| $[\text{MoO}_2\text{L}^1]$ (1) | 277(51814), 345(26982) |
| $[\text{MoO}_2\text{L}^2]$ (2) | 278(45121), 385(27637) |
| $[\text{MoO}_2\text{L}^3]$ (3) | 277(23258), 388(15223) |
| $[\text{MoO}_2\text{L}^4]$ (4) | 279(25123), 365(15921) |
| $[\text{MoO}_2\text{L}^5].\text{EtOH}$ (5) | 277(26126), 355(15711) |
| $[\text{MoO}_2\text{L}^6].\text{DMF}$ (6) | 276(23470), 330(16352) |
| $[\text{MoO}_2\text{L}^7]$ (7) | 275(22768), 346(16939) |

**Figure 5.2.** Electronic absorption spectrum of $[\text{MoO}_2\text{L}^1]$ (**1**).

The NMR spectra (^1H and ^{13}C) of **1–3**, **5** were recorded using CDCl_3 and **4** and **7** with $\text{DMSO}-d_6$. The ^1H NMR spectra of the free ligands exhibit resonance in the range $\delta = 11.47\text{--}10.54$ ppm due to phenolic $-\text{OH}$, but upon complex formation the peak disappears. The aromatic peaks for the complexes appear in the region $\delta = 7.34\text{--}6.80$ ppm, while the aliphatic protons ($-\text{CH}$, $-\text{CH}_2$ and CH_3) are observed in $\delta = 4.25\text{--}1.10$ ppm region. The detailed NMR data has been included in the experimental section. The representative ^1H

NMR spectrum of complex **2** is shown in Figure 5.3. The peaks observed in the ^{13}C NMR spectra of **1–7** at $\delta = 157.32\text{--}113.41$ ppm region have been assigned to aromatic carbons, while the aliphatic protons appear at $\delta = 75.41\text{--}14.19$ ppm region. The representative ^{13}C NMR spectrum of **2** is shown in Figure 5.4. Due to the symmetry present in **2**, half of the total number of protons and carbon atoms appear in the ^1H and ^{13}C NMR spectra, respectively.

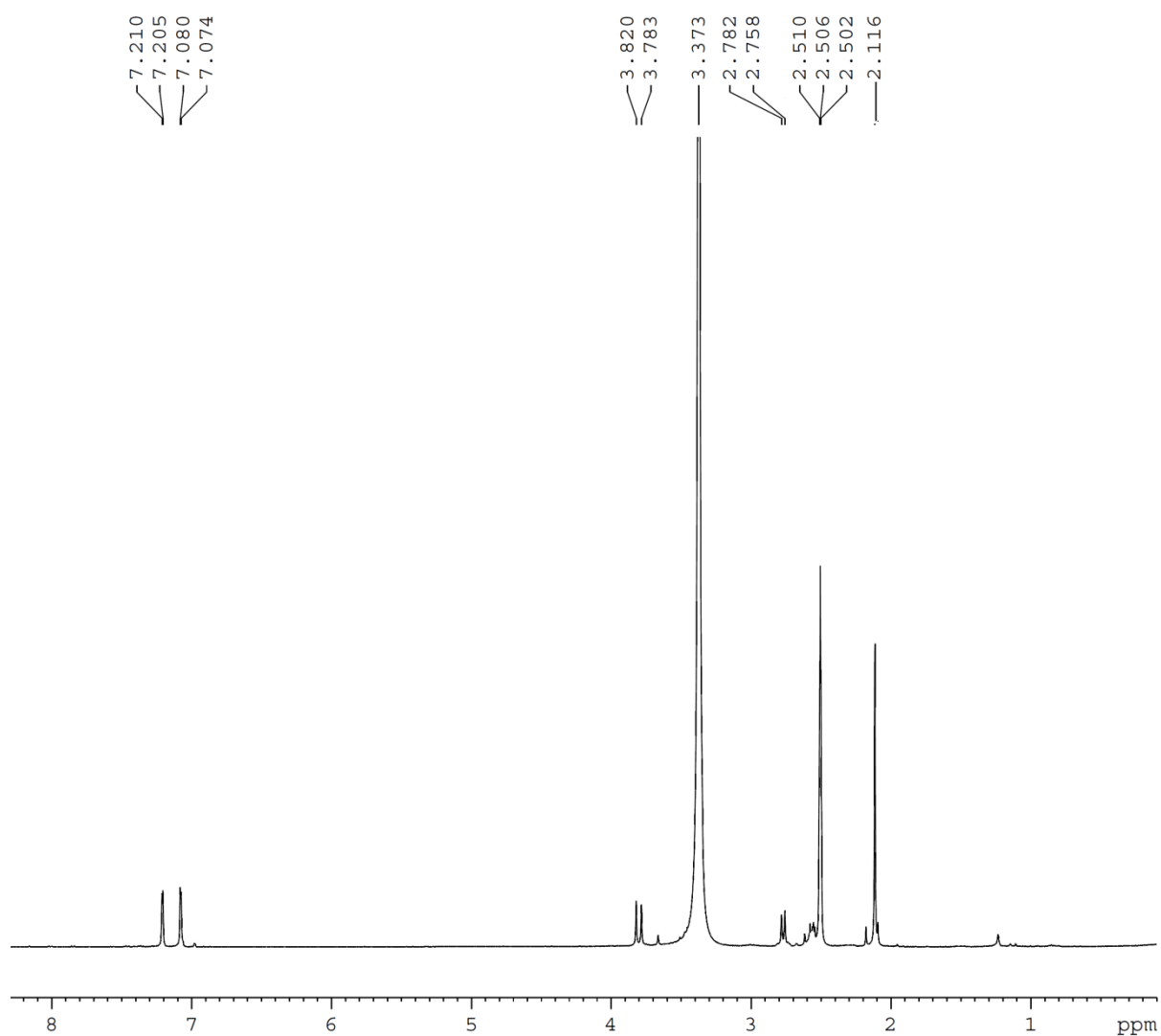


Figure 5.3. ^1H NMR spectrum of $[\text{MoO}_2\text{L}^2]$ (**2**).

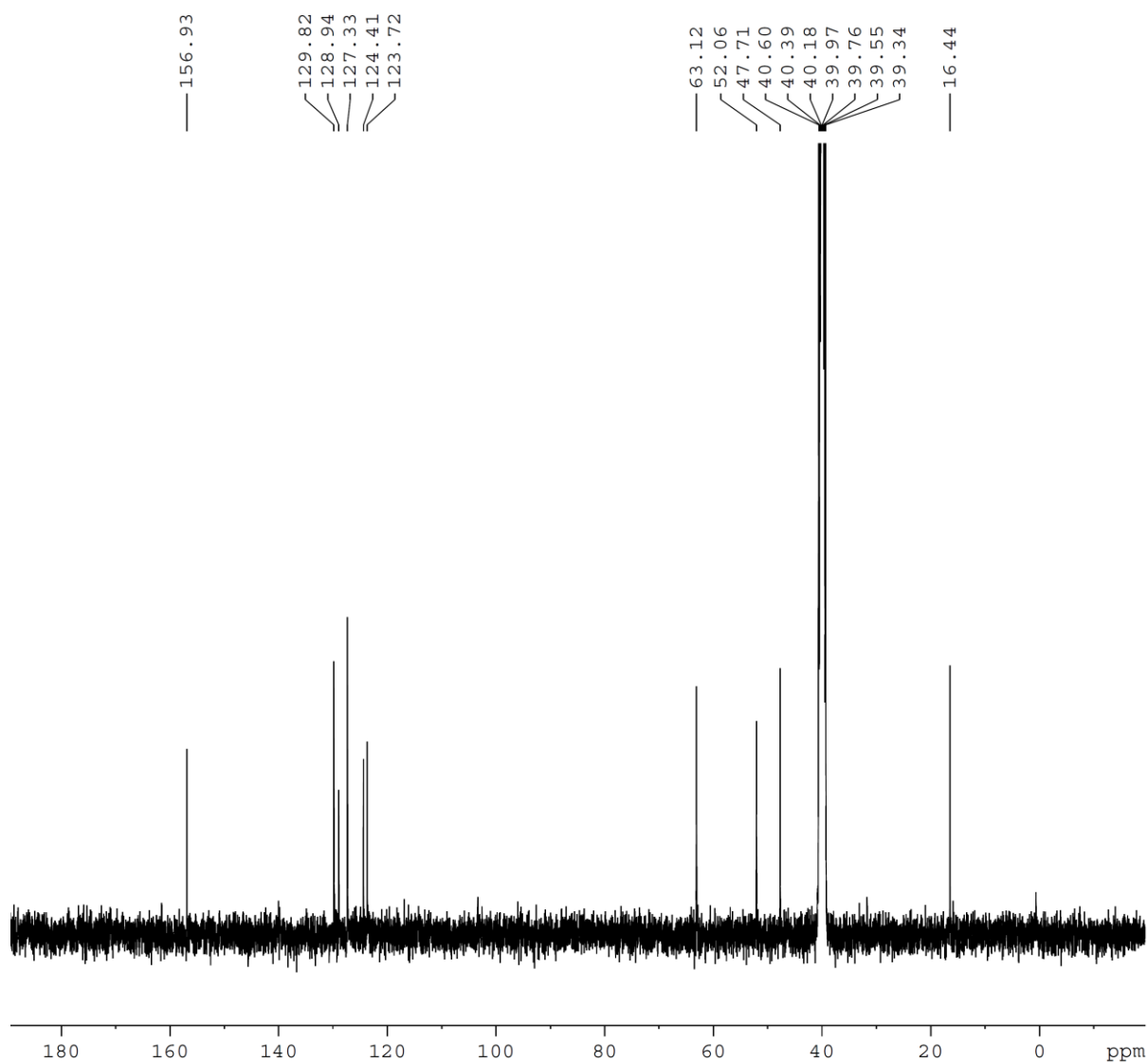


Figure 5.4. ^{13}C NMR spectrum of $[\text{MoO}_2\text{L}^2]$ (**2**) in CDCl_3 .

5.3.3. ESI-MS. ESI-MS of complexes (**1–7**) have been recorded in acetonitrile solution. Mass spectral analysis for **1–4** and **7** show molecular ion peaks at m/z 612.94, 523.31, 607.42, 636.72 and 727.12 respectively, whereas **5** and **6** shows the peaks for $[\mathbf{5} - \text{EtOH}]^+$ and $[\mathbf{6} - \text{DMF} - \text{H}]^+$ at 468.46 and 592.48, respectively. In addition to the molecular ion peak, **1** shows peaks at m/z 621.58 and 533.81 corresponding to $[\mathbf{1} - \text{CH}_3 + \text{Na}]^+$ and 533.81 $[\mathbf{1} - \text{Br}]^+$. Figures 5.5, 5.6 and 5.7 depict representative ESI-MS spectra of complexes **1**, **2** and **7**, respectively.

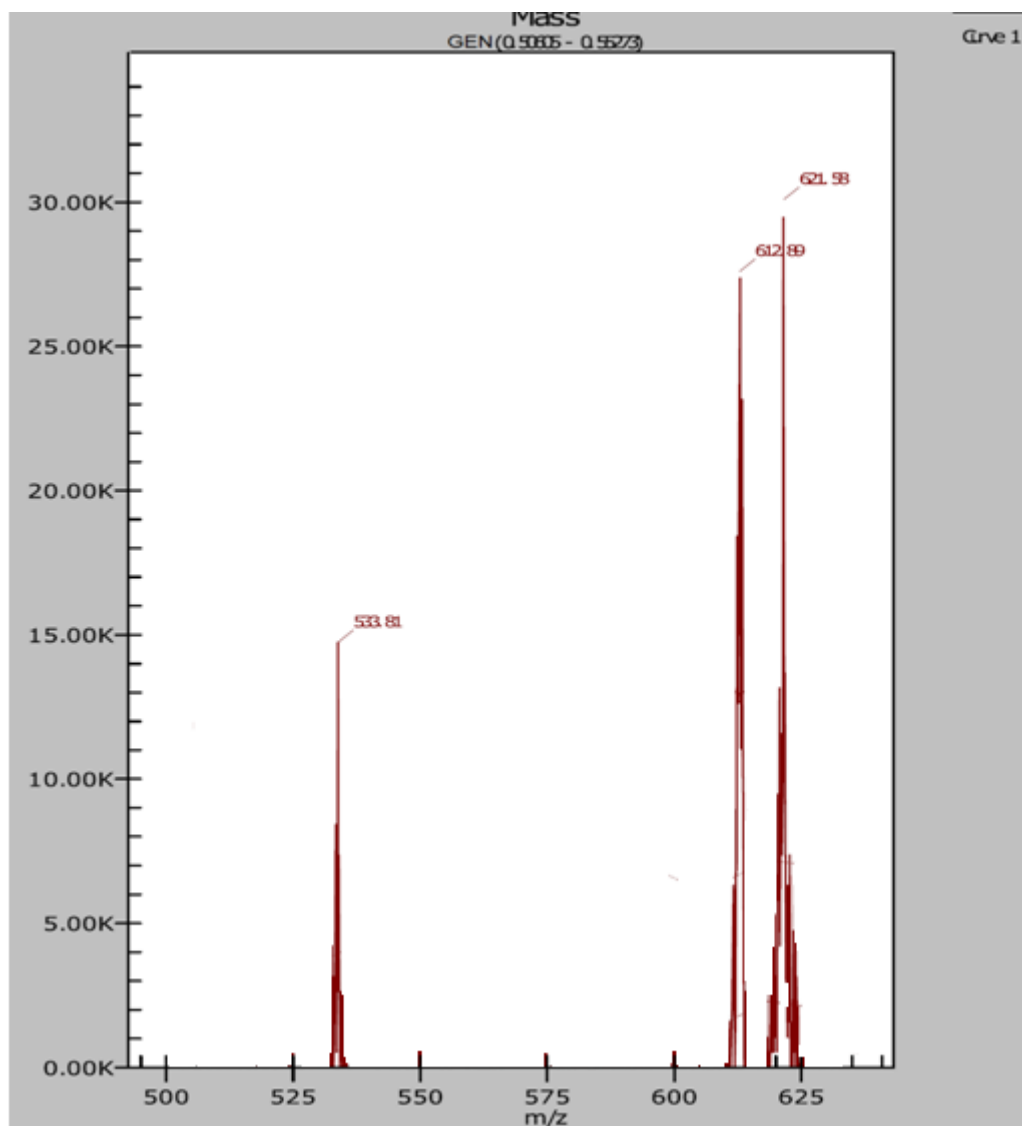


Figure 5.5. ESI-MS of $[\text{MoO}_2\text{L}^1]$ (**1**) in CH_3CN .

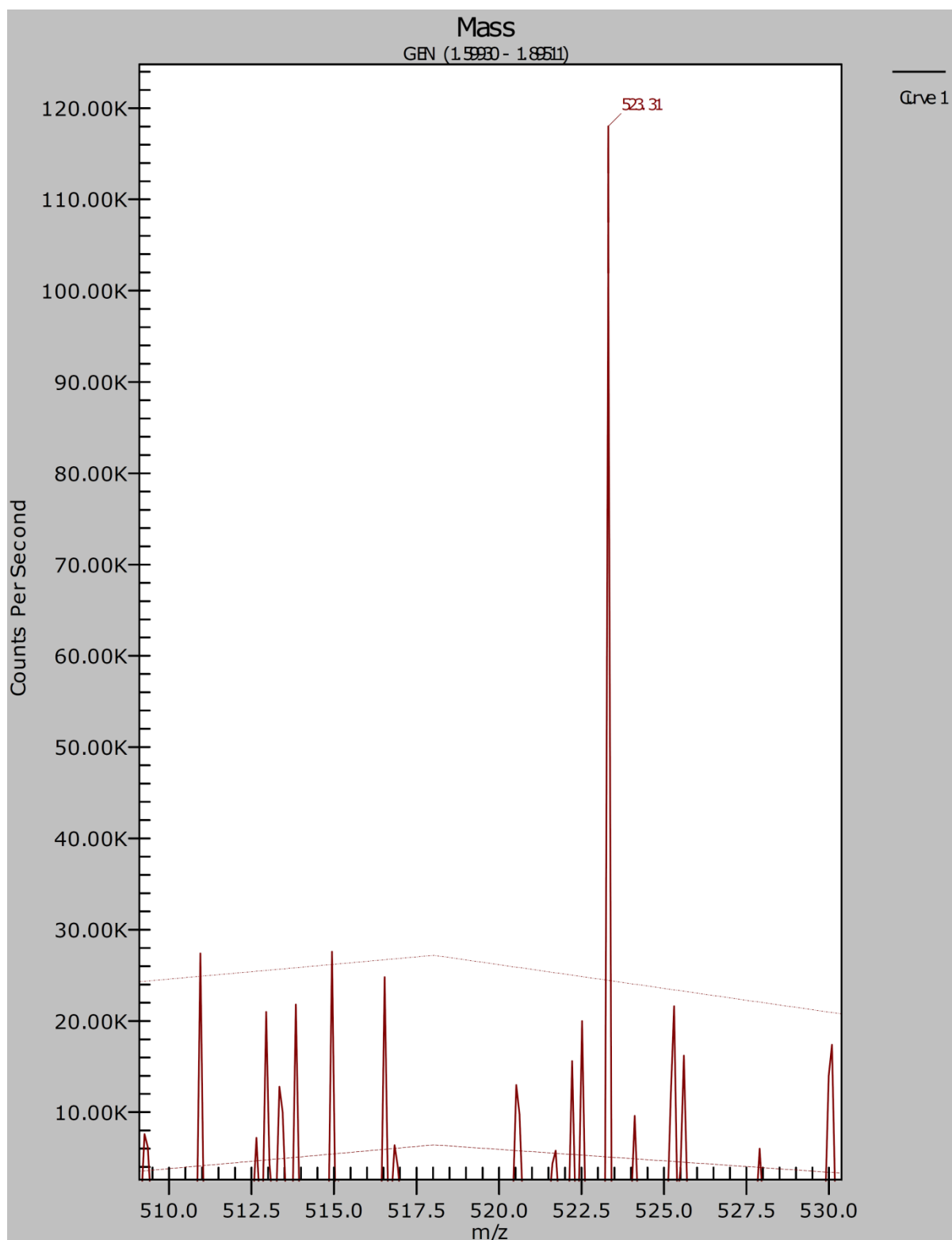


Figure 5.6. ESI-MS of $[\text{MoO}_2\text{L}^2]$ (**2**) in CH_3CN .

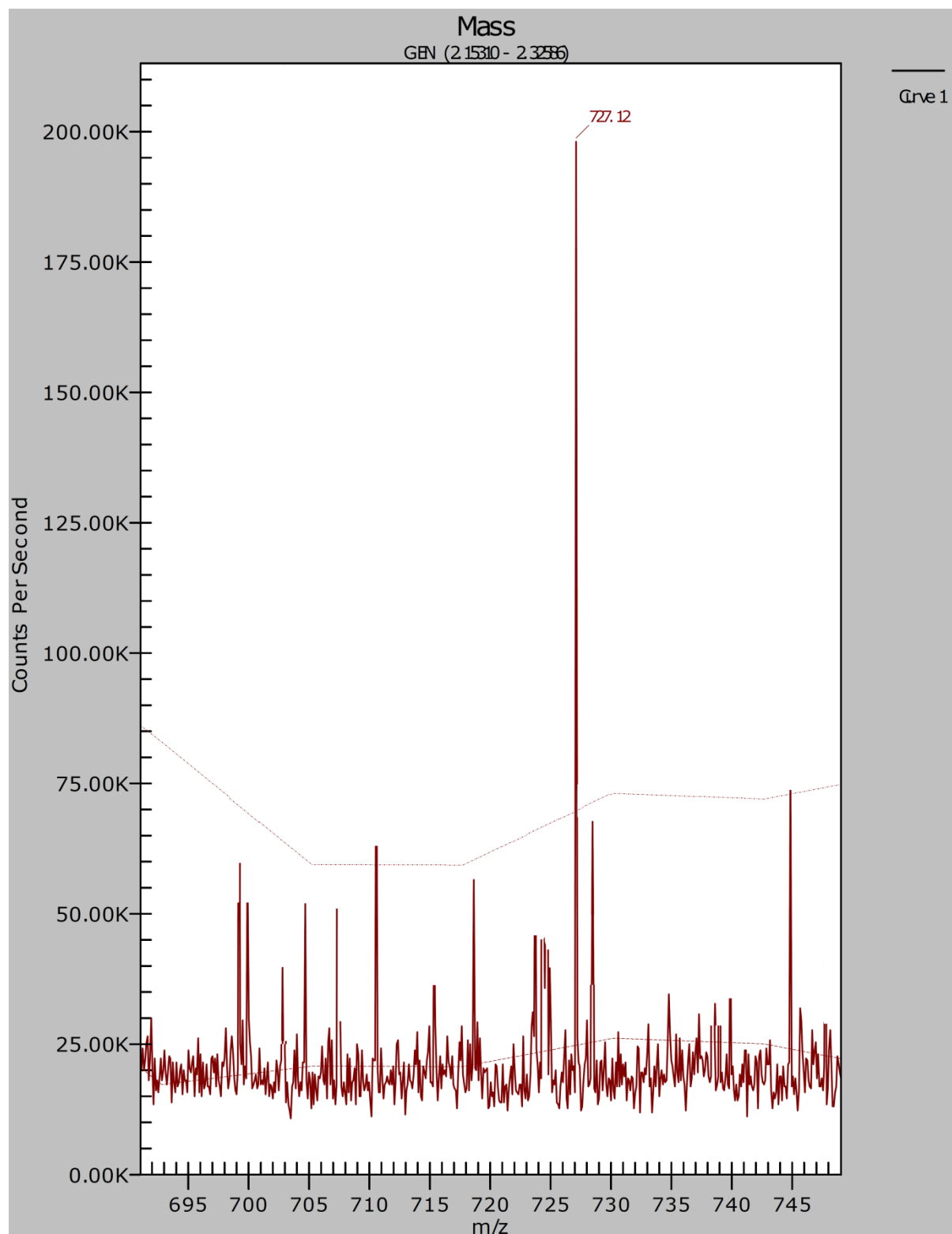


Figure 5.7. ESI-MS of $[\text{MoO}_2\text{L}^7]$ (**7**) in CH_3CN .

5.3.4. Electrochemical Properties

The electrochemical properties of complexes (**1–7**) have been examined in DMF solution by cyclic voltammetry using a Pt working electrode, Pt auxiliary electrode, and an Ag/AgCl reference electrode using 0.1 M TBAP as electrolyte. All the complexes show a quasi-reversible single electron wave ($\Delta E_p = 151\text{--}179$ mV) in the cathodic region at $E_{1/2}$ range -1.28 to -1.33 V, which is assigned to the Mo(VI)/ Mo(V) reduction.^{29c} The ligand is redox inactive in the potential window of -1.0 to -1.6 V in the cathodic region. The one-electron nature of this reduction has been tentatively established by comparing its current height with that of the standard ferrocene-ferrocenium couple under the same experimental conditions. The potential data are listed in Table 5.3. A representative voltammogram of complex **7** is depicted in Figure 5.8.

Table 5.3. Cyclic voltammetric results for $[\text{MoO}_2\text{L}^{1-7}]$ (**1–7**) at 298 K.^[a]

| Complex | $E_{1/2}$ (V) | ΔE_p (mV) |
|---|---------------|-------------------|
| $[\text{MoO}_2\text{L}^1]$ (1) | -1.29 | 154 |
| $[\text{MoO}_2\text{L}^2]$ (2) | -1.30 | 155 |
| $[\text{MoO}_2\text{L}^3]$ (3) | -1.32 | 175 |
| $[\text{MoO}_2\text{L}^4]$ (4) | -1.31 | 179 |
| $[\text{MoO}_2\text{L}^5].\text{EtOH}$ (5) | -1.28 | 151 |
| $[\text{MoO}_2\text{L}^6].\text{DMF}$ (6) | -1.33 | 177 |
| $[\text{MoO}_2\text{L}^7]$ (7) | -1.30 | 170 |

^[a]**1–7** in DMF at a scan rate of 100 mV s^{-1} . $E_{1/2} = (E_p^a + E_p^c)/2$, where E_p^a and E_p^c are anodic and cathodic peak potentials vs. Ag/AgCl, respectively. $\Delta E_p = E_p^a - E_p^c$.

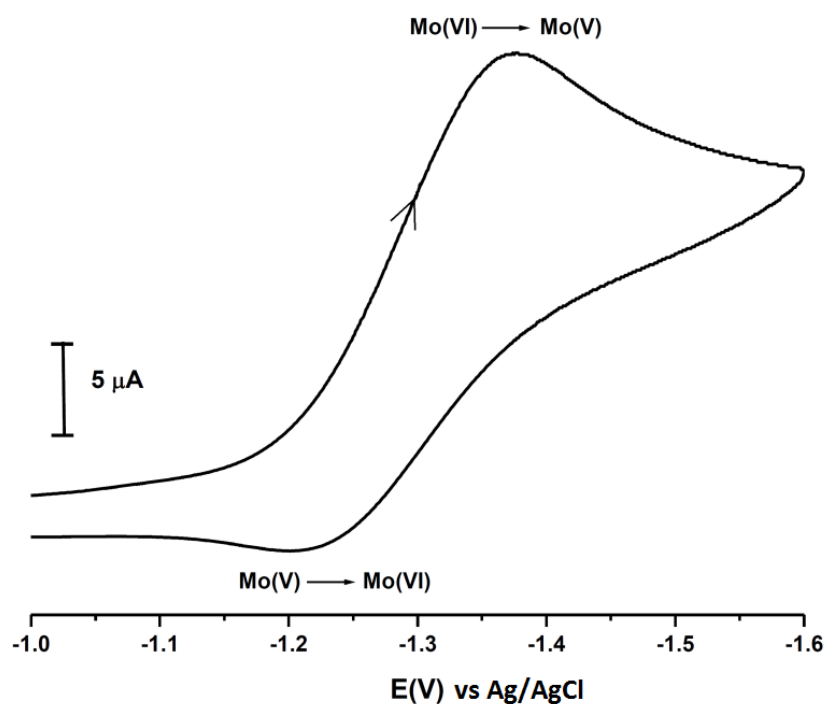


Figure 5.8. Cyclic voltammogram of $[\text{MoO}_2\text{L}^7]$ (**7**) showing reduction ($\text{Mo(VI)} \rightarrow \text{Mo(V)}$) at the molybdenum(VI) center.

5.3.5. Description of X-ray structures of $[\text{MoO}_2\text{L}^{1-6}]$ (**1-6**)

The solid state structures of complexes **1-6** are shown in Figure 5.9, selected bond parameters are listed in Table 5.4. The asymmetric unit of all these complexes consists of a complete formula unit with the exception of complex **2**, which belongs to point group C_2 . Complexes **5** and **6** had EtOH and DMF, respectively, as solvent of crystallization. All complexes exhibit the same structural features with some conformational differences arising from steric and electronical requirements of the individual ligands. At the metal site, the MoO_2 -fragment with its double bonded oxygen atoms is only slightly affected by ligand effects. The $\text{Mo}=\text{O}$ bonds are in a very narrow range [1.701(2)–1.719(2) Å, mean value: 1.710(5) Å] as are the $\text{O}=\text{Mo}=\text{O}$ bond angles [107.8(1)°–109.7(2)°, mean value: 108.7(6)°]. In each case, the ligand expands the coordination sphere of the Mo atom to a distorted octahedron via two oxygen and two nitrogen atoms (Figure 5.10). Small bond length variations are observed in case of the corresponding Mo–O bonds [1.932(3)–1.959(3) Å, mean value: 1.944(8) Å] but larger ones in case of the much weaker Mo–N bonds [2.303(3)–2.399(3) Å, mean value 2.347(41) Å]. In addition, bond angles are

sensitive to ligand variations. Especially, the bond angle between the two *trans* positioned oxygen atoms of the ligand shows a strong influence [$\angle(\text{O1-Mo1-Mo2})$: $151.6(1)^\circ - 160.1(1)^\circ$, mean value $156.2(33)^\circ$]. Within the ligand, the conformation of the $-\text{CH}_2-\text{CH}_2-$, respectively $-\text{CHMe}-\text{CH}_2-$ bridge is very similar in all complexes as the corresponding torsion angles [$\angle(\text{N1-C15-C16-N2})$, Table 5.4] demonstrate [$53.3(2)^\circ - 57.1(5)^\circ$, mean value: $55.8(14)^\circ$]. Most of the conformational differences between the different ligands, however, are picked up from the neighboring atoms C7 and C14 as the torsion angles C7-N1-C15-C16 [$-155.7(3)^\circ - -170.0(3)^\circ$, mean value: $164.3(55)^\circ$] and C15-C16-N2-C14 [$-161.6(3)^\circ - -171.2(2)^\circ$, mean value: $168.0(51)^\circ$] reveal. Therefore these two atoms constitute the rotatable linkage between the nitrogen atoms on the one side and the oxygen atoms of the phenyl rings on the other side, which allow the phenyl groups of the ligand to adopt different orientations relative to each other with respect to the different substituents they bear. Dihedral angles between the phenyl groups therefore vary from $41.3(1)^\circ$ to $66.4(1)^\circ$.

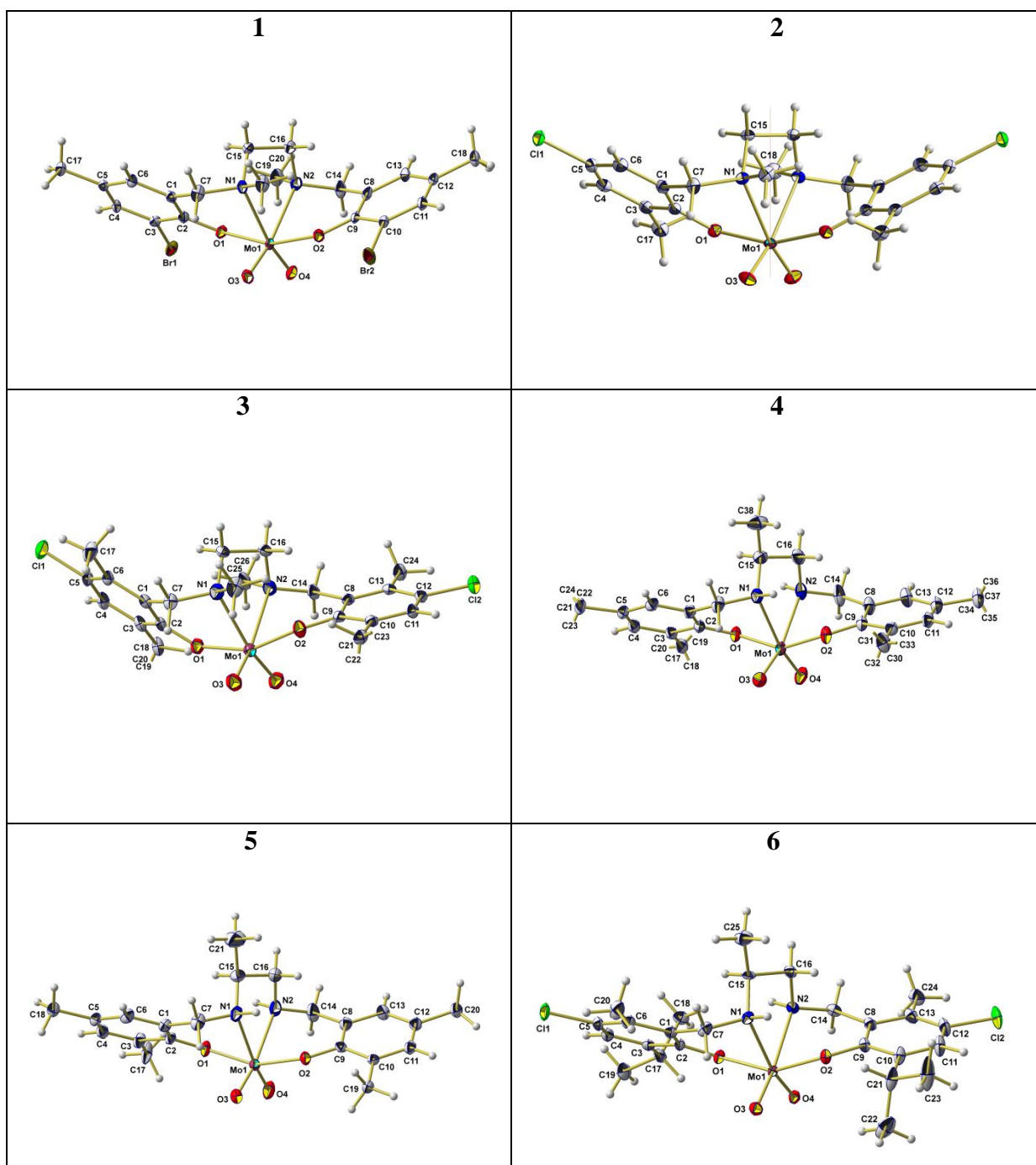


Figure 5.9. Ball-and-stick models of complexes $[\text{MoO}_2\text{L}^{1-6}]$ (1–6) with atomic numbering scheme used. For clarity solvent molecules as well as atoms of the CH_3 -groups of the *i*-propyl and *t*-butyl groups of $[\text{MoO}_2\text{L}^3]$ (3) and $[\text{MoO}_2\text{L}^4]$ (4) have been omitted. In case of $[\text{MoO}_2\text{L}^2]$ (2) the twofold rotation axis of point group C_2 has been drawn in orange and only atoms of the asymmetric unit have been labelled. With exception of the hydrogen

atoms, which are drawn as spheres of arbitrary radius, all other atoms are represented as thermal displacement ellipsoids of 50% probability level.

Table 5.4. Selected bond parameters of [MoO₂L¹⁻⁶] (1-6)

| | 1 | 2 ¹ | 3 | 4 | 5 | 6 |
|--------------------|----------|----------------|----------|-----------|----------|----------|
| Bond distance [Å] | | | | | | |
| Mo(1)-O(1) | 1.950(3) | 1.943(2) | 1.948(2) | 1.946(1) | 1.932(3) | 1.945(2) |
| Mo(1)-O(2) | 1.959(3) | 1.943(2) | 1.938(2) | 1.941(1) | 1.947(3) | 1.948(2) |
| Mo(1)-O(3) | 1.705(3) | 1.713(2) | 1.705(2) | 1.705(2) | 1.713(3) | 1.708(2) |
| Mo(1)-O(4) | 1.711(3) | 1.713(2) | 1.701(2) | 1.715(2) | 1.716(3) | 1.719(2) |
| Mo(1)-N(1) | 2.399(3) | 2.390(2) | 2.387(3) | 2.329(2) | 2.311(4) | 2.303(3) |
| Mo(1)-N(2) | 2.396(3) | 2.390(2) | 2.389(3) | 2.345(2) | 2.318(3) | 2.311(3) |
| Bond angles [°] | | | | | | |
| O(1)-Mo(1)-O(2) | 160.1(1) | 158.97(9) | 156.6(1) | 151.55(6) | 156.9(1) | 153.1(1) |
| O(1)-Mo(1)-O(3) | 98.2(1) | 98.07(6) | 97.3(1) | 99.19(7) | 98.2(2) | 100.0(1) |
| O(1)-Mo(1)-O(4) | 93.7(1) | 94.15(6) | 94.0(1) | 99.22(7) | 96.5(1) | 96.8(1) |
| O(1)-Mo(1)-N(1) | 79.6(1) | 79.22(5) | 76.1(1) | 76.85(6) | 79.0(1) | 78.4(1) |
| O(1)-Mo(1)-N(2) | 84.1(1) | 83.95(6) | 81.6(1) | 80.08(6) | 84.4(1) | 81.8(1) |
| O(2)-Mo(1)-O(3) | 93.5(1) | 94.15(6) | 97.1(1) | 96.99(6) | 94.1(1) | 96.6(1) |
| O(2)-Mo(1)-O(4) | 97.9(1) | 98.08(6) | 99.1(1) | 97.45(7) | 97.7(1) | 97.8(1) |
| O(2)-Mo(1)-N(1) | 84.6(1) | 83.95(6) | 85.4(1) | 79.68(6) | 81.7(1) | 80.8(1) |
| O(2)-Mo(1)-N(2) | 79.9(1) | 79.22(5) | 79.5(1) | 77.76(6) | 77.2(1) | 76.2(1) |
| O(3)-Mo(1)-O(4) | 108.7(2) | 108.7(1) | 107.8(1) | 108.88(8) | 109.7(2) | 108.2(1) |
| O(3)-Mo(1)-N(1) | 88.8(1) | 89.09(7) | 90.3(1) | 90.81(7) | 89.4(2) | 89.6(1) |
| O(3)-Mo(1)-N(2) | 161.7(1) | 161.86(7) | 164.2(1) | 163.33(7) | 161.9(2) | 162.7(1) |
| O(4)-Mo(1)-N(1) | 162.1(1) | 161.86(7) | 160.6(1) | 160.31(7) | 160.9(2) | 162.1(1) |
| O(4)-Mo(1)-N(2) | 89.2(1) | 89.09(7) | 88.0(1) | 87.59(7) | 87.7(2) | 88.5(1) |
| N(1)-Mo(1)-N(2) | 73.8(1) | 73.52(8) | 74.1(1) | 72.75(6) | 73.4(1) | 73.9(1) |
| Torsion angles [°] | | | | | | |
| C(1)-C(7)-N(1)- | 59.7(4) | 55.8(2) | 52.0(4) | 68.3(2) | 63.5(5) | 62.5(4) |

| | | | | | | |
|-------------------------------------|----------|-----------|----------|-----------|----------|-----------|
| C(15) | | | | | | |
| C(7)-N(1)-C(15)- | - | -161.7(2) | - | -167.0(2) | - | -168.2(3) |
| C(16) | 163.2(3) | | 155.7(3) | | 170.0(3) | |
| N(1)-C(15)- | 56.0(4) | 53.3(2) | 56.9(4) | 55.2(2) | 57.1(5) | 56.5(3) |
| C(16)-N(2) | | | | | | |
| C(15)-C(16)- | - | -161.7(2) | - | -171.2(2) | - | -172.8(3) |
| N(2)-C(14) | 161.6(3) | | 168.5(3) | | 172.2(4) | |
| C(16)-N(2)- | 57.1(4) | 55.8(2) | 62.2(4) | 67.1(3) | 68.3(5) | 70.4(4) |
| C(14)-C(8) | | | | | | |
| Angle between both phenyl rings [°] | | | | | | |
| C(1)-C(6)/C(8)- | 66.4(1) | 63.45(5) | 54.5(1) | 43.0(1) | 53.5(2) | 41.3(1) |
| C(13) | | | | | | |

¹As the asymmetric unit of $[\text{MoO}_2\text{L}^2]$ (**2**) consists of half a molecule missing data have been included using the symmetry related values.

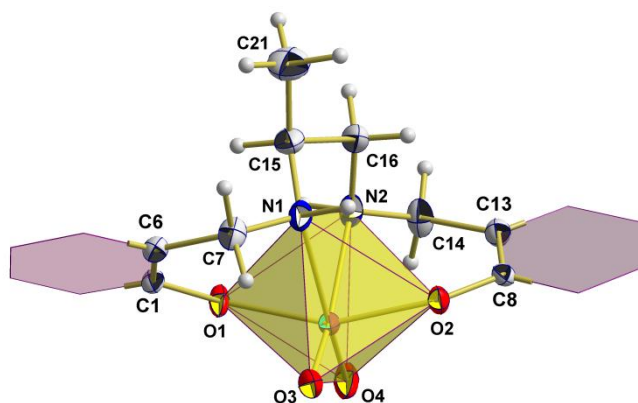


Figure 5.10. The coordination sphere of the Mo atom and the conformational flexible parts of the ligand of $[\text{MoO}_2\text{L}^5]$ (**5**). Phenyl groups are visualized as hexagons.

5.3.6. DNA binding studies

Solution phase stability

The solution phase stability was studied over a period of 72 h at 25 °C for all the dioxidomolybdenum(VI) complexes (**1–7**) with the aid of electronic absorption spectroscopic studies. All the complexes were stable and did not show any change in the electronic absorption spectra after incubation at 25 °C for 72 h (Figure 5.11).

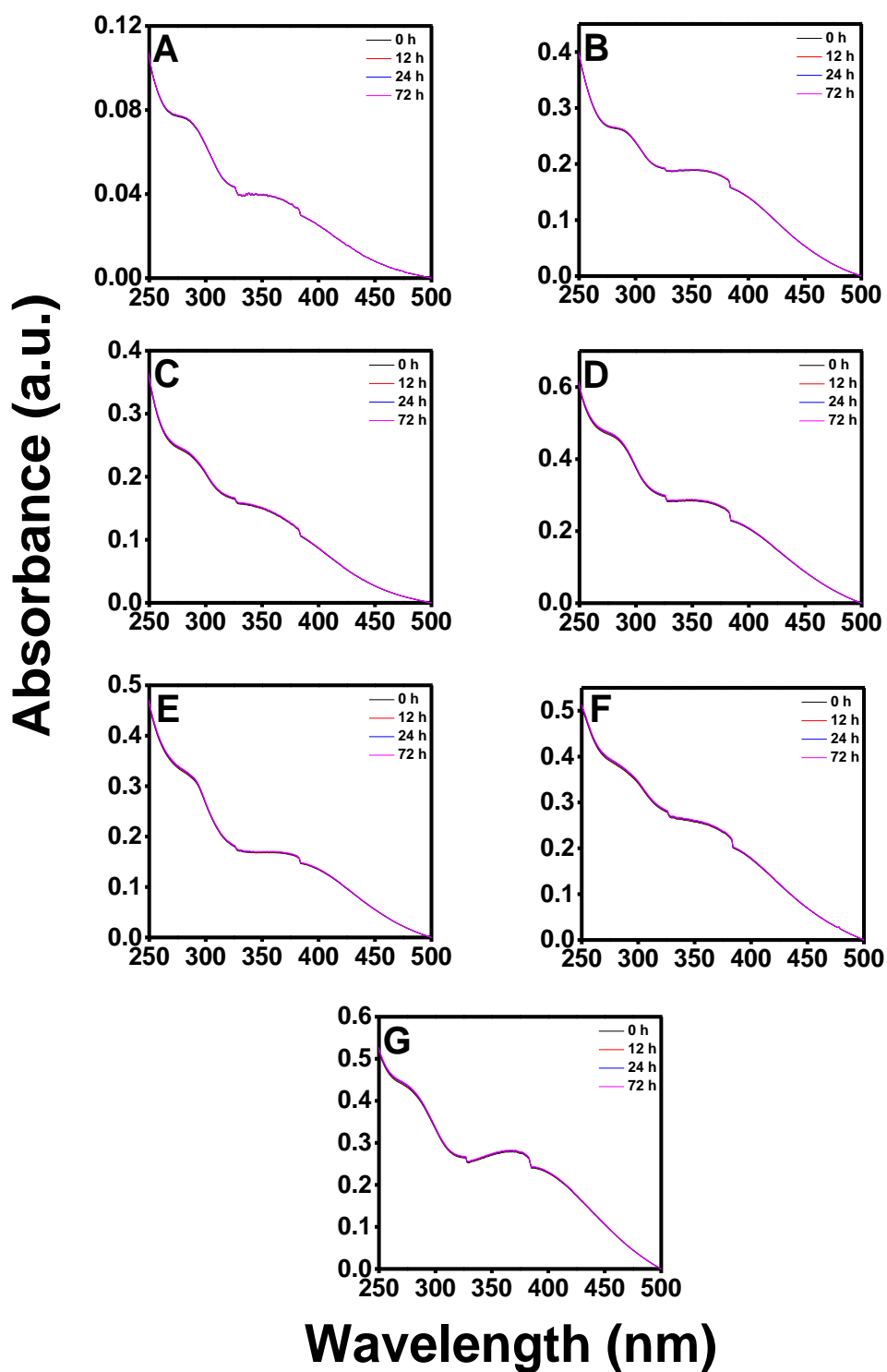


Figure 5.11. Absorption spectral traces of [MoO₂L¹] (1) (A), [MoO₂L²], (2) (B), [MoO₂L³], (3) (C), [MoO₂L⁴], (4) (D), [MoO₂L⁵], (5) (E), [MoO₂L⁶], (6) (F) and

[MoO₂L⁷], (**7**) (**G**) (25 μM each) in 10 mM Tris-HCl buffer (pH 8.0) containing 1% DMF. The spectra were recorded up to 72 h at room temperature.

Absorption spectroscopic studies

At first, the equilibrium binding constant (K_b) of the dioxidomolybdenum(VI) complex **1–7** with CT-DNA was determined with the aid of UV-vis titration experiments (Figure 5.12 and Table 5.5). Complexes **1–7** have in particular two distinct absorption bands in the region 388–330 and 279–275 nm which is attributed to L–Mo(dπ) LMCT and intra-ligand transitions, respectively. On addition of CT-DNA to the complex solution, the UV-vis absorption bands in the region 390–275 nm showed a hypochromic shift for all the complexes (Figure 5.12) which indicated the interaction between the dioxidomolybdenum (VI) complexes with CT-DNA. The observed hypochromicity of **1–7**, in the intra-ligand transition band may be due to the interaction between the electronic states of the chromophores of the ligands and the DNA bases.^{52,53,54}

Table 5.5. DNA binding parameters for complexes [MoO₂L^{1–7}] (**1–7**)

| Complex | Binding constant (K_b) ^a (M ⁻¹) | ΔT_m ^b (°C) |
|--|--|--------------------------------|
| [MoO ₂ L ¹], 1 | 1.06×10^4 | +1.50 |
| [MoO ₂ L ²], 2 | 4.74×10^5 | +3.00 |
| [MoO ₂ L ³], 3 | 8.85×10^4 | +0.50 |
| [MoO ₂ L ⁴], 4 | 2.61×10^4 | +1.00 |
| [MoO ₂ L ⁵], 5 | 5.37×10^4 | +0.50 |
| [MoO ₂ L ⁶], 6 | 1.08×10^4 | +0.50 |
| [MoO ₂ L ⁷], 7 | 2.43×10^4 | +1.00 |

^a DNA binding constants were determined by the UV-vis spectral method.

^b Change in the melting temperature of CT-DNA.

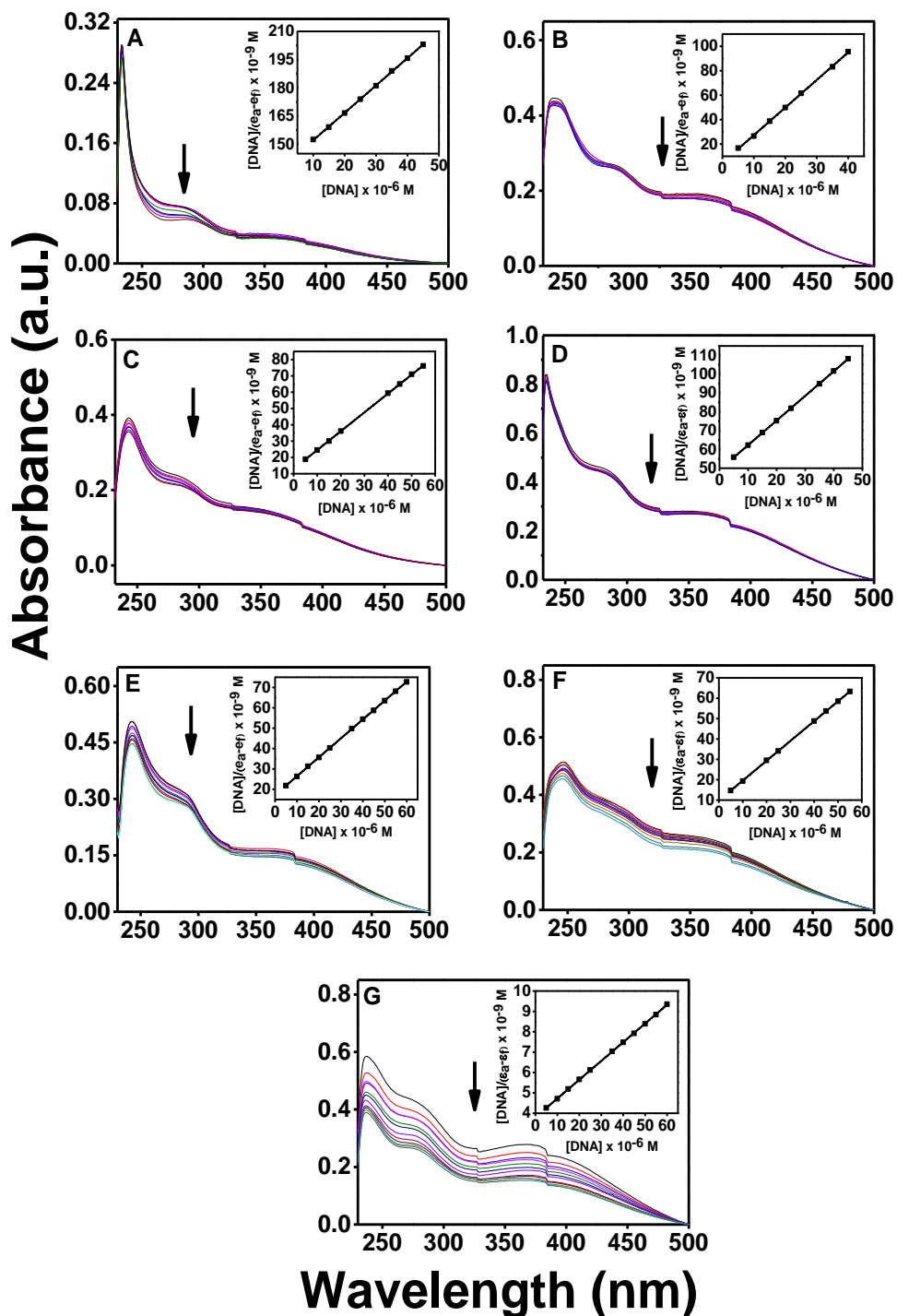


Figure 5.12. Electronic absorption spectra of $[\text{MoO}_2\text{L}^1]$ (1) (A), $[\text{MoO}_2\text{L}^2]$, (2) (B), $[\text{MoO}_2\text{L}^3]$, (3) (C), $[\text{MoO}_2\text{L}^4]$, (4) (D), $[\text{MoO}_2\text{L}^5]$, (5) (E), $[\text{MoO}_2\text{L}^6]$, (6) (F) and $[\text{MoO}_2\text{L}^7]$, (7) (G) ($25 \mu\text{M}$ each) upon the titration of CT-DNA (0 – $70 \mu\text{M}$). The experiments were performed with 10 mM Tris-HCl buffer ($\text{pH } 8.0$) containing 1% DMF.

Arrow shows the changes in absorbance with respect to an increase in the CT-DNA concentration. The inset shows the linear fit of $[\text{DNA}]/(\epsilon_a - \epsilon_f)$ vs $[\text{DNA}]$ and the binding constant (K_b) was calculated using Eq. 5.1.

The binding constant (K_b) of the interaction between CT-DNA and each of the dioxidomolybdenum (VI) complexes (**1–7**) was calculated using Eq. 5.1. The data is reported in Table 5.5 which reveal that the DNA binding strength of the dioxidomolybdenum(VI) complexes are in the order **2 > 3 > 5 > 4 > 7 > 6 \approx 1**, with the K_b values of complexes ranging from 1.06×10^4 to $4.74 \times 10^5 \text{ M}^{-1}$. The binding affinity of the ligands to CT-DNA showed the binding constant (K_b) values lower than their corresponding dioxidomolybdenum (VI) complexes (Figure 5.13 and Table 5.6).

Table 5.6. Binding constant (K_b) values for the "CT-DNA-ligand" interactions.^a

| Ligand | Binding constant (K_b) (M^{-1}) |
|-----------------------------------|--|
| H₂L¹ | 3.8×10^3 |
| H₂L² | 6.7×10^3 |
| H₂L³ | 3.6×10^3 |
| H₂L⁴ | 8.6×10^3 |
| H₂L⁵ | 4.7×10^3 |
| H₂L⁶ | 8.5×10^3 |
| H₂L⁷ | 8.3×10^3 |

^a The DNA binding constant was determined by the UV-vis spectral method.

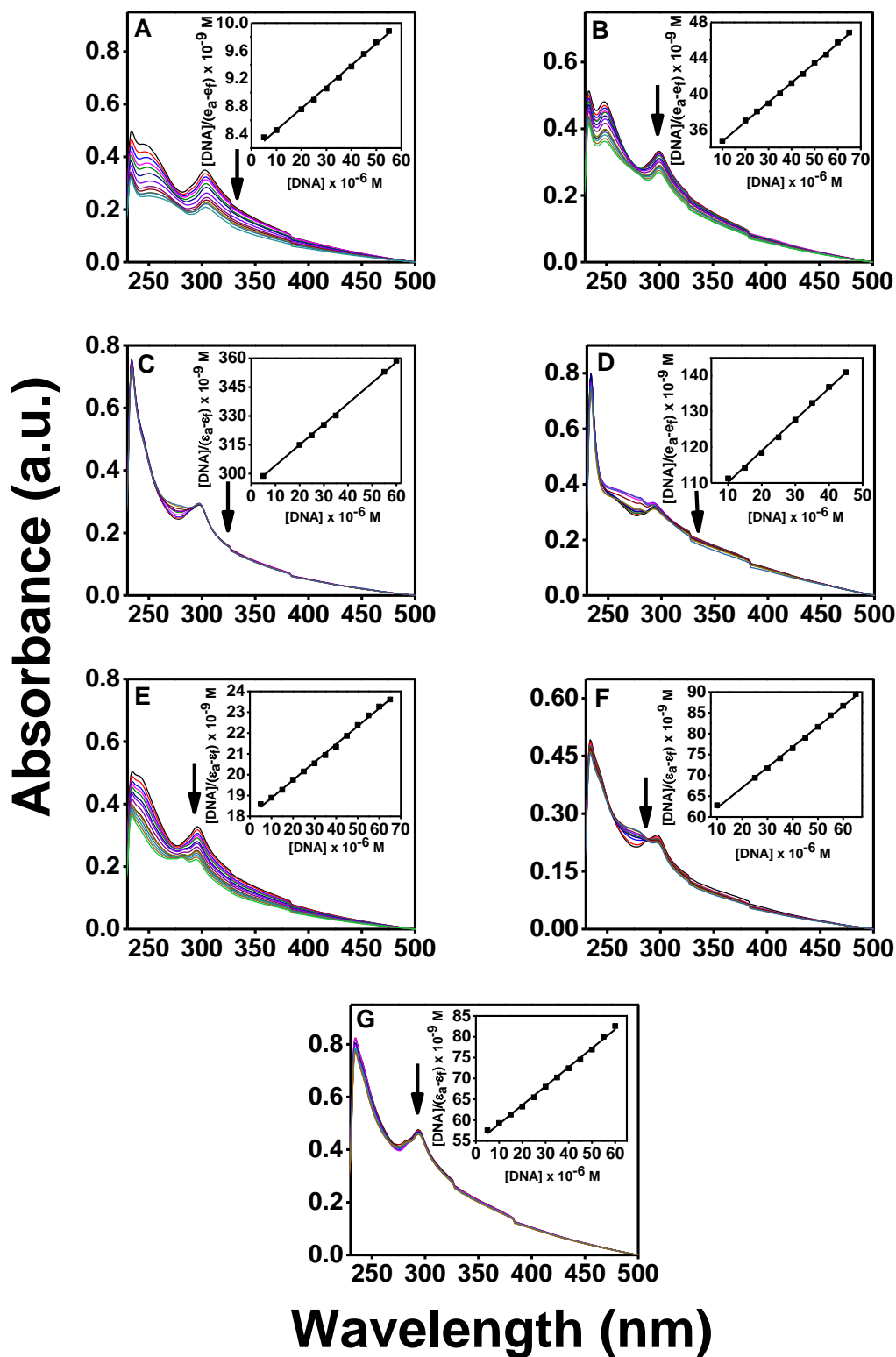


Figure 5.13. Electronic absorption spectra for H_2L^1 (A), H_2L^2 (B), H_2L^3 (C) H_2L^4 (D), H_2L^5 (E), H_2L^6 (F) and H_2L^7 (G) (25 μ M each) upon the titration of CT-DNA

(0 – 70 μM) in 10 mM Tris-HCl buffer (pH 8.0) containing 1% DMF. The inset shows the linear fit of $[\text{DNA}]/(\varepsilon_a - \varepsilon_f)$ vs $[\text{DNA}]$ from which the binding constant (K_b) was calculated using Eq. 5.1.

Thermal denaturation studies

In order to investigate the stability of the CT-DNA in absence and presence of the dioxidomolybdenum(VI) complexes **1–7**, DNA melting experiments were performed.⁵⁷ The melting temperature (T_m) of CT-DNA in absence of any complex was ~ 66 °C which is in good agreement with our previous findings.³⁵ Upon interaction with dioxidomolybdenum (VI) complexes **1** and **3–7**, the T_m of CT-DNA increased very slightly (~ 0.50 – 1.5 °C), whereas complex **2** exhibited a significant amount (~ 3.0 °C) of positive shift in the melting temperature of CT-DNA (Figure 5.14 and Table 5.5). The lower ΔT_m values for the dioxidomolybdenum(VI) complexes **1** and **3–7** suggest that these complexes interact with CT-DNA by a groove binding mode. While the larger ΔT_m value of dioxidomolybdenum(VI) complex **2** indicates that it may interact with CT-DNA through both groove binding as well as partial intercalative mode of binding.^{55,56}

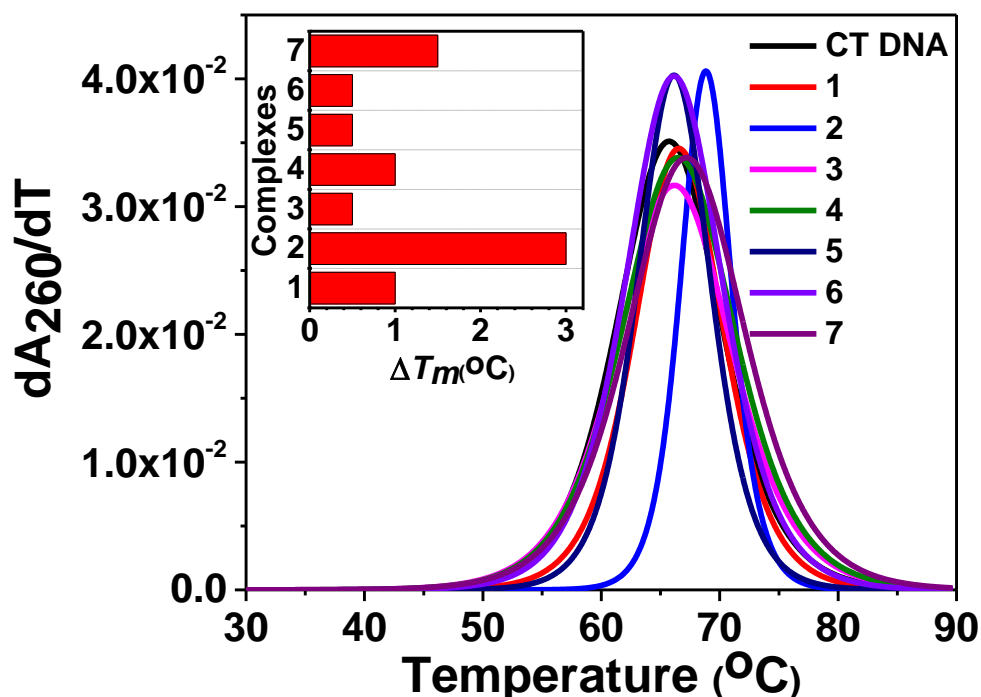


Figure 5.14. Derivative plot of thermal denaturation of CT-DNA (100 μM) in the absence and presence of $[\text{MoO}_2\text{L}^{1-7}]$ (1–7) (25 μM) in 10 mM Tris-HCl buffer (pH 8.0) containing 1% DMF. Inset shows the ΔT_m ($^\circ\text{C}$) of the complexes as compared to CT-DNA.

Circular dichroism studies

Circular dichroism (CD) spectroscopy was used in order to study the conformational changes in CT-DNA upon the interaction with complexes.⁵⁷ CT-DNA usually shows one positive band at 275 nm for base stacking interaction and a negative band at 245 nm for right-handed helicity.⁵⁷ There is less or no perturbation on the base stacking and helicity bands when a small molecule interacts with CT-DNA by groove binding and electrostatic interaction but intercalation can induce intensity changes of both bands and can modulate the right-handed B-conformation of DNA.⁵⁷ The CD spectra of 100 μM CT-DNA upon the interaction with the dioxidomolybdenum(VI) complexes (4–7) showed very slight changes, for the positive band at 275 nm as well as for the negative band at 245 nm (Figure 5.15). The dioxidomolybdenum(VI) complexes (1–3) exhibited minor alteration in the negative band at 245 nm while only complex 2 exhibited a moderate shift in the

positive ellipticity for the band at 275 nm. This suggests that the interaction of the dioxidomolybdenum(VI) complexes (**1** and **3–7**), were either electrostatic or groove binding in nature while complex **2** which showed intensity changes in both the negative and positive bands may possibly interact with CT-DNA by a partial intercalative mode of binding.

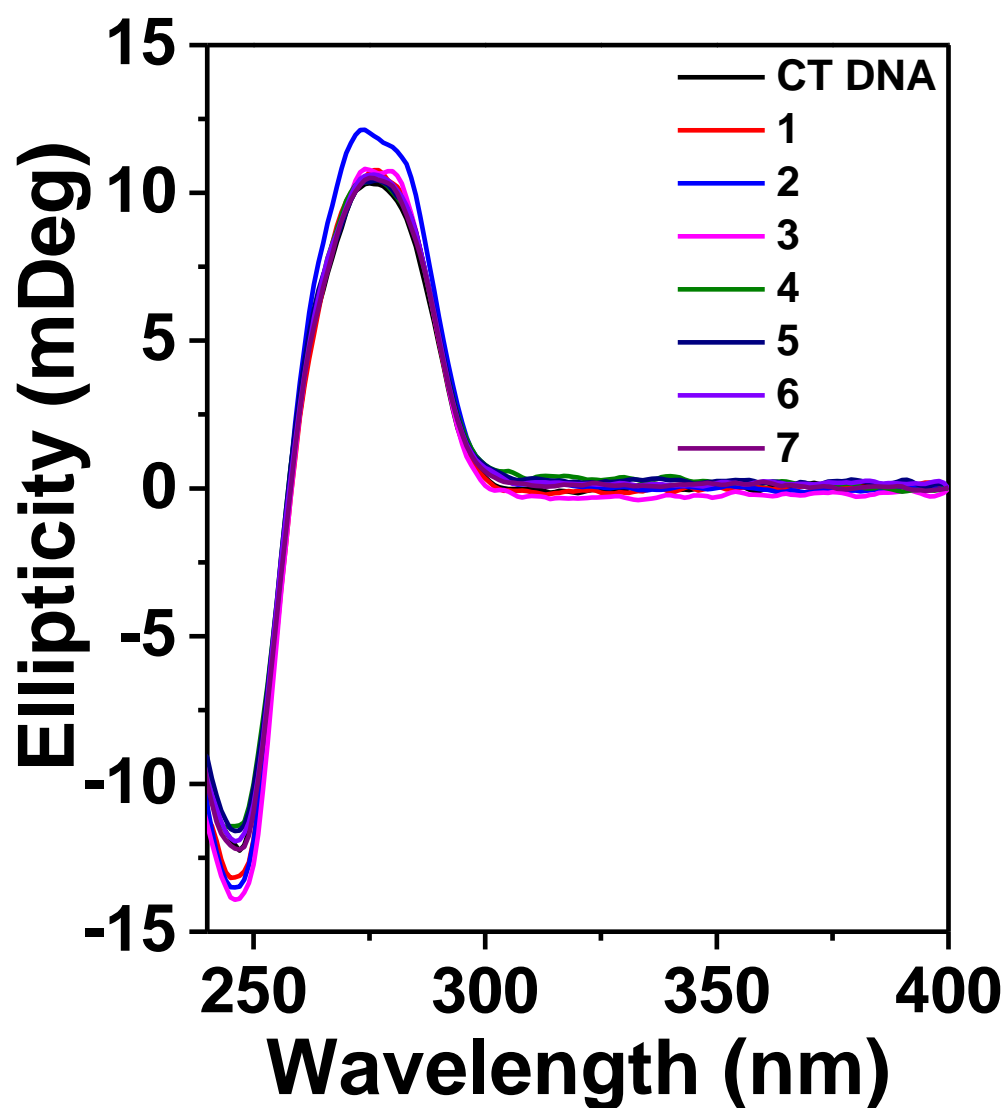


Figure 5.15. Circular dichroism spectra of CT-DNA (100 μM) in the presence and absence of $[\text{MoO}_2\text{L}^{1-7}]$ (**1–7**) (25 μM). The experiment was done in 10 mM Tris-HCl buffer (pH 8.0) containing 1% DMF. The path length of the cuvette was 10 mm.

Competitive binding studies

The thermal denaturation and the circular dichroism experiments hinted that the dioxidomolybdenum (VI) complexes (**1** and **3–7**), bind to CT-DNA possibly through groove binding mode and complex **2** possibly by groove and partial intercalative binding mode. Therefore in order to find out the binding mode of the complexes with CT-DNA, we performed competitive binding experiments with three fluorescent dyes DAPI, MG and EB. DAPI and MG are mainly minor and major groove binders respectively, while EB binds to DNA through intercalation.^{34b,d} The titration of the DAPI bound CT-DNA with increasing amount of the complex concentration led to the quenching of the emission intensity of the DAPI bound CT-DNA at 455 nm (Figure 5.16). This indicated the displacement of the bound DAPI to CT-DNA by the dioxidomolybdenum (VI) complexes (**1–7**) (Figure 5.16). Complex **2** exhibited the highest quenching (~38%), followed by complex **1** and **3** (~30% each) (Figure 5.16). Complexes **4–7** showed the least quenching of the fluorescence intensity at 455 nm of ~25% each (Figure 5.16). Hence our data clearly showed that the dioxidomolybdenum (VI) complex **1–7** binds to the CT-DNA through minor groove binding mode.

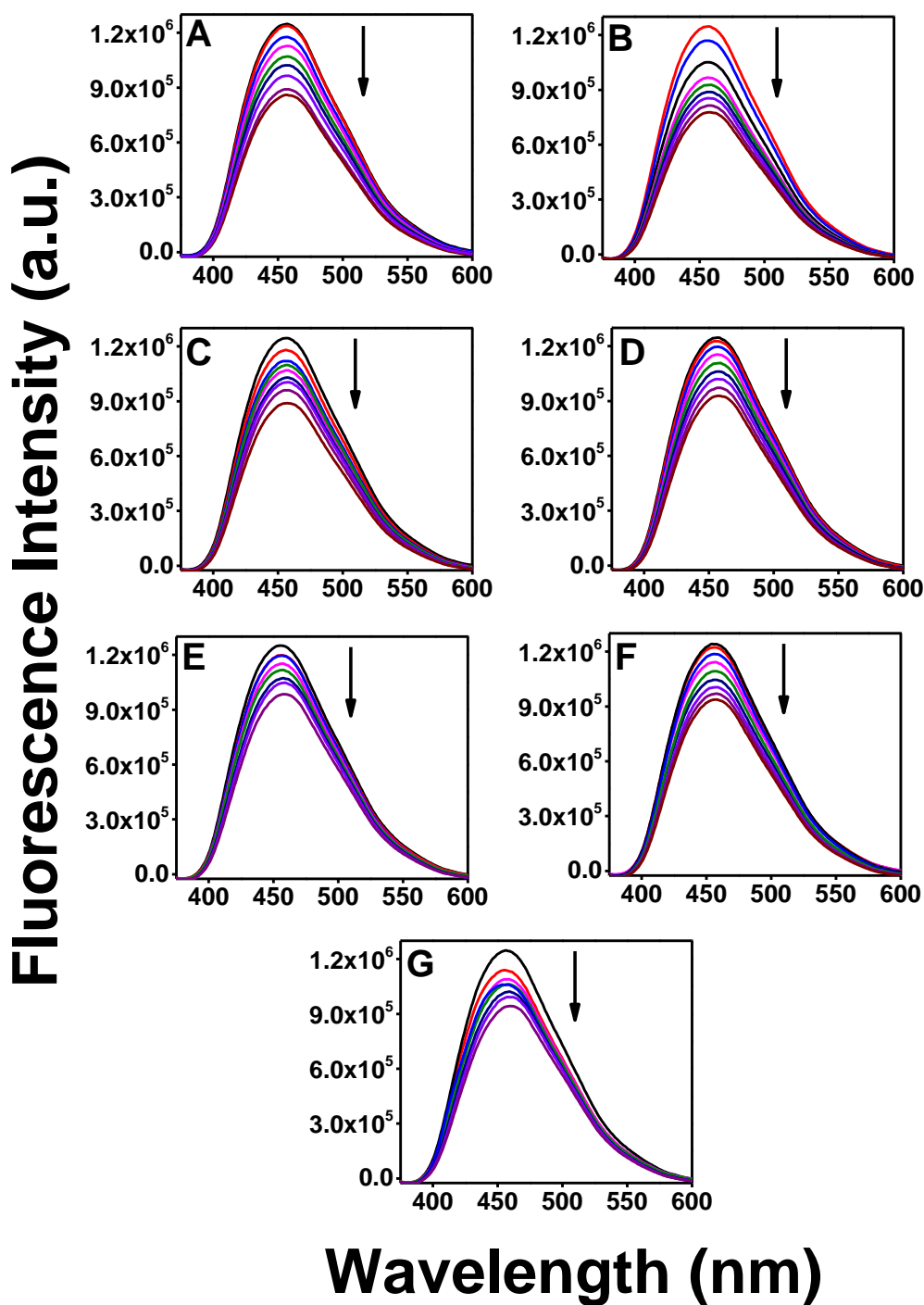


Figure 5.16. Fluorescence emission spectra of DAPI (2 μM) bound to CT-DNA (50 μM) in the presence of $[\text{MoO}_2\text{L}^1]$, **1** (A), $[\text{MoO}_2\text{L}^2]$, **2** (B), $[\text{MoO}_2\text{L}^3]$, **3** (C), $[\text{MoO}_2\text{L}^4]$, **4** (D), $[\text{MoO}_2\text{L}^5]$, **5** (E), $[\text{MoO}_2\text{L}^6]$, **6** (F) and $[\text{MoO}_2\text{L}^7]$, **7** (G) (0–90 μM) in 10 mM Tris–HCl buffer (pH 8.0) containing 1% DMF. The arrow indicates the effect of increasing the

concentration of the complex on the fluorescence emission of DAPI bound CT-DNA. The excitation and emission band width were 2.5 and 5.0 nm respectively.

In order to assess whether the complexes interacted with CT-DNA by major groove binding, MG bound CT-DNA was titrated with increasing concentration of the complexes. The decrease in the emission intensity of the MG bound CT-DNA at 672 nm upon the addition of the complexes indicated that the complexes also interacted with CT-DNA by major groove binding mode (Figure 5.17). Complex **2** showed the highest quenching of the emission intensity at 672 nm of ~21% followed by complex **3**, **5**, **6** and **7**, which exhibited quenching in the range of ~11-14 % (Figure 5.17). The least quenching of the emission intensity at 672 nm was showed by the complex **1** and **4** of ~5% each (Figure 5.17). Therefore our results revealed that the dioxidomolybdenum(VI) complexes (**1–7**) interacted with CT-DNA partially by major groove binding mode.

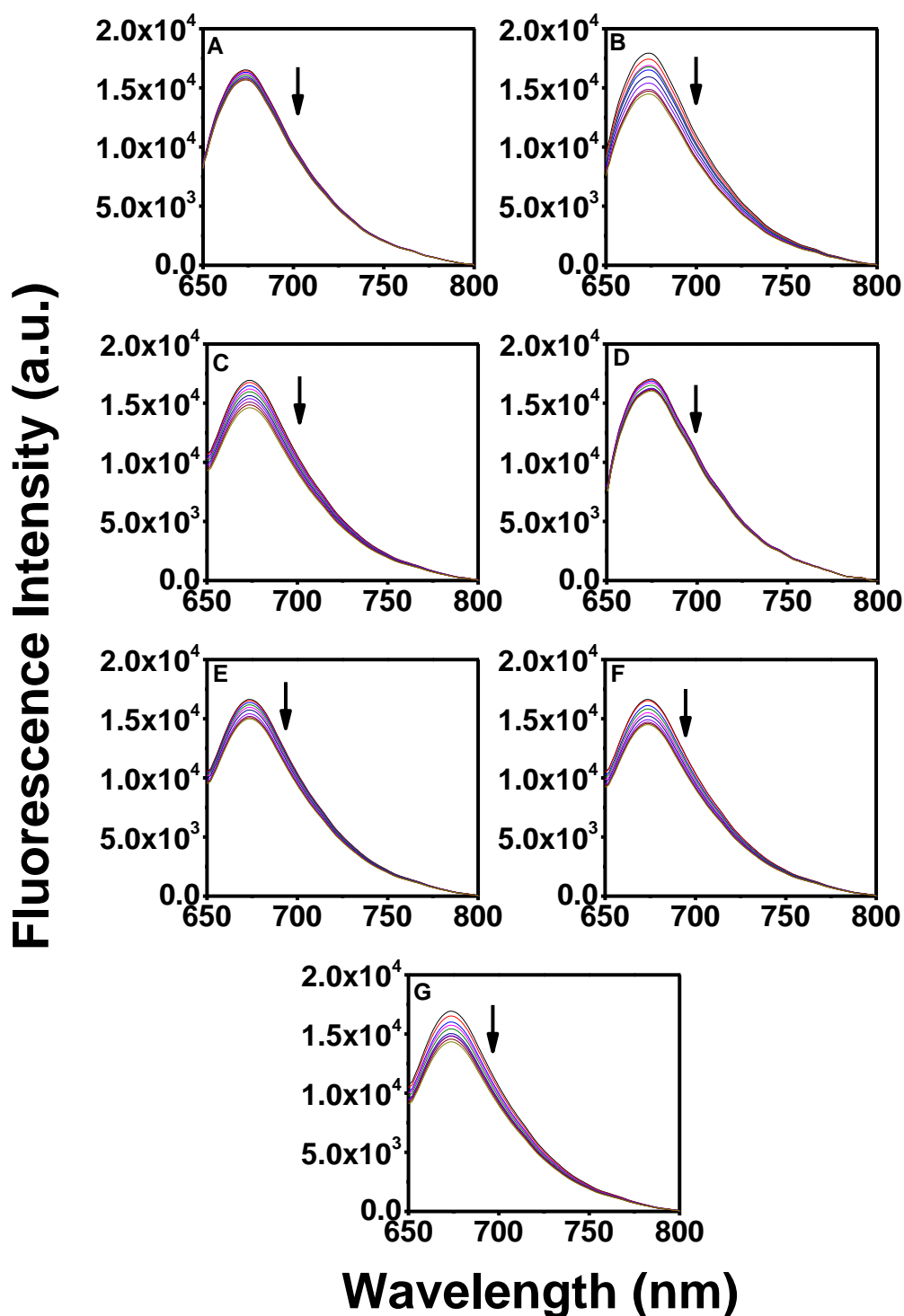


Figure 5.17. Fluorescence emission spectra of MG (2 μM) bound to CT-DNA (50 μM) in the presence of $[\text{MoO}_2\text{L}^1]$, **1** (A), $[\text{MoO}_2\text{L}^2]$, **2** (B), $[\text{MoO}_2\text{L}^3]$, **3** (C), $[\text{MoO}_2\text{L}^4]$, **4** (D), $[\text{MoO}_2\text{L}^5]$, **5** (E), $[\text{MoO}_2\text{L}^6]$, **6** (F) and $[\text{MoO}_2\text{L}^7]$, **7** (G) (0–90 μM) in 10 mM Tris–HCl buffer (pH 8.0) containing 1% DMF. The arrow indicates the effect of increasing the

concentration of the complex on the fluorescence emission of MG bound CT-DNA. The excitation and emission band width were 5 and 10.0 nm respectively.

Similar competitive experiments were also performed with EB bound CT-DNA. The addition of the dioxidomolybdenum (VI) complexes **1** and **3–7** to EB bound CT-DNA negligibly quenched (< 2%) the emission intensity of EB bound CT-DNA at 597 nm (Figure 5.18), while complex **2** exhibited a quenching of ~23% at the similar wavelength (Figure 5.18). This clearly revealed that among all the complexes only complex **2** interacted with the CT-DNA by partial intercalation which is in good agreement with our thermal denaturation and the circular dichroism studies.

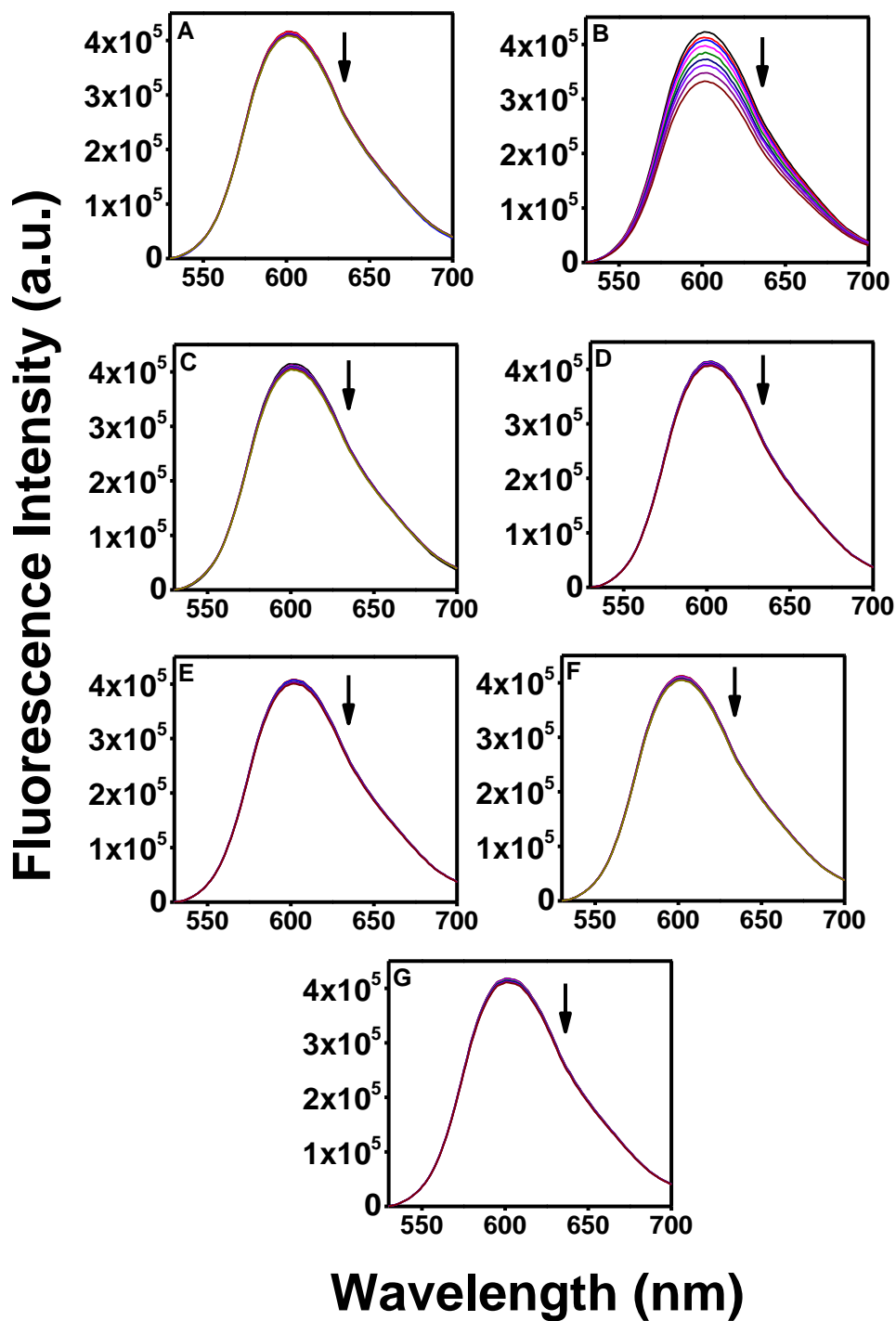


Figure 5.18. Fluorescence emission spectra of EB (2 μM) bound to CT-DNA (50 μM) in the presence of $[\text{MoO}_2\text{L}^1]$ (1) (A), $[\text{MoO}_2\text{L}^2]$, (2) (B), $[\text{MoO}_2\text{L}^3]$, (3) (C), $[\text{MoO}_2\text{L}^4]$, (4) (D), $[\text{MoO}_2\text{L}^5]$, (5) (E), $[\text{MoO}_2\text{L}^6]$, (6) (F) and $[\text{MoO}_2\text{L}^7]$, (7) (G) (0–90 μM) in 10 mM Tris-HCl buffer (pH 8.0) containing 1% DMF. The arrow indicates the effect of

increasing the concentration of the complex on the fluorescence emission of EB bound CT-DNA. The excitation and emission band width were 2.5 and 5.0 nm respectively.

5.3.7. DNA cleavage studies

Chemical-induced DNA cleavage. The chemical induced DNA cleavage capability of the dioxidomolybdenum (VI) complexes **1–7** (1–100 μM) was studied using 300 ng supercoiled pUC19 DNA in 50 mM Tris-HCl buffer (pH 8.0) containing 1% DMF in the dark in the presence of 0.5 mM hydrogen peroxide as the oxidising agent. The dioxidomolybdenum (VI) complexes do not exhibit any chemical-induced DNA cleavage activity (data not shown).

Photo-induced DNA cleavage. Photo-induced DNA cleavage experiments were performed to find out whether the dioxidomolybdenum (VI) complexes **1–7** possess any photo-nuclease activity. The photo-induced DNA nuclease activity of complexes **1–7** upon irradiation of UVA light of 350 nm for 3 h in the absence and presence of the dioxidomolybdenum (VI) complexes was studied using 300 ng supercoiled (SC) pUC19 DNA in 50 mM Tris-HCl buffer (pH 8.0) containing 1% DMF (Figure 5.19). The decrease in the supercoiled pUC19 DNA (Form I) and subsequent formation of nicked circular DNA (Form II) and linear DNA (Form III) indicated the extent of the DNA cleavage. The percentage of net DNA cleavage by the complexes was estimated using Eq. 5.3:

$$\text{Net DNA cleavage \%} = \frac{\text{Form IIs} + 2 \times \text{Form IIIs}}{\text{Form Is} + \text{Form IIs} + 2 \times \text{Form IIIs}} - \frac{\text{Form IIc} + 2 \times \text{Form IIc}}{\text{Form Ic} + \text{Form IIc} + 2 \times \text{Form IIc}} \quad \text{Eq. 5.3}$$

The subscripts “s” and “c” refers to the sample and control, respectively.⁵⁸

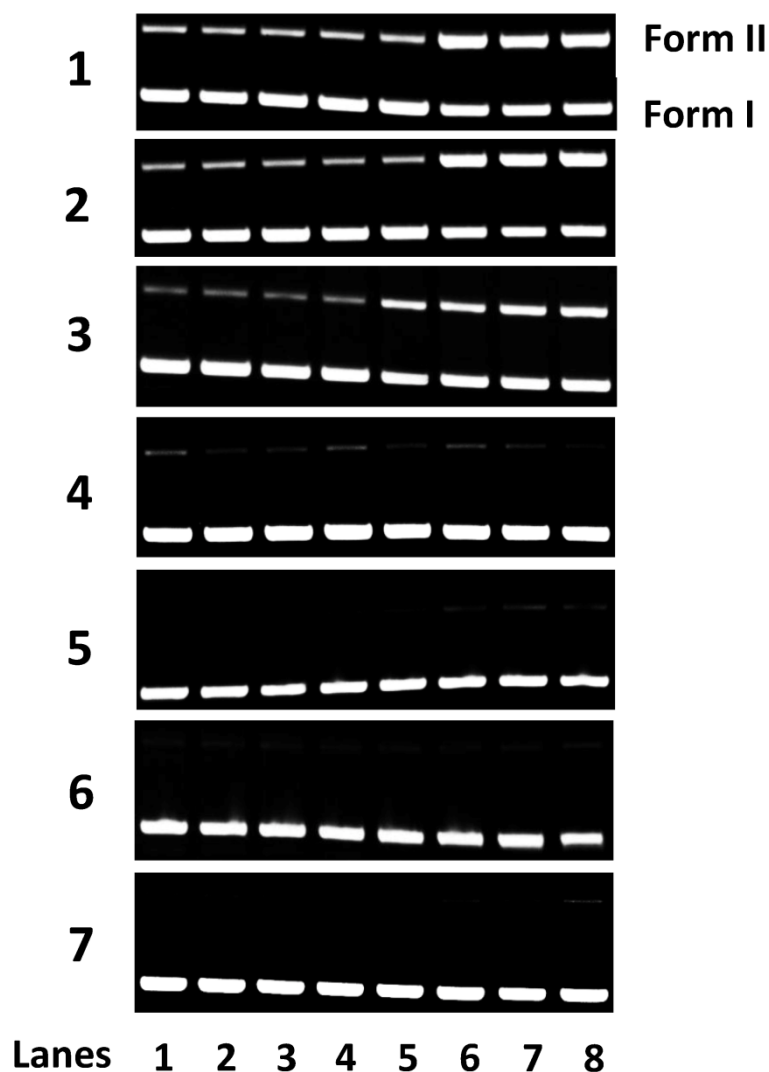


Figure 5.19. Gel diagram showing concentration dependent DNA cleavage by $[\text{MoO}_2\text{L}^{1-7}]$ (**1-7**); 300 ng of SC pUC19 DNA at different concentrations of the complexes [1–100 μM in 50 mM Tris-HCl buffer (pH 8.0) containing 1% DMF] was photo-irradiated with UVA at 350 nm for 3 h. Lanes 1–8: 1, 2.5, 5.0, 7.5, 10, 50, 75, and 100 μM of $[\text{MoO}_2\text{L}^{1-7}]$ (**1-7**).

The DNA cleavage activity of the dioxidomolybdenum (VI) complexes **1-7** were carried out in a concentration dependent manner from 1–100 μM . The net DNA cleavage percent by **1-7** was plotted with increasing concentration of the dioxidomolybdenum(VI) complexes (Figure 5.20). The photo-induced DNA cleavage activity of the complexes **4-7**

at a concentration of 100 μM complexes was between 6–8%. The complex **1**, **2** and **3** exhibited a DNA cleavage of ~21%, ~23% and ~20% at a concentration of 50 μM which saturated at a concentration of 100 μM (Figure 5.20). At this concentration the photo-nuclease activity of complex **1–3** was approximately ~24%, ~28% and ~23% respectively. This indicated that complex **2** has the highest photo-nuclease activity among the complex series. Cleavage activity of the dioxidomolybdenum(VI) complexes (**1–7**) varies because of the different functional group present in their ligand moieties.^{34b,d} Control experiments revealed that neither DMF (1%) nor the ligand molecules H_2L^{1-7} at a concentration of 100 μM showed any photo-induced DNA cleavage activity, implying that DMF and the ligands are cleavage inactive under similar experimental conditions (Figure 5.21).

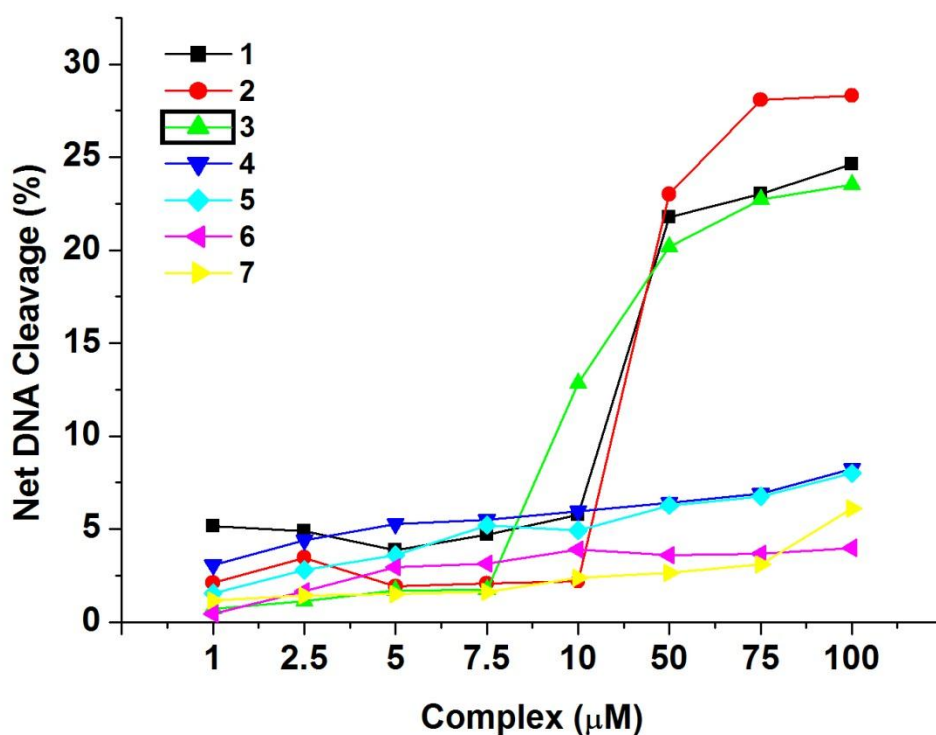


Figure 5.20. Concentration dependent DNA cleavage of $[\text{MoO}_2\text{L}^{1-7}]$ (**1–7**); 300 ng of SC pUC19 DNA at different concentration of the complexes [1–100 μM in 50 mM Tris-HCl buffer (pH 8.0) containing 1% DMF] was photo-irradiated with UVA at 350 nm for 3 h. The net DNA cleavage percent was calculated using Eq. 5.3.

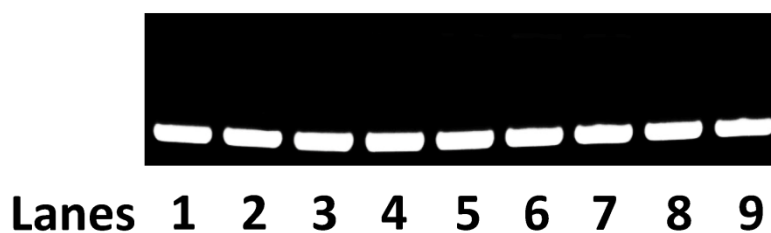


Figure 5.21. Gel diagram showing the effect of DMF (1%) and ligands on the photo-induced cleavage of SC pUC19 DNA. 300 ng SC pUC19 DNA was photo-irradiated in absence and presence of 1% DMF and various ligands (100 μ M) with UVA at 350 nm for 3 h. Lane 1, DNA only; Lane 2, DNA in presence of 1% DMF; Lane 3, DNA + $\mathbf{H}_2\mathbf{L}^1$; Lane 4, DNA + $\mathbf{H}_2\mathbf{L}^2$; Lane 5, DNA + $\mathbf{H}_2\mathbf{L}^3$; Lane 6, DNA + $\mathbf{H}_2\mathbf{L}^4$; Lane 7, DNA + $\mathbf{H}_2\mathbf{L}^5$; Lane 8, DNA + $\mathbf{H}_2\mathbf{L}^6$; Lane 9, DNA + $\mathbf{H}_2\mathbf{L}^7$.

Since the photo-induced DNA cleavage activity of the complexes **4–7** were less than $\sim 8\%$, the mechanistic aspect of the photo nuclease activity exhibited by these complexes was not explored. Only the photo-induced DNA cleavage activity of complexes **1–3** was investigated in the presence of various additives to understand the mechanistic pathways involved in the photo-cleavage reactions. The DNA cleavage reaction involving molecular oxygen can proceed in two mechanistic pathways: (a) a type-II process involving singlet oxygen species ($^1\text{O}_2$), or (b) by a photo-redox pathway involving reactive hydroxyl radicals (OH).⁵⁹ To find out the pathway taken by the complexes to exhibit photo-induced DNA cleavage activity, the amount of nicked circular DNA formed in the presence of complex and the additives was analysed. The net nicked circular DNA (Form II) percentage (% NC DNA) by **1–3** was plotted against the various additives (Figure 5.22). The addition of singlet oxygen quenchers like NaN_3 and L-histidine, inhibited the nicked circular DNA percentage of **2** substantially by ~ 11 and $\sim 10\%$, respectively (Figure 5.22 and 5.23). In presence of hydroxyl radical quenchers such as KI and D-mannitol, the % NC DNA of **2** was restrained by $\sim 6\%$ and $\sim 2\%$, respectively (Figure 5.22 and 5.23). For the dioxidomolybdenum (VI) complexes **1** and **3** the inhibition in the presence of the additives was negligible ranging between 1–3% (Figure 5.22 and 5.23). Therefore, from the above mechanistic studies it can be concluded that the photo-induced DNA cleavage activity of complex **2** probably proceeds *via* singlet oxygen

pathway. The mechanistic pathways involved for the photo induced DNA cleavage activity of dioxidomolybdenum(VI) complexes **1** and **3** cannot be stated with certainty.

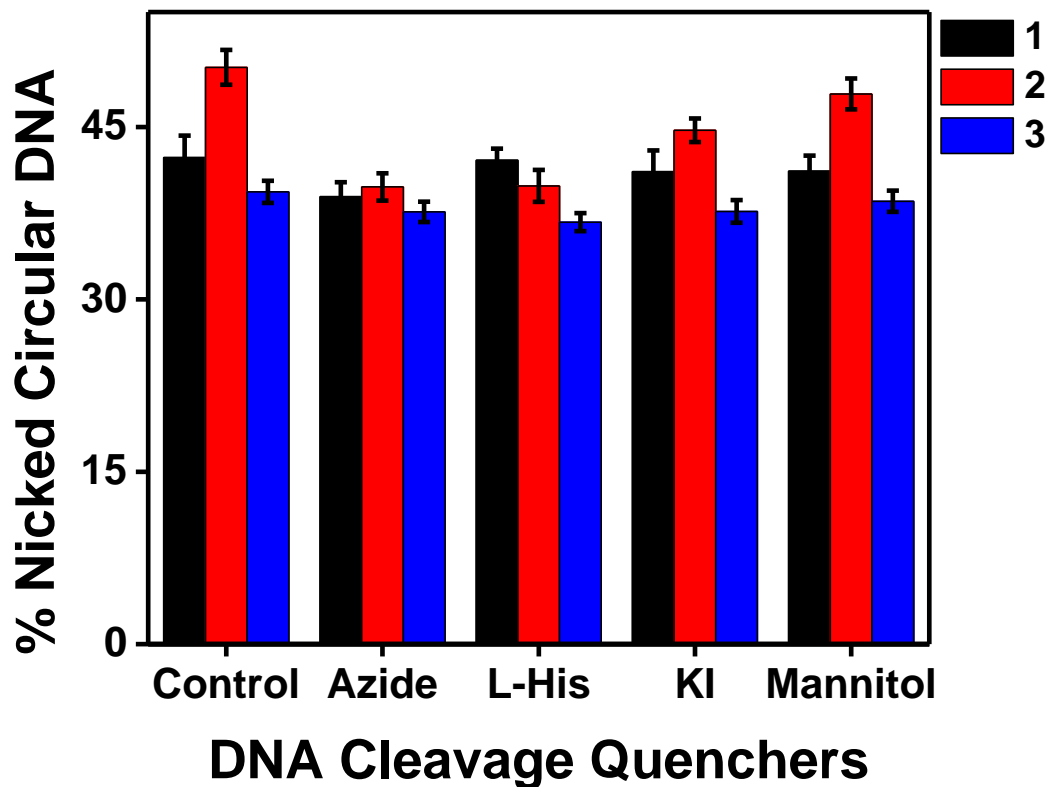


Figure 5.22. DNA cleavage of SC pUC19 DNA by $[\text{MoO}_2\text{L}^{1-3}]$ (**1–3**) in presence of various additives in 50 mM Tris-HCl buffer (pH 8.0) containing 1% DMF. SC pUC19 DNA (300 ng) in the presence of various additives was photo-irradiated with UVA at 350 nm for 3 h in presence of $[\text{MoO}_2\text{L}^{1-3}]$ (**1–3**) (100 μM). The additive concentrations were: sodium azide (0.5 mM), L-histidine (0.5 mM), KI (0.5 mM) and D-mannitol (0.5 mM).

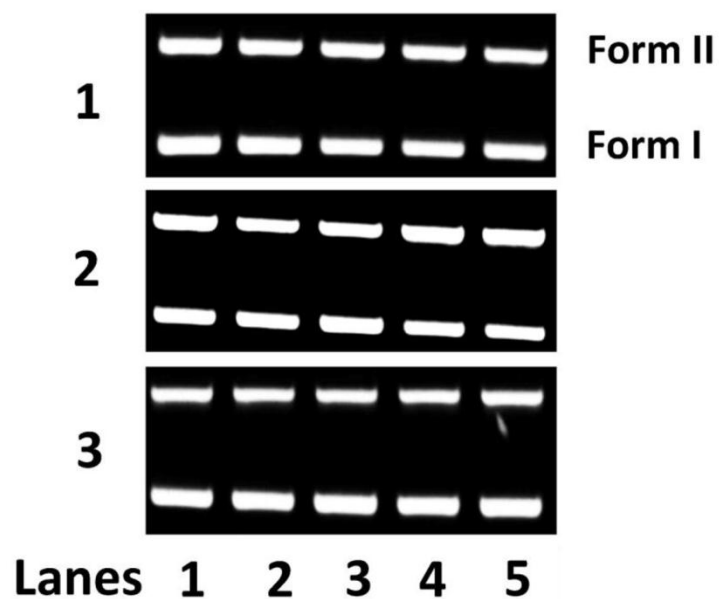


Figure 5.23. Gel diagram depicting cleavage of SC pUC19 DNA by **1–3** in presence of various additives in 50 mM Tris-HCl buffer (pH 8.0) containing 1% DMF. SC pUC19 DNA (300 ng) in the presence of various additives was photo-irradiated at 350 nm for 3 h with $[\text{MoO}_2\text{L}^{1-3}]$ (**1–3**) (100 μM). The additive concentrations were: sodium azide (0.5 mM), L-histidine (0.5 mM), KI (0.5 mM) and D-mannitol (0.5 mM). Lane 1, DNA + complex; Lane 2, DNA + complex + sodium azide; Lane 3, DNA + complex + L-histidine; Lane 4, DNA + complex + KI; Lane 5, DNA + complex + D -mannitol.

5.3.8. Cytotoxicity

The study clearly showed that the cytotoxicity of the reported complexes (**1–7**) depends on the nature of the compounds (the phenolato and diamine substituents present in the ligand backbone), its concentration and cell type (Figure 5.24). Among all the compounds, **6** is the most potent cytotoxic agent and capable of killing 50% of the cancer cell population at a concentration of 10 $\mu\text{g/ml}$. Complexes **5** and **7** were found effective at higher concentration (100 and 50 $\mu\text{g/ml}$) but their cytotoxicity decreases with a decrease in concentration. The toxicity of these two compounds was found indifferent to the cancer cell type. Complex **2** showed a very unique cytotoxic property. It showed almost five fold higher cytotoxicity against HT-29 with respect to HeLa at all concentration. A similar kind of response was also observed for MoO_2L^1 (**1**) but the magnitude of the variation was less in comparison to MoO_2L^2 (**2**). Among all the compounds, complexes **3** and **4** were found relatively less cytotoxic and capable of killing 30–40% of cancer cell population even at a concentration of 100 $\mu\text{g/ml}$. Complexes **1–4** showed a lower IC_{50} for HT-29 than the same for HeLa, **5** showed almost same IC_{50} for both the cell line whereas in case of complexes **6** and **7** a reverse trend was observed. Complex **6** has lowest IC_{50} among all the compounds for both type of cancer cell lines. The complexes also showed higher antiproliferative activity as compared to the ligands or metal precursor, $\text{MoO}_2(\text{acac})_2$ ($\text{IC}_{50} > 250 \mu\text{M}$). A plausible elucidation is that by coordination, the polarity of the ligand and the central metal ion are reduced through the charge equilibration, which favors permeation of the complexes through the lipid layer of the cell membrane.³⁴

Loss of nuclear integrity (fragmentation) is common for many metal complexes which actually exhibit their action by intercalating with nucleic acids and destabilizing the DNA.⁶⁰ Keeping this perspective in mind here we looked for the nuclear damage. For this purpose cells were stained with DAPI after 36 h of treatment. Surprisingly, here we did not notice any sign of nuclear damage (Figure 5.25). In all the samples, nucleus was found intact and of conventional shape and size. However, during this microscopy based investigation we noticed abrupt variation in cytoskeletal organization of the cells. Cytoskeleton of cell is majorly comprised of actino-myosin filamentous network. Among the components, F-actin plays a major role in determining the cell shape and adherence

which in turn govern the physiology of the cells.⁶¹ Now a days a number of cytotoxic drugs are available that actually works on cytoskeleton.^{51,62} Our investigation revealed that, the compounds which exhibited cytotoxicity in MTT assay actually disrupt the colony of both HeLa and HT-29. This was most evident in case of complexes **1** and **5–7**. Especially in case of complex **6**, both type of cancer cells started producing elongated actin stress fibre unlike their characteristic morphology. Our MTT data showed that at 100 µg/ml concentration **2** showed higher activity against HT-29 than HeLa. The microscopy study demonstrated that, under the exposure of complex **2**, both the cells started losing their individualistic appearance in the colony and seems as a fused system. The cells under the exposure of complexes **3** and **4** appeared less perturbed. The studies altogether suggest that these set of compounds exhibit cytotoxic effect by disrupting the cytoskeletal organization of the cells.

In the recent past, some oxidomolybdenum(VI) complexes have been reported to have significant cytotoxic activities against various human cancer cell lines including HL-60 and K562 (leukemia), A-549 (lung cancer), HeLa (cervical carcinoma) and MCF-7 (breast carcinoma).^{24a-1,25–27} Among our synthesized Mo(VI)-salan complexes, **5**, **6** and **7** have been found to exhibit comparable^{25c,27a} or higher^{26a,25c} cytotoxicity than some of the other reported Mo complexes against HeLa. A table containing the IC₅₀ values of the **1–7** and some of the known anticancer drug is provided in Table 5.7.^{30,63,64} The lower antiproliferative behavior of **3** and **4** in both cell lines could be attributed to their reduced solubility, and the steric bulk^{33a,e} of the ortho ^{iso}Pr and ^{tert}Bu group, respectively, inhibiting interaction with cellular target. However, no clear cytotoxicity order is observed based on electronic effects. The solubility factor plays a major role in the antiproliferative activity of the complexes as has previously been cited for other salan complexes of vanadium and titanium.^{30,33g,i} Though **6** also has an ortho ^{iso}Pr group but the asymmetry present in its ligand backbone could possibly result in making this complex substantially more active than its symmetrical analogue, **3**. The IC₅₀ values of **6** and **7** are comparable to salan complexes of Ti and V against HT-29 cancer cells.^{33a,e,j} These biological observations emphasize on the significance of fine tuning the ligand environment to execute higher cytotoxicity, and thus encourage further development and analysis of the mechanistic action of this family of complexes.

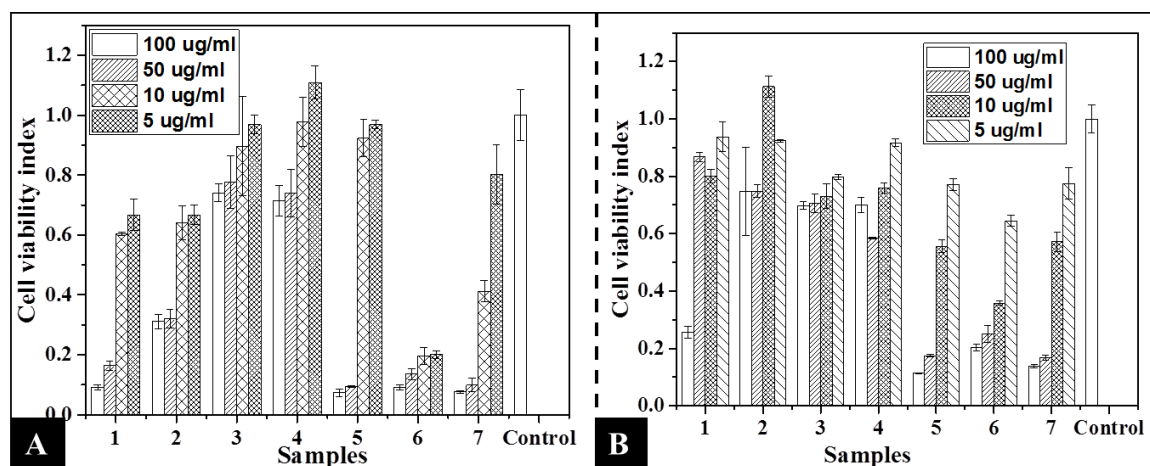


Figure 5.24. Cytotoxicity of $[\text{MoO}_2\text{L}^{1-7}]$ (1–7) against HT-29 (A) and HeLa cells (B) after 48 h exposure. The experiments were performed in quadruplets and the data were expressed as mean \pm S.D.

Table 5.7. Antiproliferative effect of complexes (1–7) against HT-29 and HeLa cell lines after 48 h exposure.

| Complexes | IC ₅₀ (in μM) | |
|---------------------------------------|--------------------------------------|--------|
| | HT-29 | HeLa |
| $[\text{MoO}_2\text{L}^1]$, 1 | 32.52 | 102.94 |
| $[\text{MoO}_2\text{L}^2]$, 2 | 51.94 | 275.20 |
| $[\text{MoO}_2\text{L}^3]$, 3 | 201.94 | 209.89 |
| $[\text{MoO}_2\text{L}^4]$, 4 | 221.81 | 217.16 |
| $[\text{MoO}_2\text{L}^5]$, 5 | 57.88 | 42.18 |
| $[\text{MoO}_2\text{L}^6]$, 6 | 2.62 | 10.74 |
| $[\text{MoO}_2\text{L}^7]$, 7 | 11.79 | 30.48 |
| Cisplatin | 70 | 12.2 |
| Cyclophosphamide | 21.5 | 1689 |
| Tamoxifen | 9.3 | 8.82 |
| 5-Fluorouridine | 0.3 | 2.85 |

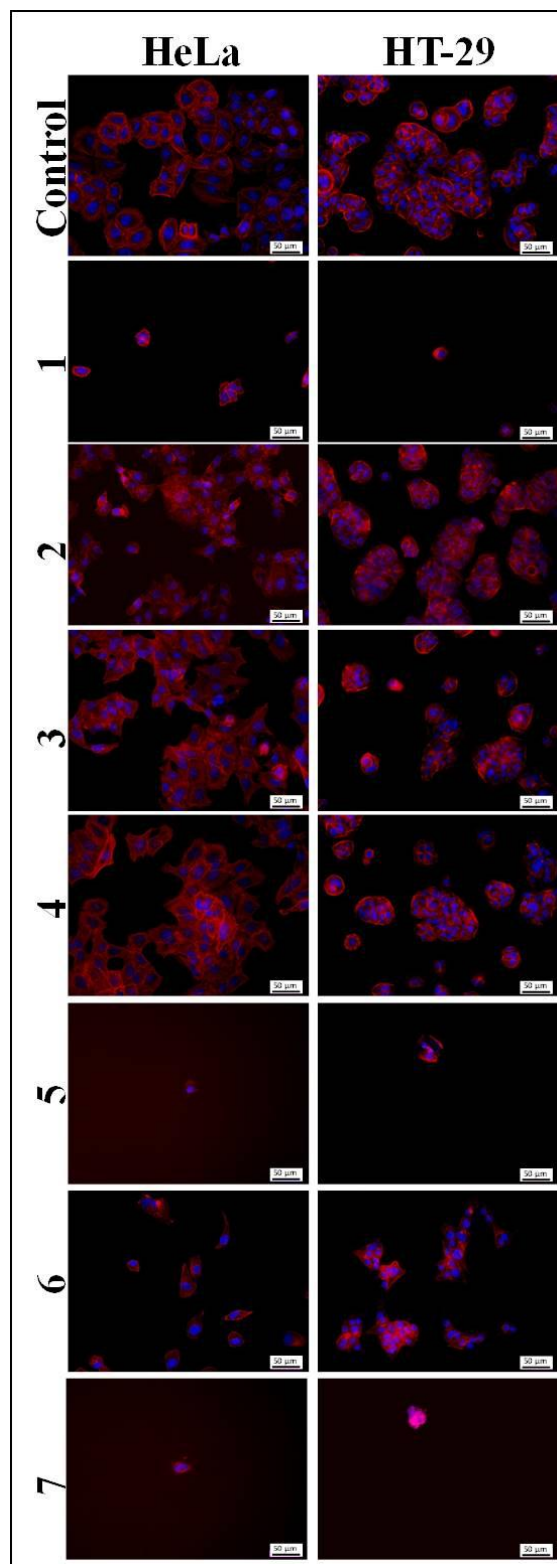


Figure 5.25. Morphology of HeLa and HT-29 cells treated with complexes (1–7) for 36 h. Cells were stained with DAPI (Blue color – nucleus) and TRITC Phalloidin (Red color- F-actin) and visualized under fluorescent microscope.

5.4. CONCLUSION

Seven tetradentate salen ligands (H_2L^{1-7}) and their corresponding *cis*-dioxidomolybdenum(VI) complexes, $[MoO_2L^{1-7}]$ (**1–7**), were synthesized and characterized by various analytical techniques (IR, UV-vis, 1H and ^{13}C NMR spectroscopy, ESI-MS and cyclic voltammetry). The molecular structures of $[MoO_2L^{1-6}]$ (**1–6**) were solved by single crystal X-ray diffraction analysis. The asymmetric unit of all these complexes consists of a complete formula unit with the exception of complex **2**, which belongs to point group C_2 . All complexes have a distorted octahedral geometry with the ONNO ligand coordinated in a folded fashion to the molybdenum centre. The conformational differences which arise are due to the steric and electronic requirements of the individual ligands and most of the differences are picked up from the neighboring atoms C7 and C14, as revealed from their torsion angles.

These complexes showed moderate DNA binding propensity with binding constants ranging from 10^4 – 10^5 M^{-1} . The experimental results showed that the complexes **1–7** effectively interact with CT-DNA by both minor and major groove binding mode, while complex **2** additionally interacts by partial intercalative mode of binding. The dioxidomolybdenum (VI) complexes (**1–3**) showed moderate photo-induced cleavage of pUC19 supercoiled plasmid DNA. The results from the mechanistic study suggest that the photolytic DNA cleavage of complex **2** proceeded *via* singlet oxygen pathway. The results obtained are significant in the context that dioxidomolybdenum (VI) complexes showing only DNA photo-cleavage activity but no chemical nuclease activity are sparse.

Among the series of complexes synthesized, remarkable cytotoxic results were obtained for complexes **6** and **7** against both HT-29 colon and HeLa cervical carcinoma cells. The higher cytotoxicity of these complexes can be correlated to their better solubility in DMSO, which is of particular interest to therapeutic applications^{33g} in addition to the effect of substituents in the ligand backbone, which might affect its interaction in the cell medium. The results encourage further insights into the mechanism of anticancer activity, and test on other cancer cell lines is the scope of future research.

5.5. REFERENCES

- (1) (a) Farrell, N. *Coord. Chem. Rev.* **2002**, *232*, 1–4. (b) Transition Metal Complexes as Drugs and Chemotherapeutic Agents, Farrell, N. in “Catalysis By Metal Complexes”, James, B. R. and Ugo, R., Eds., Kluwer Academic Press (**1989**). ISBN 9027728283. (c) Uses of Inorganic Chemistry in Medicine, Farrell, N., Ed., Royal Society of Chemistry (1999). ISBN 0854044442.
- (2) Platinum-Based Drugs in Cancer Therapy, Kelland, L.R. and Farrell, N. Eds., in “Cancer Drug Discovery and Development”, Teicher, B. A., Ed. Humana Press (2000). ISBN 0896035999.
- (3) Ott, I. *Coord. Chem. Rev.* **2009**, *253*, 1670–1681.
- (4) Quiroga, A. G.; Navarro Ranninger, C. *Coord. Chem. Rev.* **2004**, *248*, 119–133.
- (5) Metcalfe, C.; Thomas J. A. *Chem. Soc. Rev.* **2003**, *32*, 215–224.
- (6) Fanelli M.; Formica, M.; Fusi, V.; Giorgi, L.; Micheloni, M.; Paoli, P. *Coord. Chem. Rev.* **2016**, *310*, 41–79.
- (7) Bergamo, A.; Sava, G. *Chem. Soc. Rev.* **2015**, *44*, 8818–8835.
- (8) Singh, A. K.; Pandey, D. S.; Xu, Q.; Braunstein, P.; *Coord. Chem. Rev.* **2014**, *270–271*, 31–56.
- (9) Cutillas, N.; Yellol, G. S.; de Haro, C.; Vicente, C.; Rodriguez, V.; Ruiz, J. *Coord. Chem. Rev.* **2013**, *257*, 2784–2797.
- (10) de Almeida, A.; Oliveira, B. L.; Correia, J. D. G.; Soveral G.; Casini, A. *Coord. Chem. Rev.* **2013**, *257*, 2689–2704.
- (11) Graf, N.; Lippard, S. J. *Adv. Drug Deliv. Rev.* **2012**, *64*, 993–1004.
- (12) Metallotherapeutic Drugs and Metal-Based Diagnostic Agents: The use of metals in Medicine Gielen M. and Tiekink E. R. T., John Wiley & Sons, Hoboken, (**2005**) pp 584.
- (13) Bharti, N.; Maurya, M. R.; Naqvi, F.; Bhattacharya, A.; Bhattacharya, S.; Azam, A. *Eur. J. Med. Chem.* **2000**, *35*, 481–486.
- (14) Manegold, C.; Gatzemeier, U.; von Pawel, J.; Pirker, R.; Malayeri, R.; Blatter, J.; Krejcy, K. *Ann. Oncol.* **2000**, *11*, 435–440.
- (15) (a) Boulikas, T.; Vougiouka, M.; *Oncol. Rep.* **2003**, *10*, 1663–1682. (b) Wong, E.; Giandomenico, C. M. *Chem. Rev.* **1999**, *99*, 2451–2466. (c) Galanski, M.; Arion, V. B.; Jakupec, M. A.; Keppler, B. K. *Curr. Pharm. Des.* **2003**, *9*, 2078–2089. (d) Wang, D.;

- Lippard, S. J. *Nat. Rev. Drug Discovery* **2005**, *4*, 307–320. (e) Angeles-Boza, A. M.; Bradley P. M.; Fu, P. K. L.; Wicke, S. E.; Bacsa, J.; Dunbar, K. M.; Turro C., *Inorg. Chem.* **2004**, *43*, 8510–8519.
- (16) Zhang, C. X.; Lippard, S. J. *Curr. Opin. Chem. Biol.* **2003**, *7*, 481–489.
- (17) Ronconi, L.; Sadler, P. J. *Coord. Chem. Rev.* **2007**, *251*, 1633–1648.
- (18) (a) Sah, A. K.; Baig, N. *Catal. Lett.* **2015**, *145*, 905–909. (b) Fridgen, J.; Herrmann W. A.; Eickerling, G.; Santos, A. M.; Kühn, F. E. *J. Organomet. Chem.* **2004**, *689*, 2752–2761. (c) Fujihara, T.; Sasaki, Y.; Imamura, T. *Chem. Lett.* **1999**, *5*, 403–404. (d) Liu, W. S.; Zhang, R.; Huang, J. S.; Che, C. M.; Peng S. M., *J. Organomet. Chem.* **2001**, *634*, 34–38. (e) Spence, J. T.; Tocatlian, J. *J. Am. Chem. Soc.* **1961**, *83*, 816–819. (f) Cammack R.; Barber M. J.; Bray R. C. *Biochem. J.* **1976**, *157*, 469–478. (g) Vujevic, G.; Janiak, C.; *Z. Anorg. Allg. Chem.* **2003**, *629*, 2585–2590.
- (19) Qiao, Y. -L.; Dawsey, S. M.; Kamangar, F.; Fan, J. -H.; Abnet, C. C.; Sun, X. -D.; Johnson, L. L., Gail, M. H.; Dong, Z. -W.; Yu, B.; Mark, S. D.; Taylor, P. R. *J. Natl. Cancer Inst.* **2009**, *101*, 507–518.
- (20) Collison, D.; Garner, C. D.; Joule, J. A. *Chem. Soc. Rev.* **1996**, *25*, 25–32.
- (21) Nitrogen Fixation: The Chemical-Biochemical-Genetic Interface, Miller, A.; Newton W.E., (Eds), Plenum Press, NY, 1983, pp. 1–19. Advance in Nitrogen Fixation Research, C. Veeger, W.E. Newton, (Eds.), Nijhoff / Junk, Wageningen, 1984.
- (22) Hille, R. *Chem. Rev.* **1996**, *96*, 2757–2816.
- (23) Holm, R. H.; Kennepohl, P.; Solomon, E. I. *Chem. Rev.* **1996**, *96*, 2239–2314.
- (24) (a) Hussein, M. A.; Guan, T. S.; Haque, R. A.; Khadeer Ahamed, M. B.; Abdul Majid A. M. S. *Inorg. Chim. Acta* **2014**, *421*, 270–283. (b) Vrdoljak, V.; Đilović, I.; Rubčić, M.; Kraljević Pavelić, S.; Kralj, M.; Matković-Čalogović, D.; Piantanida, I.; Novak, P.; Rožman, A.; Cindrić, M. *Eur. J. Med. Chem.* **2010**, *45*, 38–48. (c) Saraiva, M. S.; Quintal, S.; Portugal, F. C. M.; Lopes, T. A.; Félix, V.; Nogueira, J. M. F.; Meireles, M.; Drew M. G. B.; Calhorda M. J. *J. Organomet. Chem.* **2008**, *693*, 3411–3418. (d) Hussein, M. A.; Guan, T. S.; Haque, R. A.; Ahamed, M. B. K.; Majid, A. M. S. A. *Polyhedron* **2015**, *85*, 93–103. (e) Thomadaki, H.; Karaliota, A.; Litos, C.; Scorilas, A. *J. Med. Chem.* **2007**, *50*, 1316–1321. (f) Feng, J.; Lu X. -M.; Wang, G.; Du, S. -Z.; Cheng, Y. -F. *Dalton Trans.* **2012**, *41*, 8697–8702. (g) Tzuberly, A.; Tshuva, E. Y. *Inorg. Chem.*

2012, *51*, 1796–1804. (h) Zhang, G.; Ta, C.; Cheng, S. -Y.; Golen, J. A.; Rheingold, A. L. *Inorg. Chem. Commun.* **2014**, *48*, 127–130. (i) Terenzi, A.; Lotsch, D.; van Schoonhoven, S.; Roller, A.; Kowol, C. R.; Berger, W.; Keppler, B. K.; Barone G., *Dalton Trans.* **2016**, *45*, 7758–7767. (j) Herchel, R.; Sindelar, Z.; Travnicek, Z.; Zboril, R.; Vanco, J. *Dalton Trans.* **2009**, 9870–9880. (k) Koepf-Maier, P.; Koepf, H. *Chem. Rev.* **1987**, *87*, 1137–1152. (l) Koepf-Maier, P. *Eur. J. Clin. Pharmacol.* **1994**, *47*, 1–16.

(25) (a) Pereira, C. C. L.; Diogo, C.V.; Burgeiro, A.; Oliveira, P. J.; Paula, M.; Marques, M.; Braga, S. S.; Paz, F. A. A.; Pillinger, M.; Goncalves, I. S. *Organometallics* **2008**, *27*, 4948–4956. (b) Marques, A. R.; Kromer, L.; Gallo, D. J.; Penacho, N.; Rodrigues, S. S.; Seixas, J. D.; Bernardes, G. J. L.; Reis, P. M.; Otterbein, S. L.; Ruggieri, R. A.; Goncalves, A. S. G.; Goncalves, A. M. L.; Matos, M. N. D.; Bento, I.; Otterbein, L. E.; Blättler, W. A.; Romão, C. C. *Organometallics* **2012**, *31*, 5810–5822. (c) Bandarra, D.; Lopes, M.; Lopes, T.; Almeida, J.; Saraiva, M. S.; Vasconcellos-Dias, M.; Nunes, C. D.; Félix, V.; Brandão, P.; Vaz, P. D.; Meireles, M.; Calhorda, M. J. *J. Inorg. Biochem.* **2010**, *104*, 1171–1177. (d) Šebestová, L.; Havelek, R.; Řezáčová, M.; Honzíček, J.; Kročová, Z.; Vinklárek, J. *Chem. Biol. Interact.* **2015**, *242*, 61–70.

(26) (a) Saraiva, M. S.; Quintal, S.; Portugal, F. C.M.; Lopes, T. A.; Félix, V.; Nogueira, J. M. F.; Meireles, M.; Drew, M. G. B.; Calhorda, M. J. *J. Organomet. Chem.* **2008**, *693*, 3411–3418. (b) Gleeson, B.; Claffey, J.; Deally, A.; Hogan, M.; Mendez, L. M. M.; Muller-Bunz, H.; Patil, S.; Tacke, M. *Inorg. Chim. Acta* **2010**, *363*, 1831–1836. (c) Honzicek, J.; Vinklarek, J.; Padelkova, Z.; Sebestova, L.; Foltanova, K.; Rezacova, M. *J. Organomet. Chem.* **2012**, *716*, 258–268. (d) Yamase, T. *Mol. Eng.* **1993**, *3*, 241–262. (e) Cindric, M.; Kajfež Novak, T.; Kraljevic, S.; Kralj, M.; Kamenar, B. *Inorg. Chim. Acta* **2006**, *359*, 1673–1680.

(27) (a) Vrdoljak, V.; Dilovic, I.; Rubc'ic, M.; Pavelic, S. K.; Kralj, M.; Matkovic'-Calogovic, D.; Piantanida, I.; Novak, P.; Rozman, A.; Cindric, M. *Eur. J. Med. Chem.* **2010**, *45*, 38–48. (b) Zhang, K.; Cui, S.; Wang, J.; Wang, X.; Li, R. *Med. Chem. Res.* **2012**, *21*, 1071–1076. (c) Feng, J.; Lu, X.; Wang, G.; Du, S.; Cheng, Y. *Dalton Trans.* **2012**, *41*, 8697–8702.

(28) (a) Katsuki, T. *Chem. Soc. Rev.* **2004**, *33*, 437–444. (b) Katsuki, T. *Coord. Chem. Rev.* **1995**, *140*, 189–214.

- (29) (a) Sergeeva, E.; Kopilov, J.; Goldberg, I.; Kol M. *Chem. Commun.* **2009**, 3053–3055. (b) Yeori, A.; Goldberg, I.; Shuster, M.; Kol, M. *J. Am. Chem. Soc.* **2006**, *128*, 13062–13063. (c) Mandal, D.; Ganguly, R.; Chatterjee, P. B.; Endo, A.; Weakley, T. J. R.; Chaudhury, M. *Struct. Chem.* **2007**, *18*, 187–193. (d) Yang, H.; Wang, H.; Zhu, C. *J. Org. Chem.* **2007**, *72*, 10029–10034. (e) Subramanian, P.; Spence, J. T.; Ortega, R.; Enemark, J. H. *Inorg. Chem.* **1984**, *23*, 2564–2572. (f) Hinshaw, C. J.; Peng, G.; Singh, R.; Spence, J. T.; Enemark, J. H.; Bruck, M.; Kristofzski, J.; Merbs, S. L.; Ortega, R. B.; Wexler, P. A. *Inorg. Chem.* **1989**, *28*, 4483–4491. (g) Whiteoak, C. J.; Britovsek, G. J. P.; Gibson, V. C.; White, A. J. P. *Dalton Trans.* **2009**, *13*, 2337–2344. (h) Lehtonen, A.; Sillanpää, R. *Polyhedron* **2005**, *24*, 257–265.
- (30) Reytman, L.; Braitbard, O.; Tshuva, E. Y. *Dalton Trans.* **2012**, *41*, 5241–5247 and references therein.
- (31) (a) Correia, I.; Pessoa, J. C.; Duarte, M. T.; Henriques, R. T.; Piedade, M. F. M.; Veiros, L. F.; Jakusch, T.; Kiss, T.; Dornyei, A.; Castro, M. M. C. A.; Geraldès, C. F. G. C.; Avecilla, F. *Chem. Eur. J.* **2004**, *10*, 2301–2317. (b) Correia, I.; Pessoa, J. C.; Duarte, M. T.; da Piedade, M. F. M.; Jackush, T.; Kiss, T.; Castro, M. M. C. A.; Geraldès, C. F. G. C.; Avecilla, F. *Eur. J. Inorg. Chem.* **2005**, 732–744.
- (32) (a) Hormnirun, P.; Marshall, E. L.; Gibson, V. C.; White, A. J. P.; Williams, D. J. *J. Am. Chem. Soc.* **2004**, *126*, 2688–2689. (b) Ogumaab, T.; Katsuki, T. *Chem. Commun.* **2014**, *50*, 5053–5056. (d) Liu, J.; Bao, Y.; Liu, Y.; Ren, W.; Lu, X. *Polym. Chem.* **2013**, *4*, 1439–1444. (e) Dean, R. K.; Dawe, L. N.; Kozak, C. M. *Inorg. Chem.* **2012**, *51*, 9095–9103. (f) Rao D. -Y., Li, B.; Zhang, R.; Wang, H.; Lu, X. -B. *Inorg. Chem.* **2009**, *48*, 2830–2836. (g) Yang, H.; Wang, H.; Zhu, C. *J. Org. Chem.* **2007**, *72*, 10029–10034. (h) Adão, P.; Avecilla, F.; Bonchio, M.; Carraro, M.; Pessoa, J. C.; Correia, I. *Eur. J. Inorg. Chem.* **2010**, 5568–5578. (h) Sun, J.; Zhu, C.; Dai, Z.; Yang, M.; Pan, Y.; Hu, H. *J. Org. Chem.* **2004**, *69*, 8500–8503. (i) Huang, Y.; Yang, F.; Zhu, C. *J. Am. Chem. Soc.* **2005**, *127*, 16386–16387.
- (33) (a) Peri, D.; Meker, S.; Manna, C. M.; Tshuva, E. Y. *Inorg. Chem.* **2011**, *50*, 1030–1038. (b) Immel, T. A.; Grütze, M.; Spate, A.; Groth, U.; Ohlschlager, P.; Huhn, T. *Chem. Commun.* **2012**, *48*, 5790–5792. (c) Grütze, M.; Zhao, T.; Immel, T. A.; Huhn, T. *Inorg. Chem.* **2015**, *54*, 6697–6706. (d) Meker S., Margulis-Goshen K., Weiss E., Magdassi S., Tshuva E. Y., *Angew. Chem. Int. Ed.* **2012**, *51*, 10515–10517. (e) Peri, D.;

- Manna, C. M.; Shavit, M.; Tshuva, E. Y. *Eur. J. Inorg. Chem.* **2011**, 4896–4900. (f) Immel, T. A.; Grützke, M.; Batroff, E.; Groth, U.; Huhn, T. *J. Inorg. Biochem.* **2012**, *106*, 68–75. (g) Glasner, H.; Tshuva, E. Y. *J. Am. Chem. Soc.* **2011**, *133*, 16812–16814. (i) Glasner, H.; Tshuva, E. Y. *Inorg. Chem.* **2014**, *53*, 3170–3176. (j) Reytman, L.; Braitbard, O.; Hochman, J.; Tshuva, E. Y. *Inorg. Chem.* **2016**, *55*, 610–618.
- (34) (a) Dash, S. P.; Panda, A. K.; Pasayat, S.; Majumder, S.; Biswas, A.; Kaminsky, W.; Mukhopadhyay, S.; Bhutia, S. K.; Dinda, R. *J. Inorg. Biochem.* **2015**, *144*, 1–12. (b) Dash, S. P.; Panda, A. K.; Pasayat, S.; Dinda, R.; Biswas, A.; Tiekink, E. R. T.; Patil, Y. P.; Nethaji, M.; Kaminsky, W.; Mukhopadhyay, S.; Bhutia, S. K. *Dalton Trans.* **2014**, *43*, 10139–10156. (c) Dash, S. P.; Pasayat, S.; Bhakat, S.; Roy, S.; Dinda, R.; Tiekink, E. R. T.; Mukhopadhyay, S.; Bhutia, S. K.; Hardikar, M. R.; Joshi, B. N.; Patil, Y. P.; Nethaji, M. *Inorg. Chem.* **2013**, *52*, 14096–14107. (d) Dash, S. P.; Panda, A. K.; Pasayat, S.; Dinda, R.; Biswas, A.; Tiekink, E. R. T.; Mukhopadhyay, S.; Bhutia, S. K.; Kaminsky, W.; Sinn, E. *RSC Adv.* **2015**, *5*, 51852–51867.
- (35) Saswati; Chakraborty, A.; Dash, S. P.; Panda, A. K.; Acharyya, R.; Biswas, A.; Mukhopadhyay, S.; Bhutia, S. K.; Crochet, A.; Patil, Y. P.; Nethaji, M.; Dinda, R. *Dalton Trans.* **2015**, *44*, 6140–6157.
- (36) (a) Banerjee, S.; Dixit, A.; Karande, A. A.; Chakravarty, A. R. *Dalton Trans.* **2016**, *45*, 783–796. (b) Banerjee, S.; Dixit, A.; Kumar, A.; Mukherjee, S.; Karande, A. A.; Chakravarty, A. R. *Eur. J. Inorg. Chem.* **2015**, 3986–3990. (c) Bhattacharyya, A.; Dixit, A.; Mitra, K.; Banerjee, S.; Karande, A. A.; Chakravarty, A. R. *MedChemComm.* **2015**, *6*, 846–851. (d) Banerjee, S.; Pant, I.; Khan, I.; Prasad, P.; Hussain, A.; Kondaiah, P.; Chakravarty, A. R. *Dalton Trans.* **2015**, *44*, 4108–4122. (e) Banerjee, S.; Dixit, A.; Karande, A. A.; Chakravarty, A. R. *Eur. J. Inorg. Chem.* **2015**, 447–457. (f) Balaji, B.; Banik, B.; Sasmal, P. K.; Maity, B.; Majumdar, R.; Chakravarty, A. R. *Eur. J. Inorg. Chem.* **2012**, 126–135. (g) Banerjee, S.; Prasad, P.; Hussain, A.; Khan, I.; Kondaiah, P.; Chakravarty, A. R. *Chem. Comm.* **2012**, *48*, 7702–7704. (h) Banik, B.; Somyajit, K.; Nagaraju, G.; Chakravarty, A. R. *Dalton Trans.* **2014**, *43*, 13358–13369. (i) Goswami, T. K.; Gadadhar, S.; Balaji, B.; Gole, B.; Karande, A. A.; Chakravarty, A. R. *Dalton Trans.* **2014**, *43*, 11988–11999.
- (37) (a) Banerjee, S.; Dixit, A.; Maheswaramma, K. S.; Maity, B.; Mukherjee, S.; Kumar, A.; Karande, A. A.; Chakravarty, A. R. *J. Chem. Sci. (Berlin, Germany)*

- 2016**, 128, 165–175. (b) Goswami, T. K.; Chakravarthi, B. V. S. K.; Roy, M.; Karande, A. A.; Chakravarty, A. R. *Inorg. Chem.* **2011**, 50, 8452–8464. (c) Fei, B.; Xu, W.; Tao, H.; Li, W.; Zhang, Y.; Long, J.; Liu, Q.; Xia, B.; Sun, W. *J. Photochem. Photobiol. B*, **2014**, 132, 36–44. (d) Zhou, X.; Sun, Q.; Jiang, L.; Li, S.; Gu, W.; Tian, J.; Liua, X.; Yan, S. *Dalton Trans.* **2015**, 44, 9516–9527.
- (38) Feng, J.; Lu, X.; Wang, G.; Du, S.; Cheng, Y. *Dalton Trans.* **2012**, 41, 8697–8702.
- (39) (a) Pasayat, S.; Dash, S. P.; Majumder, S.; Dinda, R.; Sinn, E.; Stoeckli-Evans, H.; Mukhopadhyay, S.; Bhutia, S. K.; Mitra, P. *Polyhedron* **2014**, 80, 198–205. (b) Pasayat, S.; Dash, S. P.; Saswati; Majhi, P. K.; Patil, Y. P.; Nethaji, M.; Dash, H. R.; Das, S.; Dinda, R. *Polyhedron* **2012**, 38, 198–204. (c) Pasayat, S.; Dash, S. P.; Roy, S.; Dinda, R.; Dhaka, S.; Maurya, M. R.; Kaminsky, W.; Patil, Y. P.; Nethaji, M. *Polyhedron* **2014**, 67, 1–10. (d) Dinda, R.; Ghosh, S.; Falvello, L. R.; Tomas, M.; Mak, T. C. W. *Polyhedron* **2006**, 25, 2375–2382. (e) Dinda, R.; Sengupta, P.; Ghosh, S.; Sheldrick, W. S. *Eur J. Inorg. Chem.* **2003**, 2, 363–369. (f) Dinda, R.; Sengupta, P.; Ghosh, S.; Mayer-Figge, H.; Sheldrick, W. S. *J. Chem. Soc., Dalton Trans.* **2002**, 23, 4434–4439.
- (40) Chen, G. J. -J.; McDonald, J. W.; Newton, W. E. *Inorg. Chem.* **1976**, 15, 2612–2615.
- (41) Mukhopadhyay, S.; Mandal, D.; Chatterjee, P. B.; Desplanches, C.; Sutter, J.; Butcher, R. J.; Chaudhury, M. *Inorg. Chem.* **2004**, 43, 8501–8509.
- (42) SAINT. 2008, Bruker AXS Inc.: Madison, Wisconsin, USA.
- (43) SADABS. 2008, Bruker AXS Inc.: Madison, Wisconsin, USA.
- (44) Hahn, T., ed. International Tables for Crystallography 4th ed. Vol. A Space-Group Symmetry. 1996, Kluwer Academic Publishers: Dordrecht.
- (45) Sheldrick, G. M. *Acta Cryst. A* **2008**, 64, 112–122.
- (46) Wilson A. J. C. Ed. International Tables for Crystallography. Vol. C. 1992, Kluwer Academic Publishers: Dordrecht.
- (47) Brandenburg, K. Diamond - Crystal and Molecular Visualization. 2006, Crystal Impact: Bonn, Germany.
- (48) Macrae, C. F.; Bruno, I. J.; Chisholm, J. A.; Edgington, P. R.; McCabe, P.; Pidcock, E.; Rodriguez-Monge, L.; Taylor, R.; van de Streek, J.; Wood, P. A. *Appl. Crystallogr.* **2008**, 41, 466–470.

- (49) Kumar, P.; Gorai, S.; Santra, M. K.; Mondal, B.; Manna, D. *Dalton Trans.* **2012**, *41*, 7573–7581.
- (50) Serpe, L.; Catalano, M.; Cavalli, R.; Ugazio, E.; Bosco, O.; Canaparo, R.; Muntoni, E.; Frairia, R.; Gasco, M.; Eandi, M. *Eur. J. Pharm. Biopharm.* **2004**, *58*, 673–680.
- (51) Wang, X.; Tanaka, M.; Krstin, S.; Peixoto, H. S.; de Melo Moura, C. C.; Wink, M. *Eur. J. Pharmacol.* **2016**, *789*, 265–274.
- (52) Arjmand, F.; Mohani, B.; Ahmad, S. *Eur. J. Med. Chem.* **2005**, *40*, 1103–1110.
- (53) Rajendiran, V.; Murali, M.; Suresh, E.; Sinha, S.; Somasundaram, K.; M. Palaniandavar, M. *Dalton Trans.* **2008**, 148–163.
- (54) Arjmand, F.; Aziz, M. *Eur. J. Med. Chem.* **2009**, *44*, 834–844.
- (55) An, Y.; Liu, S. D.; Deng, S. Y.; Ji, L. N.; Mao, Z. W. *J. Inorg. Biochem.* **2006**, *100*, 1586–1593.
- (56) Banerjee, S.; Hussain, A.; Prasad, P.; Khan, I.; Banik, B.; Kondaiah, P.; Chakravarty, A. R. *Eur. J. Inorg. Chem.* **2012**, 3899–3908.
- (57) Li, L.; Guo, Q.; Dong, J.; Xu, T.; Li, J. *Photochem. Photobiol. B* **2013**, *125*, 56–62.
- (58) Dai, W. M.; Lai, K. W.; Wu, A.; Hamaguchi, W.; Lee, M. Y.; Zhou, L.; Ishii, A.; Nishimoto, S. *J. Med. Chem.* **2002**, *45*, 758–761.
- (59) Sasmal, P. K.; Saha, S.; Majumdar, R.; De, S.; Dighe, R. R.; Chakravarty, A. R. *Dalton Trans.* **2010**, *39*, 2147–2158.
- (60) El-Awady, R. A.; Semreen, M. H.; Saber, M. M.; Cyprian, F.; Menon, V.; Al-Tel, T. H. *DNA repair.* **2016**, *37*, 1–11.
- (61) Jordan, M. A.; Wilson, L. *Curr. Opin. Cell Biol.* **1998**, *10*, 123–130.
- (62) Zheng, Y. -B.; Gong, J. -H.; Liu, X. -J., Wu, S. -Y., Li, Y., Xu, X. -D., Shang, B. -Y, Zhou, J.-M.; Zhu, Z. -L.; Si, S. -Y. *Sci. Rep.* **2016**, *6*, 31472.
- (63) (a) Stockert, A.; Kinder, D.; Christ, M.; Amend, K.; Aulthouse, A. *Austin J. Pharmacol. Ther.* **2014**, *2*, 6. (b) Lewis, A.; Forrester, L.; Hayes, J.; Wareing, C.; Carmichael, J.; Harris, A.; Mooghen, M.; Wolf, C. R. *Brit. J. Cancer.* **1989**, *60*, 327–331.
- (64) (a) Takara, K.; Sakaeda, T.; Yagami, T.; Kobayashi, H.; Ohmoto, N.; Horinouchi, M.; Nishiguchi, K.; Okumura, K. *Biol. Pharm. Bull.* **2002**, *25*, 771–778. (b) Petinari, L.; Kohn, L. K.; de Carvalho, J. E.; Genari, S. C. *Cell Biol. Int.* **2004**, *28*, 531–539.

Chapter 6

Synthesis, characterization and superoxide dismutase activity of Cu(II) salan complexes: Unprecedented Cu(II) catalyzed acetal formation

Chapter 6

Synthesis, characterization and superoxide dismutase activity of Cu(II) salan complexes: Unprecedented Cu(II) catalyzed acetal formation

ABSTRACT

The synthesis and characterization (elemental analysis, UV–vis spectroscopy and ESI-MS) of Cu(II) complexes ($[\text{CuL}^{1,2}]$ (**1** and **2**) and $[\text{CuL}^{3,4'}]_2$ (**3** and **4**)) using tetradentate diamino bis(phenolato) “salan” ligands, *N,N'*-dimethyl-*N,N'*-bis-(2-hydroxy-3-X-5-Y-6-Z-benzyl)-1,2-diaminoethane ($X = \text{}^i\text{Pr}$, $Y = \text{Cl}$, $Z = \text{Me}$ (H_2L^1); $X = \text{OCH}_3$, $Y = \text{allyl}$, $Z = \text{H}$ (H_2L^2)) and *N,N'*-bis-(2-hydroxy-3-X-5-Y-6-Z-benzyl)-1,2-diaminopropane ($X = \text{}^i\text{Pr}$, $Y = \text{Cl}$, $Z = \text{Me}$ (H_2L^3); $X = Y = \text{CH}_3$, $Z = \text{H}$ (H_2L^4)) have been discussed. The redox property of the complexes has been ascertained by cyclic voltammetry. The molecular structures of the complexes (**1** and **3**) have been determined by X-ray crystallography. While **1** and **2** have the expected square planar geometry, with the ligand coordinating to the metal center in the usual tetradentate fashion, an unprecedented ligand transformation occurs in the case of **3** and **4**, leading to the formation of phenolato bridged Cu(II) dimeric complexes, $[\text{CuL}^{3,4'}]_2$, having an elongated octahedron structure. The organic transformation in the ligands (H_2L^3 and H_2L^4) has been mechanistically elucidated to be Cu(II) catalysed. In order to fortify the ligand modification to be Cu(II) assisted, the corresponding Ni^{II} , Fe^{III} and Mo^{VI} complexes (**5–7**) with the same ligand environment, were synthesized and characterized. The anomaly in the ligand backbone was however not observed in the case of other transition metal complexes (**5–7**). In addition, the superoxide dismutase (SOD) activity of the Cu(II) complexes (**1–3**) has also been investigated; the activity follows the order **3** > **1** > **2**. Due to the deliquescent nature of $[\text{CuL}^{4'}]_2$ (**4**), its SOD activity could not be evaluated.

6.1. INTRODUCTION

Copper plays diverse roles in nature which involve electron transfer, O₂ binding, activation and reduction, NO²⁻ and N₂O reduction, and substrate activation.¹ These properties are largely attributed to its accessible redox states (I/II) and bioavailability.¹ Relatively high redox potential working between +0.25 and +0.75 V for the Cu(II)–Cu(I) system in copper enzymes² is utilized for direct oxidation of substrates, such as superoxide (in superoxide dismutase),³ ascorbate (in ascorbate oxidase)⁴ or catechols (in catecholase, tyrosinase or in laccases).^{5,6}

The Cu/Zn- SOD that predominates in the extracellular spaces provides a natural defense mechanism in living systems against superoxide-mediated oxidative damages such as those associated with inflammatory diseases and reperfusion as well as neurological disorders like, Parkinson's and Alzheimer's disease.⁷ However, short plasma half-life, inability to cross cell membranes, and immunogenic responses of application of natural SODs have limited their therapeutic applications.⁸ Therefore, low-molecular-weight SOD mimics are being extensively investigated as potential pharmaceutical agents for treating such diseases.⁹ In the last few years, research on biocompatible Cu(I,II) coordination compounds for their anticancer properties has boosted dramatically.¹⁰ Due to an increase in uptake of copper by malignant cells and its contribution to cancer progression, angiogenesis and metastasis, cellular copper is evolving as a promising target for developing new anti-cancer therapeutics.^{11–14}

Again, the Cu(II) salan complexes have been extensively utilised in the asymmetric Henry reaction, wherein the variation of electron properties and location of the substituents on aromatic rings have had an influence on the enantioselectivity in the reactions.¹⁵ Though copper compounds derived from dianionic salan ligand precursors have been investigated,^{15–21} yet it has not been fully explored, in context of their biological applicability. The environment around the Cu center and its conformational flexibility plays a significant role in order to mimic closely a metalloprotein in properties, for carrying out specific physiological function, such as dioxygen binding and oxygen utilization. In this respect, the tetrahydro derivative of salen ligand holds an advantage due to its greater flexibility and higher resistance to hydrolytic decomposition.²² As compared to salen, its reduced analogue coordinates more easily in a folded fashion as a

consequence of C=N bond hydrogenation.²³ The Cu-salan complexes scrutinized so far either contain tertiary amine or sterically hindered secondary amine in their ligand backbone,¹⁵⁻²¹ but no attempts to synthesize complexes with salan ligands containing unhindered secondary amines have been made.

Over the past few years, we have been studying the chemistry and biological applicability of transition metal complexes with O and N donating ligands.²⁴ As an extension of our work on the coordination and biochemistry of copper(I/II) complexes,²⁵ we have herein synthesized four novel mono- and dinuclear bis(phenoxido)-bridged Cu(II) complexes with tetrapodal salan ligands (H_2L^{1-4}). These ligands have been designed using either N, N'-ethylenediamine ($H_2L^{1,2}$) or 1,2-diaminopropane ($H_2L^{3,4}$) by one step Mannich condensation with aqueous HCHO and *o*, *p*-disubstituted phenols. The presence of tertiary amine group in the ligand ($H_2L^{1,2}$) leads to normal square planar coordination of the Cu atom to the metal center, $[CuL^{1,2}]$ (**1**, **2**), however, metallation of salan ligand containing secondary amine ($H_2L^{3,4}$) leads to an intriguing chemical transformation in the ligands by an *in situ* bonding of a pendent $-CH_2OCH_3$ group to one of the N atoms and formation of an elongated octahedron $[CuL^{3,4}]$ (**3**, **4**). The anomalous chemistry of **3** and **4** was compared with the corresponding Ni(II), Fe(III) and Mo(VI) complexes. It is noteworthy that no such chemical transformation is perceived in the corresponding molybdenum $[MoO_2L^3]$ (**5**), nickel $[NiL^3]$ (**6**) or iron $[FeL^3(Cl)]$ (**7**) complexes with H_2L^3 . Mechanistic insights into the unprecedented Cu-assisted acetal formation, with the subsequent coordination of the latter to the metal ion have been discussed. All the ligands and complexes have been characterized by various physicochemical techniques, viz., elemental analyses, IR, UV-vis and NMR spectroscopy, ESI-MS, and cyclic voltammetry. The molecular structures of the **1** and **3** have been further confirmed by single-crystal X-ray diffraction study. The Cu(II)-salan complexes have also been studied for the dismutation of superoxide anion radicals (O_2^-).

6.2. EXPERIMENTAL SECTION

6.2.1. General Methods and Materials. Chemicals were purchased from commercial sources and used without further purification. $\text{CuClO}_4 \cdot 6\text{H}_2\text{O}$, N, N'-dimethylethylenediamine and 1, 2-diaminopropane were purchased from Loba Chemie. The substituted phenols were purchased from Sigma Aldrich. Reagent grade solvents were dried and distilled prior to use. Elemental analyses were performed on a Vario ELcube CHNS Elemental analyzer. ^1H and ^{13}C NMR spectra were recorded on a Bruker Ultrashield 400 MHz spectrometer using SiMe_4 as an internal standard. Electronic spectra were recorded on a Lambda25, PerkinElmer spectrophotometer. ESI-MS were obtained on a SQ-300 MS instrument. A CH-Instruments (Model No. CHI6003E) electrochemical analyzer was used for cyclic voltammetric experiments with CH_3CN solutions of the complexes containing TBAP (tetra butyl ammonium perchlorate) as the supporting electrolyte. The three electrode measurements were carried out at 298 K with a platinum working electrode, platinum auxiliary electrode and SCE as a reference electrode. **Caution:** Although no problems were encountered during the course of this work, attention is drawn to the potentially explosive nature of perchlorates.

6.2.2. Synthesis of ligands (H_2L^{1-4}). The diamine bis-phenolato “salan” ligands (H_2L^{1-4}) were prepared by essentially the same procedure as reported in Section 5.2.2.²⁶ The resulting white compounds were filtered, washed with methanol and dried over fused CaCl_2 . Elemental analysis, NMR (^1H and ^{13}C) and IR data of the ligands confirmed their structures.

H_2L^1 : Same as reported for ligand H_2L^3 in Section 5.2.2

H_2L^2 : Yield: 86%. Anal. calc. for $\text{C}_{26}\text{H}_{36}\text{N}_2\text{O}_4$: C, 70.88; H, 8.24; N, 6.36. Found: C, 70.84; H, 8.27; N, 6.33. Main IR peaks (KBr pellet, cm^{-1}): 2966 $\nu(\text{O}-\text{H}/\text{N}-\text{H})_{\text{H-bonded}}$. ^1H NMR (CDCl_3 , 400 MHz) δ (ppm): 7.54–7.01 (2H, aromatic), 5.09–5.04 (d, 2H, $=\text{CH}_2$), 5.97 (1H, quin., $-\text{CH}_2\text{CH}=\text{CH}_2$) 3.86 (s, 3H, $-\text{OCH}_3$), 3.67 (s, 2H, $-\text{NCH}_2\text{Ar}$), 3.28 (d, 2H, $-\text{CH}_2-\text{CH}=\text{CH}_2$), 2.69 (s, 2H, $-\text{NCH}_2$), 2.30 (s, 3H, $-\text{NCH}_3$). ^{13}C NMR (CDCl_3 , 100

MHz) δ (ppm): 147.76, 145.09, 137.84, 130.45, 121.51, 120.36, 115.52, 111.46, 61.41, 55.88, 54.49, 41.97, 39.82.

H₂L³: Same as described for ligand H₂L⁶ in Section 5.2.2

H₂L⁴: Yield: 86%. Anal. calc. for C₂₇H₄₂N₂O₂: C, 76.01; H, 9.92; N, 6.57. Found: C, 76.05; H, 9.97; N, 6.52. Main IR peaks (KBr, cm⁻¹): 2981 ν (O–H/N–H)_{H-bonded}. ¹H NMR (CDCl₃, 400 MHz) δ (ppm): 7.28–7.09 (m, 4H, aromatic), 4.42–4.21 (s, 4H, ArCH₂), 3.77–3.70 (m, 2H, NCH₂), 3.18 (sextet, 1H, CHCH₃), 2.97–2.89 (s, 6H, *p*-ArCH₃), 2.57–2.32 (m, 18H, 2C(CH₃)₃), 1.26–1.22 (d, 3H, CHCH₃). ¹³C NMR (CDCl₃, 100 MHz) δ (ppm): 162.61, 162.01, 148.24, 148.08, 147.77, 147.48, 133.07, 132.88, 129.71, 129.27, 126.73, 126.37, 125.54, 125.27, 121.72, 121.26, 121.08, 120.77, 58.44, 53.49, 44.81, 44.25, 41.87, 36.53, 31.47, 31.11, 18.42.

6.2.3. Synthesis of Cu(II) complexes (1–4). Triethylamine (1 mmol) was added to a hot methanolic solution of H₂L¹⁻⁴ (1 mmol), followed by the addition of CuClO₄·6H₂O (1 mmol). The mixture was refluxed for 12 h. The resulting dark green solution was filtered and slow evaporation of the filtrate over a week, produced deep green compounds.

[CuL¹] (**1**): Yield: 74%. Anal. calc. for C₂₆H₃₆CuN₂O₂: C, 57.51; H, 6.68; N, 5.16. Found: C 57.55; H, 6.67; N, 5.19.

[CuL²] (**2**): Yield: 77%. Anal. calc. for C₂₆H₃₄CuN₂O₄: C, 62.83, H, 7.03, N, 5.43. Found: C, 62.84, H, 7.08, N, 5.41.

[CuL^{3'}]₂ (**3**): Yield: 63%. Anal. calc. for C₃₄H₃₀Cl₂Cu₂N₆O₁₀: C, 37.84; H, 2.80; N, 7.79. Found: C, 37.81; H, 2.84; N, 7.76.

[CuL^{4'}]₂ (**4**): Yield: 62%. Anal. calc. for C₅₈H₈₈N₄O₆Cu₂: C, 65.45; H, 8.33; N, 5.26. Found: C, 65.42; H, 8.35; N, 5.22.

6.2.4. Synthesis of [Ni^{II}L³] (5), [Fe^{III}L³(Cl)] (6) and [Mo^{VI}O₂L³] (7) complexes. Triethylamine (1 mmol) was added to a hot methanolic solution of H₂L³ (1 mmol), followed by the addition of 1 mmol of Ni(OAc)₂·4H₂O, anhydrous FeCl₂ and MoO₂(acac)₂ for synthesis of complexes **5–7**, respectively. Each solution mixture was

refluxed for 12 h. Red, brown and yellow crystalline residue was obtained from the reaction mixture for the Ni^{II} (**5**), Fe^{III} (**6**) and Mo^{VI} (**7**) complexes respectively.

[NiL³] (**5**): Yield: 70%. Anal. calc. for C₂₅H₃₄Cl₂N₂NiO₂: C, 57.29; H, 6.54; N, 5.34. Found: C, 57.25; H, 6.50; N, 5.37.

[FeL³(Cl)] (**6**): Yield: 63%. Anal. calc. for C₂₅H₃₄Cl₃FeN₂O₂: C, 53.93; H, 6.16; N, 5.03. Found: C, 53.88; H, 6.21; N, 5.07.

[Mo^{VI}O₂L³] (**7**): Same as complex **6** described in Section 5.2.2.

6.2.5. X-ray Crystallography

[CuL¹] (**1**): A blue platelet crystal of C₂₆H₃₆Cl₂CuN₂O₂ having approximate dimensions of 0.240 x 0.140 x 0.080 mm was mounted on a glass fiber. All measurements were made on a Rigaku XtaLAB mini diffractometer using graphite monochromated Mo-K α radiation.²⁷

The crystal-to-detector distance was 50.00 mm. Cell constants and an orientation matrix for data collection corresponded to a primitive monoclinic cell with dimensions:

The data were collected at a temperature of 20 \pm 1^oC to a maximum 2 Θ value of 55.0^o. A total of 540 oscillation images were collected. A sweep of data was done using ω oscillations from -60.0 to 120.0^o in 1.0^o steps. The exposure rate was 10.0 [sec./^o]. The detector swing angle was 29.50^o. A second sweep was performed using ω oscillations from -60.0 to 120.0^o in 1.0^o steps. The exposure rate was 10.0 [sec./^o]. The detector swing angle was 29.50^o. Another sweep was performed using ω oscillations from -60.0 to 120.0^o in 1.0^o steps. The exposure rate was 10.0 [sec./^o]. The detector swing angle was 29.50^o. Another sweep was performed using ω oscillations from -60.0 to 120.0^o in 1.0^o steps. The exposure rate was 10.0 [sec./^o]. The detector swing angle was 29.50^o. Another sweep was performed using ω oscillations from -60.0 to 120.0^o in 1.0^o steps. The exposure rate was 10.0 [sec./^o]. The detector swing angle was 29.50^o. Another sweep was performed using ω oscillations from -60.0 to 120.0^o in 1.0^o steps. The exposure rate was 10.0 [sec./^o]. The detector swing angle was 29.50^o. The crystal-to-detector distance was 50.00 mm. Readout was performed in the 0.146 mm pixel mode.

Data Reduction

Of the 51379 reflections that were collected, 12362 were unique ($R_{\text{int}} = 0.3084$). Data were collected and processed using CrystalClear (Rigaku).²⁷

The linear absorption coefficient, μ , for Mo-K α radiation is 10.304 cm⁻¹. The data were corrected for Lorentz and polarization effects.

Structure Solution and Refinement

The structure was solved by direct methods²⁸ and expanded using Fourier techniques. The non-hydrogen atoms were refined anisotropically. Hydrogen atoms were refined using the riding model. The final cycle of full-matrix least-squares refinement on F^2 was based on 12362 observed reflections and 611 variable parameters and converged (largest parameter shift was 0.00 times its esd) with unweighted and weighted agreement factors of:

$$R_1 = \Sigma ||F_o| - |F_c|| / \Sigma |F_o| = 0.1010$$

$$wR_2 = [\Sigma (w (F_o^2 - F_c^2)^2) / \Sigma w(F_o^2)^2]^{1/2} = 0.2262$$

The standard deviation of an observation of unit weight was 0.99. Unit weights were used. The maximum and minimum peaks on the final difference Fourier map corresponded to 0.51 and -0.38 e⁻/Å³, respectively.

Neutral atom scattering factors were taken from Cromer and Waber.²⁹ Anomalous dispersion effects were included in F_{calc} ;³⁰ the values for $\Delta f'$ and $\Delta f''$ were those of Creagh and McAuley.³¹ The values for the mass attenuation coefficients are those of Creagh and Hubbell.³² All calculations were performed using the CrystalStructure³³ crystallographic software package except for refinement, which was performed using SHELXL-97.³⁴

[CuL^{3'}]₂ (**3**): A blue prism, measuring 0.48 x 0.04 x 0.03 mm³ was mounted on a loop with oil. Data was collected at 22°C on a Nonius Kappa CCD FR590 single crystal X-ray diffractometer, Mo-radiation.

Crystal-to-detector distance was 30 mm and exposure time was 60 seconds per degree for all sets. The scan width was 2°. Data collection was 99.7% complete to 25° in θ . A total of 11220 merged reflections were collected covering the indices $-12 \leq h \leq 13$, $-16 \leq k \leq 16$, $-16 \leq l \leq 16$. 6739 reflections were symmetry independent and the $R_{\text{int}} = 0.0721$ indicated that the data was of average quality. Indexing and unit cell refinement indicated a triclinic P lattice. The space group was found to be $P \bar{1}$ (No.2).

The data was integrated and scaled using hkl-SCALEPACK.³⁵ This program applies a multiplicative correction factor (S) to the observed intensities (I) and has the following form:

$$S = (e^{-2B(\sin^2\theta)/\lambda^2})/\text{scale}$$

S is calculated from the scale and the B factor determined for each frame and is then applied to I to give the corrected intensity (I_{corr}).

Solution by direct methods (SHELXS, SIR97³⁶) produced a complete heavy atom phasing model consistent with the proposed structure. The structure was completed by difference Fourier synthesis with SHELXL97.^{37,38} Scattering factors are from Waasmair and Kirfel.³⁹ Hydrogen atoms were placed in geometrically idealised positions and constrained to ride on their parent atoms with C---H distances in the range 0.95–1.00 Angstrom. Isotropic thermal parameters U_{eq} were fixed such that they were 1.2 U_{eq} of their parent atom U_{eq} for CH's and 1.5 U_{eq} of their parent atom U_{eq} in case of methyl groups. All non-hydrogen atoms were refined anisotropically by full-matrix least-squares.

Details on the data collection parameters applied on the individual crystals of **1** and **3** are summarized in Table 6.1

Table 6.1. Crystal and refinement data of complexes [CuL¹] (**1**) and [CuL^{3'}]₂ (**3**)

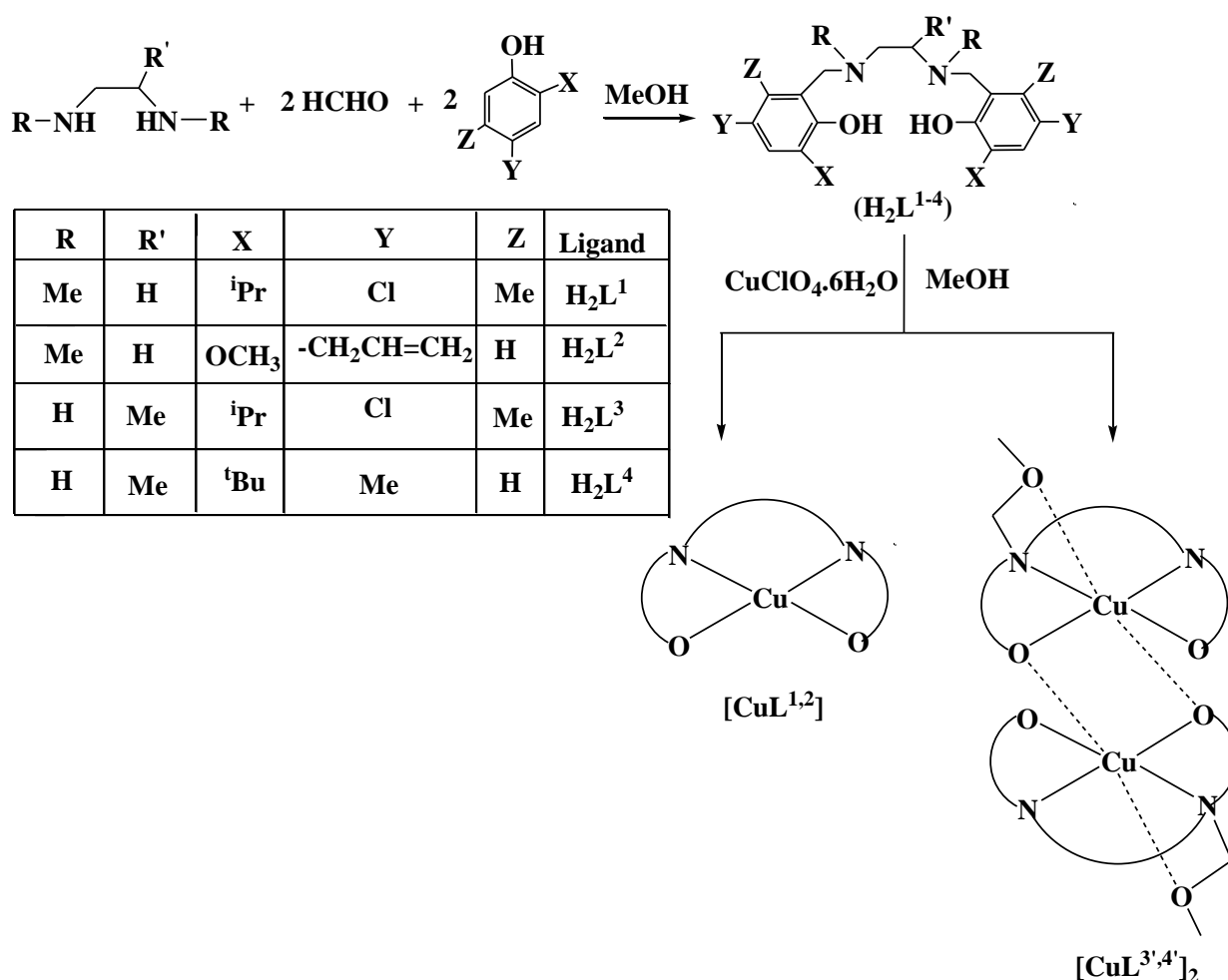
| Compound | 1 | 3 |
|---|---|---|
| Empirical Formula | C ₂₆ H ₃₆ Cl ₂ CuN ₂ O ₂ | C ₅₄ H ₇₆ Cl ₄ Cu ₂ N ₄ O ₆ |
| M | 543.03 | 1146.06 |
| Crystal system | triclinic | monoclinic |
| Space group | <i>P</i> -1 | <i>P</i> 2 ₁ /a |
| a(Å) | 14.524 (3) | 15.048(2) |
| b(Å) | 21.071(4) | 21.675(3) |
| c(Å) | 18.875(3) | 16.615(2) |
| α (°) | 90 | 90 |
| β (°) | 110.690(8) | 93.091(8) |
| γ (°) | 90 | 90 |
| V (Å ³) | 5404 (2) | 5411.2 (12) |
| Z | 8 | 4 |
| D _{calc} (g.cm ⁻³) | 1.335 | 1.417 |
| Absorption Coefficient | 1.030 mm ⁻¹ | 1.0361 mm ⁻¹ |
| F(000) | 2280 | 2408 |
| Crystal size (mm ³) | 0.240 x 0.140 x 0.080 | 0.170 x 0.150 x 0.050 |
| Theta range for data collection(°) | 3 to 27.30 | 1.546 to 27.968 |
| R ₁ [I>2σ(I)] | R1 = 0.0461 wR2 = 0.137 | R1 = 0.0361, wR2 = 0.078 |
| wR ₂ [all data] | R1 = 0.049 wR2 = 0.142 | R1 = 0.059, wR2 = 0.088 |
| S[goodness of fit] | 1.100 | 1.002 |
| max. / min. res. (e.Å ⁻³) | 1.404 and -0.842 | 0.387 and -0.341 |

6.2.6. Superoxide Dismutase activity

The SOD activity was evaluated with the nitroblue tetrazolium (NBT) method using xanthine/xanthine oxidase as the source of the superoxide anion as has been previously described.⁴⁰ However, since the compounds were not soluble in phosphate buffer (pH 7.4), stock solutions ($5 \times 10^{-6} \text{ mol dm}^{-3}$) of them were prepared in DMSO and suitable volumes (0.050–0.400 cm^3) of them were added to the cuvettes containing NBT ($4.8 \times 10^{-5} \text{ mol dm}^{-3}$) and xanthine ($1.9 \times 10^{-4} \text{ mol dm}^{-3}$). The IC_{50} was determined by plotting V/v versus the concentration of the complex, where V is the velocity of NBT reduction in the absence of the copper compound and v is the velocity of NBT reduction in the presence of the complex. The reaction was followed for 10 min and the velocity of NBT reduction was taken as the slope of the curve at 560 nm between 1 and 3 min.

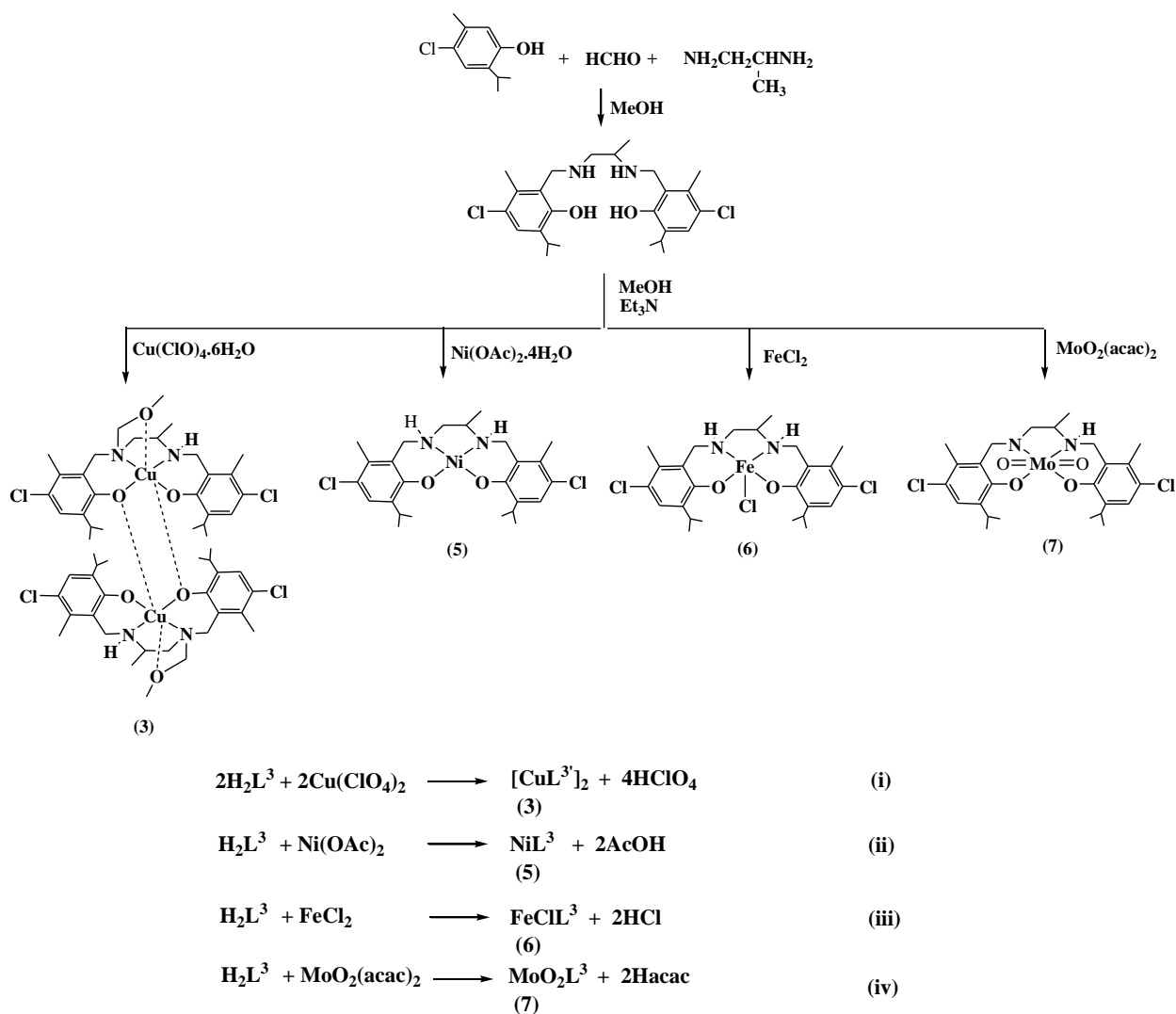
6.3. RESULTS AND DISCUSSION

6.3.1. Synthesis. The synthetic methodology for the ligand and complexes are illustrated in Scheme 6.1. Reaction of $\text{Cu}(\text{ClO}_4)_2 \cdot 6\text{H}_2\text{O}$ with tetradentate diamino bis(phenolato) (ONNO) “salan” ligands (H_2L^{1-4}) in the molar ratio of 1:1 in MeOH, resulted in the formation of the green filtrate. Cu(II) complexes (**1–4**) were obtained from the filtrate upon slow evaporation. The purity of these compounds was further confirmed by elemental analyses, UV-vis spectroscopy and ESI-MS, which were also consistent with the X-ray structures. The complexes were soluble in aprotic solvents, DMF and DMSO, and sparingly soluble in protic solvents. All the complexes were stable in both solid and solution phases.



Scheme 6.1. Schematic diagram for synthesis of Cu(II) complexes (**1–4**).

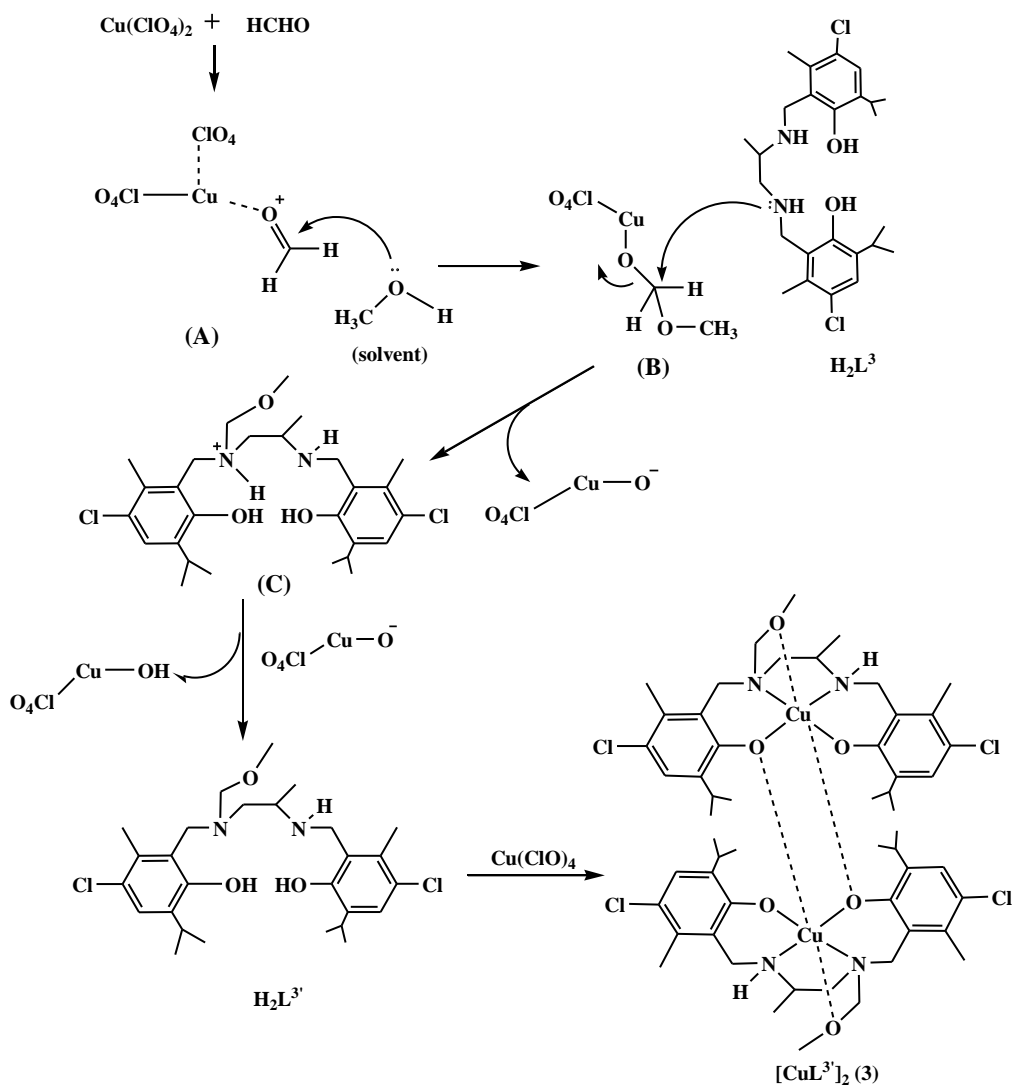
An unprecedented ligand transformation occurred upon complex formation in the case of **3** and **4** as reflected in Scheme 6.1 and as evidenced from other physico-chemical characterizations. In these complexes an extra acetal fragment (CH_2OCH_3) is bonded to the unhindered N atom of the secondary amine, which in turn is weakly coordinated to the Cu center. In addition, there is also a weak interaction of the Cu center with the phenolic O atom of the neighboring Cu molecule, resulting in the formation of a distorted elongated octahedron. Further investigation to explain the unusual transformation in the case of **3** and **4** has been done by taking $[\text{CuL}^{3'}]_2$ as a representative compound. To confirm that the organic rearrangement is copper assisted, the corresponding nickel, iron and molybdenum complexes of H_2L^3 were prepared following a similar approach, by using $[\text{Ni}(\text{OAc})_2] \cdot 4\text{H}_2\text{O}$, FeCl_2 and $[\text{MoO}_2(\text{acac})_2]$ as metal precursors. It was observed that the analogues Ni(II), Fe(III) and Mo(VI) complexes, $[\text{NiL}^3]$ (**5**), $[\text{FeL}^3(\text{Cl})]$ (**6**) and $[\text{MoO}_2\text{L}^3]$ (**7**), respectively, did not initiate the type of ligand rearrangement seen in the Cu scenario (**3**) (Scheme 6.2), and the ligand coordinated in the usual manner, as verified from other spectral and structural characterizations, thereby fortifying the mechanism to be Cu(II) catalysed.



Scheme 6.2. Synthesis of $[\text{CuL}^3]_2$ (**3**), $[\text{NiL}^3]$ (**5**), $[\text{Fe}^{\text{III}}\text{L}^3(\text{Cl})]$ (**6**) and $[\text{MoO}_2\text{L}^3]$ (**7**).

As elucidated in Scheme 6.3, the carbonyl group of HCHO (used in excess during ligand synthesis) is activated ('A') by the Lewis acid (Cu^{+2} , from CuClO_4), followed by the nucleophilic attack of methanol (used as solvent), thereby resulting in the formation of the intermediate compound 'B'. In the subsequent step, the parent ligand H_2L^3 then attacks the electrophilic center generated upon departure of $[\text{CuOClO}_4]^-$ from 'B', leading to the formation of 'C'. 'C' is then stabilized as $\text{H}_2\text{L}^{3'}$ (modified ligand) upon release of a proton to the transient $[\text{CuOClO}_4]^-$ species (forming $\text{CuClO}_4(\text{OH})$ in solution). This *in situ* generated ligand, $\text{H}_2\text{L}^{3'}$, then forms the final complex $[\text{CuL}^3]_2$ (**3**) upon reaction with the metal precursor, CuClO_4 . Presumably, the formation of the acetal fragments allows the

coordination of the oxygen atoms to the Cu(II) ion, which in turn stabilises the complex formed. Cu(II) ion is a typical example of a 3d metal ion, capable of showing the presence of a Jahn–Teller effect.⁴¹ Jahn Teller distortion effect does not occur in the case of Ni(II), Fe(III) and Mo(VI) complexes (**5–7**), wherein a regular chemistry is observed. The stability of the Cu(II) complexes, $[\text{CuL}^{3'}]_2$ is also influenced by the presence of an additional Cu–O interaction.



Scheme 6.3. Plausible reaction mechanism leading to formation of $[\text{CuL}^{3'}]_2$ (**3**).

6.3.2. Spectral Characteristics

UV-vis Spectroscopy. The electronic spectra of all the complexes were recorded in DMSO solutions. The UV-vis data of complexes **1–6** is tabulated in Table 6.2. In the spectra of **1–4** the lower energy absorptions (432–346 nm) are ascribable to ligand to metal charge transfer transitions whereas the higher energy absorptions (299–211 nm) are likely to be due to ligand centered transitions.²⁵ Weak absorptions observed in the range 625–613 nm are assigned to d–d transition in the Cu(II) complexes.²⁵ A representative spectrum of the Cu(II) complexes, [CuL¹] (**1**) is shown in Figure 6.1. UV-vis spectra of Ni(II), [NiL³] (**5**) and Fe(III), [FeL³(Cl)] (**6**) complexes is shown in Figure 6.2 and Figure 6.3 respectively. The peak at 317 nm and a shoulder band at 348 nm in [NiL³] (**5**) are attributed to the ligand to metal charge transfer bands, while the weaker d–d peak is observed at 419 nm.^{19b} The peak at higher energy, 278 nm, in [NiL³] (**5**) is due to intra ligand $\pi \rightarrow \pi^*$ transition. In [FeL³(Cl)] (**6**), the absorption maxima observed in the near-UV regions, below 300 nm are due to intra-ligand $\pi \rightarrow \pi^*$ transitions, while the peak at 487 nm is proposed to arise from charge-transfer transitions from the in-plane p_π orbital of the phenolate to the half-filled d_{π^*} orbital of Fe(III).⁴² Related results of the UV-vis spectra of MoO₂L³ (**7**) is discussed in Section 5.3.2.

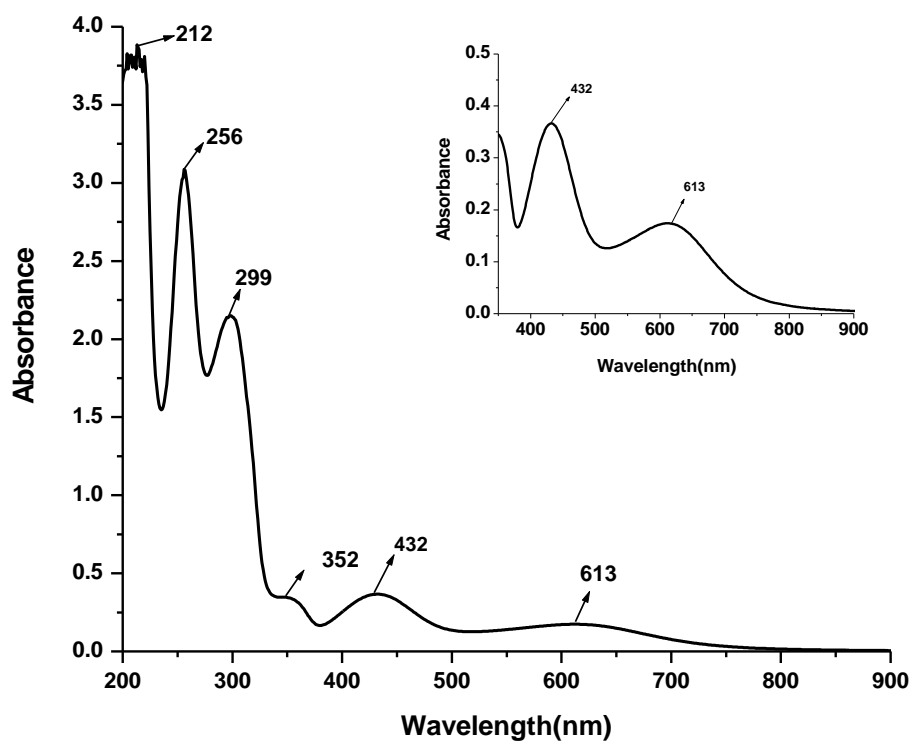


Figure 6.1. UV-vis spectrum of [CuL¹] (1) in DMSO.

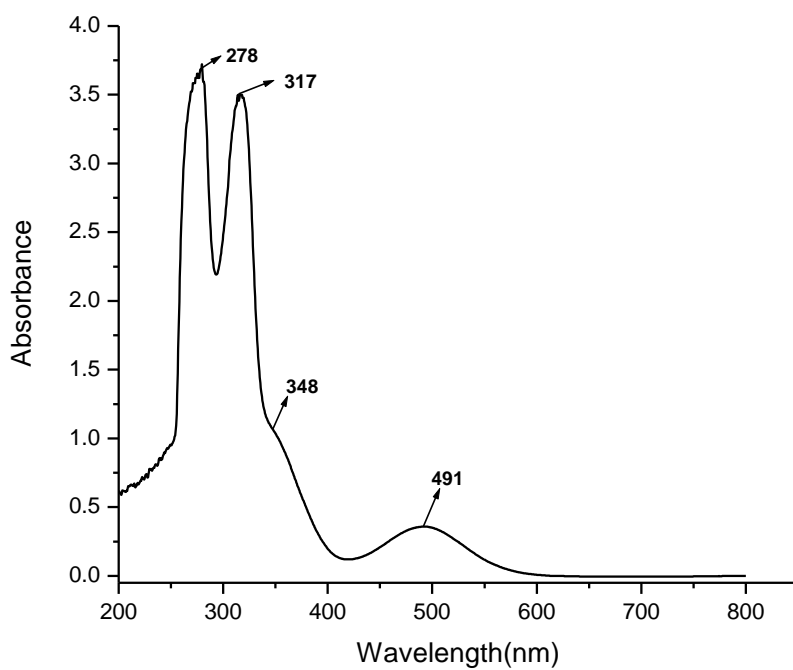


Figure 6.2. UV-vis spectrum of [NiL³] (5) in DMSO.

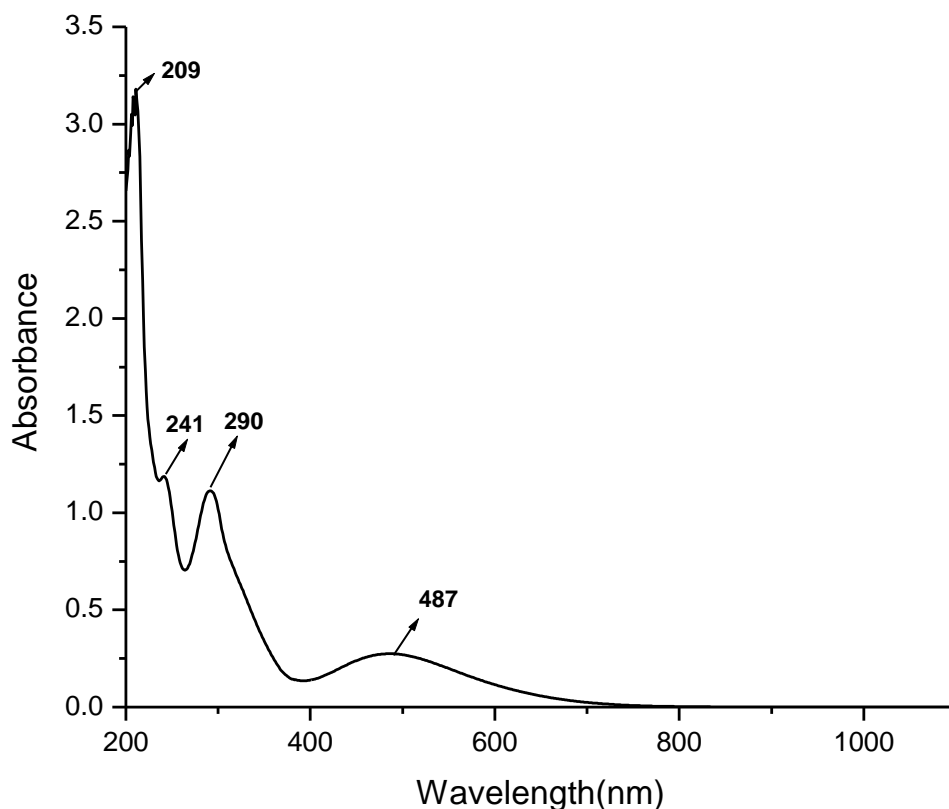


Figure 6.3. UV-vis spectrum of [FeL³(Cl)] (**6**) in DMSO.

Table 6.2. Electronic spectra for complexes [CuL^{1,2}] (**1**, **2**), [CuL^{3',4'}]₂ (**3**, **4**), [NiL³] (**5**), [FeL³(Cl)] (**6**) in DMSO

| Complex | λ_{\max}/nm ($\epsilon_{\max}/\text{M}^{-1}\text{cm}^{-1}$) |
|--|--|
| [CuL ¹] (1) | 212(31600), 256(27630), 299(12990), 352(6610), 432(9921), 613(1200) |
| [CuL ²] (2) | 215(29660), 255(23200), 285(11660), 346(5100), 429(9342), 625(1160) |
| [CuL ^{3'}] ₂ (3) | 211(30000), 254(24685), 295(12685), 353(6120), 429(9511), 617(1232) |
| [CuL ^{4'}] ₂ (4) | 211(29790), 252(23258), 294(11768), 352(5132), 419(8526), 621(1210) |
| [NiL ³] (5) | 278(24000), 317(21750), 348(558), 491(160) |
| [FeL ³ (Cl)] (6) | 209(29500), 241(9100), 290(6700), 487(940) |

6.3.3. ESI-MS. ESI-MS data of **1–5** have been recorded in the positive ion mode and that of **6** and **7** in the negative ion mode, in acetonitrile solution. ESI-MS analysis for CuL^1 (**1**) and CuL^2 (**2**) shows peaks at m/z 544.26 $[\text{M} + \text{H}]^+$ and 441.58 $[\text{M} + \text{H}]^+$ respectively, whereas $[\text{CuL}^{3'}]_2$ (**3**) and $[\text{CuL}^{4'}]_2$ (**4**) exhibits the major ionic peak at m/z 572.06 $[1/2\text{M} + \text{H}]^+$ and 532.21 $[1/2\text{M} + \text{H}]^+$, indicating coordination of the modified ligand to the Cu center in **3** and **4**. Representative spectra of Cu(II) complexes (**1** and **3**) is shown in Figure 6.4 and 6.5 respectively. The presence of a peak at m/z 523.15 $[\text{M} + \text{H}]^+$ in the ESI-MS of NiL^3 (**5**) (Figure 6.6) and three major peaks at m/z 554.32 $[\text{M} - \text{H}]^-$, 591.99 $[\text{M} + \text{K} - 2\text{H}]^-$ and 599.64 $[\text{M} + \text{FA} - \text{H}]^-$ (where FA= formic acid) in the ESI-MS of $[\text{FeL}^3(\text{Cl})]$ (**6**) (Figure 6.7) and the major peak at m/z 593.22 $[\text{M} - \text{H}]^-$ in the ESI-MS of MoO_2L^3 (**7**) (Figure 6.8), confirmed the regular coordination of the tetradentate salan ligand, H_2L^3 , to the Ni(II), Fe(III) and Mo(VI) centers, without any ligand modification.

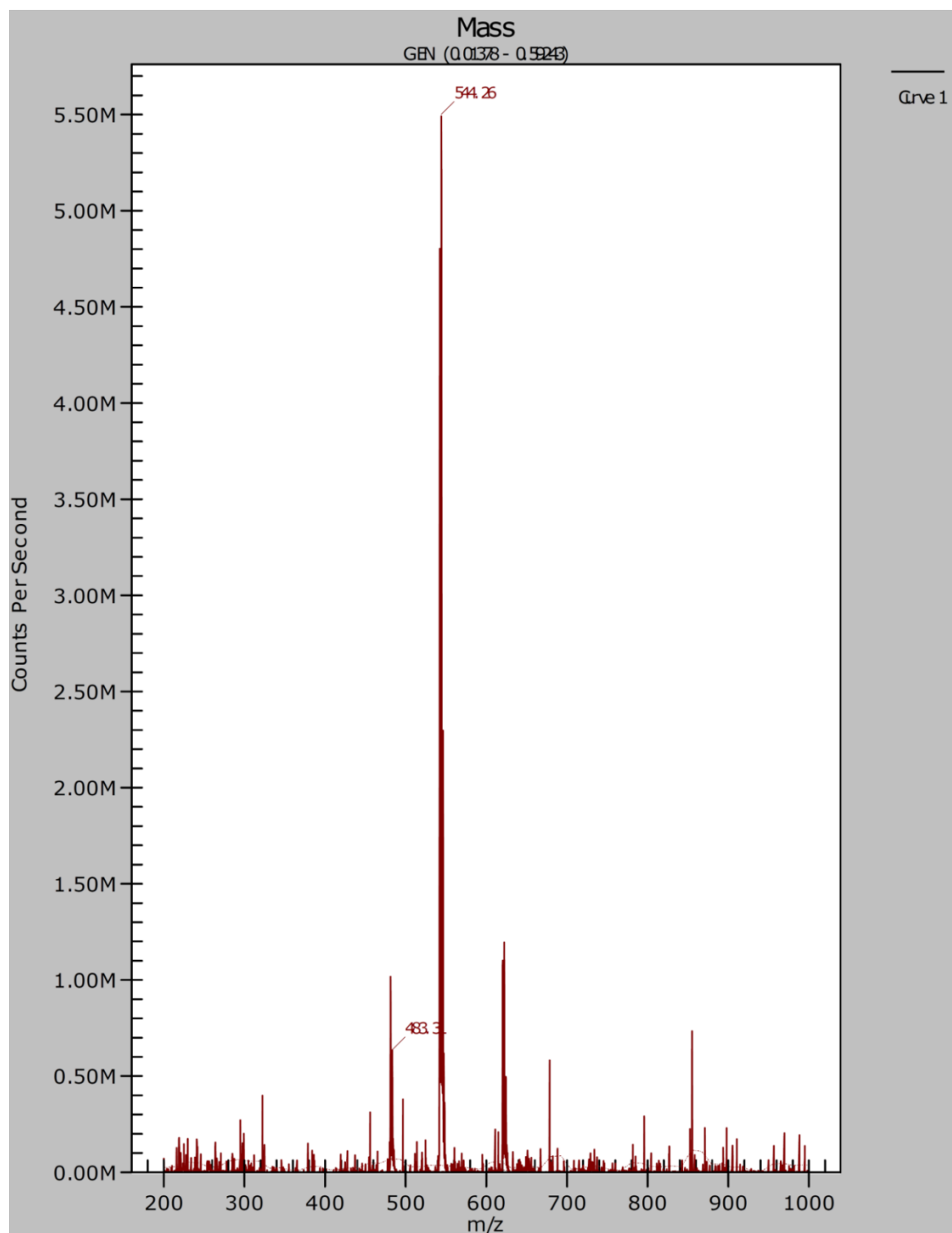


Figure 6.4. ESI-MS of $[\text{CuL}^1]$ (1) in CH_3CN .

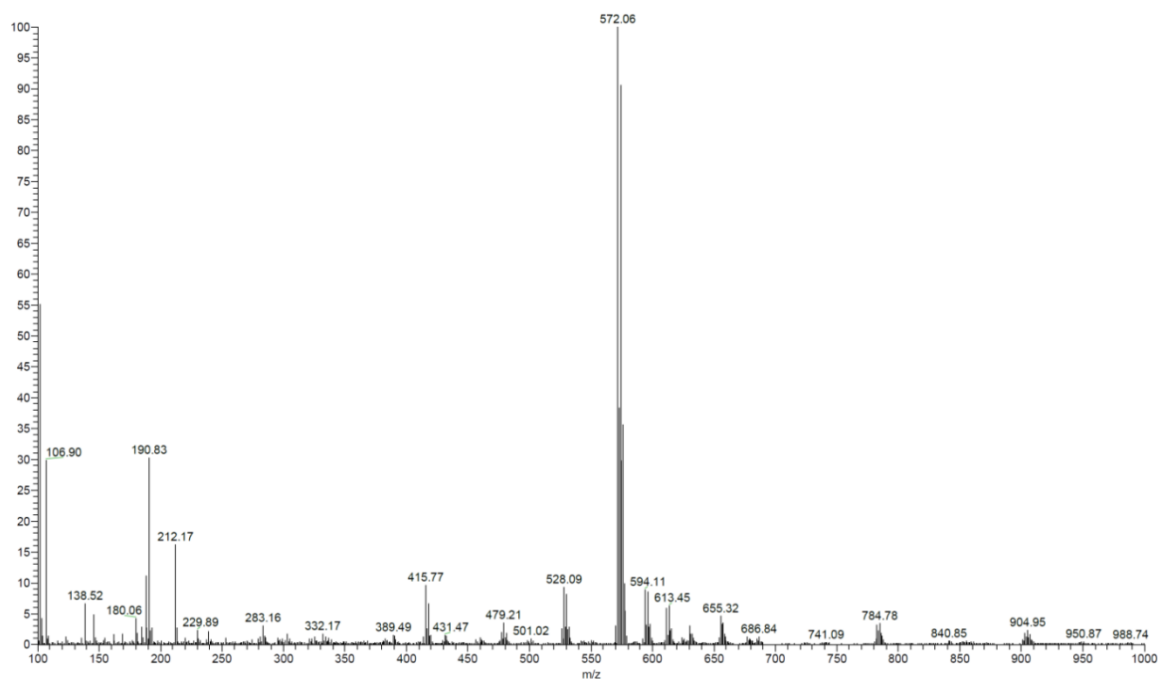


Figure 6.5. ESI-MS of $[\text{CuL}^3]_2$ (3) in CH_3CN .

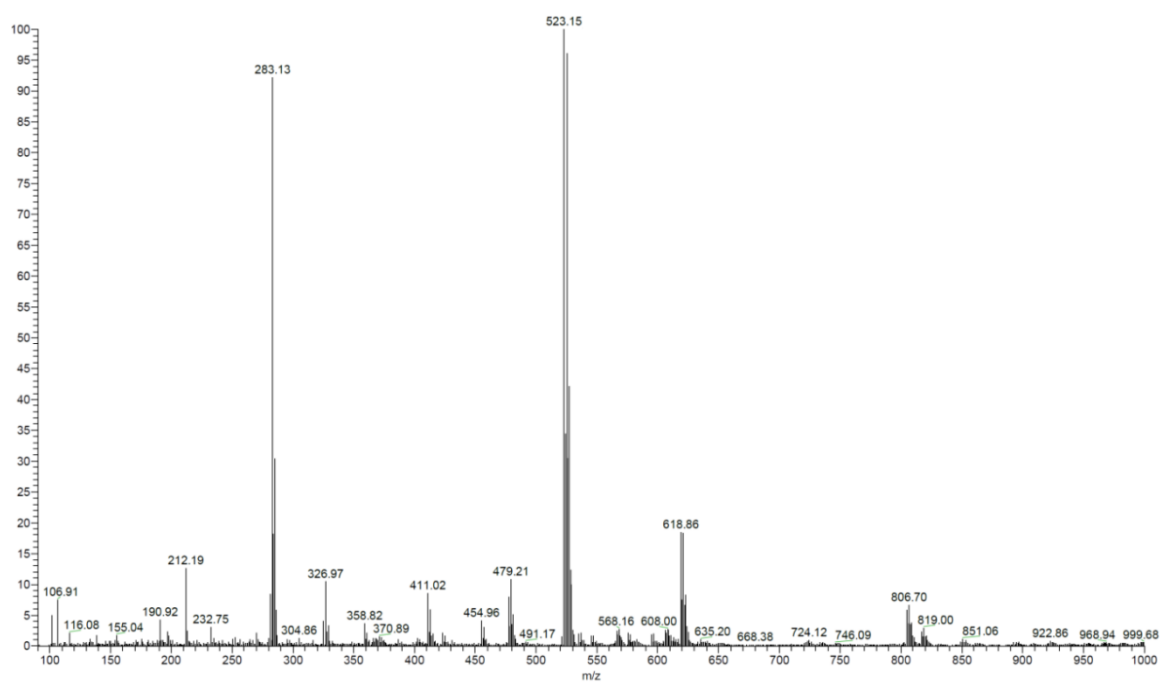


Figure 6.6. ESI-MS of $[\text{NiL}^3]$ (5) in CH_3CN .

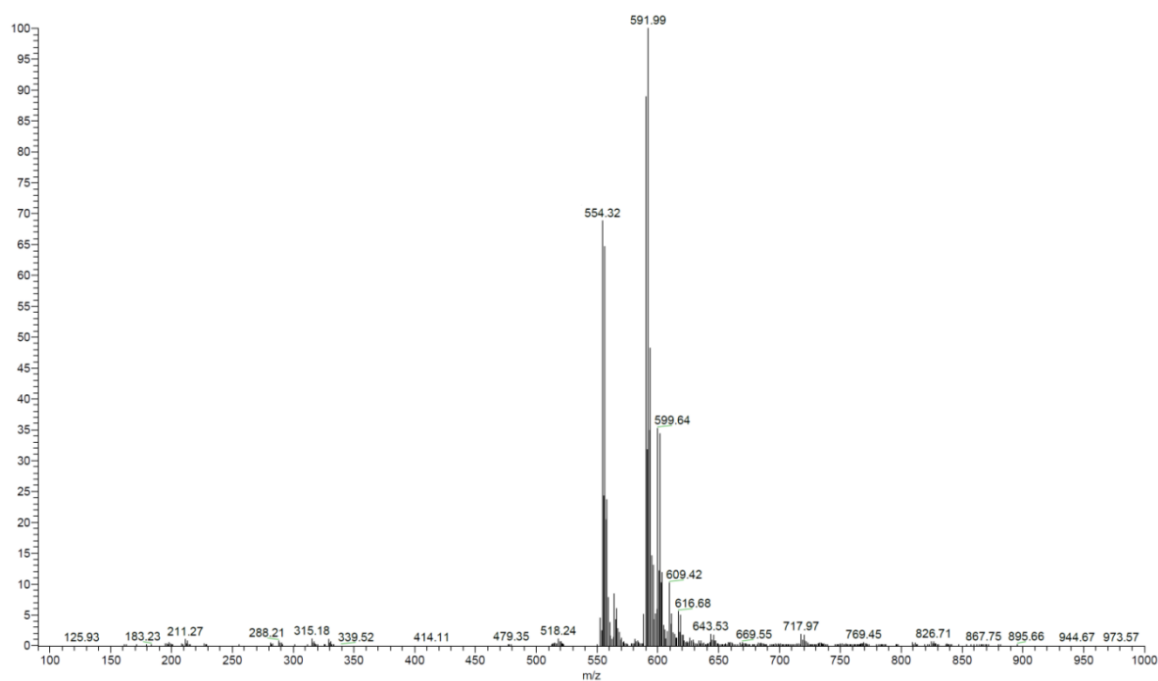


Figure 6.7. ESI-MS of $[\text{FeL}^3(\text{Cl})]$ (**6**) in CH_3CN .

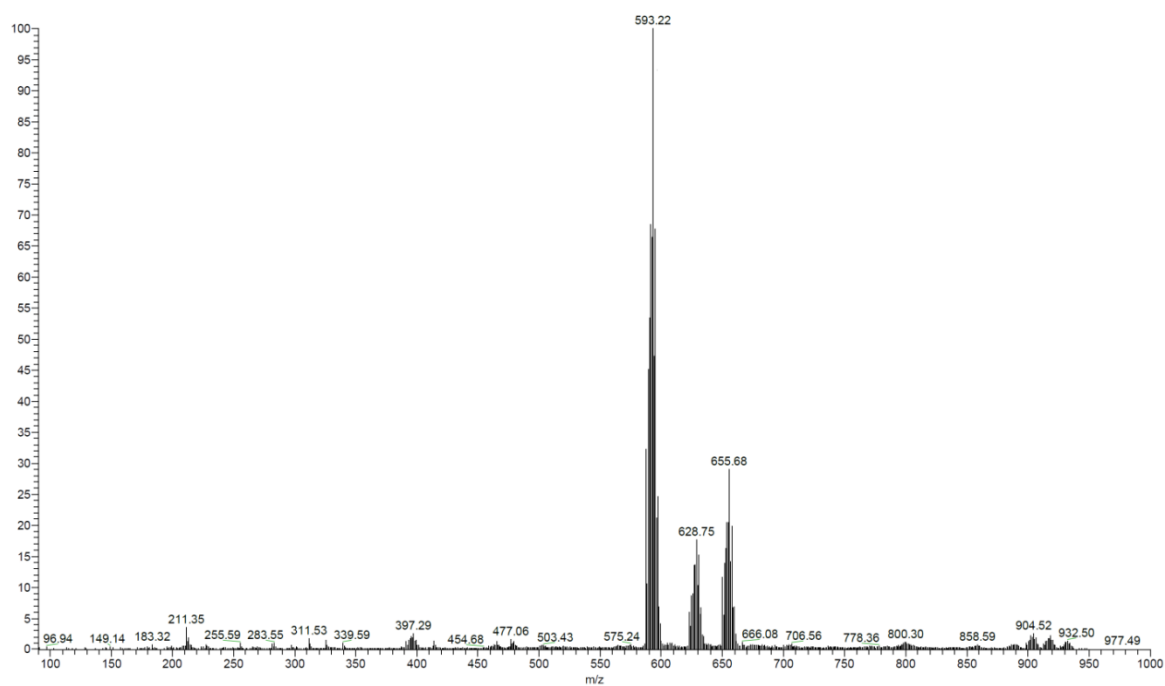


Figure 6.8. ESI-MS of $[\text{MoO}_2\text{L}^3]$ (**7**) in CH_3CN .

6.3.4. Electrochemical Properties. Electrochemical properties of the complexes have been studied by cyclic voltammetry in DMF solution (0.1 M TBAP), and the voltammetric data are listed in Table 6.3. The cyclic voltammogram of all the four complexes exhibit an irreversible reductive response within the potential window of -1.32 to -1.29 V, which is assigned to the Cu(II)/Cu(I) process.²⁵ The ligand is redox inactive in the potential window of 0 to -2 V in the cathodic region. A representative voltammogram of complex **3** is given in Figure 6.9. Single electron processes were verified by comparing the current height of the quasi-reversible reductive response with that of the standard ferrocene–ferrocenium couple under identical experimental conditions.

Table 6.3. Cyclic voltammetric^[a] results for complexes **1–4** at 298 K

| Complex | E_p^c (V) ^[a] | Complex | E_p^c (V) ^[a] |
|----------------------------------|----------------------------|--|----------------------------|
| [CuL ¹] (1) | -1.29 | [CuL ^{3'}] ₂ (3) | -1.32 |
| [CuL ²] (2) | -1.30 | [CuL ^{4'}] ₂ (4) | -1.31 |

^[a]**1–4** in DMF at a scan rate of 100 mV s⁻¹. where E_p^c is the cathodic peak potentials vs. Ag/AgCl.

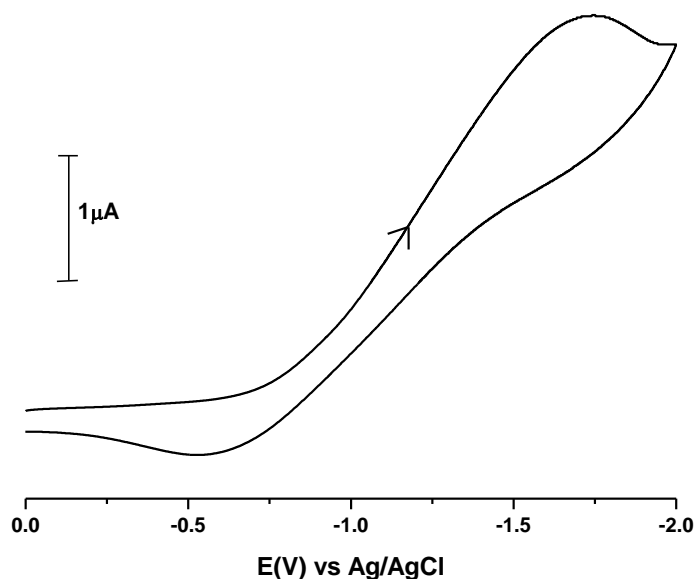


Figure 6.9. Cyclic voltammogram of **3** showing reduction (Cu(II) → Cu(I)) at the copper(II) center.

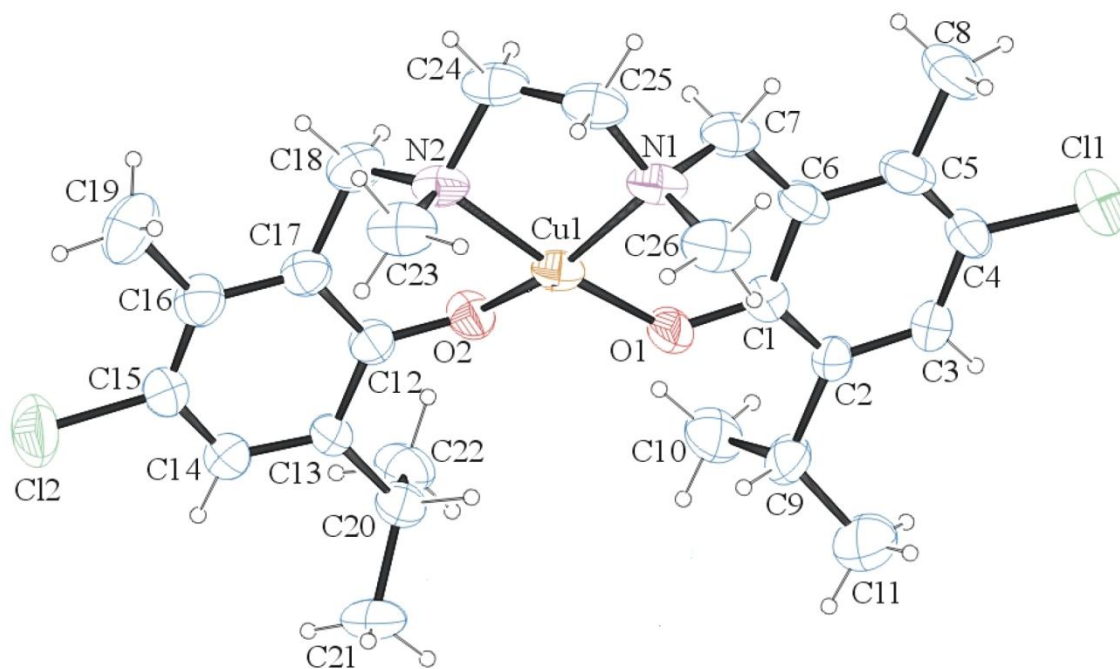
6.3.5. Description of X-ray structure of [CuL¹] (**1**) and [CuL^{3'}]₂ (**3**)

The observed elemental analysis (C, H, N) data of all the complexes (**1–4**) are consistent with their composition. In order to authenticate the molecular structures of the complexes, single crystals of **1** and **3** were analysed by X-ray crystallography.

[CuL¹] (**1**): ORTEP diagram of **1** is depicted in Figure 6.10. **1** crystallized in the monoclinic system, space group $P 2_1/c$, with the unit cell containing two molecules in the asymmetric unit. Both molecules present square-planar coordination around the Cu center with the equatorial planes defined by atoms O1, O2, N1 and N2. The planar arrangement of the chromophore is tetrahedrally distorted with the four bond angles, O(1)–Cu(1)–O(2), O(1)–Cu(1)–N(1), O(2)–Cu(1)–N(2), N(1)–Cu(1)–N(2) differing slightly from 90°. The two methyl groups on the tertiary amine are situated out of the N₂O₂ plane and positioned trans to each other. The bond parameters of **1** are tabulated in Table 6.4.

Table 6.4. Selected geometric parameters for [CuL¹] (**1**)

| Bond lengths (Å) | | | |
|------------------|-----------|-----------------|-----------|
| Cu(1)–O(1) | 1.879 (6) | Cu(1)–N(1) | 2.039 (7) |
| Cu(1)–O(2) | 1.880 (5) | Cu(1)–O(2) | 2.030 (9) |
| Bond angles (°) | | | |
| O(1)–Cu(1)–O(2) | 93.7 (3) | O(2)–Cu(1)–N(1) | 157.6 (3) |
| O(1)–Cu(1)–N(1) | 94.4 (3) | O(2)–Cu(1)–N(2) | 93.1 (3) |
| O(1)–Cu(1)–N(2) | 155.4 (3) | N(1)–Cu(1)–N(2) | 88.1 (3) |

**Figure 6.10.** ORTEP diagram of [CuL¹] (**1**) with atom labeling scheme.

[CuL^{3'}]₂ (**3**): ORTEP diagram of **3** is presented in Figure 6.11. The crystal structure of **3** revealed that each Cu(II) ion resides in a distorted octahedral environment (Figure 6.12). The asymmetric unit contains two independent molecules. The copper center is coordinated to two amine nitrogen atoms (N1, N2) and two phenolic oxygen atoms (O1, O2) in the equatorial plane. In addition, the Cu atom is also coordinated in the axial position to the phenolate O(1ⁱ) of the neighboring symmetry related molecule to form

Cu(1)–O(1)–Cu(1ⁱ)–O(1ⁱ) dimer (Figure 6.12). The oxygen atom (O3) of the CH₂–O–CH₃ moiety occupies the other axial site in the complex to complete the octahedral geometry. The intermolecular Cu(1)–O(1ⁱ) bond lengths are significantly longer compared to intramolecular Cu(1)–O(1) distance (Table 6.5). The extended intermolecular Cu(1)–O(1ⁱ) bond may be a result of hindrance due to the geometrical complexity of the involved molecules.

Table 6.5. Selected geometric parameters for [CuL^{3'}]₂ (**3**)

| Bond lengths (Å) | | | |
|--------------------------|-----------|-----------------|-----------|
| O(1)–Cu(1) | 1.971(8) | N(1)–Cu(1) | 1.968(10) |
| O(2)–Cu(1) | 1.909(8) | N(2)–Cu(1) | 2.042(9) |
| O(1 ⁱ)–Cu(1) | 2.786(10) | O(3)–Cu(1) | 2.544(9) |
| Bond angles (°) | | | |
| O(2)–Cu(1)–N(1) | 151.5(4) | O(2)–Cu(1)–O(1) | 100.2(3) |
| N(1)–Cu(1)–O(1) | 91.3(4) | O(2)–Cu(1)–N(2) | 91.9(4) |
| N(1)–Cu(1)–N(2) | 86.2(4) | O(1)–Cu(1)–N(2) | 158.7(4) |

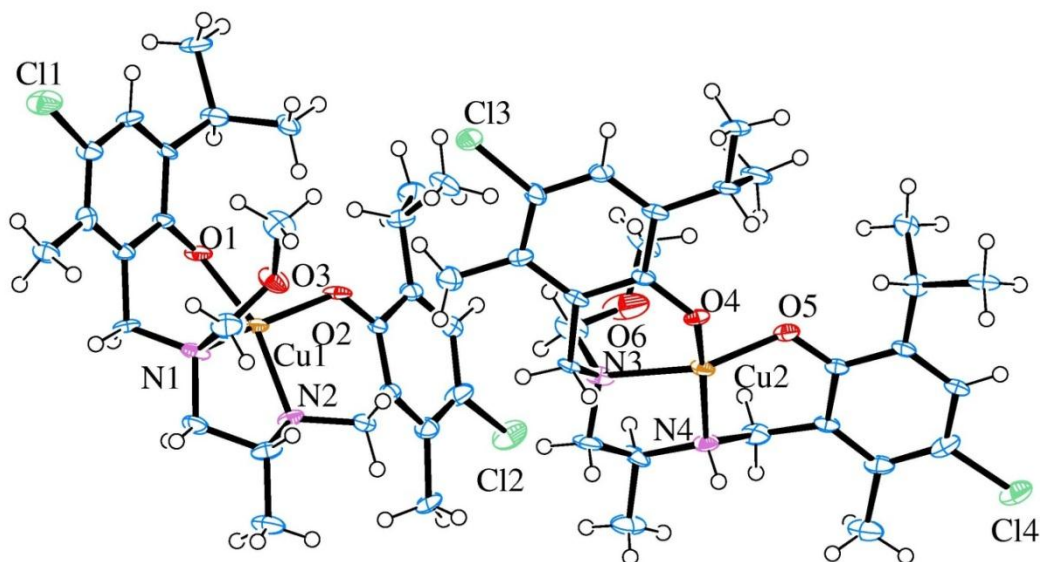


Figure 6.11. ORTEP diagram of the asymmetric unit of [CuL^{3'}]₂ (**3**) with atom labeling scheme.

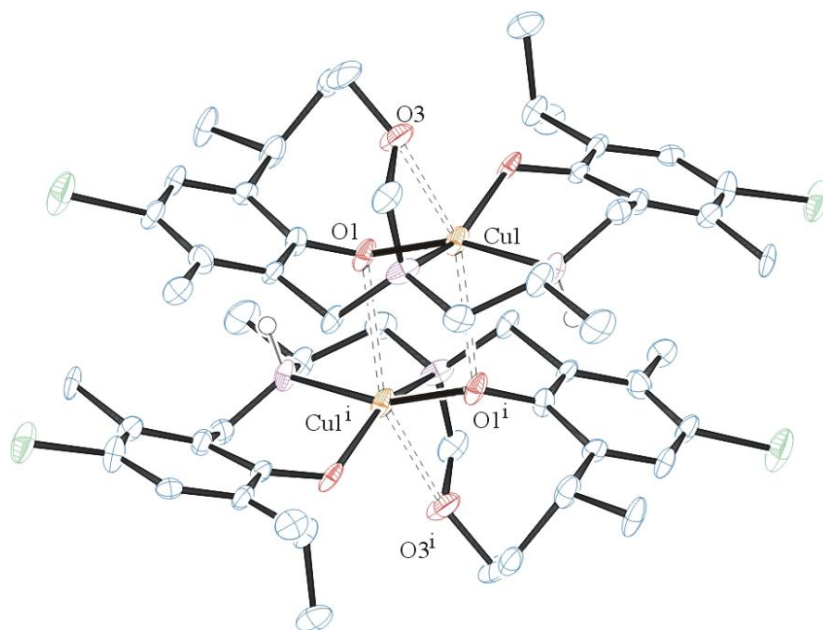


Figure 6.12. ORTEP diagram of [CuL³]₂ (**3**) showing the weak interactions.

6.3.6. Superoxide Dismutase Activity

The SOD activity of complexes **1–3** was investigated by employing the xanthine/ xanthine oxidase/ NBT system. Complex **4** could not be evaluated due to its deliquescent nature. In the presence of xanthine, xanthine oxidase generates superoxide anion at a constant rate, which promotes the reduction of NBT to formazan. This latter shows an intense absorption at 560 nm. Thus, by monitoring the increase of the absorption at 560 nm in the presence and in the absence of the copper compounds, it is possible to evaluate if they show SOD-like activity. In this regard, the concentration of the compound that decreases the velocity of NBT reduction by 50% is considered the IC_{50} . This value can be accessed by carrying out experiments with different concentrations of the compound under evaluation (Figures 6.13 and 6.14).

The IC_{50} values presented by complexes **1–3** are in the middle range observed for other copper complexes previously described in the literature (Table 6.6). It is assumed that complex **3** exists as a monomer, $CuL^{3'}$, in solution in the biological assay. The observed order of activity was $CuL^{3'} (\mathbf{3}) > CuL^1 (\mathbf{1}) > CuL^2 (\mathbf{2})$. The IC_{50} could not be determined for $CuL^2 (\mathbf{2})$ due to its low solubility in the phosphate buffer. The highest concentration that was possible to reach ($3.0 \mu\text{mol dm}^{-3}$) is lower than the IC_{50} , which means that its IC_{50} value is higher than $3.0 \mu\text{mol dm}^{-3}$.

The IC_{50} presented by $CuL^{3'}$ is twice lower than the value observed for CuL^1 . Different factors have been considered of relevance for a synthetic compound to show satisfactory SOD activity, including redox potential, ligand design and coordination environment.⁴³ The redox potential (Table 6.3) presented by the compounds described here are very similar, which suggested that it is not the driving force of the SOD activity. On the other hand, compound CuL^1 shows a square planar geometry; while the copper center in $CuL^{3'}$ is square pyramidal in solution, suggesting that a five-coordinated environment may be of relevance to increase the SOD. However, a feature that may have the highest influence on the IC_{50} values of the complexes are the substituents present in the ligand backbone.

Table 6.6. Superoxide dismutase activity (IC_{50}) presented by complexes (1–3), CuZn-SOD, $CuCl_2$ and other compounds described in the literature.

| Compound | $IC_{50}/\mu\text{mol dm}^{-3}$ |
|--|---------------------------------|
| CuL^1 ^a (1) | $1.55\pm 0.050.07$ |
| CuL^2 ^a (2) | >3.0 |
| CuL^3 ^a (3) | 0.75 ± 0.05 |
| $[Cu(BCEN)]Cl_2 \cdot 2H_2O$ ^{a, 43} | 0.179 ± 0.017 |
| $[Cu(BPAP)H_2O]Cl_2$ ^{a, 43} | 0.168 ± 0.030 |
| $[Cu(BPAH)H_2O]Cl_2$ ^{a, 43} | 0.129 ± 0.033 |
| $CuCl_2 \cdot 2H_2O$ ^{a, 43} | 0.910 ± 0.191 |
| $[Cu(en)_2Cl]$ ^{a, 44} | 1000 |
| $[(en)Cu-PMDT](ClO_4)_3$ ^{b, 45} | 41 |
| $[(en)_2Cu-Im-Cu(en)_2](ClO_4)_3$ ^{b, 45} | 52 |
| $[(en)_2Cu-M-Im-Cu(en)_2](ClO_4)_3$ ^{b, 45} | 20 |
| $(en)_2Cu-E-Im-Cu(en)_2](ClO_4)_3$ ^{b, 45} | 42 |
| $[Cu(dipsH)_2(BZDH)_2]$ ^{a, 46} | 0.94 |
| $[Cu_2(indo)_4(H_2O)_2]$ ^{a, 46} | 1.31 |
| CuZn-SOD ^{a, 44} | 0.15 |
| CuZn-SOD ^{a, 47} | 0.03 |
| CuZn-SOD ^{c, 48} | 0.0026 |

^a IC_{50} was determined by employing xanthine/xanthine oxidase-mediated reduction of NBT; ^bNBT assay in the presence of alkaline DMSO; ^c IC_{50} was determined by measuring the inhibition of the photoreduction of NBT.

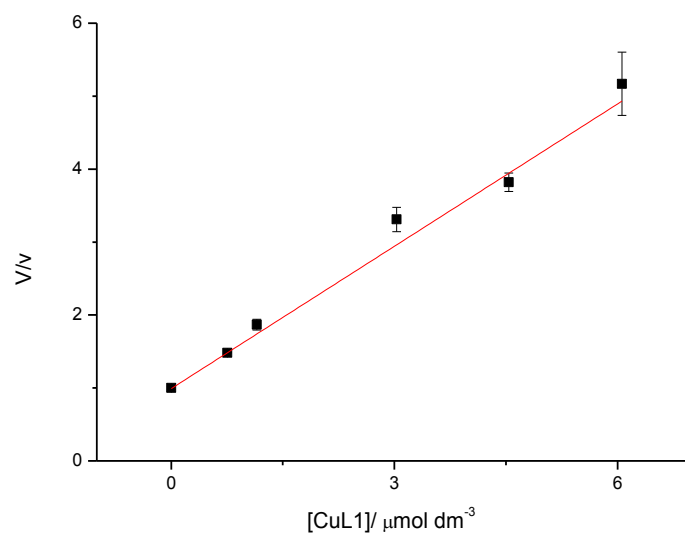


Figure 6.13. Plot of V/v vs concentration of complex **1** employed for IC_{50} calculation. V/v is the ratio between the NBT reduction rate in the absence (V) and in the presence (v) of different concentration of the complexes. The IC_{50} is the value at $V/v = 2$.

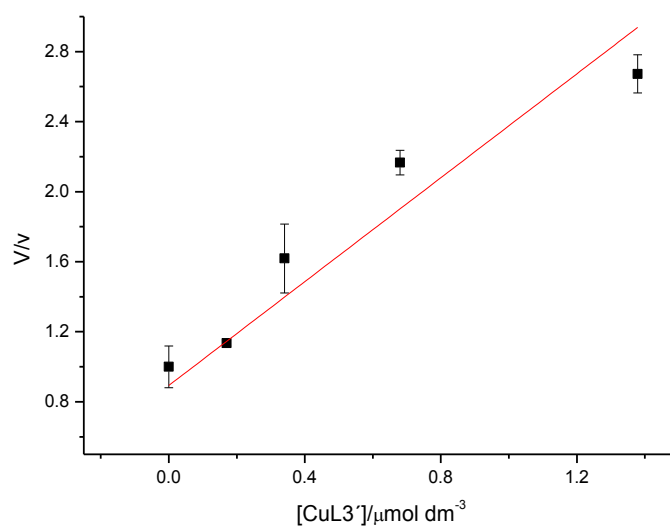


Figure 6.14. Plot of V/v vs concentration of complex **3** employed for IC_{50} calculation. V/v is the ratio between the NBT reduction rate in the absence (V) and in the presence (v) of different concentration of the complexes. The IC_{50} is the value at $V/v = 2$.

6.4. CONCLUSION

Four tetradentate diamino bis(phenolato) “salan” ligands and their corresponding Cu(II) complexes (**1–4**) have been synthesized and characterized by various physico-chemical techniques, including solving of the single crystal X-ray structure of $[\text{CuL}^1]$ (**1**) and $[\text{CuL}^{3'}]_2$ (**3**). While the coordination geometry of the asymmetric unit of complex **1** displays a near square planar geometry that of complex **3** shows a distorted elongated octahedron. The copper(II) catalyzed organic transformation in the ligands ($\text{H}_2\text{L}^{3,4}$) has been mechanistically established. Similar chemical transformation was however not observed for other transition metal complexes ($[\text{Ni}^{\text{II}}\text{L}^3]$ (**5**), $[\text{Fe}^{\text{III}}\text{L}^3(\text{Cl})]$ (**6**) and $[\text{Mo}^{\text{VI}}\text{O}_2\text{L}^3]$ (**7**)), as concluded from other analytical data. In order to ascertain the mechanism further, alternative synthetic methodology by employing different solvent medium (ethanol or acetonitrile) and using acetaldehyde as an external reagent into the reaction medium is under process. The superoxide dismutase activity of Cu(II) complexes (**1–3**) has also been probed and it is found to follow the order **3** > **2** > **1**; the SOD mimetic activity being dependent on the ligand design. Compound $[\text{CuL}^{4'}]_2$ (**4**) could not be evaluated due to its deliquescent nature.

6.5. REFERENCES

- (1) Solomon, E. I.; Heppner, D. E.; Johnston, E. M.; Ginsbach, J. W.; Cirera, J.; Qayyum, M.; Kieber-Emmons, M. T.; Kjaergaard, C. H.; Hadt, R. G.; Tian L. *Chem. Rev.* **2014**, *114*, 3659–3853 and references therein.
- (2) Ladomerskyab, E.; Petris, M. J. *Metallomics* **2015**, *7*, 957.
- (3) (a) Fukuzumi, S.; Ohtsu, H.; Ohkubo, K.; Itoh, S.; Imahori, H. *Coord. Chem. Rev.* **2002**, *226*, 71–80. (b) Tainer, J. A.; Getzoff, E. D.; Richardson, J. S.; Richardson, D. C. *Nature* **1983**, *306*, 284.
- (4) Poillon, W. N.; Dawson, C. R. *Biochim. Biophys. Acta* **1963**, *77*, 27–36.
- (5) Knowles, P. F.; Ito, N. In *Perspectives in Bio-inorganic Chemistry*; Jai Press LTD: London, **1994**; Vol. 2, pp 207.
- (6) Banu, K. S.; Chattopadhyay, T.; Banerjee, A.; Bhattacharya, S.; Suresh, E.; Nethaji, M.; Zangrando, E.; Das, D. *Inorg. Chem.* **2008**, *47*, 7083–7093.
- (7) Gaggelli, E.; Kozlowski, H.; Valensin, D.; Valensin, G. *Chem. Rev.* **2006**, *106*, 1995–2044.
- (8) Riley, D. P. *Chem. Rev.* **1999**, *99*, 2573–2587.
- (9) Zhang, C. X.; Lippard, S. J. *Curr. Opin. Chem. Biol.* **2003**, *7*, 481–489 and references therein.
- (10) Park, K. C.; Fouani, L.; Jansson, P. J.; Wooi, D.; Sahni, S.; Lane, D. J. R.; Palanimuthu, D.; Lok, H. C.; Kovacevic, Z.; Huang, M. L. H.; Kalinowski, D. S.; Richardson, D. R. *Metallomics* **2016**, *8*, 874–886.
- (11) Denoyer, D.; Masaldan, S.; La Fontaine, S.; Cater, M. A. *Metallomics* **2015**, *7*, 1459–1476.
- (12) Jansson, P. J.; Yamagishi, T.; Arvind, A.; Seebacher, N.; Gutierrez, E.; Stacy, A.; Maleki, S.; Sharp, D.; Sahni, S.; Richardson, D. R. *J. Biol. Chem.* **2015**, *290*, 9588–9603.
- (13) Kalinowski, D. S.; Stefani, C.; Toyokuni, S.; Ganz, T.; Anderson, G. J.; Subramaniam, N. V.; Trinder, D.; Olynyk, J. K.; Chua, A.; Jansson, P. J.; Sahni, S.; Lane, D. J.; Merlot, A. M.; Kovacevic, Z.; Huang, M. L.; Lee, C. S.; Richardson, D. R. *Biochim. Biophys. Acta* **2016**, *1863*, 727–748.
- (14) Lovejoy, D. B.; Jansson, P. J.; Brunk, U. T.; Wong, J.; Ponka, P.; Richardson, D. R. *Cancer Res.* **2011**, *71*, 5871–5880.

- (15) (a) Reytman, L.; Braitbard, O.; Tshuva, E. Y. *Dalton Trans.* **2012**, *41*, 5241–5247 and references therein. (b) Adão, P.; Avecilla, F.; Bonchio, M.; Carraro, M.; Pessoa, J. C.; Correia, I. *Eur. J. Inorg. Chem.* **2010**, *35*, 5568–5578. (c) Knight, P. D.; Scott, P. *Coord. Chem. Rev.* **2003**, *242*, 125–143.
- (16) Shi, Y.; Mao, Z.; Xue, Q.; Zhu, C.; Hu, H.; Cheng, Y. *Inorg. Chem. Commun.* **2012**, *20*, 259–262.
- (17) Klement, R.; Stock, F.; Elias, H.; Paulus, H.; Pelikán, P.; Valko, M.; M. Mazúra *Polyhedron* **1999**, *18*, 3617–3628.
- (18) (a) Adão, P.; Barroso, S.; Avecilla, F.; Oliveira, M. C.; Pessoa, J. C. *J. Organomet. Chem.* **2014**, *760*, 212–223. (b) Hosseini-Monfared, H.; Soleymani-Babadi, S.; Sadighian, S.; Pazio, A.; Wozniak, K.; Siczek, M.; Mayer, P. *Transition Met. Chem.* **2015**, *40*, 255–267.
- (19) (a) Valko, M.; Boca, R.; Klement, R.; Kozisek, J.; Mazur, M.; Pelikán, P.; Morris, H.; Elias, H.; Müller, L. *Polyhedron* **1997**, *16*, 903–908. (b) Boettcher, A.; Elias, H.; Jaeger, E. G.; Langfelderova, H.; Mazur, M.; Mueller, L.; Paulus, H.; Pelikan, P.; Rudolph, M.; Valko, M. *Inorg. Chem.* **1993**, *32*, 4131–4138.
- (20) Xiong, Y.; Wang, F.; Huang, X.; Wen, Y.; Feng, X. *Chem. Eur. J.* **2007**, *13*, 829–833.
- (21) Butsch, K.; Günther, T.; Klein, A.; Stirnat, K.; Berkessel, A.; Neudörfl, J. *Inorg. Chim. Acta.* **2013**, *394*, 237–246.
- (22) Santini, C.; Pellei, M.; Gandin, V.; Porchia, M.; Tisato, F.; Marzano, C. *Chem. Rev.* **2014**, *114*, 815–862.
- (23) (a) Sergeeva, E.; Kopilov, J.; Goldberg, I.; Kol, M. *Chem. Commun.* **2009**, 3053–3055. (b) Yeorl, A.; Goldberg, I.; Shuster, M.; Kol, M. *J. Am. Chem. Soc.* **2006**, *128*, 13062–13063. (c) Mandal, D.; Ganguly, R.; Chatterjee, P. B.; Endo, A.; Weakley, T. J. R.; Chaudhury, M. *Struct. Chem.* **2007**, *18*, 187–193. (d) Yang, H.; Wang, H.; Zhu, C. *J. Org. Chem.* **2007**, *72*, 10029–10034. (e) Subramanian, P.; Spence, J. T.; Ortega, R.; Enemark, J. H. *Inorg. Chem.* **1984**, *23*, 2564–2572. (f) Hinshaw, C. J.; Peng, G.; Singh, R.; Spence, J. T.; Enemark, J. H.; Bruck, M.; Kristofzski, J.; Merbs, S. L.; Ortega, R. B.; Wexler, P. A. *Inorg. Chem.* **1989**, *28*, 4483–4491. (g) Whiteoak, C. J.; Britovsek, G. J. P.; Gibson, V. C.; White, A. J. P. *Dalton Trans.* **2009**, *13*, 2337–2344. (h) Lehtonen, A.; Sillanpää, R. *Polyhedron* **2005**, *24*, 257–265.

- (24) (a) Dash, S. P.; Panda, A. K.; Pasayat, S.; Majumder, S.; Biswas, A.; Kaminsky, W.; Mukhopadhyay, S.; Bhutia, S. K.; Dinda, R. *J. Inorg. Biochem.* **2015**, *144*, 1–12. (b) Dash, S. P.; Panda, A. K.; Pasayat, S.; Dinda, R.; Biswas, A.; Tiekink, E. R. T.; Patil, Y. P.; Nethaji, M.; Kaminsky, W.; Mukhopadhyay, S.; Bhutia, S. K. *Dalton Trans.* **2014**, *43*, 10139–10156. (c) Dash, S. P.; Pasayat, S.; Bhakat, S.; Roy, S.; Dinda, R.; Tiekink, E. R. T.; Mukhopadhyay, S.; Bhutia, S. K.; Hardikar, M. R.; Joshi, B. N.; Patil, Y. P.; Nethaji, M. *Inorg. Chem.* **2013**, *52*, 14096–14107. (d) Dash, S. P.; Panda, A. K.; Pasayat, S.; Dinda, R.; Biswas, A.; Tiekink, E. R. T.; Mukhopadhyay, S.; Bhutia, S. K.; Kaminsky, W.; Sinn, E. *RSC Adv.* **2015**, *5*, 51852–51867.
- (25) Saswati, Chakraborty, A.; Dash, S. P.; Panda, A. K.; Acharyya, R.; Biswas, A.; Mukhopadhyay, S.; Bhutia, S. K.; Crochet, A.; Patil, Y. P.; Nethaji, M.; Dinda, R. *Dalton Trans.* **2015**, *44*, 6140–6157.
- (26) Mukhopadhyay, S.; Mandal, D.; Chatterjee, P. B.; Desplanches, C.; Sutter, J.; Butcher, R. J.; Chaudhury, M. *Inorg. Chem.* **2004**, *43*, 8501–8509.
- (27) CrystalClear: Rigaku Corporation, 1999. CrystalClear Software User's Guide, Molecular Structure Corporation, (c) 2000. Pflugrath, J. W. (1999) *Acta Cryst.* D55, 1718–1725.
- (28) SIR2004: Burla, M. C.; Caliandro, R.; Camalli, M.; Carrozzini, B.; Cascarano, G.L.; De Caro, L.; Giacovazzo, C.; Polidori, G.; Spagna R. 2005.
- (29) Cromer, D. T.; Waber, J. T.; "International Tables for X-ray Crystallography", Vol. IV, The Kynoch Press, Birmingham, England, Table 2.2 A (1974).
- (30) Ibers, J. A.; Hamilton, W. C. *Acta Cryst.* **1964**, *17*, 78.
- (31) Creagh, D. C.; McAuley, W. J.; "International Tables for Crystallography", Vol C, (A.J.C. Wilson, ed.), Kluwer Academic Publishers, Boston, Table 4.2.6.8, 1992, pp 219–222.
- (32) Creagh, D. C.; Hubbell, J. H.; "International Tables for Crystallography", Vol C, (A. J. C. Wilson, ed.), Kluwer Academic Publishers, Boston, Table 4.2.4.3, 1992, pp 200–206.
- (33) CrystalStructure 4.0: Crystal Structure Analysis Package, Rigaku Corporation (2000–2010). Tokyo 196-8666, Japan.
- (34) SHELX97: Sheldrick, G. M. *Acta Cryst.* **2008**, *A64*, 112–122.

- (35) Otwinowsky, Z.; Minor, W. In: *Methods in Enzymology*; Carter, C. W., Jr., Sweet, R. M., Eds.; Academic Press: New York, 1997, 276, 307–326.
- (36) (a) Altomare, A.; Burla, C.; Camalli, M.; Cascarano, L.; Giacovazzo, C.; Guagliardi, A.; Moliterni, A. G. G.; Polidori, G.; Spagna, R. *J. Appl. Cryst.* **1999**, 32, 115–119. (b) Altomare, A.; Cascarano, G.; Giacovazzo, C.; Guagliardi, A. *J. Appl. Cryst.* **1993**, 26, 343.
- (37) (a) Sheldrick G. M. SHELXL-97, Program for the Refinement of Crystal Structures. University of Göttingen, Germany, 1997. (b) Sheldrick G. M. (2013) Crystal structure refinement with SHELXL. *Acta Cryst.* **2015**, C71, 3–8.
- (38) Mackay, S.; Edwards, C.; Henderson, A.; Gilmore, C.; Stewart, N.; Shankland, K.; Donald, A.; *MaXus: a computer program for the solution and refinement of crystal structures from diffraction data*. University of Glasgow, Scotland, **1997**.
- (39) Waasmaier, D.; Kirfel, A. *Acta Cryst. A.* **1995**, 51, 416.
- (40) Ribeiro, T. P.; Fernandes, C.; Melo, K. V.; Ferreira, S. S.; Lessa, J. A.; Franco, R. W. A.; Schenk, G.; Pereira, M. D.; Horn Jr, A. *Free Radic. Biol. Med.* **2015**, 80, 67–76.
- (41) Koval, I. A., Schuitema, A. M.; Driessen, W.L.; Reedjik J. *J. Chem. Soc., Dalton Trans.* **2001**, 3663–3667.
- (42) Hasan, K.; Fowler, C.; Kwong, P.; Crane, A. K.; Collins, J. L.; Kozak, C. M. *Dalton Trans.* **2008**, 2991–2998.
- (43) Terra, W. S.; Ferreira, S. S.; Costa, R. O.; Mendes, L. L.; Franco, R. W. A.; Bortoluzzi, A. J.; Resende, J. A. L. C.; Fernandes, C.; Horn Jr., A. *Inorg. Chim. Acta* **2016**, 450, 353–363.
- (44) Anacona, J. R.; Gutierrez C.; Rodriguez-Barbarin, C. *Monatshefte fur Chemie* **2004**, 135, 785–792.
- (45) Patel, R. N.; Singh, N.; Shukla, K. K.; Gundla, V. L. N. *Spectrochim. Acta Part A* **2005**, 61, 1893–1897.
- (46) O'Connor, M.; Kellett, A.; McCann, M.; Rosair, G.; McNamara, M.; Howe, O.; Creaven, B. S.; McClean, S.; Kia, A. F. A.; O'Shea, D.; Devereux, M. *J. Med. Chem.* **2012**, 55, 1957–1968.
- (47) Weser, U.; Schubotz, L. M.; Lengfelder, E. *J. Mol. Catal.* **1981**, 13, 249–261.
- (48) Suksrichavalit, T.; Prachayasittikul, S.; Piacham, T.; Isarankura-Na-Ayudhya, C.; Nantasenamat, C.; Prachayasittikul, V. *Molecules* **2008**, 13, 3040–3056.

Chapter 7

Conclusion and Scope for Further Research

7.1. A Brief Resume of the Work Embodied in this Dissertation and Concluding Remarks

The aim of this dissertation was to explore in depth certain aspects of the chemistry of a series of variable valence transition metal (V, Ru and Ir) complexes of some selected bi- and tridentate ON, ONO, ONN donating azo ligands and Mo and Cu complexes of tetradentate ONNO salan ligands. Major emphasis was given to the structural and spectroscopic characterization of the synthesized complexes as well as the study of their chemical, electrochemical, magnetic and pharmacological properties. The following chapter-wise summary of the work presented in this dissertation reveals the extent to which the above-mentioned objectives are fulfilled.

Chapter 2 deals with the synthesis of ethoxido bridged divanadium(IV/IV) complexes $[(VOL^{1-3})_2(\mu-OEt)][Et_3NH]$ (**1–3**) of three azo dyes, 2-(2'-carboxy-5'-X-phenylazo)-4-methylphenol (H_2L^1 , X = H; H_2L^2 , X = NO₂) and 2-(2'-carboxy-5'-Br-phenylazo)-2-naphthol (H_2L^3), differing in the substituents of the phenyl ring, in order to discern their influence, if any, on their redox potentials, biological activity and magnetochemistry. All the synthesized ligands and the vanadium(IV) complexes are successfully characterized by various physicochemical techniques, viz. elemental analysis, IR, UV-vis and NMR spectroscopy, ESI-MS and cyclic voltammetry. Molecular structures of complexes **1** and **3** have been determined by X-ray crystallography. Antiferromagnetic exchange interaction was observed between the vanadium d^1-d^1 centers of the complexes and this phenomenon was also established theoretically. The complexes were also screened for their *in vitro* cytotoxicity against HT-29 and HeLa cancer cell lines. The results confirmed the antiproliferative effect of all the complexes (**1–3**) and their specificity over particular cell type, with **1** being the most potent against HeLa cancer cell line (IC₅₀ 1.92 μM).

In **Chapter 3** the synthesis of three new monooxidovanadium(IV), $[V^{IV}OL^{1-3}]_2$ (**1–3**) and two new alkoxido bridged trioxidovanadium(IV), $[V^{IV}_3O_3(\mu-OMe)_3(\mu_3-OMe)L^{4,5}]_2$ (**4** and **5**) complexes have been reported, which were obtained upon reaction of 2-((2-X)-diazol)-4-methylphenol (where X = benzo[1,3]dioxol-5-yl (HL¹), phenyl (HL²) and 4-methoxyphenyl (HL³)), 1-(2-(thiazol-2-yl)diazenyl)naphthalene-2-ol (HL⁴) and 2-(2-(thiazol-2-yl)diazenyl)-4-methylphenol (HL⁵) with VOSO₄·5H₂O. The synthesized

complexes were successfully characterized by elemental analysis, IR and UV-vis spectroscopy, ESI-MS and their redox properties studied by cyclic voltammetry. Molecular structure of **4** has been determined by single crystal X-ray diffraction study. X-ray structure showed the molecule to be composed of three slightly distorted octahedral vanadium atoms forming an almost butterfly-shaped V_3O_4 unit similar to the well-known 3Fe-4S iron sulfur cluster. The complexes were probed for their *in vitro* insulin-mimetic activity against insulin responsive L6 myoblast cells. The complexes (**1–5**) have been screened for their cytotoxicity in human breast adenocarcinoma cell line, MCF-7. The cytotoxicity of the complexes is affected by the functional groups on the arylazo ligand backbone. IC_{50} values of the complexes were found to be comparable with clinically referred chemotherapeutic drug, cisplatin. The insulin-mimetic activity of **1–5** was probed on rat L6 myoblast cells. The percent glucose uptake of the complexes was found to be significant as compared to insulin, where complex **2** ($25 \mu\text{M}$) proved to be most potent. In order to further confirm whether these compounds act via insulin signaling pathway, immunoblot analysis for IRS-1 protein was carried out.

Chapter 4 describes the reaction of 2-(aryloxy)phenols (HL) with $[\text{Ru}(\text{PPh}_3)_3\text{Cl}_2]$ in an ethanolic medium under basic conditions to afford two organometallic Ru(II) complexes, $[\text{RuL}(\text{PPh}_3)_2(\text{CO})]$, **1** and $[\text{RuL}(\text{PPh}_3)_2(\text{CH}_3\text{CN})]$, **2**. A similar reaction of HL with $\text{Ir}(\text{PPh}_3)_3\text{Cl}$ results in formation of the organometallic Ir(III) complex, $[\text{IrL}(\text{PPh}_3)_2(\text{H})]$ (**3**). The 2-(aryloxy)phenolate ligand is coordinated to the metal center in each complex (**1–3**) as a tridentate C, N, O-donor via C-H activation of the ligand. The sixth coordination site in the equatorial plane of **1–3** is occupied by CO, CH_3CN and H^- , respectively. The plausible solvent assisted mechanistic pathway for the unprecedented CO coordination to the Ru(II) center in the case of **1** has been explained. The synthesized complexes have been characterized by various spectroscopic techniques (viz., IR, UV-vis and NMR spectroscopy), ESI-MS and their electrochemical behavior studied by cyclic voltammetry. Molecular structures of **1–3** have been determined by X-ray crystallography.

In **Chapter 5** the synthesis and structural characterization of seven hexacoordinated *cis* dioxidomolybdenum(VI) complexes, $[\text{MoO}_2\text{L}^{1-7}]$ (**1–7**) derived from various substituted tetradentate diamino-bis(phenolato) “salan” ligands, *N,N'*-dimethyl-*N,N'*-bis-(2-hydroxy-3-

X-5-Y-6-Z-benzyl)-1,2-diaminoethane $\{(X = \text{Br}, Y = \text{Me}, Z = \text{H} (\text{H}_2\text{L}^1); X = \text{Me}, Y = \text{Cl}, Z = \text{H} (\text{H}_2\text{L}^2); X = \text{}^i\text{Pr}, Y = \text{Cl}, Z = \text{Me} (\text{H}_2\text{L}^3)\}$ and *N,N'*-bis-(2-hydroxy-3-X-5-Y-6-Z-benzyl)-1,2-diaminopropane $\{(X = Y = \text{}^t\text{Bu}, Z = \text{H} (\text{H}_2\text{L}^4); X = Y = \text{Me}, Z = \text{H} (\text{H}_2\text{L}^5); X = \text{}^i\text{Pr}, Y = \text{Cl}, Z = \text{Me} (\text{H}_2\text{L}^6); X = Y = \text{Br}, Z = \text{H} (\text{H}_2\text{L}^7)\}$ containing O–N donor atoms, have been discussed. The formation of dioxidomolybdenum(VI) complexes was confirmed by elemental analysis, IR, UV-vis and NMR spectroscopy, ESI-MS and cyclic voltammetry measurements. Molecular structures of **1–6** were solved by X-ray crystallography. X-ray crystallography showed the O₂N₂ donor set to define an octahedral geometry in each case. The asymmetric unit of all the complexes consists of a complete formula unit with the exception of **2**, which belongs to point group C₂. The complexes (**1–7**) showed moderate DNA binding propensity with binding constants ranging from 10⁴–10⁵ M⁻¹. The experimental results showed that the complexes **1–7** effectively interact with CT-DNA by both minor and major groove binding mode, while complex **2** additionally interacts by partial intercalative mode of binding. The dioxidomolybdenum (VI) complexes (**1–3**) showed moderate photo-induced cleavage of pUC19 supercoiled plasmid DNA. All the complexes (**1–7**) were tested for their *in vitro* antiproliferative activity against HT-29 and HeLa cancer cell lines. IC₅₀ values of the complexes in HT-29 cell line follow the order **6** < **7** << **1** < **2** < **5** << **3** < **4** while the order was **6** << **7** < **5** < **1** << **3** < **4** < **2** in HeLa cells. Some of the complexes proved to be as active as the clinical referred drugs, and the greater potency of **6** and **7** (IC₅₀ values of **6** are 2.62 and 10.74 μM and that of **7** is 11.79 and 30.48 μM in HT-29 and HeLa cells, respectively) may be dependent on the substituents in the salan ligand environment coordinated to the metal.

In **Chapter 6** the synthesis and characterization (elemental analysis, UV–vis spectroscopy and ESI-MS) of Cu(II) complexes ([CuL^{1,2}] (**1** and **2**) and [CuL^{3,4}]₂ (**3** and **4**)) using tetradentate diamino bis(phenolato) “salan” ligands, *N,N'*-dimethyl-*N,N'*-bis-(2-hydroxy-3-X-5-Y-6-Z-benzyl)-1,2-diaminoethane (X = ⁱPr, Y = Cl, Z = Me (H₂L¹); X = OCH₃, Y = allyl, Z = H (H₂L²)) and *N,N'*-bis-(2-hydroxy-3-X-5-Y-6-Z-benzyl)-1,2-diaminopropane (X = ⁱPr, Y = Cl, Z = Me (H₂L³); X = Y = CH₃, Z = H (H₂L⁴)) have been studied. The redox property of the complexes has been ascertained by cyclic voltammetry. Molecular structures of the complexes (**1** and **3**) have been determined by X-ray crystallography. While **1** and **2** have the expected square planar geometry, with the ligand

coordinating to the metal center in the usual tetradentate fashion, an unprecedented ligand transformation occurs in the case of **3** and **4**, leading to the formation of phenolato bridged Cu(II) dimeric complexes, $[\text{CuL}^{3,4'}]_2$, having an elongated octahedron structure. The organic transformation in the ligands (H_2L^3 and H_2L^4) has been mechanistically elucidated to be Cu(II) catalysed. In order to fortify the ligand modification to be Cu(II) assisted, the corresponding Ni^{II} , Fe^{III} and Mo^{VI} complexes (**5–7**) with the same ligand environment, were synthesized and characterized. The anomaly in the ligand backbone was however not observed in the case of other transition metal complexes (**5–7**). In addition, the superoxide dismutase (SOD) activity of the Cu(II) complexes (**1–3**) has also been investigated; the activity follows the order **3** > **1** > **2**. Due to the deliquescent nature of $[\text{CuL}^{4'}]_2$ (**4**), its SOD activity could not be evaluated.

7.2. Scope for Further Research

There is further scope for research in relation to the catalytic activities of the synthesized molybdenum and vanadium complexes (in the bromoperoxidation, deperoxidation and the oxidation of benzoin) and platinum group organometallic complexes (in hydrogenation reaction). Other pharmacological activities (insulin-mimetic activity of the vanadium (IV) dimers, hydrolase and catecholase activity of the Cu(II) complexes, the DNA and protein binding and cleavage and the antimicrobial activity) of the complexes can be studied. Interaction of the synthesized complexes with bioligands and proteins of the blood and cytosol can be studied to understand biospeciation processes in the biofluids and potential pharmacologically active species in the organism. Moreover, using the synthesized ligand systems, mixed transition metal complexes can be prepared. In addition, mixed-valence divanadium(IV,V) species can be synthesized from the divanadium(IV) complexes analogues by controlled potential electrolysis (CPE). Considering the attractive chemical and physical properties pertaining to catalysis, sensor technology, magnetochemistry and bioinorganic chemistry of polyoxidovanadates, the variable temperature magnetic susceptibility measurements of the trinuclear vanadium(IV) arylazo complexes can be carried out.

Dissemination

Papers published in cited Journals (SCI)

1. ‘Highly Stable Hexacoordinated Nonoxidovanadium(IV) Complexes of Sterically Constrained Ligands: Syntheses, Structure and Study of Antiproliferative and Insulin Mimetic Activity’, S. P. Dash, S. Pasayat, S. Bhakat, **Satabdi Roy**, R. Dinda, E. R. T. Tiekink, S. Mukhopadhyay, S. K. Bhutia, M. R. Hardikar, B. N. Joshi, Y. P. Patil, M. Nethaji, *Inorg. Chem.* **2013**, *52*, **14096**.
2. Synthesis, structural studies and catalytic activity of dioxidomolybdenum(VI) complexes with aroylhydrazones of naphthol-derivative’, S. Pasayat, S. P. Dash, **Satabdi Roy**, R. Dinda, S. Dhaka, M. R. Maurya, W. Kaminsky, Y. P. Patil, M. Nethaji, *Polyhedron* **2014**, *67*, **1**.
3. ‘Versatile Reactivity and Theoretical Evaluation of Mono- and Dinuclear Oxidovanadium(V) Compounds of Aroylazines: Electrogeneration of Mixed-Valence Divanadium(IV,V) Complexes’, S. P. Dash, **Satabdi Roy**, M. Mohanty, M. F. N. N. Carvalho, M. L. Kuznetsov, J. C. Pessoa, A. Kumar, Y. P. Patil, A. Crochet, R. Dinda, *Inorg. Chem.* **2016**, *55*, **8407**.
4. ‘Synthesis, Structure and Cytotoxicity of a Series of Dioxidomolybdenum(VI) Complexes Featuring Salan ligands’, **Satabdi Roy**, M. Mohanty, S. Pasayat, S. Majumder, K. Senthilguru, I. Banerjee, H. Reuter, R. Dinda, *J. Inorg. Biochem.* DOI: **10.1016/j.jinorgbio.2017.04.015**
5. ‘Synthesis, Characterization and DNA Interaction Study of cis-Dioxidomolybdenum(VI) Complexes Derived from Diamino Bis(phenolato) Ligands’ **Satabdi Roy**, A. Chakraborty, A. Biswas, S. Majumder, A. Banerjee, R. Dinda, **Satabdi Roy**, A. Chakraborty, A. Biswas, S. Majumder, A. Banerjee, and R. Dinda, *J. Coord. Chem.* (Under Revision).
6. Mono- and dimeric oxidomolybdenum(V and VI) complexes, cytotoxicity, DNA interaction studies: Unprecedented Mo assisted C=N bond cleavage of salophen ligands, S. Majumder, S. Pasayat, A. K. Panda, S. P. Dash, **Satabdi Roy**, A. Biswas, M. E. Varma, B. N. Joshi, E. Garribba, W. Kaminsky, A. Crochet, R. Dinda, *Inorg. Chem.* (Under Revision).

7. 'Chemistry of Oxidomolybdenum(IV) and -(VI) Complexes with ONS Donor Ligands: Synthesis, Theoretical Evaluation and Oxo-Transfer Reactions', Saswati, **Satabdi Roy**, S. P. Dash, , R. Acharyya, W. Kaminsky, V. Ugone, E. Garribba, C. Harris, J. M. Lowe, and R. Dinda, *New J. Chem.* (Submitted).
8. 'Magnetic exchange coupling interaction of μ -ethoxido bridged azo functionalized oxidovanadium(IV) dimeric anions: Synthesis, X-ray structure, characterization and cytotoxicity', **Satabdi Roy**, Saswati, S. P. Dash, M. Böhme, A. Buchholz, W. Plass, K. Senthilguru, M. Reichelt, H. Reuter, W. Kaminsky and R. Dinda. *Inorg. Chem.* (Manuscript under preparation)
9. 'Synthesis, characterization and biological evaluation of oxidovanadium(IV)-azo complexes: Antiproliferative and insulin-mimetic agents' **Satabdi Roy**, S. Majumder, S. P. Dash, M. Varma, M. R. Hardikar, B. N. Joshi and R. Dinda. (Manuscript under preparation)
10. 'Synthesis, characterization and superoxide dismutase activity of Cu(II) salan complexes: Unprecedented Cu(II) catalyzed acetal formation', **Satabdi Roy**, W. Kaminsky, A. H. Jr. and R. Dinda. (Manuscript under preparation)
11. 'Synthesis, characterization and study of reactivity of Ru and Ir complexes of 2-arylazophenols: Solvent assisted CO insertion and formation of metal (Ru, Ir)-carbon bond,' **Satabdi Roy**, E. Sinn, W. Kaminsky and R. Dinda. (Manuscript under preparation).

Papers published in Conference Proceedings

1. **Satabdi Roy**, M. Mohanty, S. Majumder, A. Banerjee and R. Dinda, 'Dioxidomolybdenum(VI) complexes featuring O-N donor ligands: Synthesis, Characterization, DNA Interaction and Cytotoxicity', *International Conference on 'Recent Advances In Materials Chemistry' (RAMC 2017), Utkal University, Bhubaneswar, India, 24–26 February, 2017.*
2. S. Majumder, **Satabdi Roy**, W. Kaminsky, E. Sinn and R. Dinda, 'Molecular and supramolecular structures of oxidomolybdenum(VI) complexes with aroylhydrazones of acetylacetone: Synthesis, characterization and study of biological activity', *Sixth*

International Conference on Metals in Genetics, Chemical Biology and Therapeutics (ICMG-2016), Bangalore, India, 17–28 February, 2016.

3. **Satabdi Roy**, S. Majumder, P. A. Lay, H. Reuter, W. Plass, R. Dinda “Oxidovanadium(IV) azo complexes: Synthesis, Characterization, magnetochemistry and biological relevance”, *18th CRSI National Symposium in Chemistry, Indian Institute of Nano Science and Technology and Panjab University, India, 5–7 February, 2016.*

4. **Satabdi Roy**, S. Majumder, B. N. Joshi, R. Dinda, A. Crochet, “Mono and dinuclear oxido bridged vanadium(IV) multidentate azo complexes: Potent cytotoxic and insulin-mimetic agent ”, *National Symposium on Modern Trends in Chemistry(MTIC-XVI), Jadavpur University, India, 3–5 December, 2015.*

5. S. Majumder, **Satabdi Roy**, H. Reuter, and Rupam Dinda, “Dioxidomolybdenum(VI) complexes of aroylhydrazones: synthesis, structure and study of reactivities”, *17th CRSI National Symposium in Chemistry, NCL, Pune, India, 6-8 February, 2015.*

6. **Satabdi Roy**, S.P. Dash, S. Majumder, A. Levina, P. A. Lay, H. Reuter and R. Dinda, “Synthesis, Characterization and Cancer Cell Cytotoxicity of Ethoxo Bridged Azo Functionalized DinuclearOxidovanadium(IV) Complexes”, *41st International Conference on Coordination Chemistry (ICCC41), SNIC Singapore, 21–25 July, 2014.*

7. **Satabdi.Roy**, S. P. Dash, W. Kaminsky and R. Dinda, “Ethoxo bridged dioxidodivanadium (IV) complexes featuring azo ligands: Synthesis, structure and study of reactivity”, *16th CRSI National Symposium in Chemistry, IIT Bombay, India, 7–9 February, 2014.*

8. S. Pasayat, **Satabdi Roy**, S. P. Dash, Saswati, W. Kamisky and R. Dinda, “Synthesis, structural and biological evaluation of dioxidomolybdenum(VI) complexes: Metal mediated metal-metal bond formation”, *International conference on Recent Trends in Organometallic compounds and their Industrial applications (OMCA-2013), KIIT Bhubaneswar, India, 5–7 February, 2013.*

9. S. P. Dash, **Satabdi Roy**, Sagarika Pasayat, Saswati, Yogesh P. Patil M. Nethaji and Rupam Dinda, “Synthesis and Characterization of a Series of Hexacoordinated Non-oxo Vanadium(IV) Complex”, *15th CRSI National Symposium in Chemistry (NSC-15), BHU, India, 1–3 February, 2013.*

Curriculum Vitae

Satabdi Roy

Research Scholar

Department of Chemistry

National Institute of Technology, Rourkela

Rourkela-769008, Odisha, India

Research experience

a. Doctoral Research (July 2012 – January 2017)

Supervisor: Dr. Rupam Dinda, Department of Chemistry, National Institute of Technology Rourkela, India,

Research area: Coordination and Bioinorganic Chemistry

b. Project undertaken during M.Sc (March 2011)

Title: “Determination of the purity of the oil sample of Guggul plant by analysis of its Chemical constants.”

Supervisor: Dr. M. Z. Siddiqui, Processing and Product Development Division, Indian Institute of Natural Resins and Gums (ICAR), Ranchi.

Analytical Techniques

Spectroscopic Techniques: Acquisition and analysis of ^1H , ^{13}C , ^{31}P , ^{51}V NMR, FT-IR, UV-vis spectra and ESI-MS.

Recording and interpretation of cyclic voltammetry. Thin layer chromatography

X-Ray Crystallography: Interpretation of X-ray crystal structure

Software: MERCURY, ORTEP & Origin.

Education Profile

2011 Post graduation (**M.Sc., Specialisation: Organic Chemistry**), University Department of Chemistry, Ranchi University, Jharkhand, India.

2009 Graduation (**B.Sc. Hons. in Chemistry**), Jamshedpur Women's College, Jamshedpur, Ranchi University, Jharkhand, India.

2006 Higher Secondary (**12th**), ICSE Board, Kerala Samajam Model School, Jamshedpur, Jharkhand, India.

2004 Secondary (**10th**), ICSE Board, Kerala Samajam Model School, Jamshedpur, Jharkhand, India.

Honors and Fellowship

- Senior Research Fellowship (July 2014–Continuing)
- Junior Research Fellowship (July 2012–July 2014)
- Qualified GATE 2012
- University Gold Medal (M. Sc. Chemistry, Ranchi University)

Personal Profile

- Date of Birth 10th March, 1988
- Nationality Indian
- Permanent Address C-302, Orchid Residency,
Road No. 7(Ext.), Sonari,
Jamshedpur-831011,
Jharkhand, India